Polymeric thin films for integrated optics.

Sharma, Prem Kumar

Abstract.

This thesis presents the results from the characterisation of the linear optical properties of various polymers and the energy transfer process between several dye pairs in polymeric waveguides. The polymers and dyes were considered for their use in solid state thin film wavelength tuneable light sources.

The optical waveguiding properties of the polymers were investigated, and the results of the experiments are reported. Also the fundamental concepts of waveguiding in thin films are presented. The techniques of processing the thin films, input and output coupling of the light and analysis of the results is discussed.

The mechanism of non-radiative energy transfer between dye pairs was investigated as a means of efficiently exciting the acceptor dye. The theory is discussed. Also the results of both the steady state and time resolved experiments, used to determine the efficiency of the process, are reported. Efficient energy transfer has been observed in a rhodamine dye system and also between newly developed BASF dyes.

Several models are proposed to explain an upconversion observed in a dye doped polymer waveguide. Here fluorescence was observed by exciting the dye in the long wavelength tail of the absorption band. A model based on the thermal population of electrons to higher vibrational levels, from where they can be promoted to the first excited electronic state, is shown to best explain the phenomenon.

Acknowledgements.

I would like to acknowledge my supervisor Professor David Bloor without whose guidance I would not be in a position to submit, I would also like to thank Dr. Graham Cross for his help and advice in the research and for proof reading this thesis, also to David Gray for help with some of the temperature dependence experiments. I would also like to acknowledge Dr. Garry Rumbles and Dr. Trevor Smith from Imperial College for invaluable discussions and allowing me time on the time correlated single photon counting equipment and fluorimeter at Imperial, to them I am greatly indebted, and also to Julia Elliot, from Imperial College, for the work on some of the fluorescence spectra used in this thesis. Also I would like to thank Dr. K. Davidson from Lancaster University for using their time correlated single photon counting equipment. I would like to acknowledge my supervisor from GEC - Marconi Dr. Mike Worboys for discussions as to the course of the research, and Mark Walmsley for help on some of the theoretical work on the thermal upconversion.

I would like to thank the SERC and GEC - Marconi for the funding of this research. Also I would like to thank the Institute of Physics for their financial contribution towards the cost of attending the annual ACS symposium, August 1991 in New York.

Finally I would like to thank all those dear to me without whose support I would not be inspired, especially to my parents to whom I dedicate this thesis.

Polymeric Thin Films for Integrated Optics.

by

Prem Kumar Sharma, BSc (Hons.).

A thesis submitted for the degree of

Doctor of Philosophy

at the University of Durham, Applied Physics Group,

Department of Physics.

June 1992.

Contents

List of figure captions.

Chapter 1

Chapter 2

Chapter 3

Chapter 4

Chapter 5

List of tables.

Chapter 2

Chapter 3

Chapter 4

Declaration.

I hereby declare that the work reported in this thesis has not previously been submitted for any degree and is not being currently submitted in candidature for any other degree.

Signed P. K. Sharma

The work reported in this thesis was carried out by the candidate. Any work not carried out by the candidate is acknowledged in the main text.

Signed D Bloor

PhD Supervisor

Signed P. K. Sharma

Candidate

Statement of copyright.

CHAPTER 1.

Introduction.

1.1 Background.

It is becoming increasingly more important today for communication to be fast and efficient. This seems to be true not only for long range communications, such as between countries, but also in short range communications, such as between integrated circuits. It is primarily for these reasons that more people are looking towards optical communication as a possible solution to the problem.

The field of integrated optics has been based on the fact that light waves can be guided in very thin dielectric layers, which was first realised experimentally in the early 1960's. Due to their small dimensions, higher speed, low power requirements, greater bandwidth capability and immunity from electromagnetic interference, it is expected that optical components could replace electrical circuitry. By shaping and combining appropriate layers the light waves can be manipulated as desired. Thus light can be guided, modulated, deflected, filtered, radiated into space, or, by using laser action, be generated in a thin film structure. Advances are being made in optical device structures with the desired properties. Integrated optical devices for computing and signal processing have been fabricated in Lithium Niobate ($LiNbO_3$) [Tsai C. S., (1988)], [Syms R. R. A., (1988)]. This has been one of the principal materials to implement some of the structures mentioned above. It is a piezoelectric, birefringent crystal with a low optical transmission loss and a high electro - optic coefficient. However, it is not suitable for fabricating lasers and detectors. Monolithic integration of devices such as lasers, modulators, and photodetectors have made recent advances using semiconductor

materials [Forrest S. R., (1987)], [Suematsu Y. and Arai S., (1987)], such as gallium arsenide and indium phosphide.

Due to the potential of optical device fabrication, the field of integrated optics has attracted attention and, with fibre optic technology, the possibility of the development of an all optical communication system. An integrated optics system requires the combination of individual components, this factor affects the choice of materials to be used. Sources, guiding and coupling components can be accommodated by using all - optical components. Detecting and controlling components however, can be achieved more easily by employing lower frequency inputs involving photo - electric, electro - optic, acousto - optic or other effects.

A great deal of research is being undertaken in the field of polymeric thin films as active and passive materials. Organic materials have been considered for some time to be viable materials for integrated optics [Zyss J., (1985)], [Stegeman G. I. et al., (1987)]. Polymers have been used in the development of linear waveguides, Schriever R. et al., (1985), have extensively studied waveguiding in poly(methylmethacrylate) (PMMA) thin films and in optically recorded strip waveguides in PMMA. Reuter R. et al., (1988), have investigated various polyimides as waveguide materials. Polymers have also been used in the fabrication of nonlinear waveguides. Glenn R. et al., (1987), have described a process for the production of waveguides in polymer matrices by solvent aided indiffusion of organic dopant materials. Using suitable dopants, waveguides can be made which show nonlinear optical properties. Low loss channel waveguides are currently being produced using many different types of polymers. Booth B. L., (1989), reviews some of the techniques for fabricating channel waveguides in polymers and some of the covering processes, materials, waveguide performance and applications. Thus providing a perspective on the flexibility and

versatility for fabricating polymer channel waveguides for practical integrated optical applications. Active devices incorporating polymeric waveguides have been developed for example, modulators [Ender D. A. et al., (1988)], refracting lenses [Righini G. C. and Molesini G., (1988)], tapers [Hewak D. W. and Lit J. W. Y., (1988)], thermooptic switches [Diemeer M. B. J. et al., (1989)], sensors [Taylor H. F., (1987)] and noise filters [Thylen L., (1987)]. As for sources, solid thin film energy transfer dye lasers have been fabricated in thin polymer films [Muto S. et al., (1987a)], where energy transfer has been used to cover a wide range of emission wavelengths .

Thus with the current trends in polymer thin film research for integrated optics, the aim of this work was primarily to look at designing wavelength tuneable light sources for integrated optics. Organic dyes, excited with a pump source, have been used as the amplifying medium in dye lasers. Solid thin film energy transfer dye lasers (ETDL) have been shown to have a high practical value as compact, variable wavelength, light sources. Thin film ETDL have been developed by doping donor - acceptor dye pairs into a polymer waveguide [Muto S. et al., (1987b)]. Energy transfer between dye pairs can improve the lasing efficiency of an acceptor dye with the donor dye exciting it over a wide range of wavelengths. By using a proper mixture of dyes, energy transfer can provide a way of extending the wavelength region in which lasing is achieved. Hence this thesis reports the study of energy transfer between dye pairs in a polymer matrix. The waveguiding properties of the polymers, with a view to designing integrated lasing structures, are also reported.

Chapter 2 describes waveguiding, and introduces some of the theory and principles involved, along with the material requirements. Also it looks at different thin film fabrication methods that have been developed, in particular dipping and spinning. Several waveguiding input/output geometries are also considered, prism and grating

couplers are discussed in detail. The results from the waveguiding experiments performed on different polymers are presented.

The important requirements of dyes for dye laser applications is outlined in chapter 3. The investigation of the absorption and fluorescence properties of the dyes in thin polymer films, in order to select certain dyes as candidates for energy transfer, is presented. The advantages and the implications of a nonradiative energy transfer process on these properties are explored.

Chapter 4 discusses the mechanism of energy transfer and looks at the Förster formulation of the process. In order to investigate the extent of the energy transfer, the effect of the acceptor dye concentration on the donor dye fluorescence lifetime is monitored. The results from a detailed analysis of the fluorescence lifetimes of the dyes used are presented.

Chapter 5 reports on the results of an investigation into an upconversion process seen in a dye doped polymer waveguide. In the experiment the dye doped polymer waveguide was excited in the long wavelength tail of its absorption spectrum, and fluorescence at shorter wavelengths was observed. Several models have been proposed and the results from experiments performed to test these models are reported.

Before considering waveguiding an understanding of the fundamentals of the interaction light with matter and the concept of the refractive index of a material is required.

1.2 Linear optics.

When an electric field is applied across a sample, the negative and positive charges of the constituent molecules move in opposite directions and a polarisation is

induced. If the electric field is alternating, the polarisation also alternates, moreover the frequency of the polarisation is the same as that of the applied field. Considering just a single atom with one electron, this oscillating dipole radiates an electromagnetic wave of the same frequency as the oscillation but of a different phase, which depends on the restoring forces between electron and nucleus. The resultant wave thus has a phase which is a combination of the incident and re-radiated wave.

If the sample is of thickness d, then the phase difference between a wave travelling through the sample and a wave travelling in a vacuum is proportional to d. It appears as if the wave travelling in the sample propagates more slowly than the wave through a vacuum. The ratio between the velocities is known as the refractive index of the material.

$$n = c / \text{velocity in the sample.}$$

What has been assumed is that light propagates only in the forward direction. However the radiation pattern of an oscillating dipole has a $\sin\theta$ term (θ is the angle between the axis of the dipole and the direction of observation). The reason for forward radiation is that the phase of the radiation from every dipole is determined by the phase of the wave incident upon it. Therefore, even though each individual dipole does radiate in all directions, any radiation not in the forward direction is out of phase with the radiation in that same direction from other dipoles and does not build up. Only in the forward direction are all the dipoles phased correctly. They form a phased array of antennas.

Re-radiation of the same fraction of the incident wave allows the radiation to build up in the forward direction and interfere destructively in all other directions. If one dipole, or a group of dipoles, radiates a different fraction, some of the re-radiated

wave is visible in other directions (called scattered or incoherent radiation). The tendency to scatter is strong in materials with many impurities. All the energy used to drive the oscillating dipole is not necessarily re-radiated as an electromagnetic wave. Normally it is not just the electron which is made to oscillate, but the ensemble of electron and nucleus; moreover, there are interactions between the atoms. At certain frequencies part of the driving energy causes vibrations of the atoms, and heats the material, i.e. part of the incident energy is absorbed.

As mentioned earlier, the induced polarisation, in a medium, is proportional to the applied alternating field and has the same frequency. This can be expressed as :

$$P = \chi(\omega)\, E(\omega) e^{-i\omega t} + \text{complex conjugate} \qquad (1.1)$$

where : P - induced polarisation.

$E(\omega)$ - applied alternating electric field.

ω - frequency of the applied field.

$\chi(\omega)$ - susceptibility of the material which is related to the refractive index by :

$$n^2 = 1 + \chi(\omega) \qquad (1.2)$$

Substituting an expression for $\chi(\omega)$ [Marcuse D., (1974)] into (1.2) it can be shown that :

$$n^2 = 1 + \frac{Ne^2}{m} \frac{4\pi}{\omega_0^2 - 2i\gamma\omega - \omega^2} + \text{complex conjugate} \qquad (1.3)$$

where:

m - electron density of the medium.

e - charge on an electron.

m - mass of an electron.

ω_0 - natural frequency of an electron.

γ - damping constant.

For the case of $\gamma = 0$ (no damping), n is a real quantity, and its dependence on frequency is shown below in figure (1.1) as a solid line. If $\gamma \neq 0$, n becomes complex. The imaginary part is a measure of the absorption and becomes large in the vicinity of ω_0.

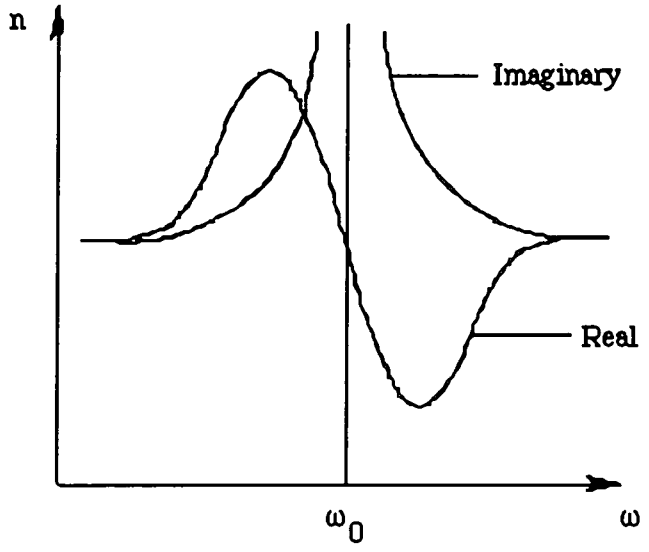

Figure (1.1) Refractive index dispersion graph.

1.3 References.

Booth B. L.,"Low loss channel waveguides in polymers.", J. Light. Tech., Vol 7, No 10, pp 1445-1453, (1989).

Diemeer M. B. J., Brons J. J. and Trommel E. S.,"Polymeric optical waveguide switch using the thermooptic effect.", J. Light. Tech., Vol 7, No 3, pp 449-453, (1989).

Ender D. A., Moshrefzadeh R. S., Boyd G. T., Leichter L. M., Liu J. C., Henry R. M. and Williams R. C., "Polmerc and organic crystalline films for electro - optic applications.", SPIE, Vol 971 Nonlinear optical properties of organic materials, pp 144-153, (1988).

Forrest S. R.,"Optoelectronic Integrated Circuits.", Proc. IEEE., Vol 75, No 11, pp 1488-1497, (1987).

Glenn R., Goodwin M. J. and Trundle C.,"Solvent-Assisted Indiffusion: A new method for the production of nonlinear waveguides in polymer matrices.", J. Mol. Elect., Vol 3, pp 59-66, (1987).

Hewak D. W. and Lit J. W. Y.,"Fabrication of tapers and lenslike waveguides by a microcontrolled dip coating procedure.", Appl. Opt., Vol 27, No 21, pp 4562-4564, (1988).

Marcuse D.,Theory of dielectric optical waveguides, Academic Press, New York, (1974).

Muto S., Uchida H. and Nakamura K.,"Characteristics of thin-film energy-transfer dye laser with DFB oscillator-amplifier system.", Elect. and Comm. Jap. Part 2., Vol 70, No 8, pp 95-101, (1987a).

Muto S., Shiba F., Iijima Y., Hattori K. and Ito C.,"Solid thin-film energy-transfer dye lasers.", Elect. Comm. Jap. Part 2., Vol 70, No 1, pp 21-31, (1987b).

Reuter R., Franke H. and Feger C.,"Evaluating polyimides as lightguide materials.", Appl. Opt., Vol 27, No 21, pp 4565-4571, (1988).

Righini G. C. and Molesini G.,"Design of optical waveguide homogenous refracting lenses", Appl. Opt., Vol 27, No 20, pp 4193-4199, (1988).

Schriever R., Franke H., Festl H. G. and Krätzig E., "Optical waveguiding in doped poly(methyl methacrylate)", Polymer, Vol 26, pp 1423-1427, (1985).

Stegeman G. I., Seaton C. T. and Zanoni R.,"Organic films in non-linear integrated optics structures.", Thin solid films, Vol 732, pp 231-263, (1987).

Suematsu Y. and Arai S.,"Integrated Optics Approach for Advanced semiconductor Lasers.", Proc. IEEE., Vol 75, No 11, pp 1472-1487, (1987).

Syms R. R. A.,"Advances in channel waveguide lithium niobate integrated optics.", Opt. Quan. Elect., Vol 20, pp 189-213, (1988).

Taylor H. F.,"Application of guided wave optics in signal processing and sensing.", Proc. IEEE., Vol 75, No 11, pp 1524-1535, (1987).

Thylen L.,"Wavelength and noise filtering characteristics of coupled active and passive waveguides.", IEEE. J. Quan. Elect., Vol QE-23, No 11, pp 1956-1961, (1987).

Tsai C. S.,"Integrated-optical device modules in $LiNbO_3$ for computing and signal processing.", J. Mod. Opt., Vol 35, No 6, pp 965-977, (1988).

Zyss J.,"Nonlinear Organic Materials for Inegrated Optics: a Review.", J. Mol. Elect., Vol 1, pp 25-45, (1985).

CHAPTER 2.

Waveguiding.

The aim of this chapter is to introduce some of the fundamental concepts of waveguiding. Some thin film fabrication methods will be discussed in section (2.2), paying particular attention to spinning and dipping. In section (2.3) input and output waveguide couplers are investigated, looking at different forms of couplers. Prism coupling is explained in detail, since this was the technique used in most cases. Grating couplers are also discussed in some detail with different grating fabrication methods.

In section (2.4) the results of experiments performed with different polymers - making thin film waveguides and characterising them - are presented. Also results from experiments on various oxygenated polymers from the University of Namur are presented.

2.1 Theoretical considerations of waveguiding in thin films.

An optical waveguide is sometimes considered as three media, a film, an air space above and a substrate below, as shown in figure (2.1).

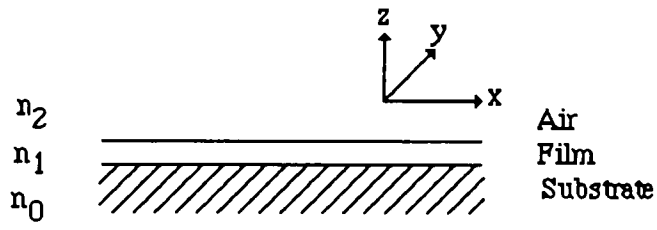

Figure (2.1) A schematic diagram of an optical waveguide.

For the thin film to allow the propagation of a mode and act like a dielectric waveguide, it is necessary but not sufficient that, the refractive index of the film must be higher than that of the substrate. The thin film must also be transparent at the wavelength of interest.

The solutions to Maxwells equations that match the boundary conditions at the film-substrate and film-air interfaces indicate three possible modes of propagation :

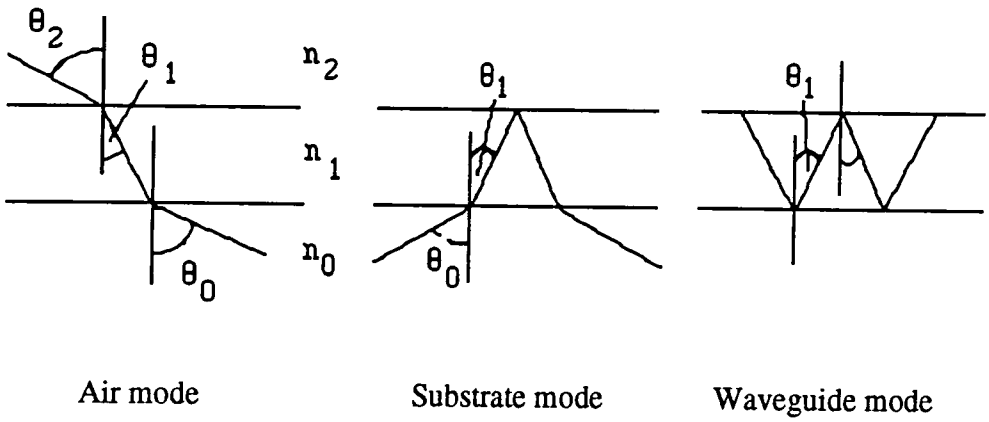

Air mode Substrate mode Waveguide mode

Figure (2.2) A schematic diagram illustrating the three possible modes of propagation.

These modes can be described by Snell's law of refraction and the total internal reflection phenomenon in optics.

Above in figure (2.1) $n_1 > n_0 > n_2$ - then from Snell's law :

$$\frac{\sin\theta_2}{\sin\theta_1} = \frac{n_1}{n_2} \qquad \text{and} \qquad \frac{\sin\theta_0}{\sin\theta_1} = \frac{n_1}{n_0}$$

The waveguided modes follow a zigzag path which can be represented by two wavevectors A_1 and B_1. These can be divided into horizontal and vertical components.

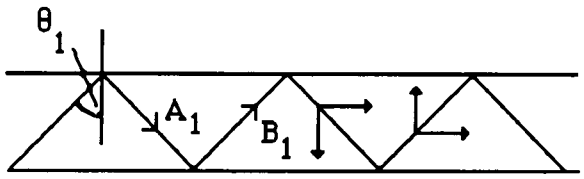

Figure (2.3) The zig zag path of a waveguided mode and its components.

The horizontal components of A_1 and B_1 are equal indicating that the waves propagate with a constant speed in a direction parallel to the film. The vertical component of A_1 represents a downward travelling wave and that of B_1 an upward travelling wave. When these two are superimposed they form a standing wave field pattern across the thickness of the film. By changing θ_1, the directions of A_1 and B_1 are changed and hence the horizontal and vertical components. This changes the wave velocity parallel to the film as well as the standing wave field pattern across the film.

The waves discussed above are plane waves. They are TE (transverse electric) waves if they contain the field components E_y, H_z, H_x. They are TM waves if they contain the field components H_y, E_x, E_z. The wavevectors A_1 and B_1 thus have a magnitude kn_1 where $k = \omega/c$, ω - the angular frequency of the light wave, c - speed of light in a vacuum. The wavevectors are normals of the wavefronts which are reflected back and forth across the film at the two interfaces. The condition then for the multiply reflected waves to add in phase, is that the total phase change for one round trip up and down should be equal to $2m\pi$, where m is an integer.

The vertical components of A_1 and B_1 have a magnitude $kn_1\cos\theta_1$. The phase change for the plane wave to cross the thickness W of the film twice (up and down) is then $2kn_1W\cos\theta_1$. Also the wave suffers a phase change of $-2\Phi_{12}$ and $-2\Phi_{10}$ due to

the total reflection at the upper and lower boundaries respectively. Hence in order for the waves to interfere constructively :

$$2kn_1 W\cos\theta_1 - 2\Phi_{10} - 2\Phi_{12} = 2m\pi.$$

This is the condition for waveguide modes. Here m is the order of the mode. According to Born and Wolf, (1970) on the theory of total reflection :

$$\tan\Phi_{12} = \frac{\sqrt{n_1^2 \sin^2\theta_1 - n_2^2}}{n_1 \cos\theta_1}$$

$$\tan\Phi_{10} = \frac{\sqrt{n_1^2 \sin^2\theta_1 - n_0^2}}{n_1 \cos\theta_1} \qquad (2.1)$$

for TE waves and

$$\tan\Phi_{12} = \frac{n_1^2\sqrt{n_1^2 \sin^2\theta_1 - n_2^2}}{n_2^2 n_1 \cos\theta_1}$$

$$\tan\Phi_{10} = \frac{n_1^2\sqrt{n_1^2 \sin^2\theta_1 - n_0^2}}{n_0^2 n_1 \cos\theta_1} \qquad (2.2)$$

for TM waves.

To avoid confusion it is desirable to describe the longitudinal propagation constant ß, and the wave velocity v as :

$$ß = kn_1\sin\theta_1 \quad \text{and} \quad v = c(k/ß).$$

hence $q = kn_1\cos\theta_1$, the transverse wave number.

$$q = \sqrt{k^2 n_1^2 - \beta^2} \tag{2.3}$$

If we assume that the upward and downward travelling waves interfere constructively i.e.

$$2kn_1 W\cos\theta_1 - 2\pi = 2m\pi \tag{2.4}$$

then from the definition of q given in equ.(2.3) it follows that :

$$qW = (m+1)\pi \tag{2.5}$$

substituting (2.5) into (2.3) we derive a quantisation condition on the longitudinal propagation constant β :

$$\beta^2 = k^2 n_1^2 - \left(\frac{(m+1)\pi}{W}\right)^2$$

This gives a characteristic plot of β vs k as shown in figure (2.4). It can be seen that whilst TEM (transverse electromagnetic) modes can have $\beta = 0$ when $k = 0$, for TE (and similarly for TM) modes there are *cut off* values of k (equivalently, of the angular frequency ω) corresponding to $\beta = 0$. For frequencies below cut off, values for k_c are given by :

$$k_c n_1 = \frac{(m+1)\pi}{W}$$

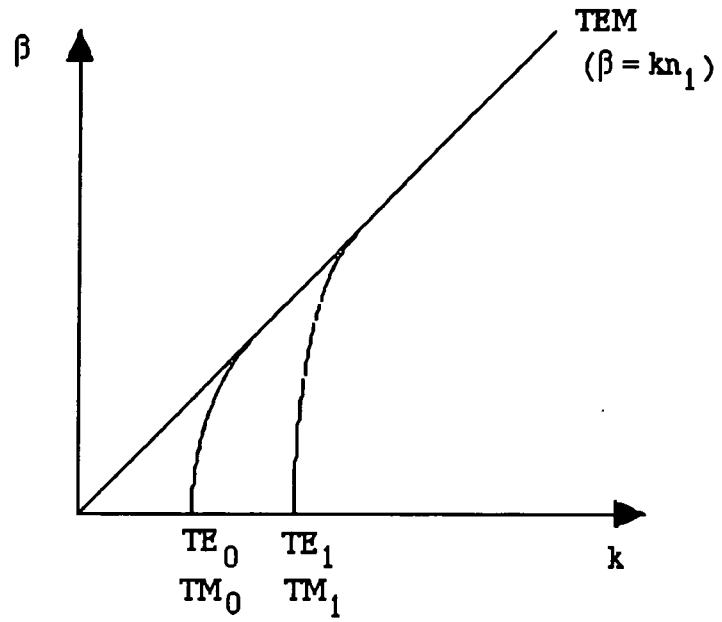

Figure (2.4) A typical β vs k plot.

In order to render the results of the above description independent of parameters such as, refractive index and guide thickness, and express them in a general form, normalised variables u, v, b are defined as :

$$u^2 = a^2(k^2n_1^2 - \beta^2)$$

$$v^2 = a^2k^2n_1^2$$

$$b = 1 - u^2/v^2$$

In general, the quantity b is a normalised propagation constant, and v is the normalised frequency. It is convenient therefore to express the result in terms of b and v :

$$b = 1 - \left(\frac{N'\pi}{2v}\right)^2$$

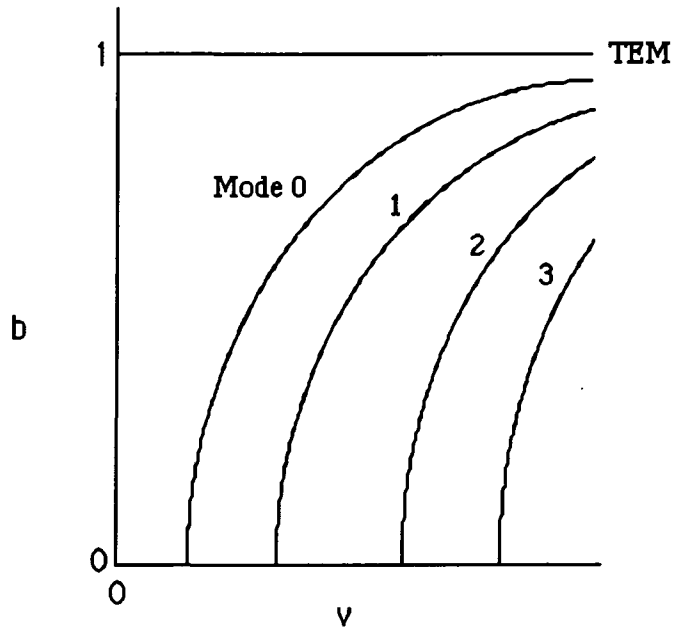

Figure (2.5) A typical plot of b vs v.

The plots of b vs v form the most general version of the numerical results of a waveguide dispersion relation (eigenvalue equation). The derivation of the eigenvalue equation was first established by Tien and Ulrich, (1970). The solution of the eigenvalue equation will yield the phase velocity and, by differentiating, the group velocity. This latter quantity may be found more directly from consideration of the Goos - Häenchen effect occurring at the waveguide boundaries [Kogelnik H. and Weber H. P., (1974)]. Here there is a lateral shift of the reflected ray with respect to the incident ray. This occurs because, if one thinks of the incident beam as composed of a set of plane waves, each elementary wave will have a slightly different angle of incidence. Since the phase change on reflection depends on the angle of incidence, the reflected beam will not be a perfect reconstitution of the incident beam at the point of incidence.

Thus associated with the reflection at the dielectric interface there is an apparent ray penetration depth. Physically this corresponds to an evanescent field in the material of lower refractive index.

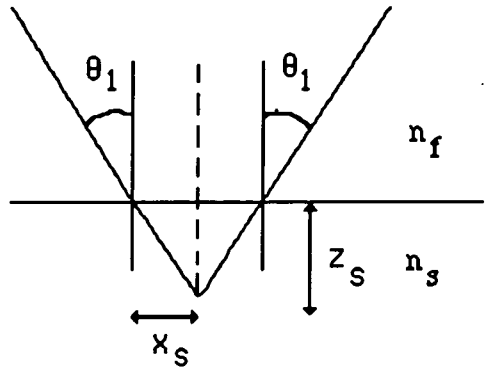

Figure (2.6) A schematic diagram showing the Goos - Häenchen shift.

To obtain a zig - zag model of the light propagation in the waveguide the Goos - Häenchen shifts at the film - substrate and film - cover interfaces [Burke, (1971)] must be taken into account. As a consequence of the ray penetration, the guide appears to have an effective thickness which is larger than the actual guide thickness and the reflected ray is shifted laterally relative to the incident ray, as shown in figure (2.6). This lateral ray shift is an important element in the understanding of the flow of energy in dielectric waveguides in terms of the ray picture. In figure (2.6) :

$$z_s = \frac{x_s}{\tan\theta_1} \qquad (2.6)$$

Thus for TE modes :

$$kx_s = \frac{\tan\theta_l}{\sqrt{N^2 - n_s^2}}$$

and for TM modes :

$$kx_s = \frac{\tan\theta_l}{\sqrt{N^2 - n_s^2}} \Big/ \left(\frac{N^2}{n_s^2} + \frac{N^2}{n_f^2} - 1 \right)$$

$N = n_f \sin\theta$ - the effective guide index.

2.2 Thin film waveguide fabrication methods.

Up until now we have considered the theoretical aspects of light propagation in waveguides. It has been shown that waveguiding is dependent on the refractive index difference between the waveguiding region and the surrounding media. A great many techniques have been established for producing the required index difference. Each method has its advantages and disadvantages. The choice of a specific technique of waveguide fabrication depends on the desired application, and on the available facilities.

Thin films for optical waveguides have certain requirements. Firstly, since, light is transmitted in the plane of the film, the material used for the waveguiding layer has to be of good optical quality and free of scattering centres. Secondly, the boundaries between the film - substrate and film - cladding should be smooth to avoid losses caused by scattering at the interfaces. The degree of *smoothness* required for negligible scattering depends upon the refractive index difference across the boundary, and the order of the mode. The film must also have no optical absorption at the wavelength of interest.

Methods used to produce waveguiding layers can be divided into two classes : those in which a layer is made by the deposition of a material on a substrate, and those in which the higher index layer is produced in the substrate itself by some chemical or physical reaction. In the first type, the index change between the guide and the substrate is discontinuous, whereas in the second type, a gradual index change occurs.

2.2.1 Reaction with dopant atoms.

2.2.1.1 Diffused dopants :

In this method dopant atoms on the surface of the substrate are diffused into the substrate, to produce a refractive index change in the substrate [Schmidt R. V. and Kaminow I. P., (1974)]. The refractive index change depends on the atoms diffused into the guide. Since diffusion must be performed below the relatively low temperatures at which glasses or polymers melt, it is a slow process.

2.2.1.2 Ion migration :

By applying an electric field to a heated glass plate, ions in the glass can be made to migrate to the negative electrode. In a sodium doped glass plate for example, a SiO_2 surface layer free of Na can be produced in this fashion. [Izawa T. and Nakagome H., (1972)] used this method to form a buried waveguide, that is one where the waveguide is created within the substrate.

2.2.1.3 Ion implantation :

When a solid is bombarded by heavy ions, these can be implanted in the solid. Due to the mechanism by which the ions lose their energy in the solid, the concentration of implanted ions in the solid has a Gaussian profile. In fused silica, the implanted ions

and the lattice displacements caused by the implantation process produces an increase in the refractive index. This method also produces buried waveguides. Implantation of substitutional dopants has also been used by [Rao E. V. K. and Moutonnet D., (1975)] to produce waveguides in CdTe, GaP and ZnTe.

2.2.2 Deposition techniques.

2.2.2.1 Sputtering :

Sputtering is the process in which atoms or molecules are removed from a solid by bombardment of atoms or ions with high energies, usually in excess of 30eV. The atoms (or molecules) removed from the surface of a target are allowed to deposit on the surface of a substrate. The slow accumulation of particles on the substrate with appreciable energy, is the reason for the good quality and durability of the sputtered films produced.

2.2.2.2 Plasma polymerisation :

If an electrical discharge is passed through a gas containing an organic compound with low molecular weight, polymerisation can occur, and, under the proper conditions, a smooth, clear, pinhole free film can be made to form on the walls and on the electrodes of the apparatus. The thickness of such films can range from 200Å to several micrometers. Using this technique [Tien, (1972)] have grown good optical waveguides.

2.2.2.3 Spinning and Dipping :

Many organic and polymeric materials can be deposited on to substrates to form waveguides using these techniques. Spinning is a technique whereby a solution of the

material required in a thin film form is put on a substrate which is then spun around on an axis normal to its surface. This has the effect of spreading the solution in a thin film over the substrate and removing any excess solution, the solvent evaporates leaving a thin film of the polymer. The viscosity of the solution and, to a lesser extent, the number of revolutions per minute are the critical factors determining the thickness of the film produced. Reasonable quality films can be produced using this method, e.g. a 20% $^{w}/_{w}$ solution of Poly-4-vinyl pyridine in butanol was spun at 2000 rpm and 1400 rpm, then baked at 165°C in a vacuum oven for 1 hour. This produced films of 2.5 μm and 2.8 μm respectively. See figures (2.7) for the interference fringes used to determine the thickness of the films.

Dipping is a technique whereby the substrate is dipped into a solution of polymer and solvent and withdrawn slowly. The sample is then usually baked under vacuum to remove any residual solvent. By varying the withdrawal velocity and the viscosity of the solution, the thickness of the film can be reasonably accurately controlled. Provided highly pure materials are used excellent quality waveguides, with very low optical losses can be fabricated. There are many advantages of this method :

a) Waveguides may be made extremely quickly.

b) This is a relatively inexpensive technique.

c) There is no need for any sophisticated equipment.

d) The technique allows the waveguide to be doped, e.g. with dyes, nonlinear optical materials, and be easily fabricated.

Figure (2.8) shows a schematic diagram of the dipper used. This was built in the workshop at Durham University. The relationship between dipping speed and the thickness of the film produced is described by Yang et al., (1980) as :

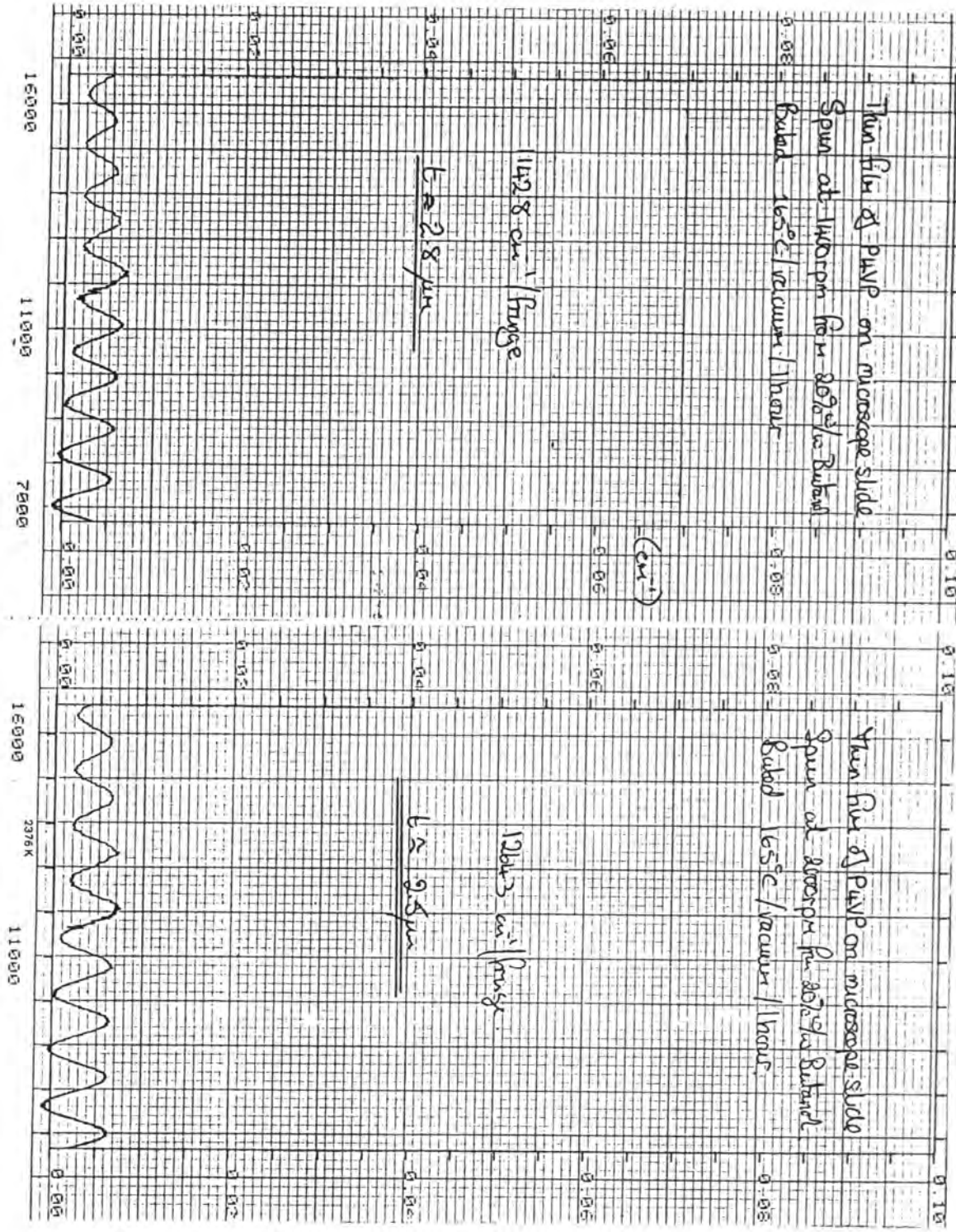

Figure (2.7) Interference fringes used to determine the thickness of the films.

$$t_p = J\xi\left(\frac{\eta-\eta_s}{\eta_0}\right)^{0.84}\left(\frac{\eta U}{g\rho_s}\right)^{0.5}$$

where :

t_p - thickness of the solid polymer coating.

J - flow rate.

ξ - ρ_S/ρ_p, ratio of the densities of the solvent and polymer.

η, η_S, $\eta_{O,}$ - viscosity of the solution, solvent and ....

U - withdrawal speed.

g - acceleration due to gravity.

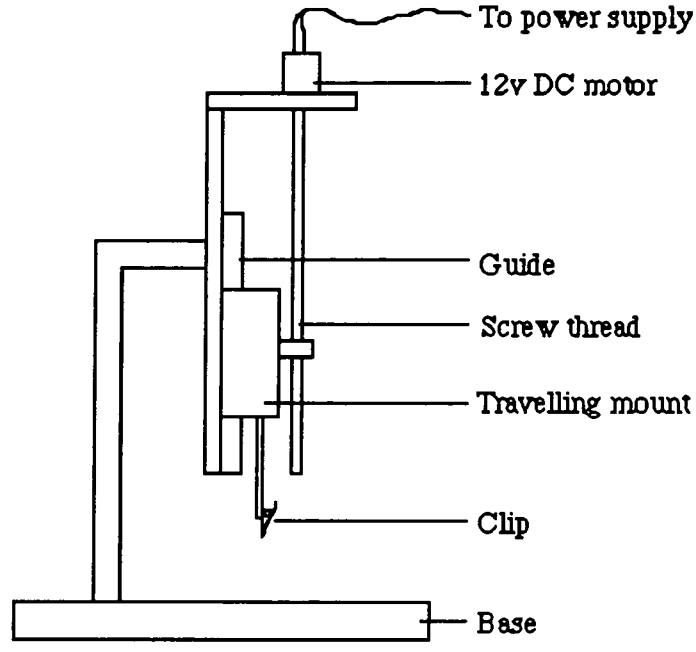

Figure (2.8) A schematic diagram of the dipper.

The thickness of the film can be measured in several different ways. A surface profiler can be used, it measures the vertical displacement of a stylus tip as it traverses across the surface of a film.

The film thickness can also be measured from the analysis of interference fringes from the film [Wells P. J., (1990)] obtained from a transmission spectrometer, where the thickness is shown to be :

$$t \approx \frac{1}{2n_f f}$$

where t - thickness of the film.

n_f - refractive index of the film.

f - separation of the interference maxima measured in wavenumbers.

The thickness can also be determined from the analysis of the synchronous angles for coupling light into a film using a prism, which will be discussed in more detail later.

2.3 Input and Output waveguide couplers.

There many ways to launch light into a waveguide. The basic aim of all couplers is to convert the energy of a light beam into a mode (or modes) which is guided by the thin film dielectric layer. There are several types of beam couplers to thin films, and generally they fall into two categories. Transverse couplers : direct focussing and end - butt, and longitudinal couplers : prism, grating and tapered.

The principal characteristics of any coupler are its efficiency and mode selectivity. Coupling efficiency is usually given as a fraction of the total power in the optical beam, which is coupled into (or out of) the waveguide. Alternatively, it may be specified in terms of a coupling loss in dB. For a mode selective coupler, efficiency can be determined independently for each mode.

The basic definition of coupling efficiency is given by :

$$\eta_m = \frac{\text{Power coupled into (or out of) the } m\text{th order mode}}{\text{Total power in optical beam prior to coupling}}$$

and coupling loss (in dB) is defined as :

$$\text{loss} = 10 \log \frac{\text{Total power in optical beam prior to coupling}}{\text{Power coupled into (or out of) the } m\text{th order mode}}$$

The coupling efficiency depends mostly on the degree of matching between the field of the optical beam and that of the waveguide mode.

2.3.1 Transverse Couplers.

2.3.1.1 Direct focussing :

This is the simplest method of coupling light into a waveguide, and is sometimes referred to as *end - fire* coupling. The transfer of beam energy to a given waveguide mode is accomplished by matching the beam field to the waveguide mode field. The coupling efficiency can be calculated from the overlap integral of the beam field and the waveguide mode field [Nakamura M. et al., (1973)]. This method is particularly useful for coupling laser beams to the fundamental waveguide mode, due to the Gaussian beam profile and the TE_0 waveguide mode shape. Also the beam diameter must be closely matched to the waveguide thickness for optimum coupling. Since film thicknesses are of the order of several micrometers, alignment is very critical. Figure (2.9) shows a schematic diagram of an end fire apparatus.

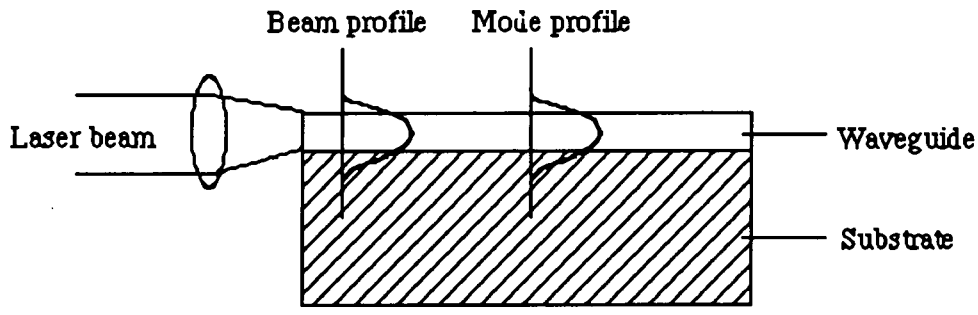

Figure (2.9) A schematic diagram of an end fire apparatus.

2.3.1.2 End - butt coupling :

This method is similar to end focussing, but involves the source in physical contact with the waveguide, and allows very efficient coupling between a semiconductor laser (or any other solid state laser) and a waveguide, since the thickness of the waveguide can be made approximately equal to the light emitting layer in the laser.

2.3.2 Longitudinal Couplers.

2.3.2.1 Prism Coupling :

A prism is clamped to the film as shown in figure (2.10). A narrow gap between the surface of the film and the base of the prism is provided by dust particles.

In order to be able to excite all the possible waveguide modes in the film, the refractive index of the prism, n_p, should be larger than that of the film, n_1. An incoming laser beam is totally reflected at the prism base and because of this a standing wave field is formed which continues below the base of the prism decreasing exponentially. The part of the wave below the base of the prism is called an evanescent field. The boundary conditions of the electromagnetic fields at the prism base require

that the fields above and below the prism base have the same horizontal component. If the horizontal component of the wavevector A_1 or B_1 equals that of the incoming wave in the prism, the wave in the prism is coupled exclusively to this waveguide mode, and the laser beam is said to be in a synchronous direction (i.e phased matched). Hence it is possible to couple the light wave to any waveguide mode by simply choosing an appropriate angle for the incoming laser beam. The excitation of a light wave into a film by the penetration of an evanescent field is known as optical tunneling.

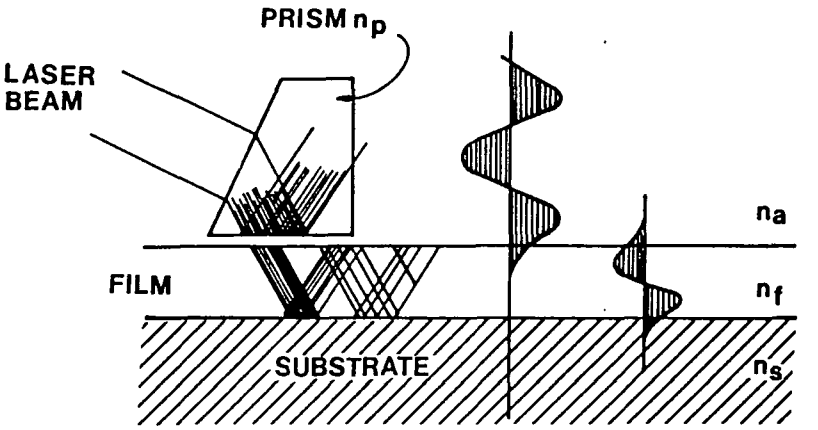

Figure (2.10) A prism clamped to a film.

As can be seen from figure (2.10) the coupling is due to the overlap, in the air gap, of the two evanescent fields from the prism and the film. Hence the size of the air gap is crucial to the coupling. Once light has been coupled in to the film it will be seen as a streak across the film. The waveguide mode is visible because of inhomogeneities in the film, which scatter light.

If another prism is clamped to the film light can be coupled out. The efficiencies of these couplers, both input and output has been calculated [Tien P. K., (1971)] and it has been shown that the optimum efficiency is 81% provided the coupling strength and intensity of the laser beam is uniformly distributed over the entire coupling length.

The condition for phase matching is derived below :

From Snell's law :-

$$\frac{\sin\alpha}{\sin\varphi} = \frac{n_a}{n_p} = \frac{1}{n_p}$$

$$\sin\alpha = \frac{\sin\varphi}{n_p}$$

so $$\alpha = \frac{\sin^{-1}(\sin\varphi)}{n_p}$$

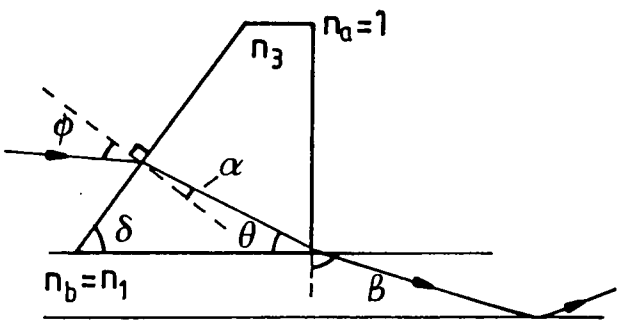

Figure (2.11) A schematic diagram of the phase matching conditions

Now the light being coupled into the film enters at an angle θ, which is :-

$$\theta = 180 - (90-\alpha) - \delta \tag{2.7}$$

As explained before, to couple to a mode, the horizontal components of the wavevectors and the incoming wave in the prism must be equal, and so the horizontal component of the refractive index is given by :

$$n_{eff} = n_p \cos\theta \tag{2.8}$$

Hence by measuring the angle φ, which is determined by aligning the prism so that the reflected beam coincides with the incident beam and rotating the prism to the mode, it is possible to determine the n_{eff} of the film, provided that the refractive index and angle of the prism are known.

For an asymmetric slab waveguide the equations used to give the effective guide thickness and the normalised frequency are [Kogelnik H. and Weber H. P., (1974)]:-

$$V\sqrt{1-b} = m\pi + \tan^{-1}\left(\sqrt{\frac{b}{1-b}}\right) + \tan^{-1}\left(\sqrt{\frac{b+a}{1-b}}\right) \tag{2.9}$$

for TE modes.

Where :

$V = kf\sqrt{n_1^2 - n_0^2}$

f - film thickness.

$k = 2\pi/\lambda$ free space wavevector.

n_1, n_0, n_2 - refractive indicies.

m - mode order (m = 0,1,2,...)

$$b = \frac{N^2 - n_0^2}{n_1^2 - n_0^2}$$ N - effective guide index = ß/k

b - known as the normalised guide index.

$$a = \frac{n_0^2 - n_2^2}{n_1^2 - n_0^2}$$ - a measure of the asymmetry.

For TM modes :

$$V\left(\frac{n_1}{n_0}\sqrt{q_0}\right)\sqrt{1-b} = m\pi + \tan^{-1}\left(\sqrt{\frac{b}{1-b}}\right) + \tan^{-1}\left(\sqrt{\frac{b+a(1-bd)}{1-b}}\right) \qquad (2.10)$$

Where :

$$b = \left(\frac{N^2 - n_0^2}{n_1^2 - n_0^2}\right)\left(\frac{n_1^2}{n_0^2 q_0}\right)$$

$$q_0 = \frac{N^2}{n_1^2} + \frac{N^2}{n_0^2} - 1$$ - reduction factor

$$a = \left(\frac{n_1}{n_2}\right)^4\left(\frac{n_0^2 - n_2^2}{n_1^2 - n_0^2}\right)$$

$$d = \left(1 - \frac{n_0^2}{n_1^2}\right)\left(1 - \frac{n_2^2}{n_1^2}\right)$$

A program was written in BASIC on an Apricot computer by [Wells P. J., (1990)] incorporating the above equations which could calculate the film thickness and index from the experimental parameters.

2.3.2.2 Grating couplers :

A grating coupler, like a prism coupler, functions to produce a phase matching between a particular waveguide mode and an unguided optical beam which is incident at an angle to the surface of the waveguide :

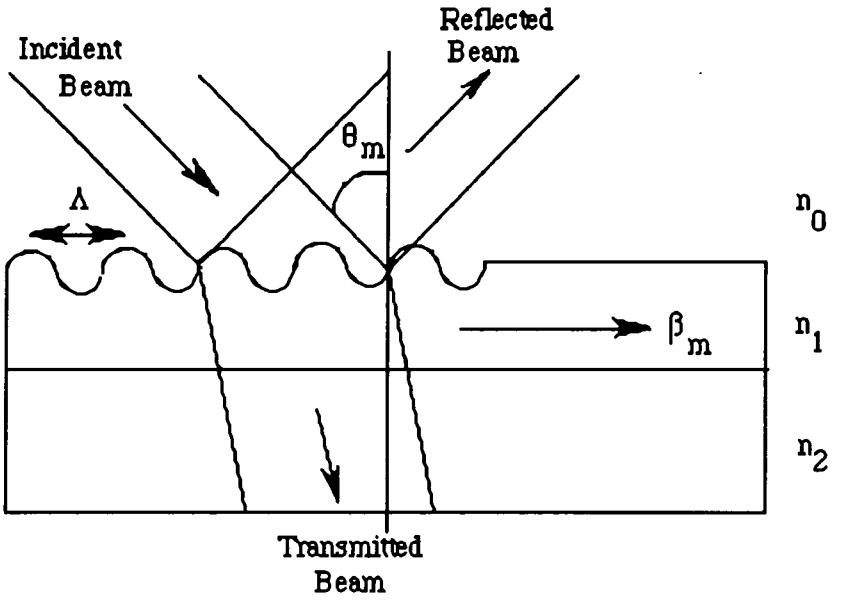

Figure (2.12) Schematic diagram of a grating coupler.

The phase matching condition which must be satisfied is given below :

$$\beta_m = kn_1\sin\theta_m = (2\pi/\lambda)n_1\sin\theta_m$$

A laser beam incident on the phase grating at an angle θ_m has a phase variation in the x direction according to $\exp\{i(2\pi/\lambda_0)(\sin\theta_m)x\}$. As the beam passes through the grating, it obtains an additional spatial phase modulation $\Delta\Phi\sin(2\pi/\Lambda)$, $\Delta\Phi$ – the amplitude of the spatial phase modulation caused by the grating and is sometimes called the phase depth of the grating ; Λ - periodicity of the grating. The light wave reaching

the top surface of the film contains many Fourier components, $\exp\{i(2\pi/\lambda_0)(\sin\theta_m + m(2\pi/\Lambda))x\}$, where m is an integer. If one of these components matches the wave motion of one of the waveguide modes of the film, the light beam is exclusively coupled to this mode and the light energy is fed into the film.

As mentioned earlier - due to its periodic nature, the grating perturbs the waveguide modes in the region underneath the grating, thus causing each one of them to have a set of spatial harmonics, with propagation constants in the x direction given by :

$$\beta_v = \beta_0 + \frac{v2\pi}{\Lambda}$$

where $v = 0, \pm1, \pm2, \ldots$, and where Λ is the periodicity of the grating. The fundamental factor β_0 is approximately equal to the β_m of the particular mode in the waveguide region not covered by the grating. The phase matching condition can be satisfied, due to the negative values of v, such that :

$$\beta_0 = kn_1\sin\theta_m \qquad \text{even though } \beta_m > kn_1$$

Since all of the spatial harmonics of each mode are coupled to form the complete surface wave field in the grating region, energy introduced from the beam into any one of the spatial harmonics is eventually coupled into the fundamental ($v = 0$) harmonic as it travels past the grating region. This fundamental harmonic is very close to, and eventually becomes, the β_m mode outside the grating region. Thus the grating region can be used to selectively transfer energy from an optical beam to a particular waveguide mode by properly choosing the angle of incidence. The grating can also be

used as an output coupler because, by its reciprocity, energy from the waveguide modes will be coupled out at specific angles θ_m, corresponding to a particular mode.

The optimum coupling efficiency of approximately 80% is theoretically possible when coupling a Gaussian beam with a grating. However, typical unblazed gratings (with symmetrical profiles) generally have efficiencies of 10 to 30%. The principal reason for this is that much of the incident energy is usually transmitted through the guide and lost in the substrate, because unlike a prism, the grating does not operate in a total internal reflection mode. By blazing the grating coupler the efficiency is greatly improved to approximately 95%.

The principal advantage of a grating coupler is that, once fabricated, it is an integral part of the waveguide structure. Hence, its coupling efficiency remains constant and is not altered appreciably by mechanical disturbances or ambient conditions. Perhaps the greatest disadvantage of the grating coupler is that it is very difficult to fabricate, requiring the use of sophisticated masking and etching techniques, as the spacing should be on the order of a wavelength.

2.3.3 Grating fabrication methods.

Many methods of fabricating a grating have been established. A few of the popular techniques will be discussed :

2.3.3.1 Ion beam milling :

Using this technique the substrate is first coated with a photoresist and exposed with an interference pattern produced by a laser. Development of the photoresist produces a relief grating, through which a grating can be milled into the substrate using a high power laser [Nakamura M. et al., (1973)].

2.3.3.2 Reactive Ion etching :

The photoresist is made in the same way as in ion milling but the grating is etched using a plasma which reacts with the surface to remove molecules.

2.3.3.3 Holographic grating :

Essentially this process involves the interference of two laser beams in the material of interest, thus producing a holographic grating. This grating could either be permanent e.g. UV laser interference pattern in a polymer [Kogelnik H. and Shank C. V., (1971)] & [Kaminow I. P. et al., (1971)] or a transient grating, i.e. the laser producing the grating is also exciting the laser action [Shank C. V. et al., (1971a)] & [Chandra S. et al., (1972)]. The grating is produced as result of the modulation of the refractive index and gain induced by the intense optical radiation.

2.3.3.4 Electron Beam Lithography :

By exposing an electron resist to the electron beam of a scanning electron microscope (SEM) it is possible to etch a high resolution grating pattern [Turner J. J. et al., (1973)].

From all of the methods outlined above the fabrication of a holographic grating offers the best prospect for tuneability, due to the fact that the angle of incidence of the two beams determines the pitch of the grating which is a critical factor in the wavelength selection. But a holographic grating is very difficult to set up in practice. Since there was access to a SEM, electron beam lithography was tried.

The electron beam in a SEM can be suitably controlled so as to pattern a grating of a pre-defined pitch on an electron sensitive material. Turner J. J. et al., (1973) have

have used Poly(methyl methacrylate), PMMA. This method was used to etch a mask which could be used many times later to define a grating in a glass substrate. A grating in a glass substrate is more permanent than a grating in a polymer, and thus can be re-used with different polymers. Figure (2.13) shows the steps involved in defining a mask.

Once the mask has been fabricated a similar procedure is used to etch a grating on a substrate. Figure (2.14) shows the steps involved.

The experiment was performed as follows : A 1000Å layer of aluminium was thermally evaporated onto a glass slide. Thin films were dipped from a solution of 1 g PMMA and 20 ml dichloromethane on to the Al layer at speeds of 5 and 10 mm/min. The films were baked in a vacuum oven for 15 minutes at 100°C, to remove any residual solvent.

The thicknesses of the films were measured using an ellipsometer. The film dipped at 5 mm/min showed to have a very irregular surface and thus was not used. This could have been due to the limitations of the dipper to be able to produce smooth films at this speed. The film dipped at 10 mm/min was much smoother and the result obtained from the ellipsometer was much more reproducible. The average thickness was 1807Å and the refractive index 1.526.

The sample was then mounted on a SEM stub and exposed to the electron beam of the SEM. The beam could be electronically controlled so as to pattern a grating. Several gratings were patterned with different parameter settings, e.g beam current, spot size, scan rate.

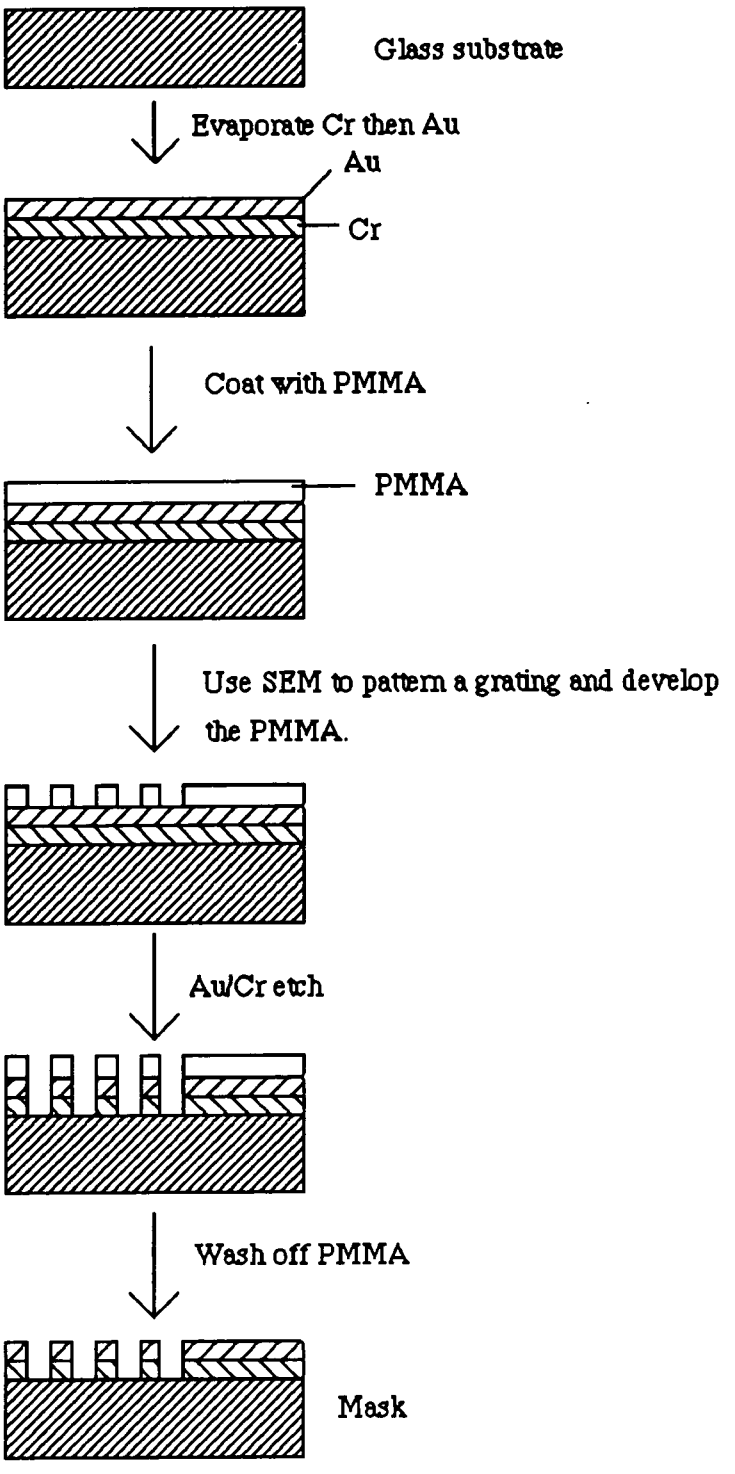

Figure (2.13) Steps involved in making a mask.

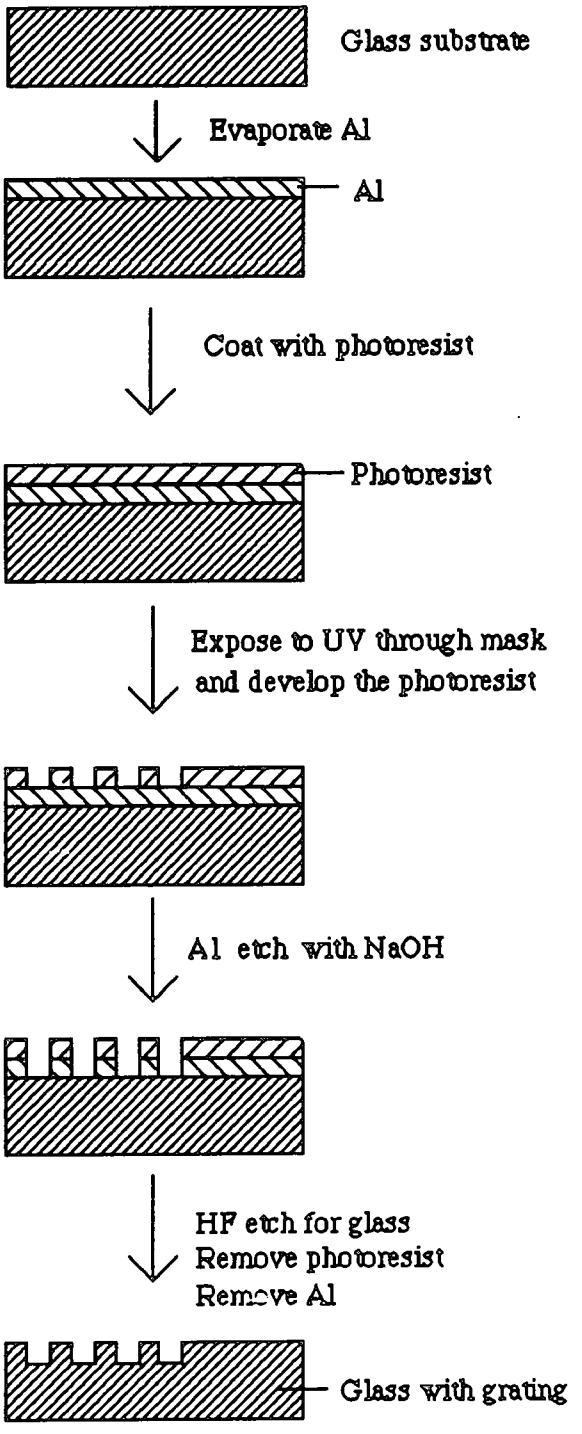

Figure (2.14) Steps involved in making a grating.

After exposure the exposed electron resist was developed with Microposer 312 for 30 seconds and then left to dry. It was then immersed in an Al etch for 2 minutes, and rinsed with water. The Al etch contained 30 parts ortho - phosphoric acid, 2 parts nitric acid and 0.7 parts water.

The developed masks were viewed under an optical phase microscope, which can pick up any surface variation and display it in contrast. Photograph (2.1) shows the best result obtained. The calibration on the photograph is 9 mm = 10 μm, from this it can be calculated that the pitch of the grating is 1.6 μm. This is a very good result for the first attempt at this method.

This result proves that this method is a good and viable one. But, however, due to the lack of SEM time available at Durham University and the inability of the SEM at Marconi to suitably electronically scan, no further gratings could be made in this fashion.

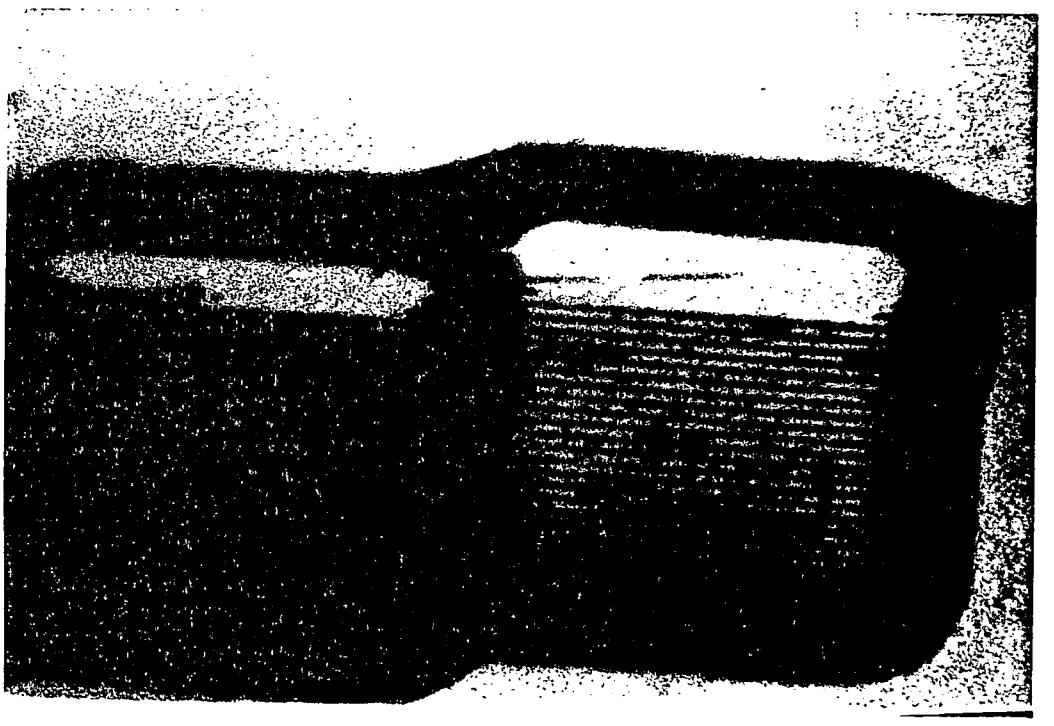

2.4 Experimental results from waveguiding in polymer films.

It is important to know the linear optical properties of polymer films when considering them as potential host materials for waveguiding.

2.4.1 Measurement of various polymer film indices.

Thin films of poly(4-vinylpyridine) (P4VP) were made using the dipping method. Linear P4VP was used as obtained from Polymer Science. This was dissolved in Isopropyl Alcohol (IPA) and microscope slides (n_S = 1.5049 at 632.8nm) were used as the substrates. The slide, after it had been cleaned with acetone and allowed to dry, was dipped into the bulk solution and withdrawn at a controlled speed. The speed at which the slide is withdrawn, as mentioned earlier, is crucial to the actual thickness of the film. It was found that the faster the withdrawal speed the thicker the film that was produced.

Once the film was cast on to the slide it was allowed to dry. The two prisms to be used were cleaned with acetone and dried. They were then carefully clamped to the film, ensuring that no scratches were made on the film. The prisms used were 60° angle prisms with a refractive index of 1.723 at 632.8nm. The right angle of the prism was positioned as close to the centre of the rotation stage as possible to prevent walk off during rotation. Whilst clamping the prism to the film a coupling spot could be observed as a silvery area on the base of the prism. This indicates good optical contact between the film and the prism.

A 10 mW Helium Neon (HeNe) laser emitting at 623.8nm was used as the light source. The system was aligned so that the laser beam refracted through the prism on to

the coupling spot. The stand was rotated until the beam was normal to the sloping face of the prism. The angle reading was set to zero, so that all subsequent readings were referenced to this point. The stage was rotated until a waveguide mode was seen as a streak across the film. Fine tuning was employed to find the position of maximum intensity. This angle was noted as a mode angle. This procedure was continued until all the modes were found.

Using equations (2.7 - 2.10), it is possible, from the incident angle of a light beam entering a waveguide mode, to calculate the refractive index of that mode, and thus the film index and the thickness averaged over the modes. The actual film thickness was measured using the interference fringes produced by the film in a spectrophotometer.

The results from an experiment to find the refractive index of P4VP films are given in table (2.1):

Mode	Vernier measurement (±5min)	mode index
normal angle	93°55	----
TE2	92°55	1.5215
TE1	90°00	1.5447
TE0	88°00	1.5598

Table (2.1) Mode indices of a P4VP film.

Film index = 1.5647 @ 632.8nm
Film thickness = 2.2μm (±0.001μm) averaged over the modes.

A second set of measurements were made on a thinner film, with a smaller number of modes as can be derived from the equation for the effective guide thickness, equation (2.7). The results for the second film are shown in table (2.2) :

mode	vernier measurement (±5min)	mode index
normal angle	94°40	----
TE1	92°15	1.5329
TE0	88°35	1.5610

Table (2.2) Mode indices of a P4VP film.

Film index = 1.5710 @ 632.8nm

Film thickness = 1.44μm (±0.001μm) averaged over the modes.

In the experiment the bulk birefringence, i.e the difference in refractive index in TE and TM modes, was zero and so all the measurements were taken in the TE mode.

Various other polymers were also characterised in the same way. The results from this investigation are summarised in table (2.3) below.

Polymer	Refractive Index. (±0.001)
PMMA	1.485
PVA	1.495
TELENE	1.524
PVC	1.539
P4VP	1.565
PC	1.578

Table (2.3) The refractive indicies of several polymers investigated.

2.4.2 Linear optical properties of oxygenated polymers

The prism coupling equipment constructed has been used to characterise the optical properties of oxygenated polymers received from the University of Namur, and their interaction with nonlinear optical moieties. The polymers received from Namur were :

a) Polyethylene glycol (Three molecular weights 100,000, 30,000 and 3,400),

b) Polyoxymethylene,

c) Polyacroleine,

d) Polypivaloctone and

e) Polycaprolactone.

These have been fully characterised by ESCA at the University of Namur and Queen Mary and Westfield College, London.

Thus the initial requirement for film fabrication is the ability to obtain a solution in a volatile solvent. Four of the polymers sent by Namur namely polyoxymethylene, polyacroleine, polypivaloloctone and polycaprolactone were insoluble. The first involved using either uncommon or hazardous solvents and for the latter three good solvents were not known. Thus these polymers were not investigated in any detail.

Solvents used	Comments
Acetone	Insoluble
Isopropyl Alcohol	Insoluble
Water	Partially soluble
Chloroform	Soluble
Cyclohexanone	Insoluble
Methanol	Soluble
Amyl Acetate	Partially soluble
Butyl Acetate	Insoluble
Trichloroethylene	Very soluble
Ethandiol	Insoluble
Diethyl Ether	Insoluble
1,1,1 Trichloroethane	Insoluble
Industrial Meths.	Soluble
Chlorobenzene	Soluble
Benzene	Soluble
Xylene	Partially soluble

Table (2.4) Solubilities of Polyethylene Glycol.

The polyethylene glycols, however, were dissolved in solvents previously used at the University of Namur, and thin films were dipped. These solutions gave films that were not optically transparent and thus were not useful for waveguiding. Thus, tests were carried out to find alternative solvents that would produce better quality films for waveguiding. Table (2.4) above shows the results of the solubilities for all three molecular weights (100,000, 30,000 and 3,400) in a variety of solvents.

Trichloroethylene was found to be the best alternative solvent, and so films were dipped for optical waveguiding. Solutions were made of 10% weight ratio of the polymer in the solvent. All the solutions were clear and viscous, except the 100,000 MW which was cloudy. Despite this the films that were produced were still not optically transparent. Thus it seems that the polyethylene glycol is not a good polymer for thin film optical waveguiding.

In order to circumvent this problem an alternative oxygenated polymer, polycarbonate-bis-phenol A was used. Various solutions of polycarbonate in the solvent dichloromethane were made, these were doped with nlo molecules e.g. 2 - Acetamido - 4 - nitro - N,N-dimethylaniline (DAN) and 4 - Methyl - ((4 - nitrophenyl)methylene) benzenamine) (NMBA), at different concentrations. Figure (2.15) shows their chemical structure. Thin films were dipped onto glass microscope slides and, using the waveguiding apparatus, the refractive index and thickness were measured using the same procedure as that outlined in section 2.4.1. Table (2.5) summarizes the results. Figures (2.16-2.19) show the modal dispersion curves for DAN and NMBA doped polycarbonate, as examples of the kind of analysis performed on the results to obtain the refractive index and thickness of the films.

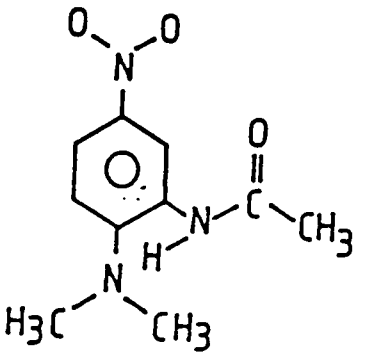

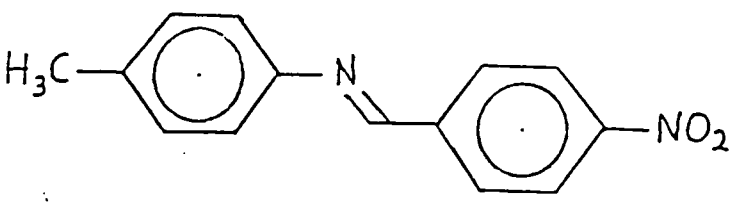

Figure (2.15) Chemical structure of DAN and NMBA.

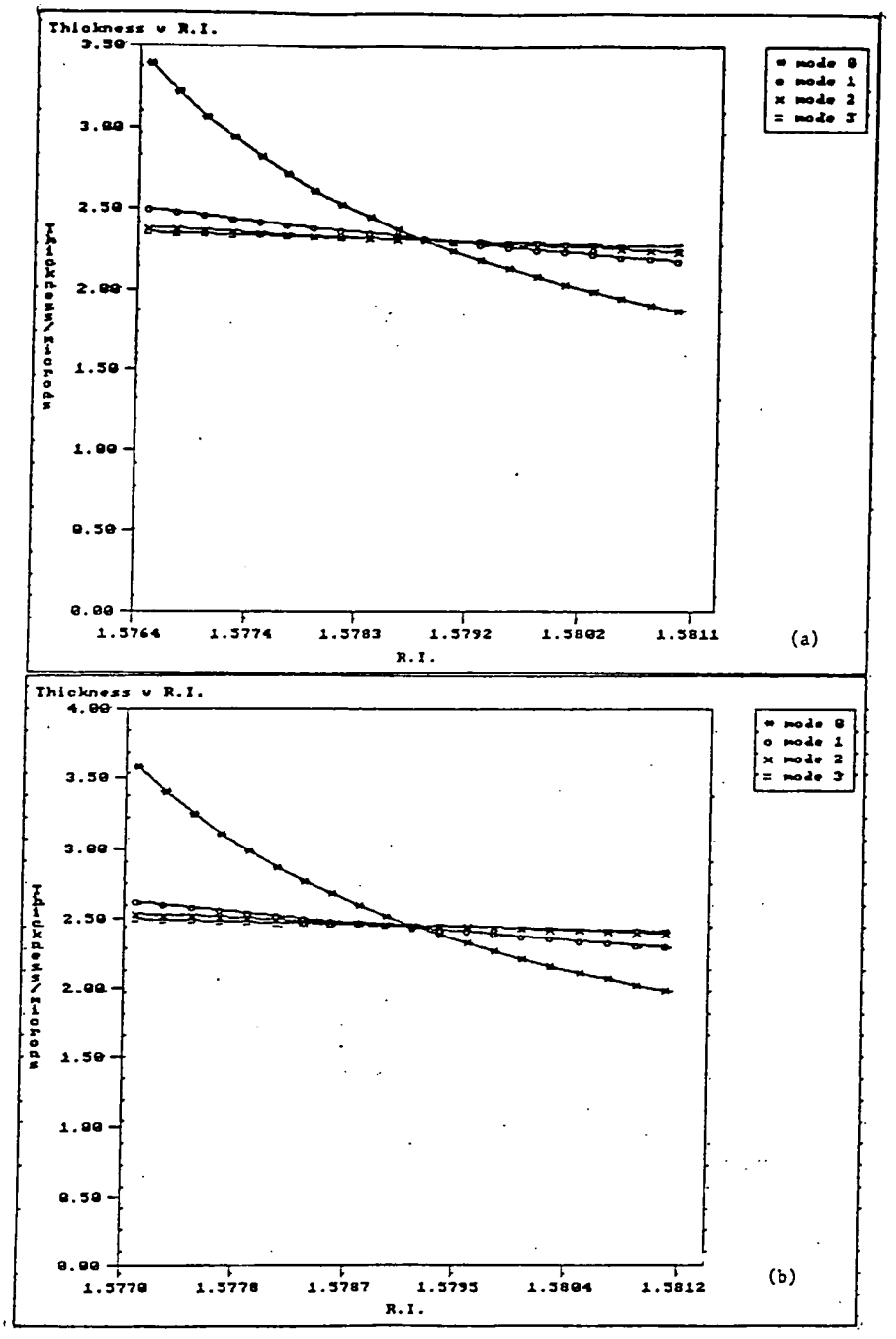

Figure (2.16) Thickness vs refractive index of DAN doped polycarbonate film. (a) 5% (b) 10%.

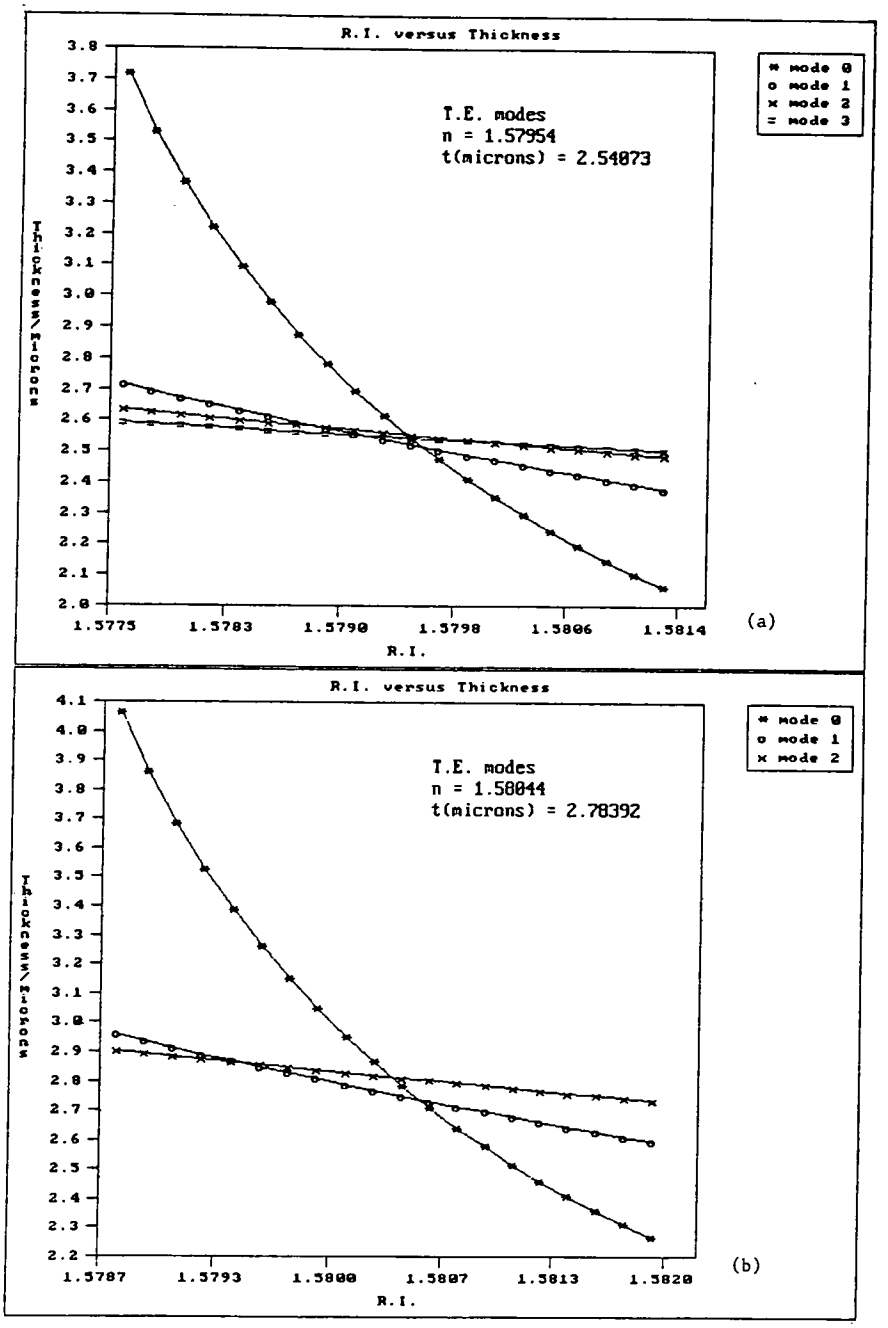

Figure (2.17) Thickness vs refractive index of DAN doped polycarbonatefilm. (a) 15% (b) 20%.

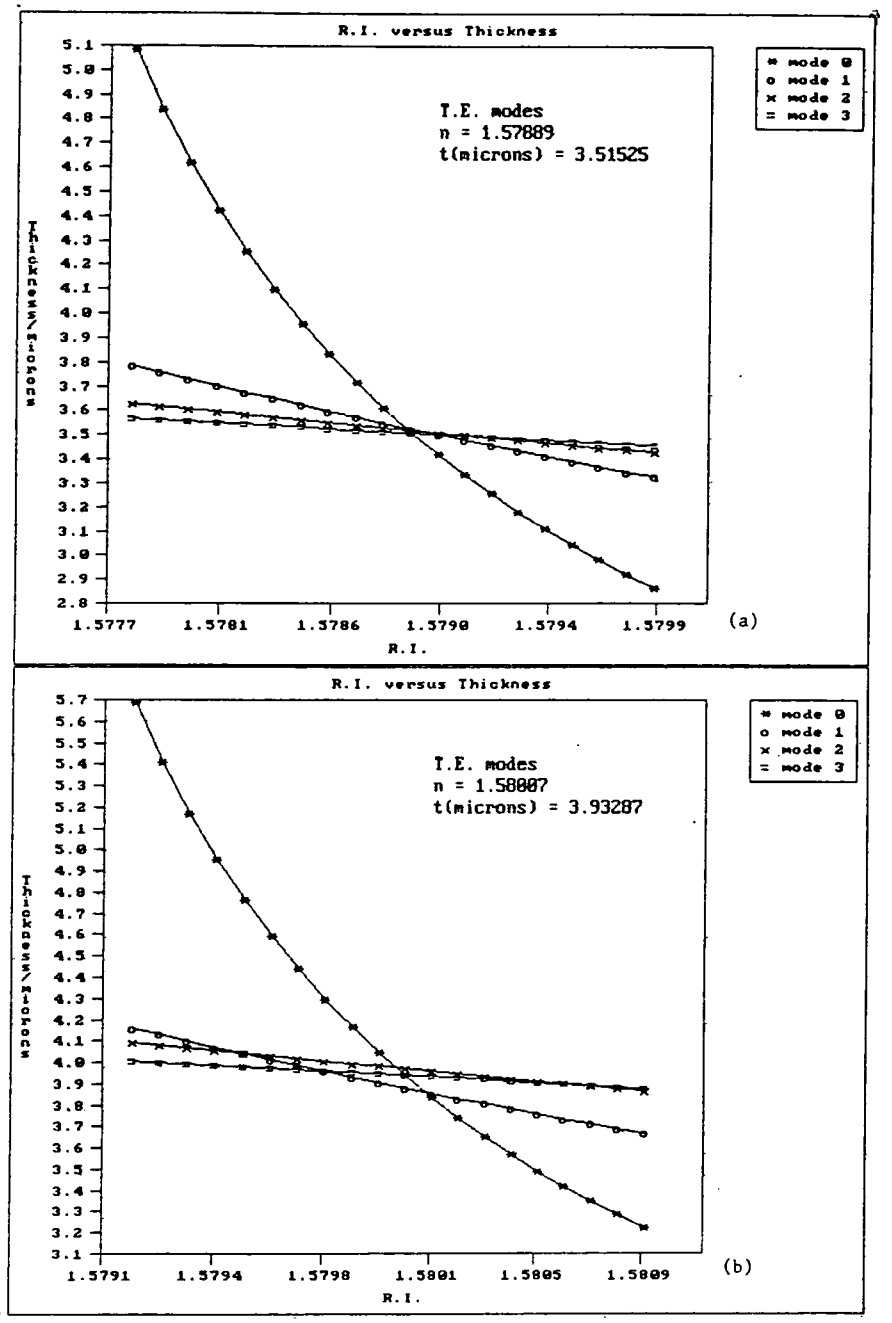

Figure (2.18) Thickness vs refractive index of NMBA doped polycarbonate film. (a) 5% (b) 10%.

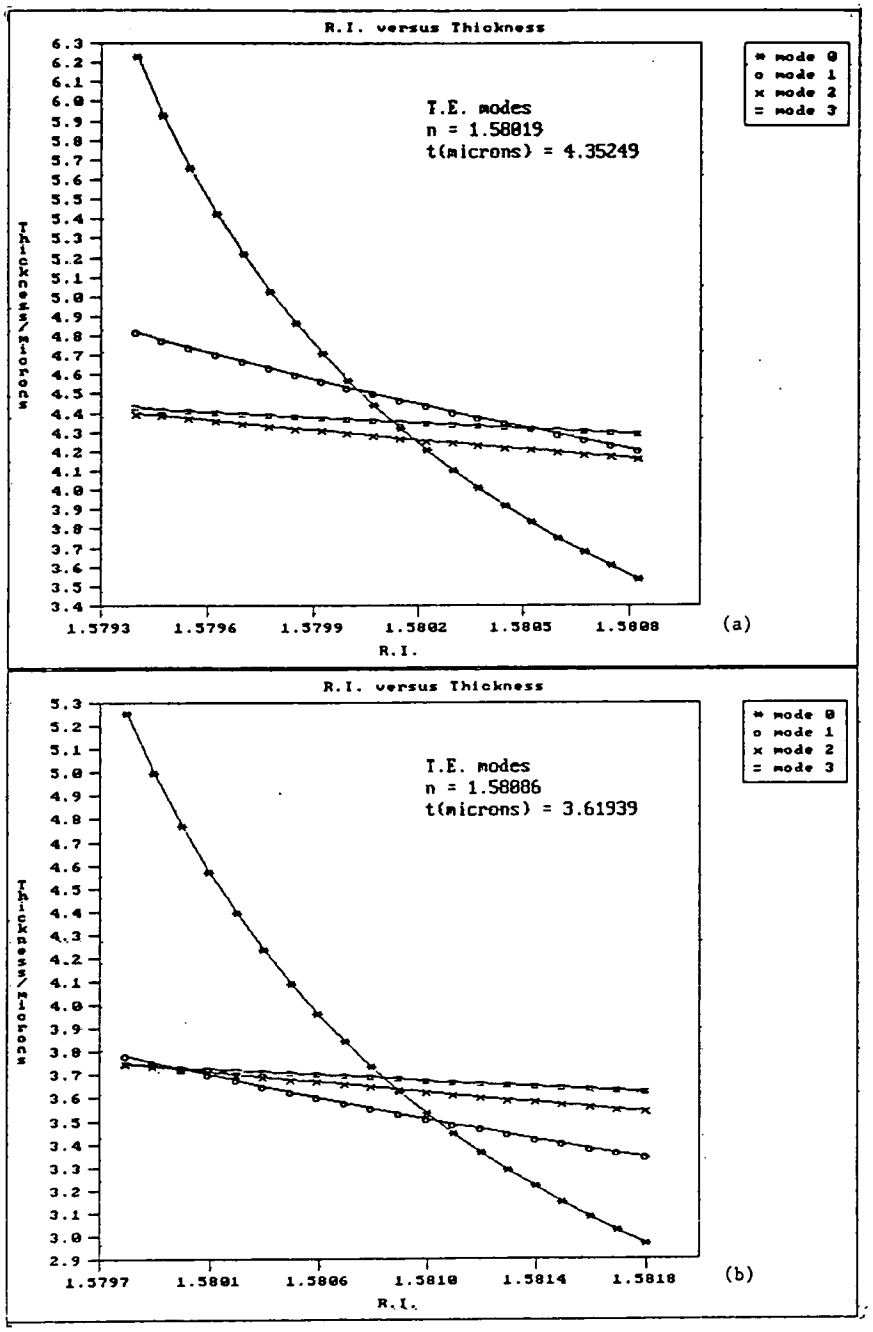

Figure (2.19) Thickness vs refractive index of NMBA doped polycarbonate film. (a) 20% (b) 30%.

NLO Doping level	Refractive Index (±0.0001)	Thickness (μm) (±0.001μm)
0 %	1.5779	2.54
5 % DAN	1.5784	2.38
10 % DAN	1.5793	2.44
15 % DAN	1.5795	2.54
20 % DAN	1.5804	2.78
5 % NMBA	1.5788	3.5
10 % NMBA	1.5800	3.9
20 % NMBA	1.5801	4.3
30 % NMBA	1.5808	3.6

Table (2.5) Results from DAN and NMBA doped polycarbonate waveguides.

These curves are generated by a computer program which calculates the effective thickness for different refractive index values of a particular mode. From these values the point of minimum deviation of these curves is determined. This point represents the film thickness and index.

Samples for further ESCA studies have been sent to the University of Namur. Compressed samples of DAN and NMBA crystals will be used to obtain reference ESCA spectra. Taken together with the ESCA spectra of the pure polymers these will enable additional features in mixed polymer - nlo compound systems to be identified. As yet I am not sure what they have determined.

The work reported in section (2.4.2) has been carried out in conjunction with research looking into guest - host interactions of various nlo doped polymer systems [Karakus Y. et al., (1991)]. Also the effect of field induced alignment (poling) of these

nlo moieties in the polymer matrix on the nonlinear effect has been monitored. It has been shown that highly doped polymers can be poled efficiently, but exhibit poor stability compared to the side chain polymers.

2.5 Conclusion.

The whole object of this exercise was to become familiar with the fundamentals of waveguiding, and the techniques of processing the materials, forming the thin films with sufficient quality to be able to waveguide, and the different preparation techniques which have been outlined. Also using prism coupling as a means of introducing light into a waveguide, it has been shown that specific modes could be selected. Other coupling techniques were also discussed. With these methods it was possible to characterise the linear optical properties of polymeric thin films, and hence determine the suitability of certain polymers for waveguiding purposes. This form of characterisation provides a good screening process for potential polymers and a reliable guide as to the performance of polymers.

2.6 References.

Born M. and Wolf E., Principles of optics., New York, Pergamon, (1970).

Burke J. J., Opt. Sci. Newslett, Vol 5, No 31, (Univ. Arizona), (1971).

Chandra S., Takeuchi N. and Hartmann S. R.,"Prism-dye laser.", Appl. Phys. Lett., Vol 21, No 4, pp 144-146, (1972).

Izawa T. and Nakagome H.,"Optical waveguide formed by electrically induced migration of ions in glass plates.", Appl. Phys. Lett., Vol 21, pp 584-586, (1972).

Kaminow I. P., Weber H. P. and Chandross E. A.,"Poly(methyl methacrylate) dye laser with internal diffraction grating resonator.", Appl. Phys. Lett., Vol 18, No 11, pp 497-499, (1971).

Karakus Y., Bloor D. and Cross G.H.,"Electro-optics in moderately doped thermopoled waveguides.", Proc. 7th International Symposium on Electrets, Berlin, (1991).

Kogelnik H. and Shank C. V.,"Stimulated emission in a periodic structure.", Appl. Phys. Lett., Vol 18, No 4, pp 152-154, (1971).

Kogelnik H. and Weber H. P.,"Rays, stored energy, and power flow in dielectric waveguides.", J. Opt. Soc. Am., Vol 64, pp 174-185, (1974).

Nakamura M., Yariv A., Yen H. W., Somekh S. and Garvin H. L.,"Optically pumped GaAs surface laser with corrugation feedback.", Appl. Phys. Lett., Vol 22, No 10, pp 515-516, (1973).

Rao E. V. K. and Moutonnet D.,"Buried optical waveguides in fused silica by high energy oxygen implantation.", J. Appl. Phys., Vol 46, pp 955-957, (1975).

Schmidt R. V. and Kaminow I. P.,"Metal diffused optical waveguides in $LiNbO_3$", Appl. Phys. Lett., Vol 25, pp 458-460, (1974).

Shank C. V. , Bjorkholm J. E. and Kogelnik H.,"Tunable distributed-feedback dye laser.", Appl. Phys. Lett., Vol 18, No 9, pp 395-396, (1971a).

Tien P. K.,"Light waves in thin films and integrated optics.", Appl. Opt., Vol 10, No 11, pp 2395-2413, (1971).

Tien P. K., Appl. Opt., Vol 11, p 637, (1972).

Tien P. K. and Ulrich R.,"Theory of prism-film coupler and thin-film light guides.", J. Opt. Soc. Am., Vol 60, No 10, pp 1325-1337, (1970).

Turner J. J., Chen B., Yang L., Ballantyne J. M. and Tang C. L.,"Gratings for integrated optics fabricated by electron microscope.", Appl. Phys. Lett., Vol 23, No 6, pp 333-334, (1973).

Wells P. J., Linear and nonlinear optical properties of poly(4-vinylpyridine) waveguides., PhD Thesis, University of London, (1990).

Yang C. C., Josefowicz J. Y. and Alexandru L.,"Deposition of ultrathin films by a withdrawal method.", Thin solid films, Vol 74, pp 117-127, (1980).

CHAPTER 3.

Absorption and Fluorescence of dye doped polymers.

3.1 Introduction.

Dye lasers have become an indispensable instrument in any spectroscopy or photochemistry laboratory. Many efforts are being made in studies aimed to improve dye lasers' efficiency and to extend their spectral range of operation.

An important component in any laser is the amplifying medium which in a dye laser is the organic dye. The development of the dye laser has been closely tied with the search for new and better dyes. The dye rhodamine 6G (R-6G) is probably the most widely employed laser dye at present. Previous dyes have been found by screening commercially available chemicals. In a survey [Gregg D. W. and Thomas S. J., (1969)] of approximately one thousand commercial dyes only four were shown to be useful. This statistic underlines the special requirements which must be met by such dyes.

Recently a series of dyes have been developed by BASF called Lumogen®F. The product line consists of four dyes developed for solar light conversion. But other applications outlined are solar engineering by fitting solar cells at the edges of fluorescence collectors, indirect illumination, markers and warning devices, photoconductors for technical instruments. Also they can be used for signs, plotters and substitutes for neon tubes. These dyes were developed for their ;

1) Great stability to light in plastics.

2) Strong luminosity.

3) Extremely high chroma.

4) Easy incorporation into plastics.

5) High heat stability.

6) Good fastness to weathering.

Thus this series of dyes are excellent candidates for further investigation as dye laser media. Reisfeld et al, (1989) have shown lasing behaviour in one of the dyes O240 in a sol gel and in solution. Thus this dye and the R300 were considered as a possible pair for energy transfer. The molecular structures of all the dyes used are shown in the appendix

Energy transfer between dyes is being studied as an alternative mechanism of efficiently exciting the dye of interest, and also a means of extending the tunable range of a dye laser. For energy transfer to take place a donor dye is required to absorb the pump radiation and transfer it to the acceptor dye. A more detailed discussion of the mechanism will be given in section (3.5). The efficiency of this process is largely dependent on the degree of spectral overlap of the fluorescence spectrum of the donor dye and the absorption spectrum of the acceptor dye. The fluorescence properties of a mixed dye system are affected by this process since, via energy transfer, fluorescence of the acceptor is observed to dominate, this is explained in section (3.5.2).

The main aim of this chapter is to present the results from the full characterisation of the absorption and fluorescence spectra of the various dyes and dye mixtures, that are of interest in the fabrication of solid thin film energy transfer dye lasers.

The results from the studies of the fluorescence lifetime measurements, of the dyes, and a detailed description of the energy transfer mechanism, will be given in the next chapter.

Compounds with conjugated double bonds absorb light at wavelengths above 200nm. All dyes in the proper sense of the word, meaning compounds having a high absorption in the visible part of the spectrum, possess several conjugated double bonds. The basic mechanism of absorption of light by dyes is the same in whatever part of the spectrum they have their longest wavelength absorption band, and will be discussed in detail in section (3.2).

Dyes are useful as laser active media [Pavlopoulos T. G. et al., (1989)], [Fletcher A. N. et al., (1987)] using their natural radiative deactivation pathways, in particular fluorescence, which will be discussed in section (3.3). Fluorescence studies of dyes are important since, in general, most dye lasers utilise the fluorescence properties of a dye since this transition will yield a high amplification factor, even at low dye concentrations. Whereas in phosphorescence, due to the strongly forbidden transition between the triplet state and the ground state, a very high concentration of the dye is necessary to obtain an amplification factor large enough to overcome the inevitable cavity losses, in fact this concentration would be higher than the solubility of the dyes in most solvents.

3.1.1 Dye lasers.

Dye lasers are generally either laser pumped or flashlamp pumped. The laser pumping configurations are summarised below, since these are more relevant to this work.

A very simple configuration for a dye laser used in many early investigations consists of a square cuvette filled with the dye solution, which is excited with a laser beam. The resonating cavity is formed by the two polished sides of the cuvette. Reflective coatings on the sides consisting of metallic or multiple dielectric layers enhance the efficiency of the cavity. In the pumping arrangement shown in figure (3.1) the population inversion in the dye solution is nonuniform along the pump laser beam, since the pump beam is attenuated in the solution.

A similar transverse arrangement, often used for nitrogen laser pumped dye lasers, involves focussing the laser beam, using a cylindrical lens, in to a line that coincides with the axis of a quartz capillary of inside diameter ≈1mm. The transmitted pump radiation is reflected back by an aluminium coating at the back surface of the capillary tube. The end faces of the tube can be either normal to the axis and act directly as cavity mirrors, or be set at the Brewster angle for use with external mirrors.

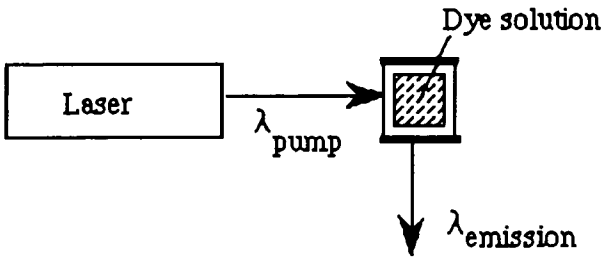

Figure (3.1) Simple transverse dye laser pumping arrangement.

A much better configuration for laser pumped dye lasers is the longitudinal arrangement, as shown in figure (3.2).

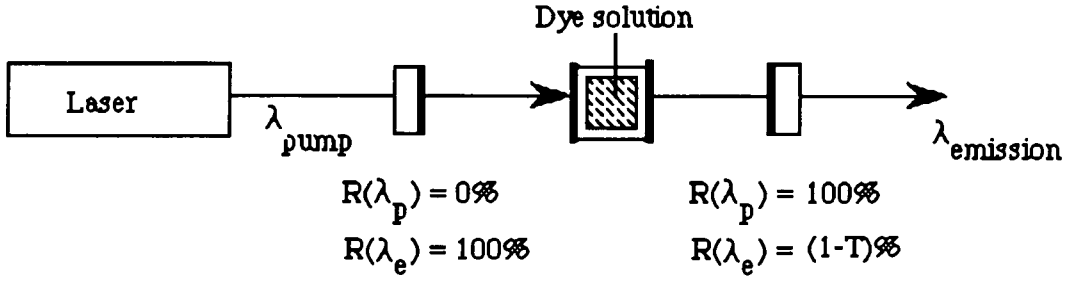

Figure (3.2) Longitudinal dye laser pumping arrangement.

In this arrangement the pump beam passes through one of the cavity mirrors of the dye laser. For an enhanced effect this is coated by a dielectric multilayer mirror with a very low reflection coefficient at the pump wavelength and a high one at the lasing wavelength.

In commercial dye lasers, where a solution of the dye is used, most of the light is absorbed in a thin outer layer of the dye solution, resulting in a non-uniform intensity laser beam. Therefore high concentrations can only be used in slab waveguide lasers, where a transverse pumping arrangement is used. The practical limit of the dye concentration is given by the fluorescence quenching effect, which reduces the fluorescence quantum yield because of the reabsorption of the fluorescence and dimerisation effects [Urisu T. and Kajiyama K., (1976)]. Thus concentration dependences on absorption and fluorescence in thin polymer films were studied, and the results are presented in section (3.4).

The techniques described above employ cells for the containment of liquid dye solutions, but even simpler arrangements are possible with solid solutions of dyes or dye crystals. Solid state dye lasers have been studied quite extensively [Muto S. et al., (1987b)], due to the number of potential advantages over liquid dye lasers. Some of these advantages have been listed below :

1) Solid state dye lasers utilise the waveguiding properties of thin dielectric films, and thus interfacing to thin film waveguides is made easier.

2) Compact size.

3) Ease of maintenance.

4) Low transmission losses.

5) Ease of fabrication.

6) High laser damage resistance of polymer matrix.

7) High dye loadings can be obtained without impairing the dye's performance.

There has been a vast amount of research in the field of dye loaded polymers investigating all facets of the photochemical and photophysical properties of the dyes and of the systems as a whole.

The photophysics and photochemistry of xanthene dyes, such as Rose Bengal and Erythrosin B, doped into various polymers have been investigated [Kamat P. V. and Fox M. A., (1984)]. Efficient dye laser waveguides have been fabricated, [Gromov D. A. et al., (1985)], from these systems. Also the refractive index change of a polymer film doped with a dye has been used to fabricate waveguides [Okamoto N. and Tashiro S., (1988)]. Rhodamine 6G has been thermally doped into a polyurethane optical solid state circuit [Matsuda A. and Iizima S., (1977)] and, by self interfering a nitrogen laser in the polyurethane to produce a periodic corrugation of the refractive index, a laser waveguide system was constructed.

As well as thin film dye lasers, dye doped polymer thin films have been used for optical phase conjugation [Egami C. et al., (1990)], third order nonlinear optics [Kuzyk M. G. and Dirk C. W., (1989)], electro-optics [Knabke G. et al., (1989)], breathing monitors [Muto S. et al., (1990)] and thin film energy transfer dye lasers [Muto S. et al., (1987a)]. The latter will be discussed in detail in section (3.5).

Alternatively dyes have also been incorporated into a matrix of silica gel [Salin F. et al., (1989)], [McKiernan J. M. et al., (1990)], and have been shown to have excellent laser efficiencies [Altman J. C. et al., (1991)], [Avnir D. et al., (1984)] with enhanced stabilities [Reisfeld R. et al., (1989)] and allow high dye concentrations [Tanaka H. et al., (1989)] without dye aggregation. The advantages of using inorganic glasses as hosts for organic dyes have been outlined by [Avnir D. et al., (1984)].

In spite of the advantages of solid state dye lasers listed above, there are some problems which prevent their practical application e.g. a notable optical degradation, a small output power and a limited range of optical wavelengths for a given dye. A method used for addressing the second of these problems and increasing the efficiency of dye lasers is energy transfer.

3.2 Absorption.

When a photon interacts with a molecule it may be absorbed, raising the molecule from its ground state to an excited state. For absorption to occur, two conditions must be satisfied. First, the energy of the photon must correspond to the energy difference between the two states. Consider a transition from a lower level whose energy is E_1 to a higher level whose energy is E_2. Then for a transition to occur the incoming photon must possess energy that corresponds to :

$$h\nu = E_2 - E_1$$

where h - Planck's constant and ν - frequency of the photon.

Second, there must be a specific interaction between the electric component of the incident radiation and the chromophore which results in a change in the dipole moment of the molecule during the transition. This can be characterised by a transition moment integral which must be non-zero.

When an electronic transition occurs within a molecule there is a large change of energy, which changes the electrostatic forces operating on the nuclei. The molecule responds to the change of forces by vibration. Thus each electronic transition is accompanied by a vibrational transition. The vibrational transitions are themselves further accompanied by rotational transitions. The vibrational and rotational transitions can be detected as fine structure in the absorption spectra of gaseous samples. But in liquid or solid samples the transitions merge together and result in a broad absorption band. The transition from the ground to the excited state via light absorption is fast (10^{-15} s) compared to the period of vibration of most molecules. So that during the absorption process the nuclei do not change their relative positions appreciably, and the dye molecule finds itself in a non-equilibrium Franck - Condon state, which is excited electronically and vibrationally, and relaxes to an excited equilibrium state within 10^{-13} - 10^{-11} s.

The exact wavelengths at which absorption occurs within a particular region are related to the structure of the molecule. A graph showing the amount of light absorbed by a substance at various wavelengths is called an *absorption spectrum*, and gives valuable information about structure.

The final intensity of light I_f, as it passes through a material of thickness l cm, with incident intensity I_i, which contains an absorbing species at a concentration of C mol litre^{-1}, can be expressed as the Beer - Lambert law :

$$I_f = I_i 10^{-\varepsilon C l} \qquad \text{or} \qquad \log\left(\frac{I_f}{I_i}\right) = -\varepsilon C l$$

Here ε is the molar extinction coefficient in units of litre mol^{-1}cm^{-1} (which is equal to $\alpha/2.303$, α - absorption coefficient), and is a measure of the probability that a particular molecule will absorb a quantum of light during its interaction with a photon. The product $\varepsilon C l$ is called the *absorbance* , A, of the sample.

The energy states that a molecule may have are characterised by the set of solutions to the Schrödinger equation. Exact solutions to the Schrödinger equation are extremely difficult to obtain, thus for large molecules it is customary to invoke the Born-Oppenheimer approximation, which is :

$$\Psi \approx \phi(\text{orbit})\chi(\text{vibration})S(\text{spin})$$

where ϕ is the electronic part of the complete wavefunction, χ is the nuclear wavefunction, and S is the spin wavefunction. This allows one to separate the transition moment integral into separate orbital, vibrational and spin components. Thus certain selection rules can be derived to predict whether the electronic transition is allowed or forbidden. These rules can be summarised as follows :

Symmetry : Transition is symmetry forbidden when the product of the symmetry portions of these functions produces an integral which is an odd function of its spatial coordinates since this results in a vanishing small transition moment integral.

Overlap : Transitions are said to be overlap, or spatially, forbidden when the two orbitals involved in the transition do not simultaneously possess large in-phase amplitudes in the same region of space.

Spin : The transition moment integral will also vanish if the spin multiplicity is not conserved during the electronic transition.

After absorption of a photon of the appropriate energy by a molecule, the energy of the molecule is raised to an excited state from which a photochemical, or any one of a number of photophysical, processes may take place.

There are four types of relaxation processes which an excited state may undergo. These are :

(i) Emission of light, i.e. a radiative transition.

(ii) A radiationless transition between two states without chemical reaction.

(iii) Electronic excitation energy transfer.

(iv) Chemical reaction.

Figure (3.3) shows the energy levels of molecular excited states and the tansitions between them. The vertical straight lines represent radiative transitions, wavy lines non-radiative transitions. The orbital arrangements and spin orientations are indicated by the boxes and arrows.

The two main excited state processes that are of interest to this research as mentioned before are fluorescence and non-radiative energy transfer. Both mechanisms will be explained in detail in sections (3.3) and (3.5).

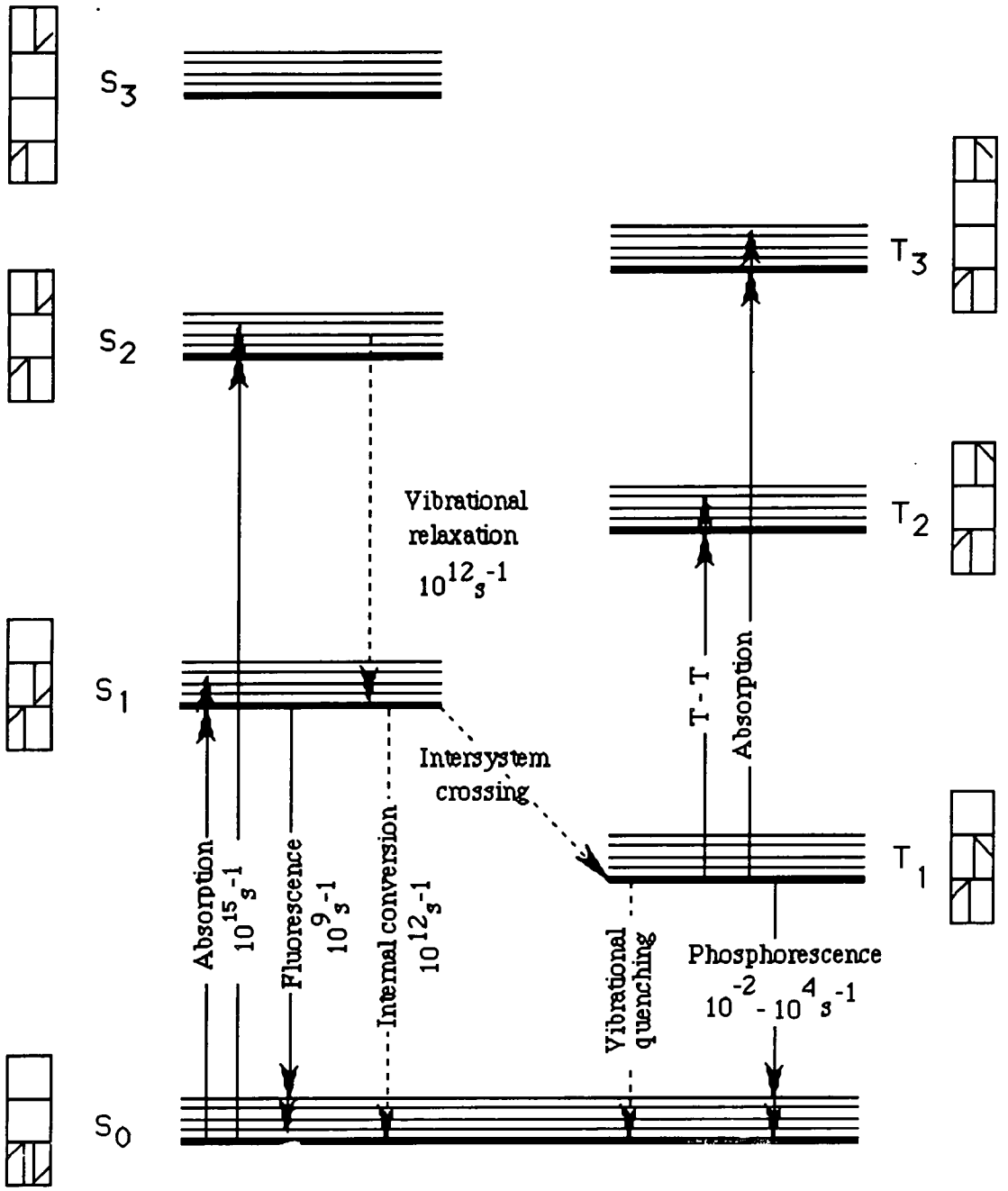

Figure (3.3) Energy levels of molecular excited states and the transitions between them.

3.3 Fluorescence.

Fluorescence is defined as the radiative transition between states of identical multiplicity. In the excited state the molecule is subjected to interactions with its environment, e.g. solvent, neighbouring molecules and lattice vibrations, and its thermal energy is discarded to the environment. These interactions cause a rapid vibrational relaxation and internal conversion in the solid or liquid state which enables the emission to take place usually from the lowest vibrational level of the first excited singlet state to the ground state. The downward transition occurs vertically, in accord with the Franck - Condon principle, and a series of lines appear as the fluorescence spectrum. The consequence of this is that the longest absorbed and shortest emitted wavelength maximum usually corresponds to the 0 - 0 transition, i.e. between the lowest vibrational levels of both electronic states. A mirror image relationship then usually exists between absorption and emission spectra. This can be seen clearly in figure (3.4) which shows the absorption and fluorescence spectra of Rhodamine 6G (R - 6G). The vibrational structure of the fluorescence spectrum is characteristic of the lower electronic state, in contrast to the structure of the absorption spectrum, and so this is a valuable method for studying vibrational characteristics of the ground state.

Further complications of dye spectra arise from temperature and concentration dependence (section (3.4)) and acid-base equilibria, for ionic dyes, with the solvent. If the temperature of a dye system is increased, higher vibrational levels of the ground state can be populated according to the Boltzmann distribution, and hence more transitions can occur from these to higher sublevels of the first excited singlet state. Consequently, the absorption spectrum becomes broader, while cooling of the system reduces the width of the absorption band and enhances the vibrational fine structure.

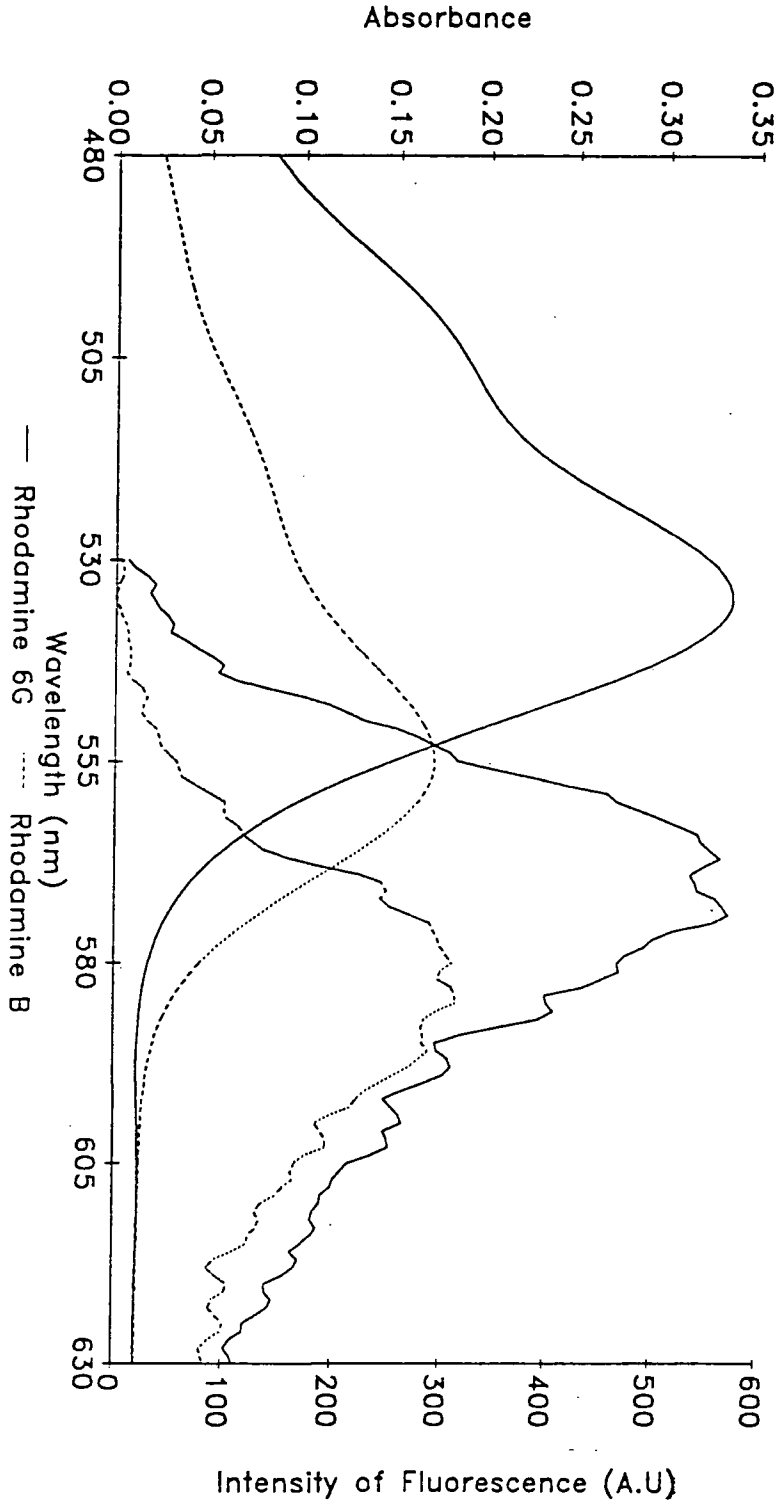

Figure (3.4) Absorption and fluorescence spectra of rhodamine 6G and rhodamine B.

3.4 Concentration effects of dyes in polymer thin films.

3.4.1 Introduction.

The concentration dependence of dye spectra is most pronounced in solutions where the solvent consists of small highly polar molecules. The spectral differences between the monomer and the dimer can be easily demonstrated. Figure (3.5) shows schematically the two main electronic energy levels of two distant dye molecules, and the splitting of the degenerate levels if they come close enough together to form a dimer.

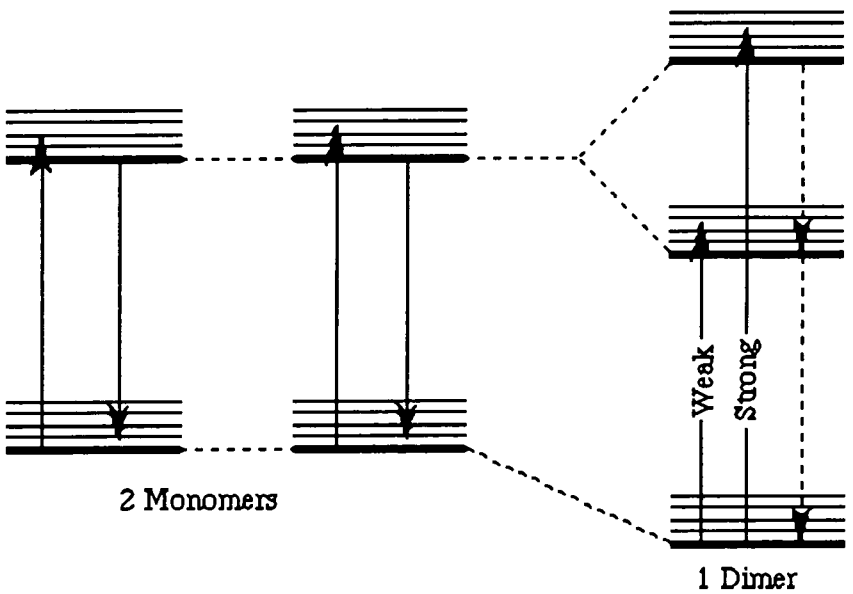

Figure (3.5) Two main electronic energy levels of two dye molecules and a dimer.

Two transitions are possible, which have different transition moments depending on the wavefunctions of the dimer. Generally the long wavelength transition has a smaller moment and so only one absorption band of the dimer is seen, lying on the short wavelength side of the monomer. This has important consequences for the

fluorescence. Since a small transition moment is coupled to a long lifetime of the excited state, these dimers would show a very slow decay of the fluorescence. This, however, makes them susceptible to quenching processes such as thermal relaxation, and in most cases the fluorescence of the dimers is completely quenched and cannot be observed.

There are several ways in which dimers can be avoided. One is to use a less polar solvent, like alcohol or chloroform. Another possibility is to add a detergent to the aqueous dye solution, which then forms micelles that contain one dye molecule each. Another, also, is to reduce the concentration of the dye molecules present.

3.4.2 Experiments and results.

The effect of the concentration of a dye in a thin polymer film, on the absorption and fluorescence properties of the system was investigated. This was done as a study to determine the optimum dye concentration before quenching effects begin to dominate.

The absorption and fluorescence properties of R-6G (Kodak) were characterised by doping the dye into a polymer, poly 4-vinyl pyridine (P4VP) (Polysciences), and dipping thin films onto glass microscope slides. All the materials were used as received from suppliers, without further purification. The effect of the concentration of the dye on the fluorescence and absorption was measured. Solutions of P4VP doped with R-6G in Iso propyl alcohol were made with different weight percentages of dye. The concentrations used were 1, 2, 5, 10, 15 and 30% (labelled 1 - 6 respectively). Table (3.1) shows the quantities of dye used, the amount of P4VP used was kept constant at 3.78 g.

Using a Perkin Elmer Lambda 9 spectrophotometer, absorption measurements, which were normalised for thickness, were recorded for each concentration, as shown in figure (3.6).

Solution	$\%^{w}/_{w}$ dye	wt of dye (g) (±0.0001 g)
1	1	0.038
2	2	0.077
3	5	0.198
4	10	0.378
5	15	0.567
6	30	1.134

Table (3.1) Quantities of rhodamine 6G used.

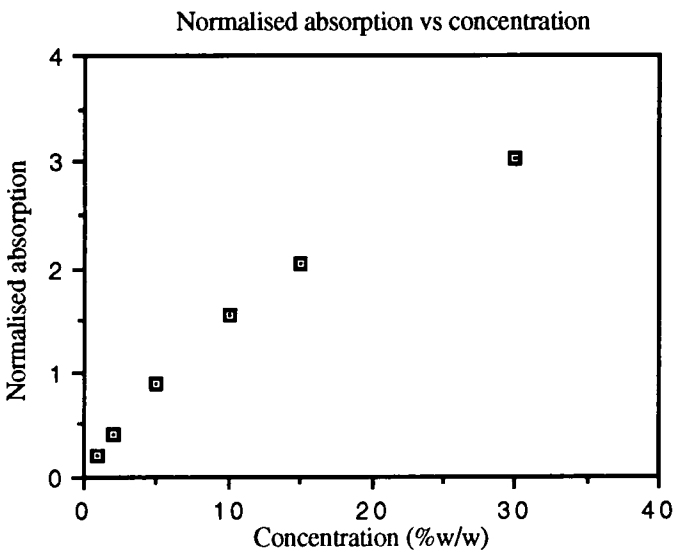

Figure (3.6) Peak absorption vs Concentration of Rhodamine 6G in a polymer thin film.

From this graph a nonlinear response is observed, attributable to the dimer formation which is seen in the spectra. This suggests, as would be expected, that concentration is important to the absorptive properties of the dye in the polymer. It is clear therefore that if the dye and polymer are to be used efficiently, the relatively low concentrations must be used, i.e. in the linear portion of the curve. From the absorption profiles, shown in figure (3.7), it can be seen that they change gradually from one peak with a shoulder to two distinct peaks, with increasing concentration. This is due to the formation of dye pairs at the high concentrations.

The fluorescence of a molecule may be quenched at high dye concentrations, so it is necessary to determine which concentration gives the maximum fluorescence. Fluorescence spectra were measured at the Royal Institution, London using a Perkin Elmer Lambda 5 Fluorimeter. The experiment required pumping the dye doped polymer film with a fixed wavelength and observing the fluorescence intensity over a range of wavelengths. The excitation wavelength chosen was 540nm which is where the absorption maxima of R-6G lies. The experimental setup was fairly simple, the surface was irradiated with a beam at the pump wavelength and the fluorescence spectra was measured emission. Figure (3.8) shows the fluorescence intensity spectra obtained. A graph of the peak values for fluorescence, taking in to account the scaling factors, is shown in figure (3.9).

From figure (3.9) it can be seen that the intensity drops sharply with the increasing dye concentration in the polymer. This, again, is possibly due to concentration effects and aggregate formation of the dye. It is clear also that the low concentrations of the dye are necessary for maximum fluorescence.

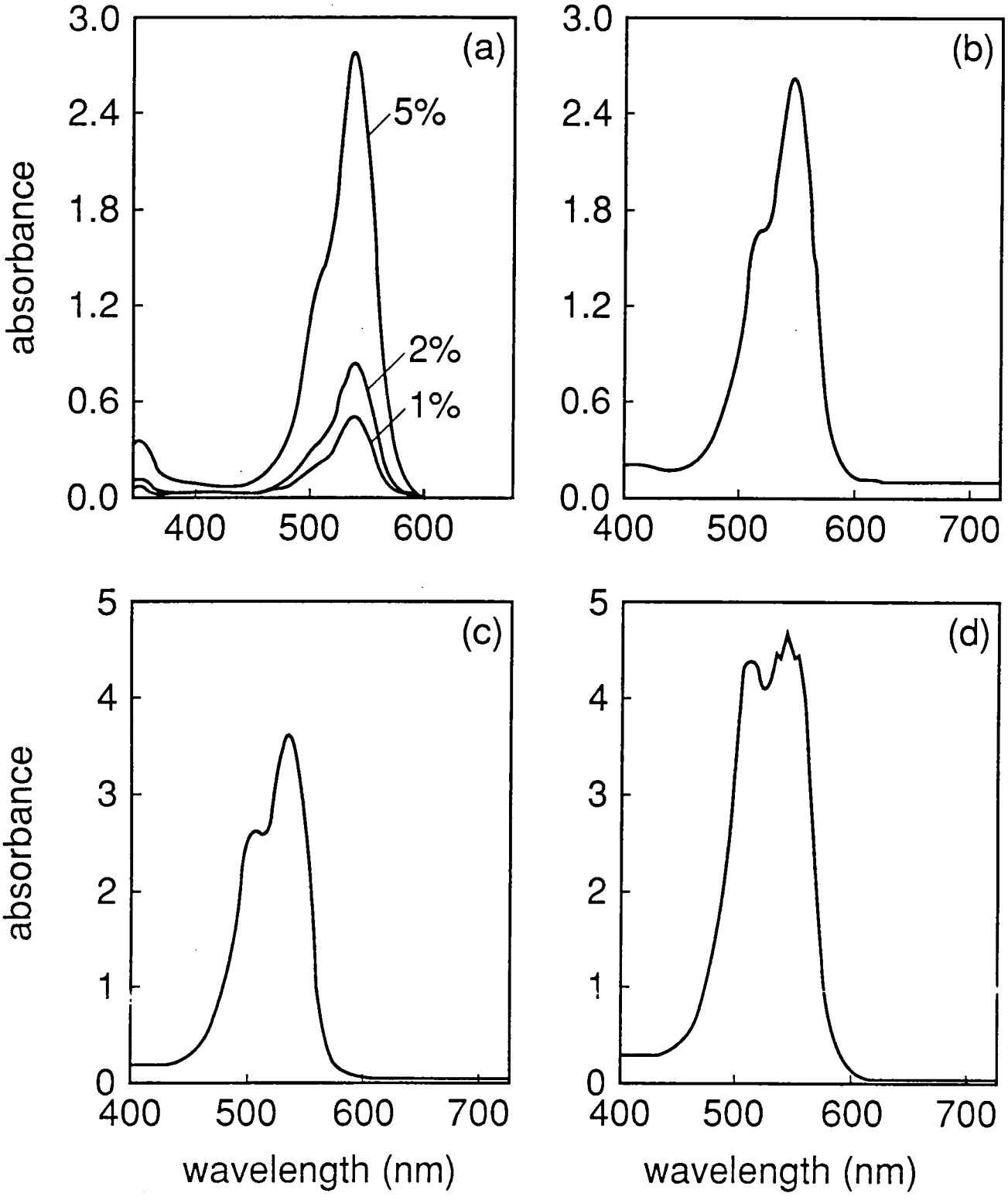

Figure (3.7) Absorption profiles of different concentrations of rhodamine 6G in a thin film.

(a) 1,2,5% (b) 10% (c) 15% (d) 30%.

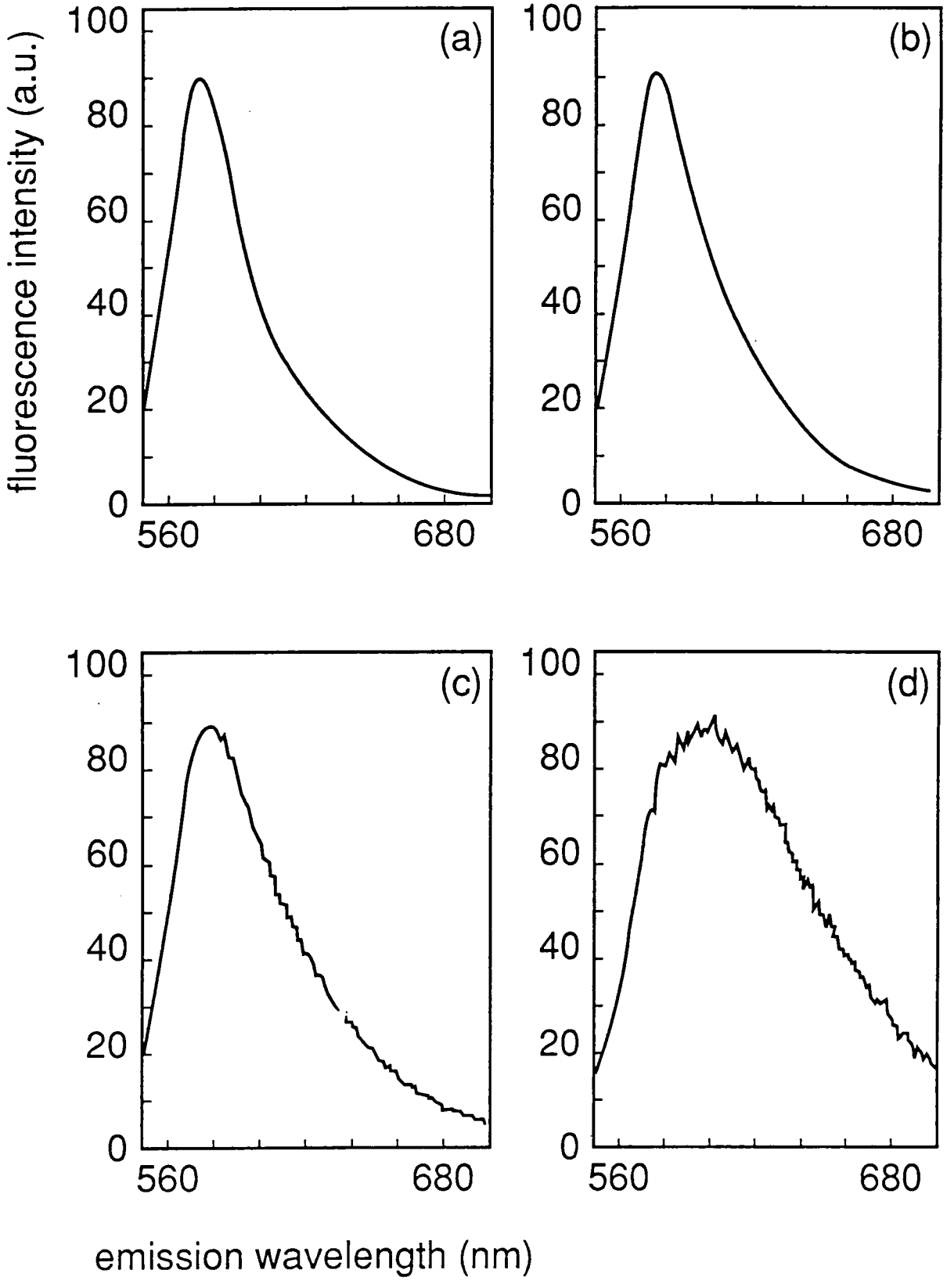

Figure (3.8) Fluorescence profiles of different concentrations of rhodamine 6G in a thin film.

(a) 1% (b) 2% (c) 5% (d) 10%

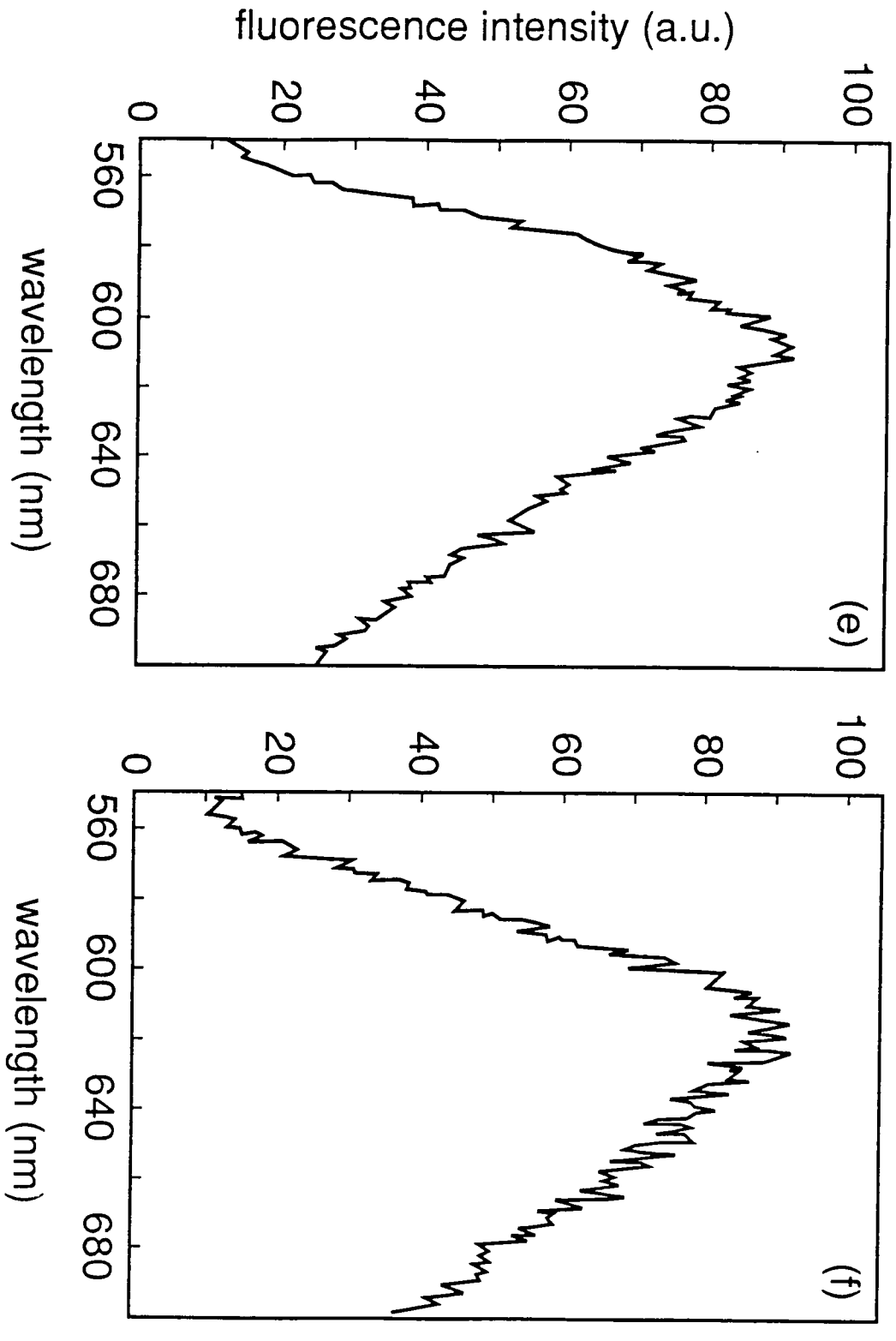

Figure (3.8) Fluorescence profiles of different concentrations of rhodamine 6G in a thin film.

(e) 15% (f) 30%.

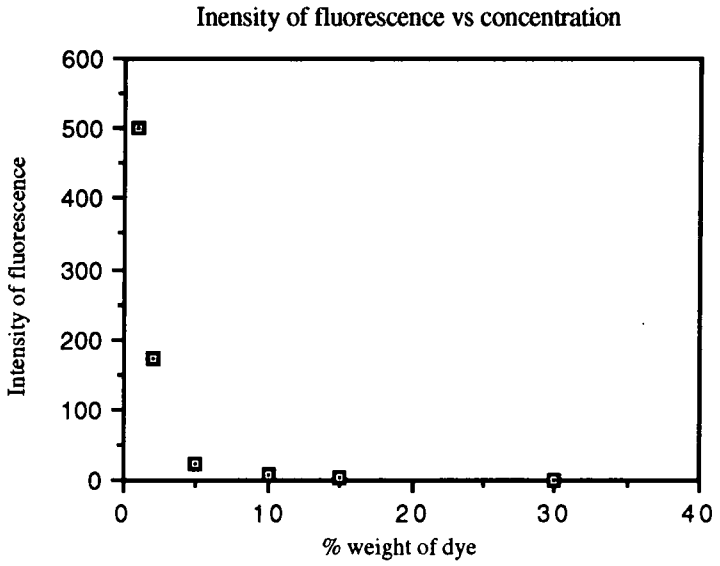

Figure (3.9) Intensity of fluorescence vs Concentration of Rhodamine 6G.

The concentration of another similar dye, Rhodamine B (to be used as the acceptor in the dye pair), was varied with respect to the polymer and the fluorescence intensity was measured. The results are shown in figure (3.10). From the graph it can be seen that the intensity of fluorescence increases with increasing concentration of dye in the polymer matrix. But eventually the fluorescence intensity levels off.

Thus for this system of doping rhodamine dyes in P4VP there seems to be an optimum dye concentration, and this is found to be about 1% $^{w}/_{w}$. At this concentration maximum intensity of fluorescence is achieved. Also the critical nature of the concentration of the dye in the polymer film has been demonstrated.

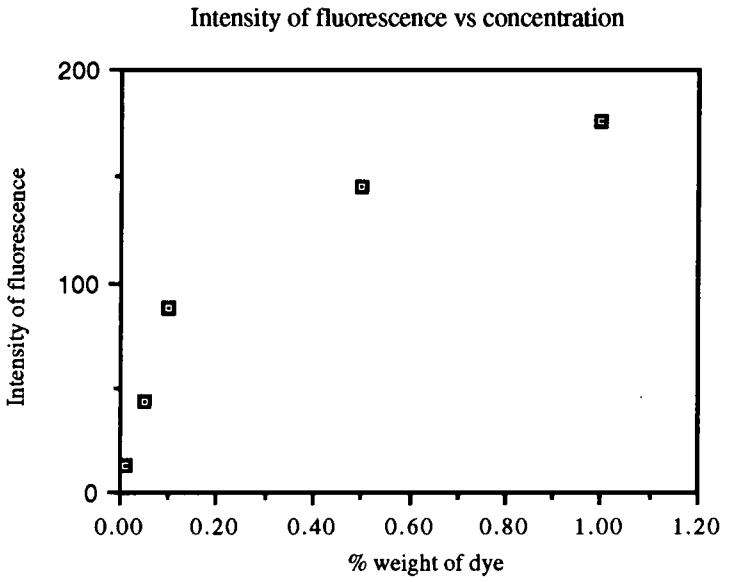

Figure (3.10) Intensity of Fluorescence vs Concentration of Rhodamine B.

3.5 Solid thin film energy transfer dye lasers.

3.5.1 Introduction.

Although a more detailed explanation of energy transfer will be given in Chapter 4, a brief explanation of the spectroscopic implications will be given in this section, followed by results from various experiments on different systems.

For energy transfer to take place a donor dye is required to absorb the pump radiation and transfer it to the acceptor dye. This energy can be transferred by direct coupling (resonance transfer of the excitation due to long range dipole-dipole interaction) or by a fluorescence absorption process, if the two spectra are sufficiently overlapped. The former mechanism is essentially nonradiative, since it does not involve the intermediacy of a photon. In essence this process relies on the degree of spectral overlap between the absorption and fluorescence spectra of the acceptor and donor dyes respectively. Thus if certain dye pairs are to be considered for energy transfer the extent

of spectral overlap must be determined. Another crucial factor is solvent compatibility of the dyes, especially if the dyes are to be dissolved into a common polymer.

Lasing can be achieved in one of a number of ways :

a) Excitation - Interference type distributed feedback [Muto S. et al., (1987)]. This involves establishing self interference of the pump beam, usually using a 90° reflecting corner, e.g. a corner of a prism. The angle of incidence of the pump beam determines the pitch of the interference pattern and hence the lasing wavelength.

b) Using a grating and mirror to form an external cavity [Muto S. et al., (1983)]. The mirror is generally partially reflecting and the grating provides tunability.

c) A grating etched onto a substrate or polymer thin film [Aoyagi Y. and Namba S., (1974)]. This grating produces a distributed feedback and thus selects a wavelength for lasing. However, the disadvantage of this method is the lack of tuneability. Once the grating is etched the pitch is fixed. One way around this problem is to etch a chirped grating, i.e one where the pitch of the grating varies along the grating, this process allows a small amount of tuneability.

3.5.2 Experiments and results.

3.5.2.1 Absorption and fluorescence spectra of some dyes.

In order to determine the degree of spectral overlap of various dye pairs in polymeric thin films the absorption and fluorescence spectra were recorded. The absorption spectra of the dyes in solution were also recorded, to note any changes in the absorption spectrum between solution and film.

The dyes used were Rhodamine 6G (R-6G), Rhodamine B (R-B), Cresyl Violet (C-V) and 3-3'-Diethylthiadicarbocyanine (DTDC). These were used since these were readily available from commercial suppliers. The polymer used was poly (vinyl alcohol) (PVA), because for the dyes in solution the solvent used was methanol and in order to keep the environment of the dye constant a similar type of polymer was used. The concentration of the dyes in methanol was 10^{-6} M. The absorption spectra recorded are shown in figure (3.11).

Thin films were dipped of PVA doped with the dyes, 2 g of PVA were dissolved with 40 ml of water and 5 x 10^{-4} M quantities of dye were used. The viscosity of the solution produced was acceptable to produce reasonably thick films. The films were dipped at 30mm/min, this produced films of 1.9 (±0.001) μm thickness.

Absorption measurements were then taken of the films. The spectra recorded are shown in figure (3.12). Table (3.3) shows the results obtained for λ_{max} of both the solutions and the films.

Dye	λ_{max}(solution)	λ_{max}(film)
R-6G	527nm	537nm
R-B	543nm	557nm
C-V	593nm	608nm
DTDC	652nm	671nm

Table (3.2) Absorption maxima of the dyes.

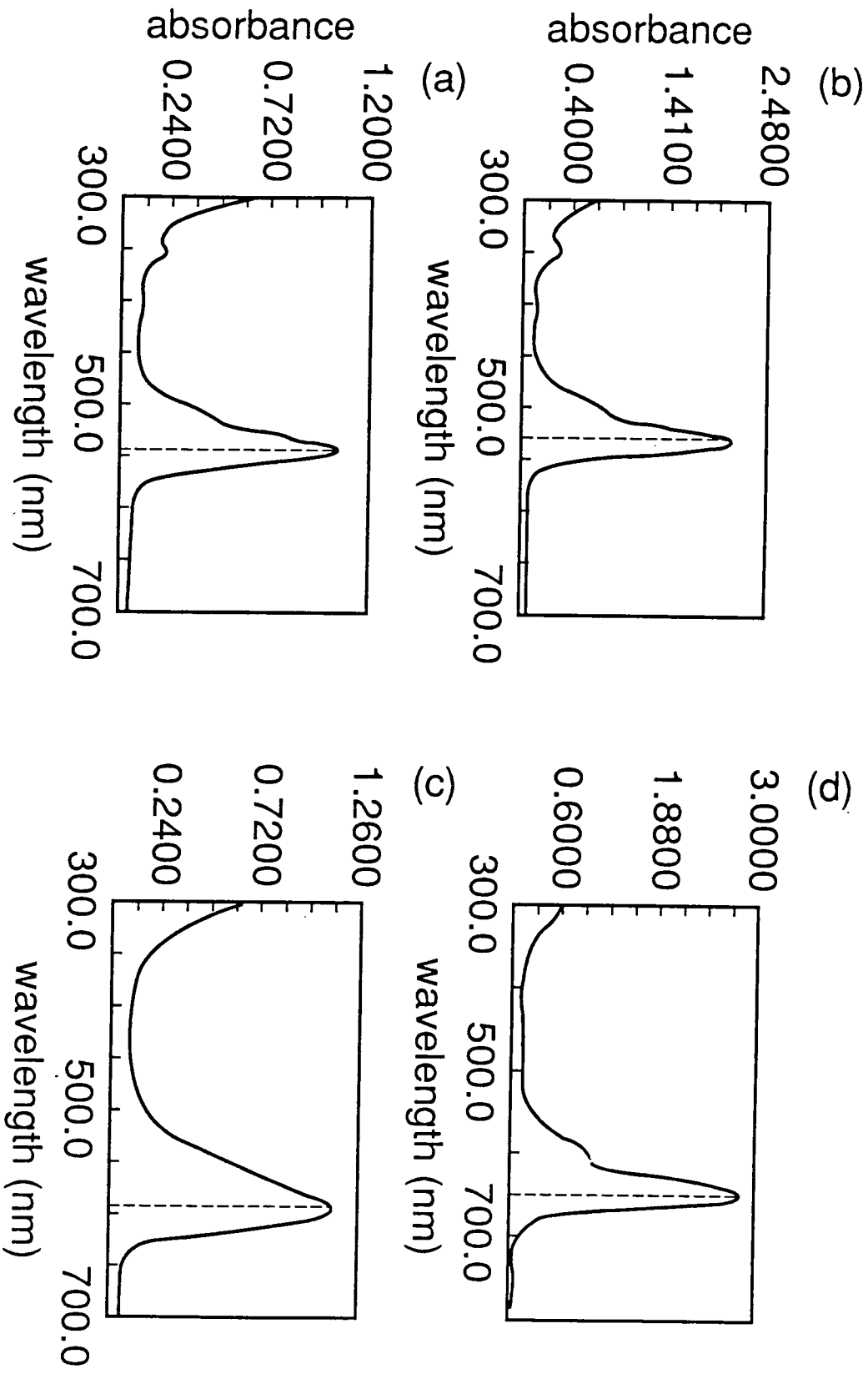

Figure (3.11) Absorption spectra of dyes in solution at 10 M (a) R-B (b) R-6G (c) CV (d) DTDC.

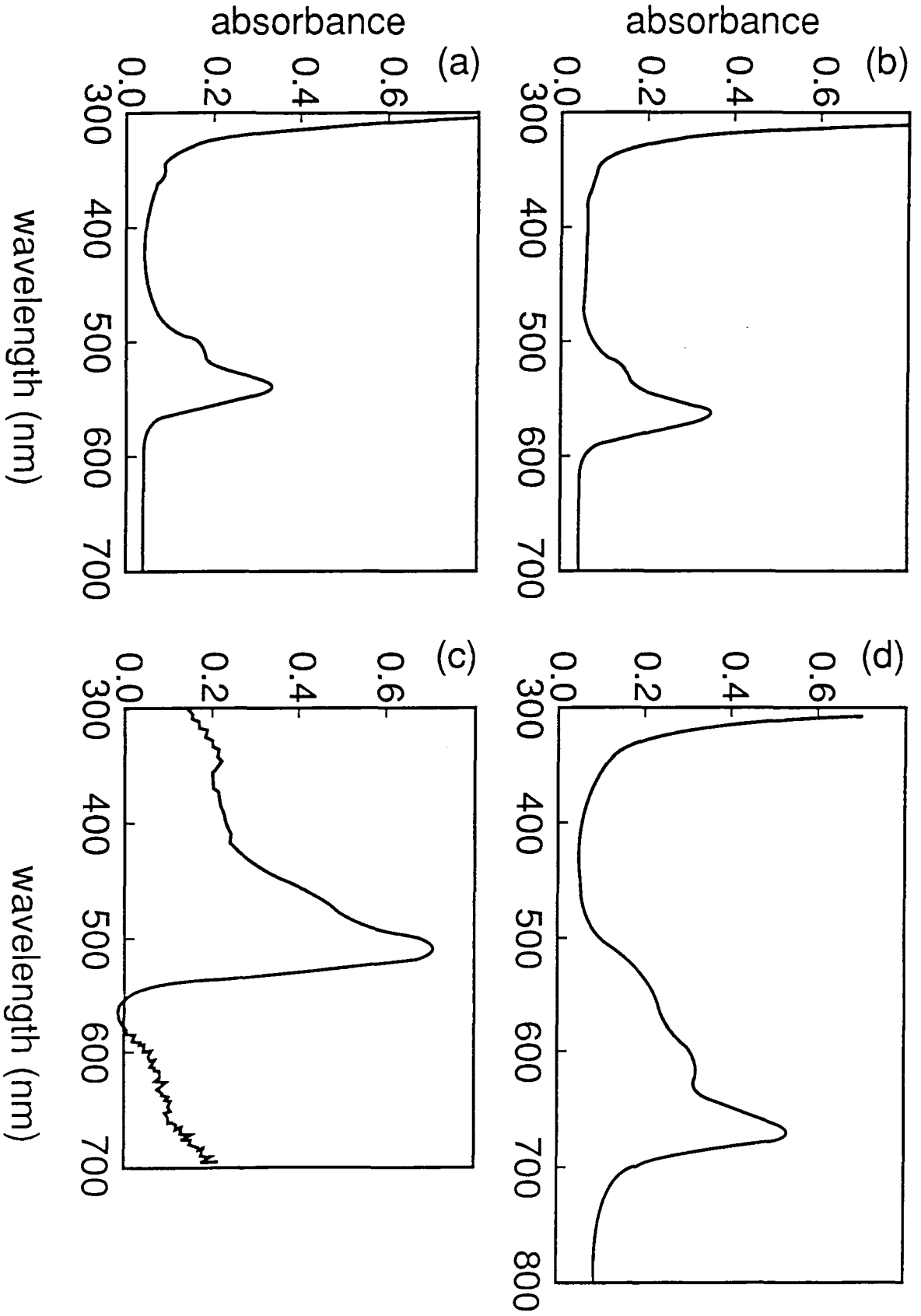

Figure (3.12) Absorption spectra of dyes in a thin film at $5*10^{-4}$M from 5% PVA in water (a) R-6G (b) R-B (c) CV(neutral) (d) DTDC.

The C-V dye did not dissolve readily in water, a small amount of HCl was added and the solution heated. The films produced had very low absorbance values.

The samples were taken to Imperial College to measure the fluorescence spectra. A mixed sample of 5 x 10^{-4} M R-B and R-6G was also made in methanol . The equipment used was the same as that outlined before see section (3.4). Initially all the films were excited at 532nm, and the emission intensity was scanned over a range of wavelengths. The experiment was then repeated but this time the excitation wavelength was the λ_{max} of the absorption of the dye in the film. The fluorescence emission spectral data was stored on a microcomputer. The results obtained are shown in figure (3.13). The table below summarises the results that were obtained :

Dye	λ_{em} (λ_{ex}=532nm)	λ_{em} (λ_{ex}=λ_{max})
R-6G	562.4nm	562.5nm
R-B	583.8nm	583.9nm
R-6G +R-B	579.5nm	578.8nm
DTDC	696nm	694.4nm

Table (3.3) Fluorescence maxima of the dyes.

From this table it can be seen that there is very little, if any within experimental error, difference in the λ_{em} between the two excitation wavelengths, as would be expected. The intensities of the spectra produced by excitation at λ_{max} were larger than those produced by excitation at 532nm. This would be expected since the absorption is larger.

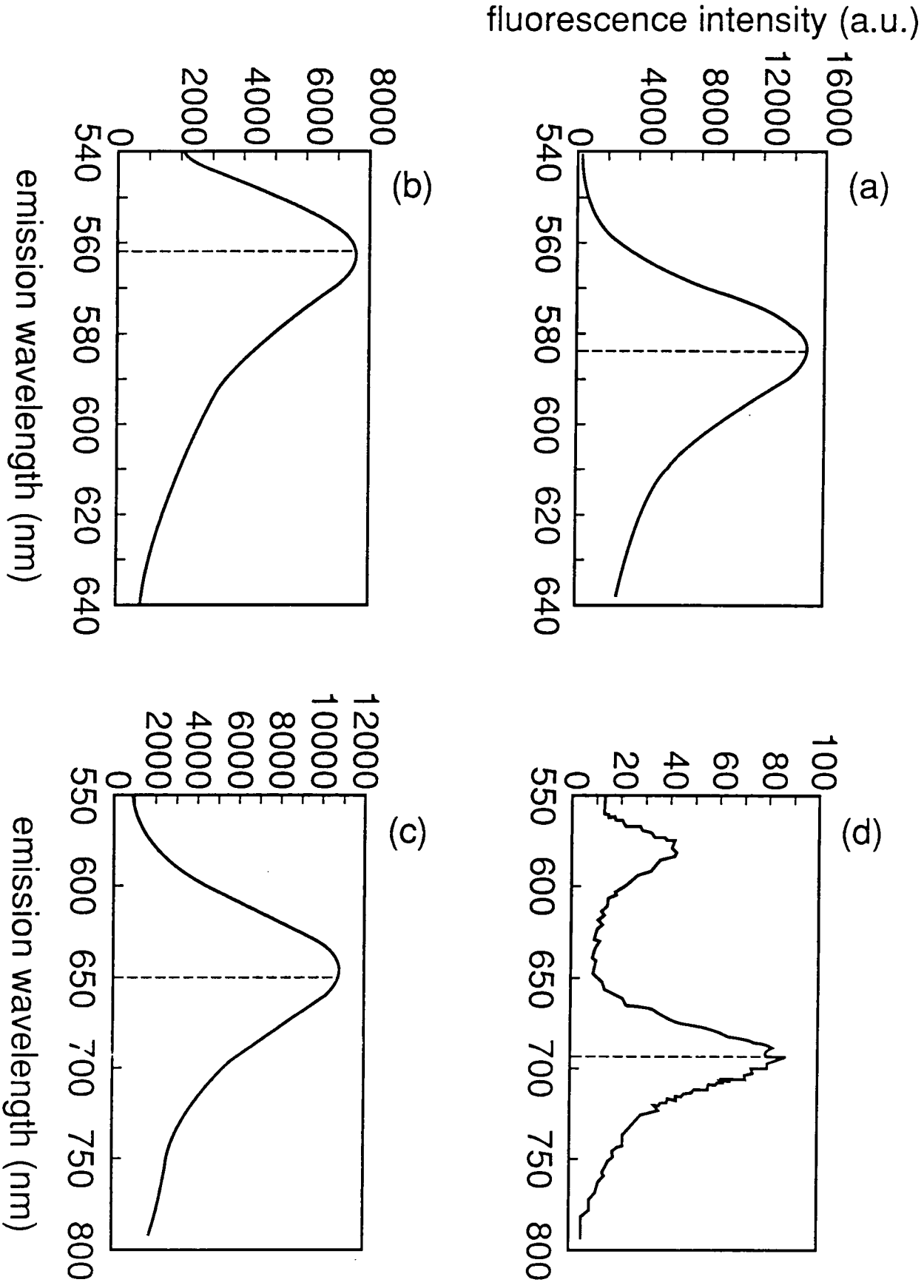

Figure (3.13) Fluorescence spectra of dyes in a thin film at $5*10^{-4}$M from 5% PVA in water (a) R-B (b) R-6G (c) CV(neutral) (d) DTDC.

Attempts were made to measure the fluorescence emission of the C-V dye in PVA, but the spectra produced were not very good since the films were of very poor quality.

Looking at the mixed R-6G and R-B system, firstly from the absorption spectrum of R-B it can be seen that it has a strong absorption at both 532nm and 542nm (the excitation wavelength chosen for the mixture which corresponds to the maximum absorption, see figure (3.14)). Thus to determine whether energy transfer was taking place, another excitation wavelength needs to be chosen where the R-6G absorbs and the R-B does not, to avoid direct excitation of R-B. From the absorption spectra of the two dyes, 460 nm was chosen as the ideal excitation wavelength. With excitation at 460nm the fluorescence emission of the mixed film over a range of wavelengths was monitored and compared with those obtained from the pure dyes. The results are shown in figure (3.15).

The peak of the fluorescence emission from the mixed dye film is close to the peak of the R-B fluorescence emission. This suggests that in the mixture, the majority of the fluorescence is due to the R-B.

But one must also consider the case where the fluorescence from the mixture may be the sum of the individual fluorescence emission of the dyes. Thus by simply fitting the individual fluorescence emission curves with the fluorescence emission curve of the mixture, one can determine whether the fluorescence emission from the sample is a linear combination of the individual emissions. This was done on a personal computer using a spreadsheet package. Figure (3.16) shows clearly that the experimental data is not the same as the computer average for the sample. The average predicts much more fluorescence on the short wavelength side of the peak, i.e in the sample some of the excited R-6G molecules do not radiatively decay via

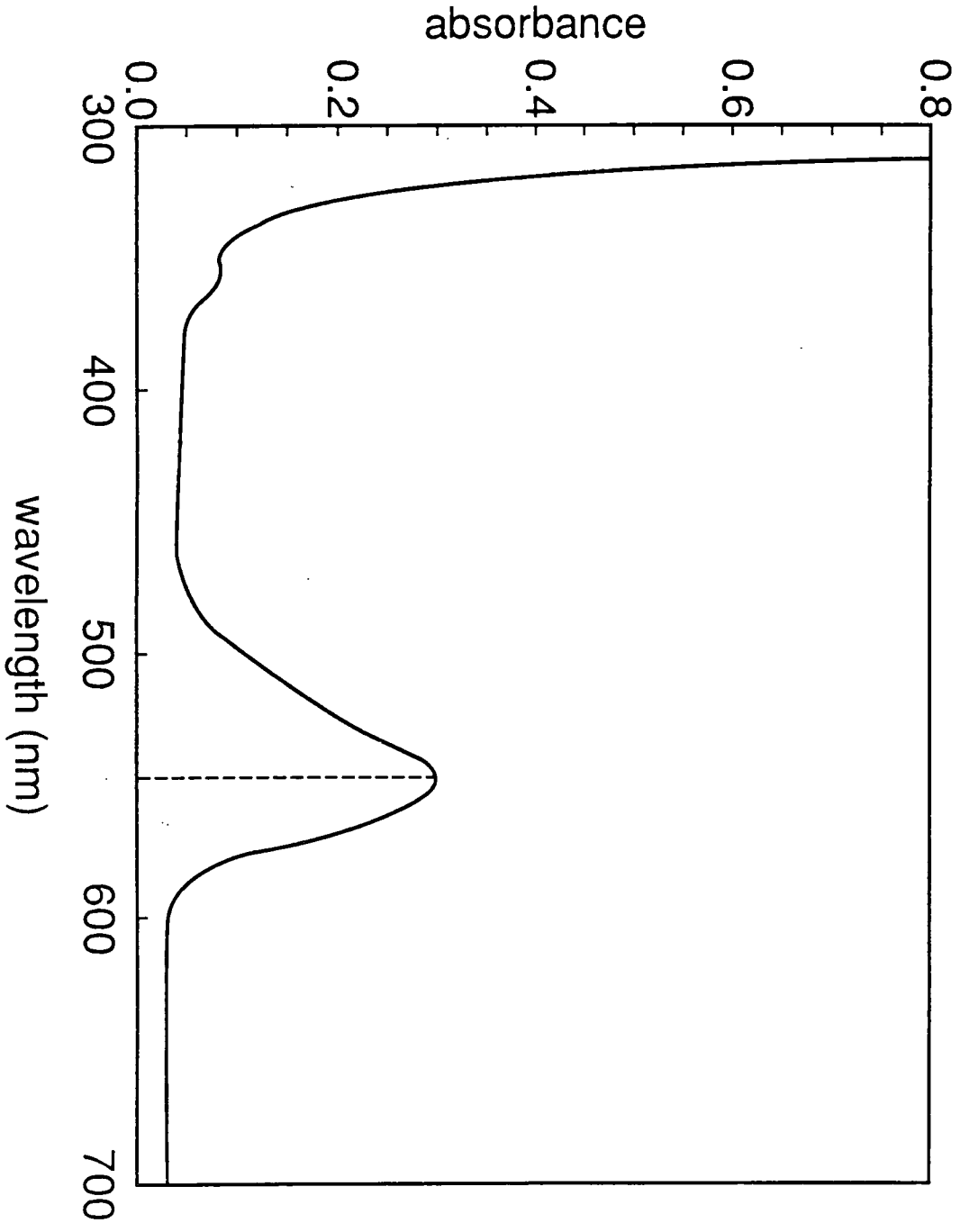

Figure (3.14) Absorption spectrum of a mixed dye system of R-B and R-6G.

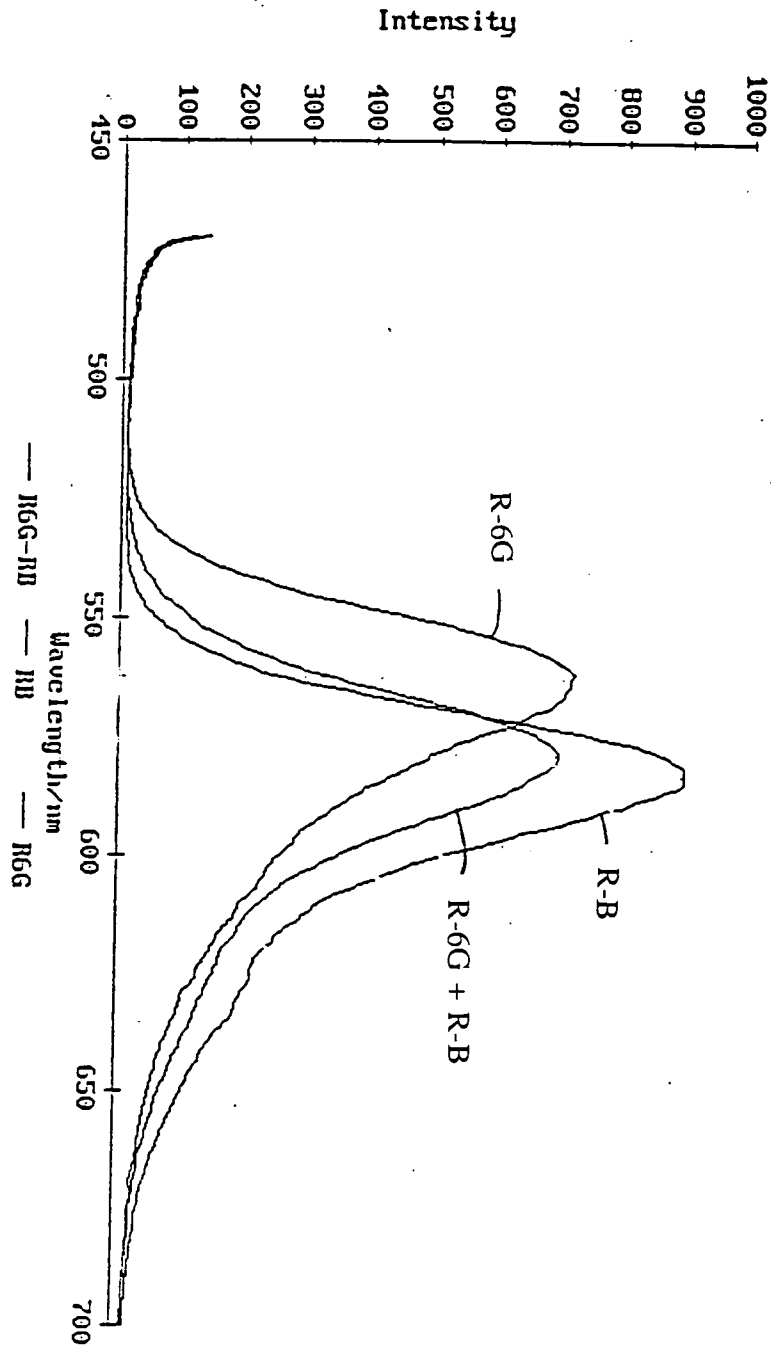

Figure (3.15) Fluorescence spectra of the pure rhodamine dyes and the mixed film excited at 460 nm.

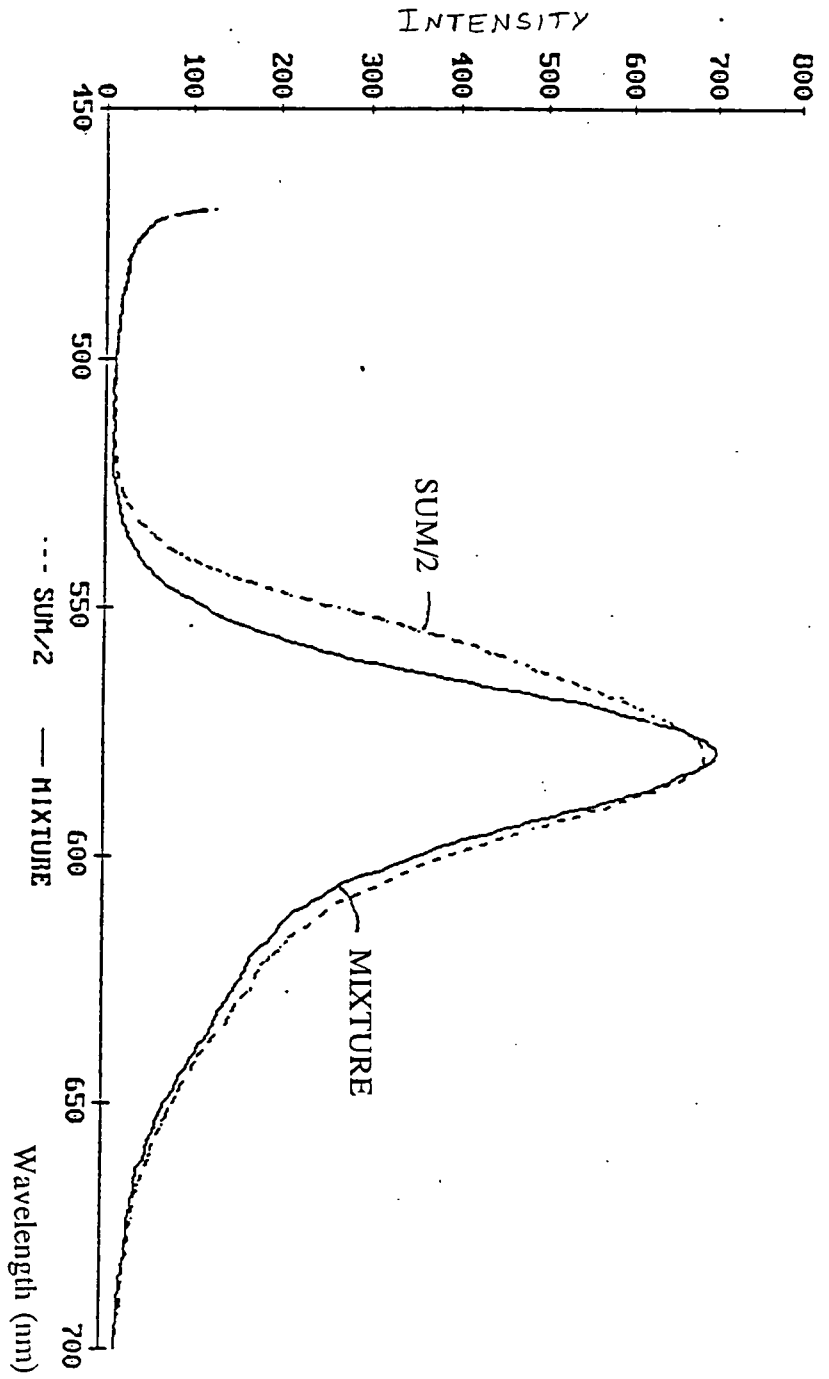

Figure (3.16) A comparison of the fluorescence emission curves of the mixed dye film and the computed average of the pure dyes.

fluorescence. Also on the long wavelength side of the average curve the signal is somewhat enhanced due to inhomogeneities in the R-B film thickness, so in actual fact it would be less than it is. Thus the average predicts less fluorescence than is actually observed in the sample.

Thus by doing this very simple exercise on the spreadsheet it was possible to determine that the fluorescence emission from the mixed dye system is not a simple linear combination of the individual dyes, and so there must be a fast competing nonradiative energy transfer process. Thus, from the relative differences of the two spectra, this seems to suggest that energy transfer was the mechanism responsible for the observed behaviour.

This process of combining the fluorescence spectra of individual dyes and then trying to match the combination to a particular mixture, provides a good means of determining how efficient these nonradiative processes are.

One would expect that for two dyes that were not chemically interacting, the absorption spectra of the mixture would be a simple linear combination of the individual dyes. This would seem a pre-requisite for the justification of energy transfer, since any deviation would imply other nonradiative processes that involve dye pairs or complexes, since as explained earlier dimer formation or complexation changes the absorption band profile. The fluorescence spectra, however, would involve nonlinearities in the combination if energy transfer was taking place. This has been observed in the rhodamine system - where the fluorescence of the acceptor dominates the total fluorescence, even though the mixture is pumped in a region of predominant donor absorption.

To examine this point further, some analytical operations were performed on the absorption and fluorescence spectra of rhodamine B and rhodamine 6G dyes individually and on a series of mixtures.

3.5.2.2 The effect of rhodamine B concentration on the absorption and fluorescence spectra of the mixed rhodamine dye system.

The dyes were doped into a matrix of poly(methyl methacrylate) (PMMA), since this polymer produced better reproducible quality films, at different concentration ratios and the effect of varying the acceptor concentration on the absorption and fluorescence spectra was observed.

The dye doped polymer solutions were made up to the concentrations ratios shown in table (3.4). The weight of R-6G was kept constant at 0.0096 g for all the solutions, and 2.651 g of PMMA in 20 ml dichloromethane was used. Films were dipped onto glass microscope slides at a speed of 30 mm/min, and left to dry. The films could not be dried in the vacuum oven because the dyes degraded at high temperatures.

R-B : R-6G	Wt R-B (g)
4 : 1	0.03946
2 : 1	0.0192
1 : 1	0.0096
0.5 : 1	0.0048
0.25 : 1	0.0024

Table (3.4) Weights of R-B used.

To quantify the ratios of the dyes in the polymer film, absorption spectra were taken of all the films. Then various linear combinations of the absorption spectra of the pure R-B and R-6G were tried, to match the absorption spectra of the mixed films i.e.

$$Abs(R\text{-}B : R\text{-}6G) = \alpha Abs\ (1{:}0) + \beta Abs(0{:}1)$$

Here α and β represent the contribution of the individual spectra to the mixed sample. The background was removed from all the spectra to avoid any unnecessary biases. Table (3.5) shows the results from this exercise. The matching of the absorption spectra can be seen in figure (3.17). The dotted line shows the variance for the fit at each wavelength. The oscillations are due to the differences in the film thickness.

Expected R-B : R-6G	R-B α	R-6G β	variance	calculated R-B : R-6G
4 : 1	7.63	0.953	0.045	8 : 1
2 : 1	2.79	0.88	0.0047	3.17 : 1
1 : 1	1.24	1.17	0.027	1.06 : 1
0.5 : 1	0.41	0.997	0.00177	0.41 : 1
0.25 : 1	0.073	0.955	0.00277	0.076 : 1

Table (3.5) Linear combinations of the individual dyes to match the absorption spectra.

From the table above it can be seen that a simple linear combination method can be used to match the individual absorption spectra of the dyes to the absorption spectra of the mixed dye film. This suggests that there are no interactions between the dyes which may have any effect on the profile of the absorption spectra. However, the actual

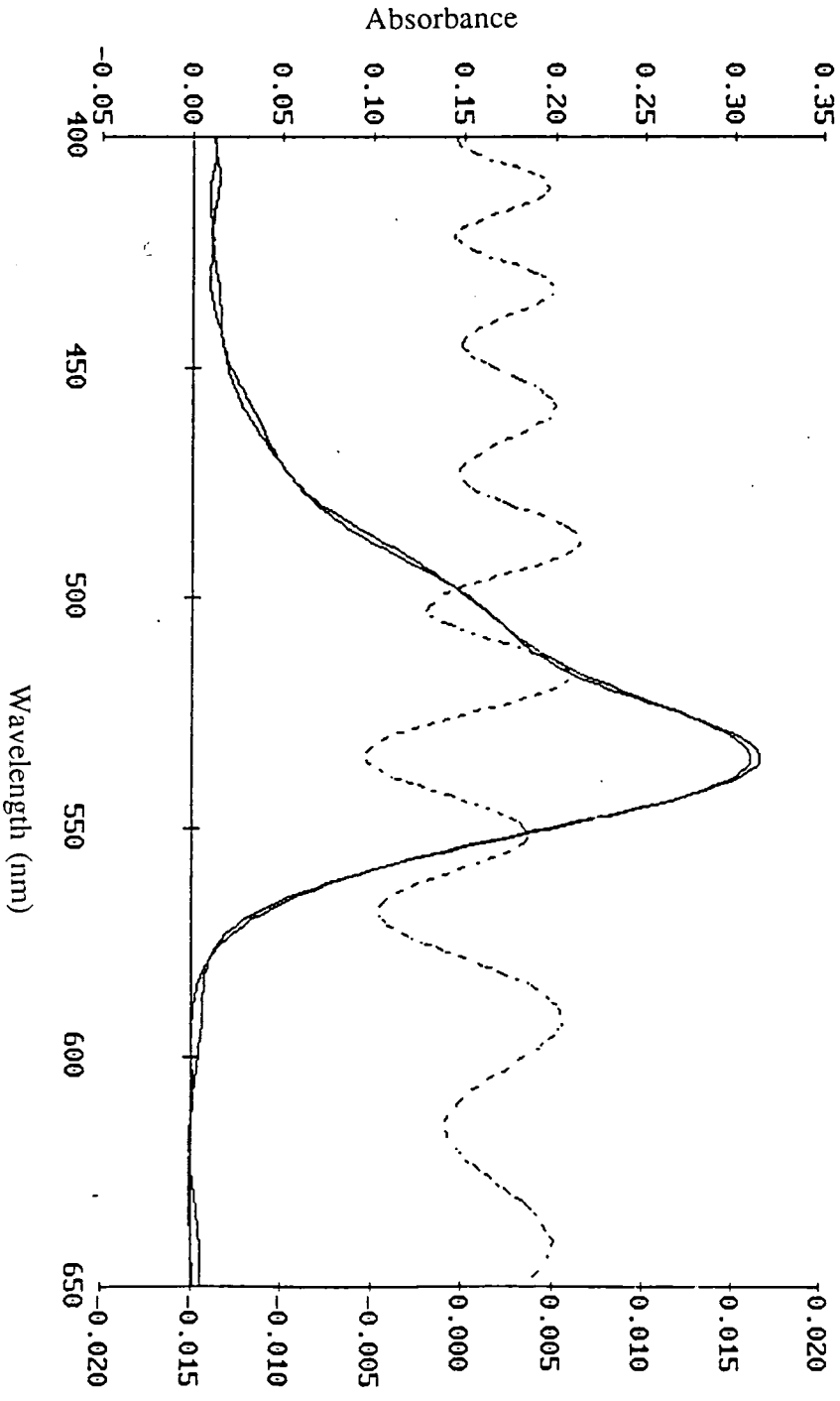

Figure (3.17) Linear combination method used to match the absorption spectra of the pure dyes to the mixed dye sample. (a) B : 6G = 1/4.

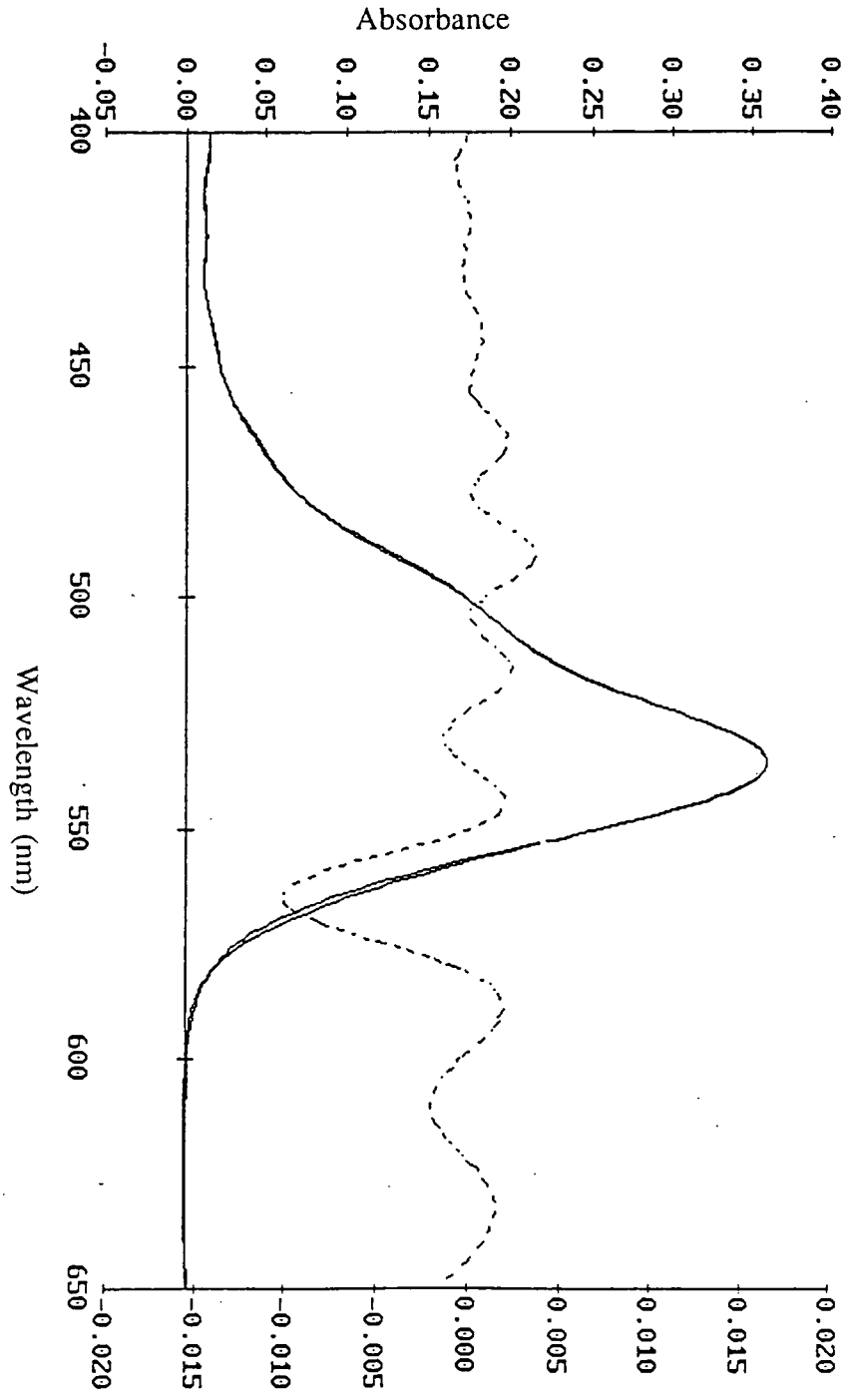

Figure (3.17) Linear combination method used to match the absorption spectra of the pure dyes to the mixed dye sample.(b) B : 6G = 1/2.

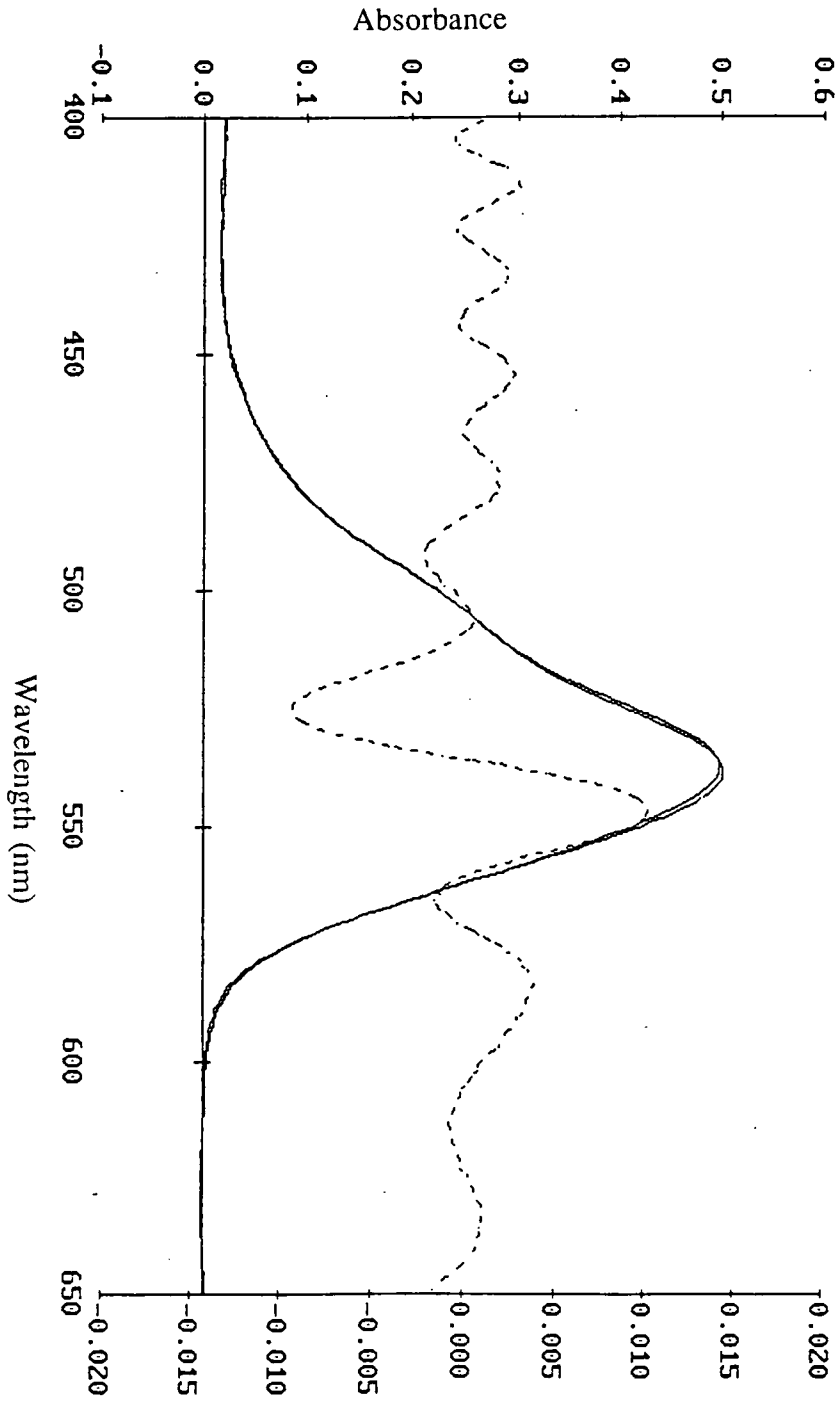

Figure (3.17) Linear combination method used to match the absorption spectra of the pure dyes to the mixed dye sample.(c) B : 6G = 1.

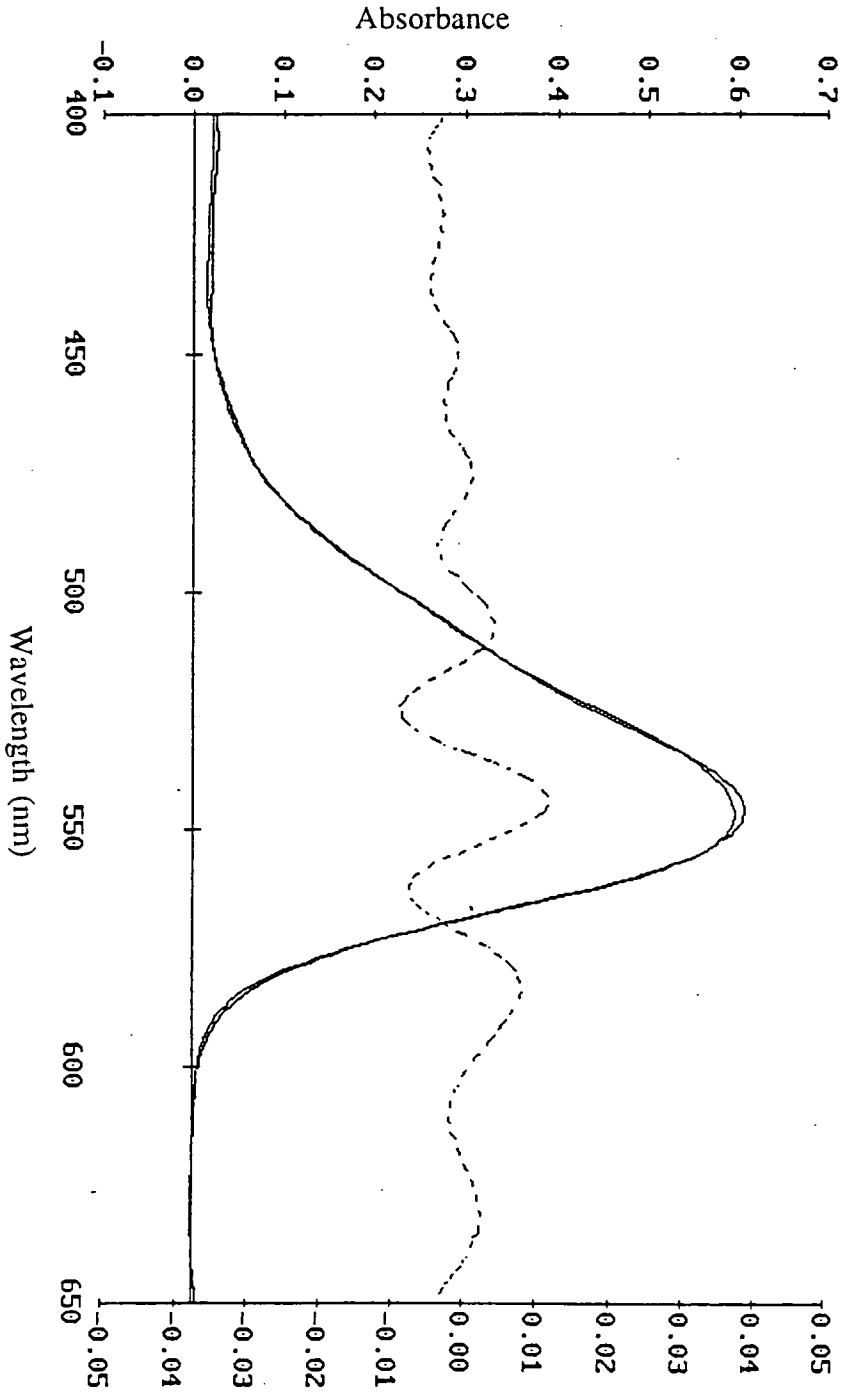

Figure (3.17) Linear combination method used to match the absorption spectra of the pure dyes to the mixed dye sample.(d) B : 6G = 2.

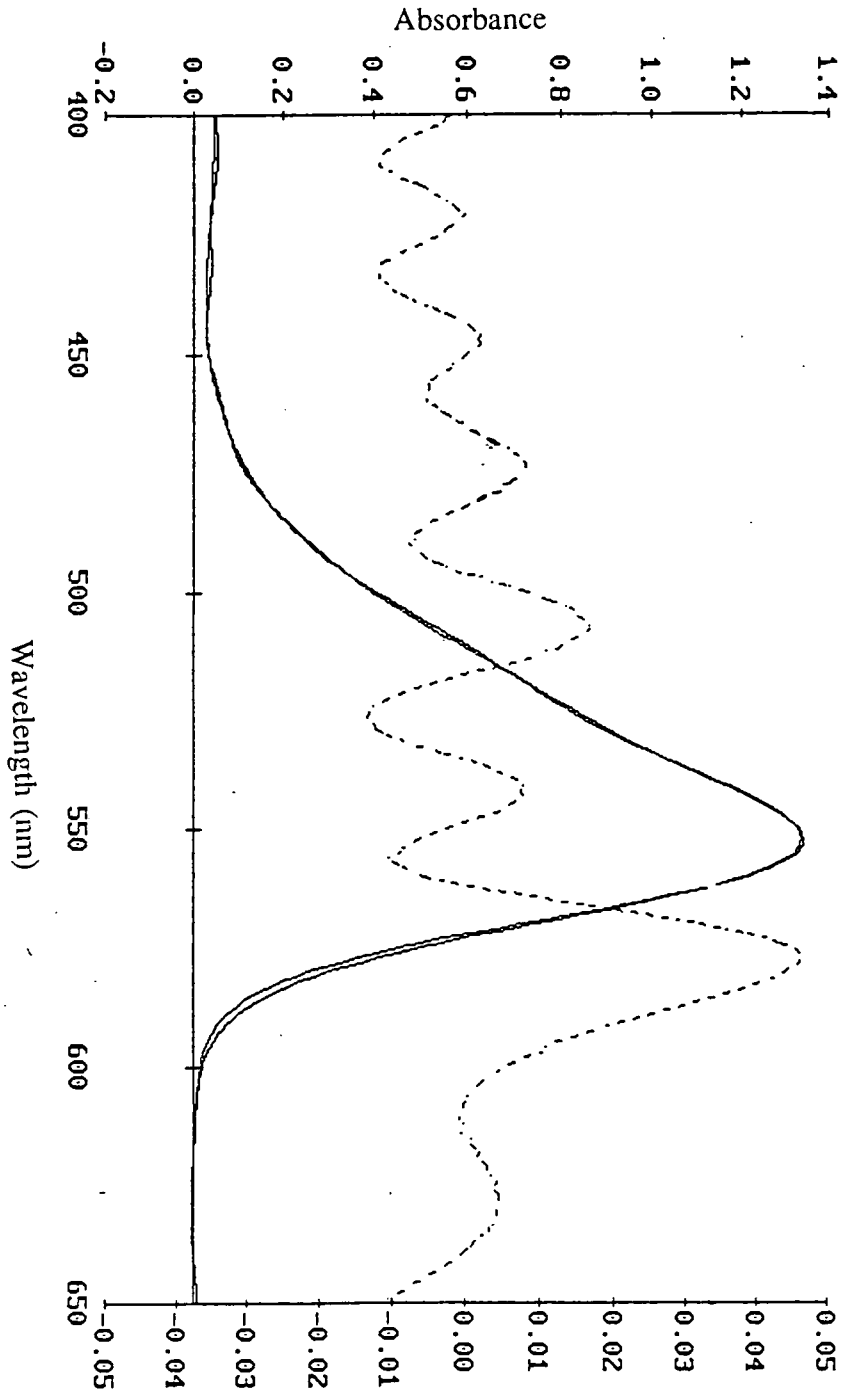

Figure (3.17) Linear combination method used to match the absorption spectra of the pure dyes to the mixed dye sample.(e) B : 6G = 4.

calculated ratios are somewhat different to those expected. This could be due to the solutions being made incorrectly, but the calculated concentration ratios will be used in all the graphs to be plotted, since these values are likely to be more accurate.

Having determined that the absorption process of each dye is independent of the other, the next stage was to determine whether the fluorescence from the mixed films is also a simple linear combination of the individual dyes, and how the contribution of the individual components vary with the concentration ratio.

Using a Perkin Elmer Lambda 5 Fluorimeter the samples were excited at 514nm, since this was the excitation wavelength used when measuring the fluorescence lifetimes reported in the next chapter, and the fluorescence emission spectra of the mixtures were recorded. See figures (3.18) for the results. Also a graph overlapping the absorption and fluorescence spectra of the pure R-B, R-6G and the 1 : 1 mixture was plotted, see figure (3.19). This graph illustrates the extent of overlap of the absorption and fluorescence spectra. The results of the linear combinations of the fluorescence spectra are shown in the table (3.6).

R-B : R-6G	R-B α	R-6G β
8 : 1	1.25	0.00
3.17 : 1	1.50	0.00
1.06 : 1	3.00	0.00
0.41 : 1	1.25	0.456
0.076 : 1	0.00	1.00

Table (3.6) Linear combination of the individual dyes to match the fluorescence spectra.

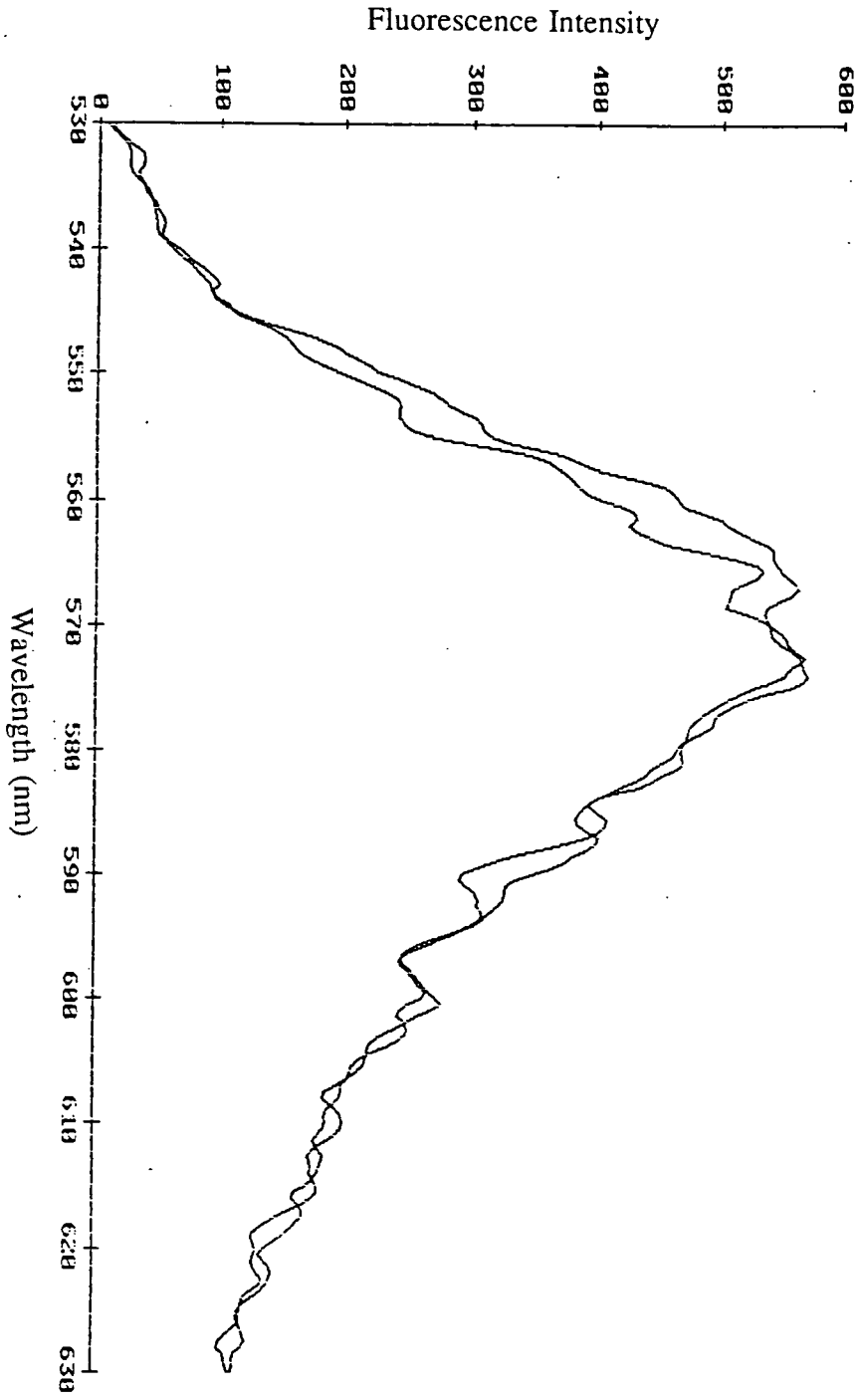

Figure (3.18) Linear combination method used to match the fluorescence spectra of the pure dyes to the mixed dye sample. (a) B : 6G = 1/4

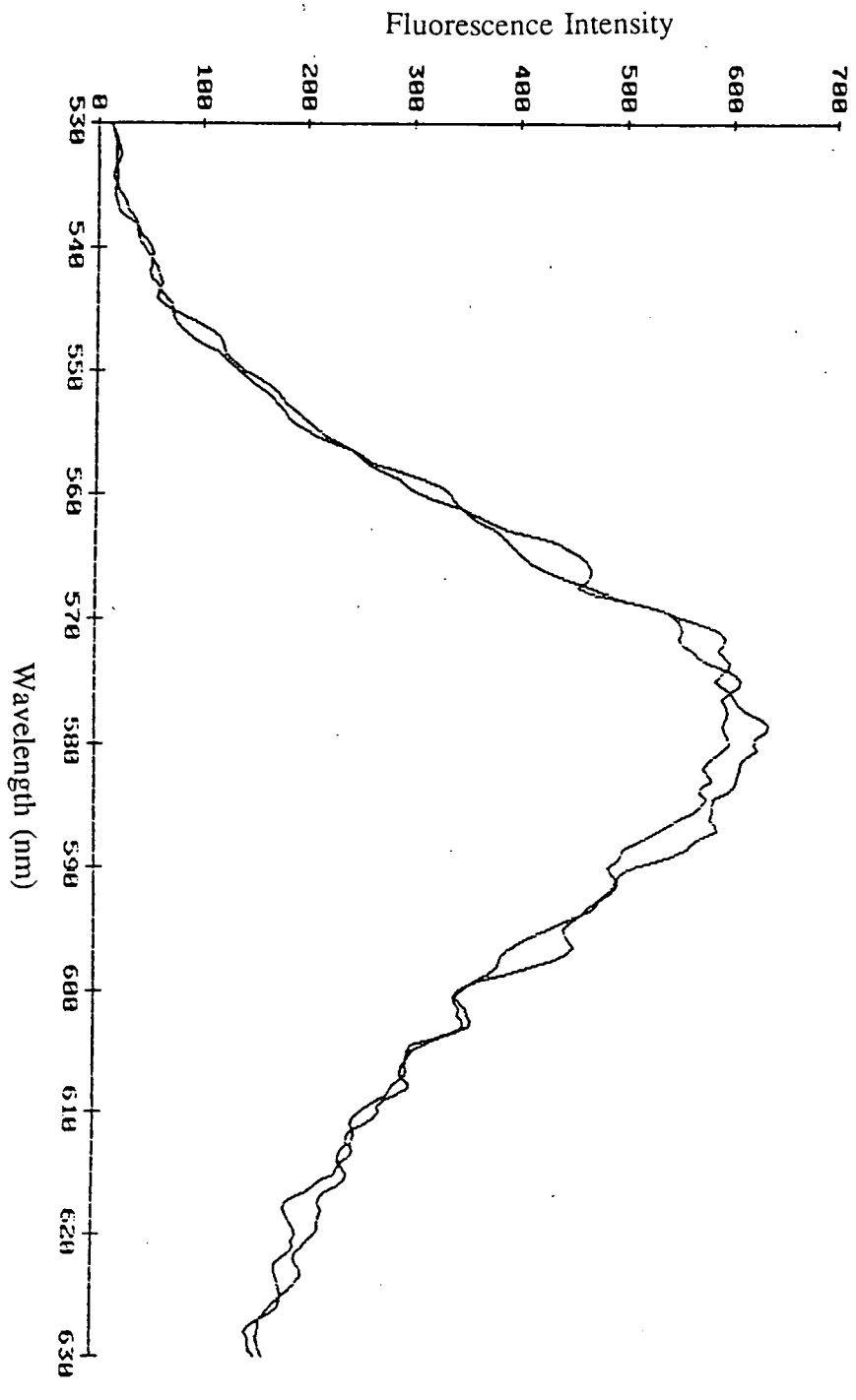

Figure (3.18) Linear combination method used to match the fluorescence spectra of the pure dyes to the mixed dye sample.(b) B : 6G = 1/2.

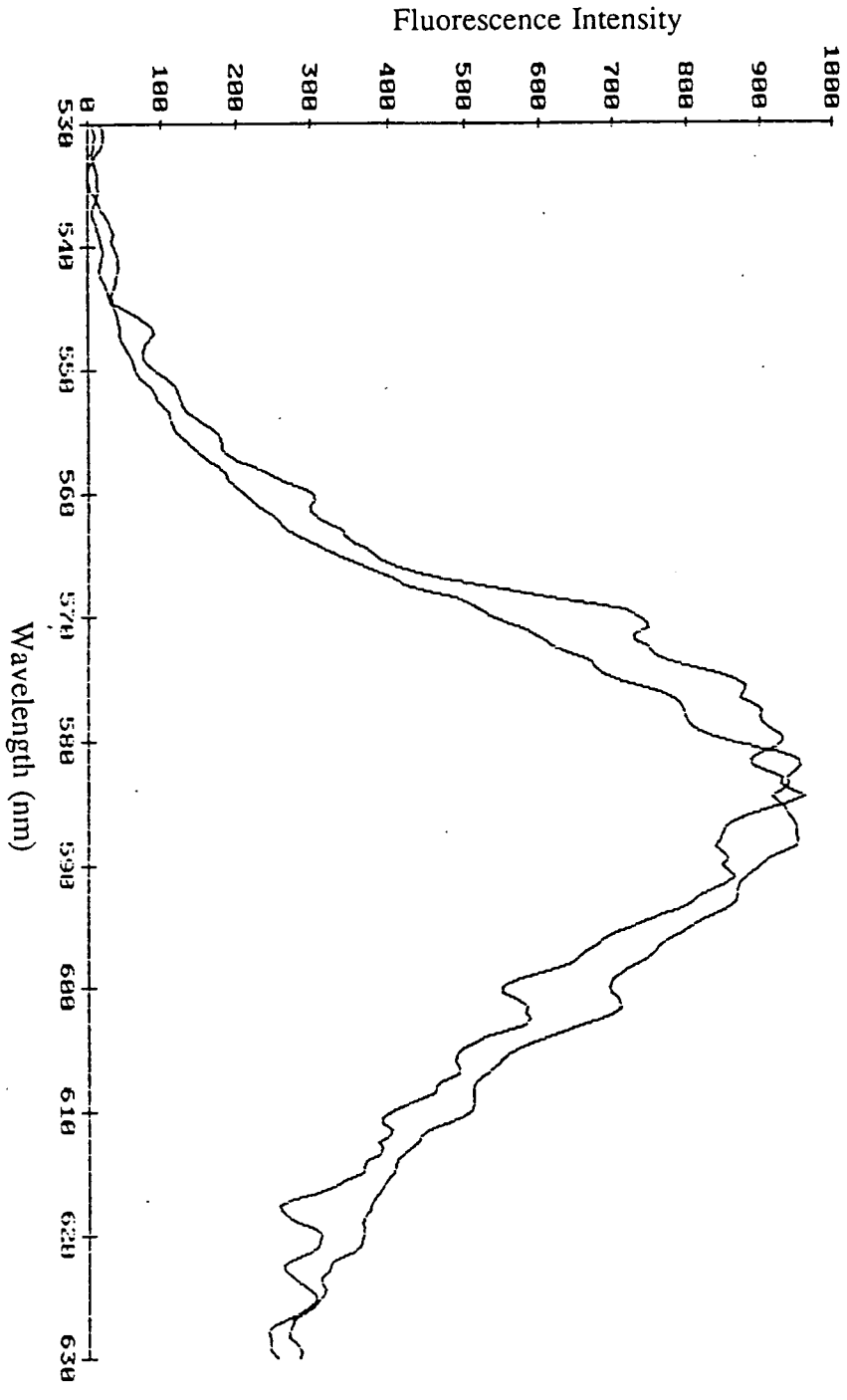

Figure (3.18) Linear combination method used to match the fluorescence spectra of the pure dyes to the mixed dye sample.(c) B : 6G = 1.

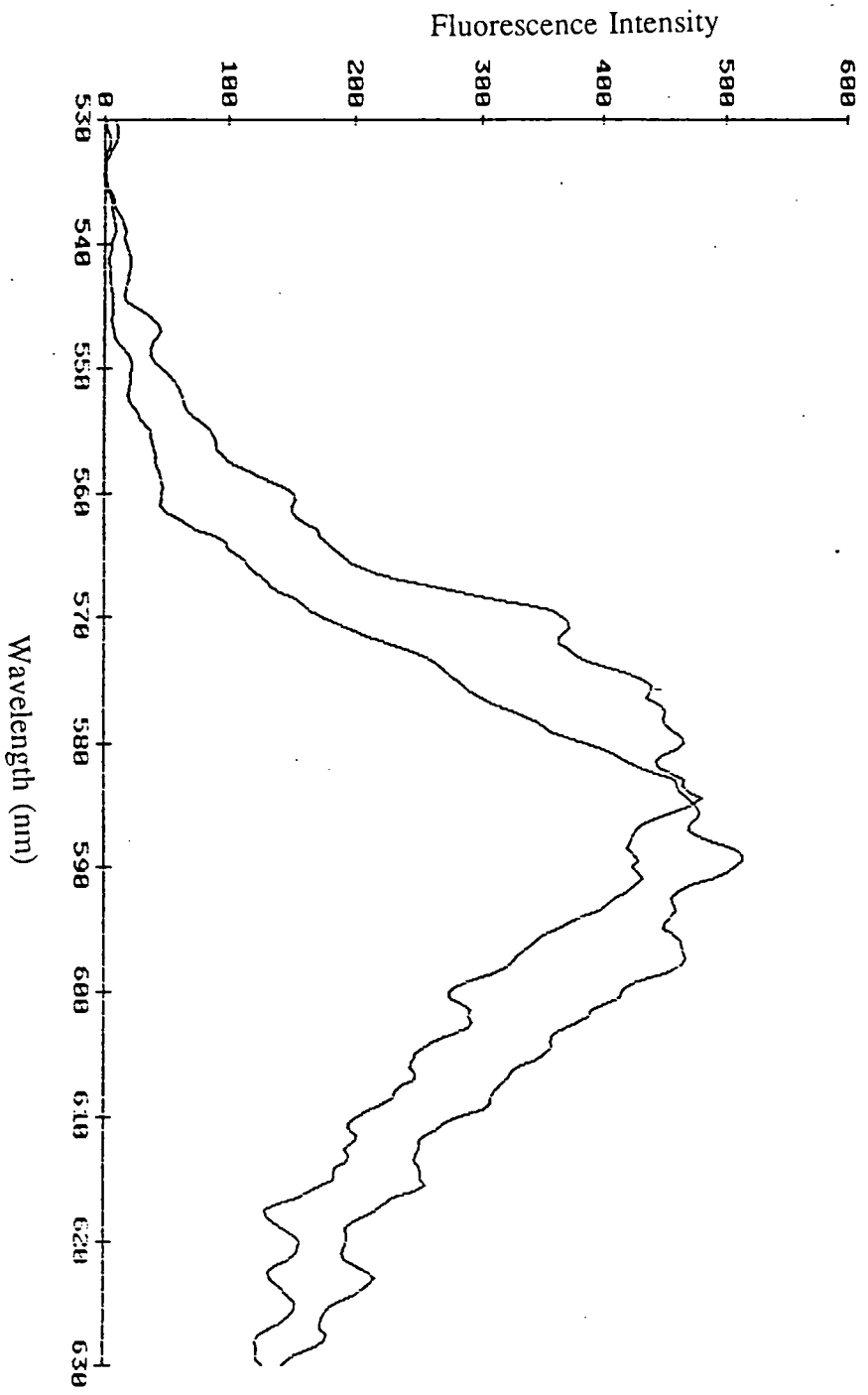

Figure (3.18) Linear combination method used to match the fluorescence spectra of the pure dyes to the mixed dye sample.(d) B : 6G = 2.

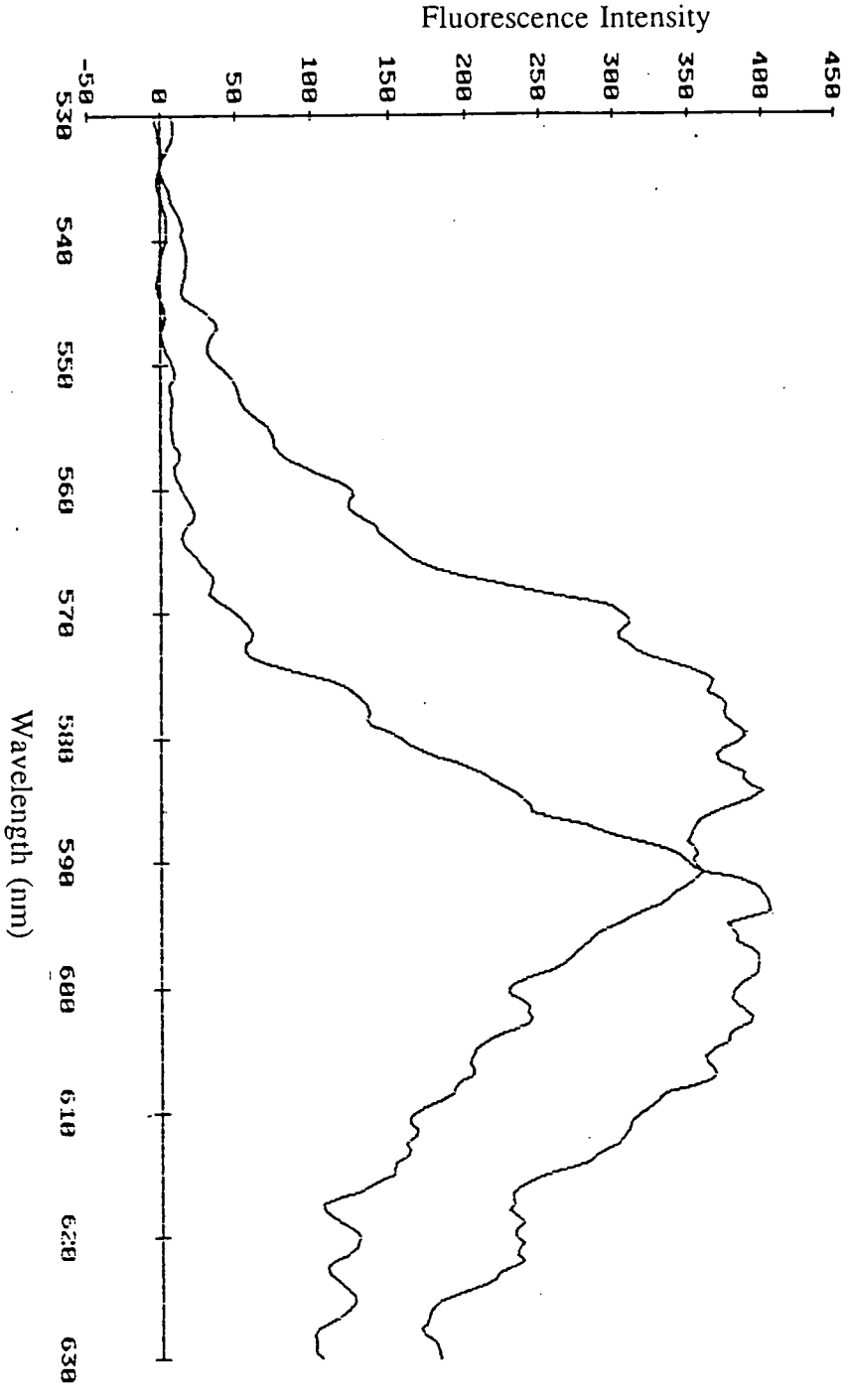

Figure (3.18) Linear combination method used to match the fluorescence spectra of the pure dyes to the mixed dye sample.(e) B : 6G = 4.

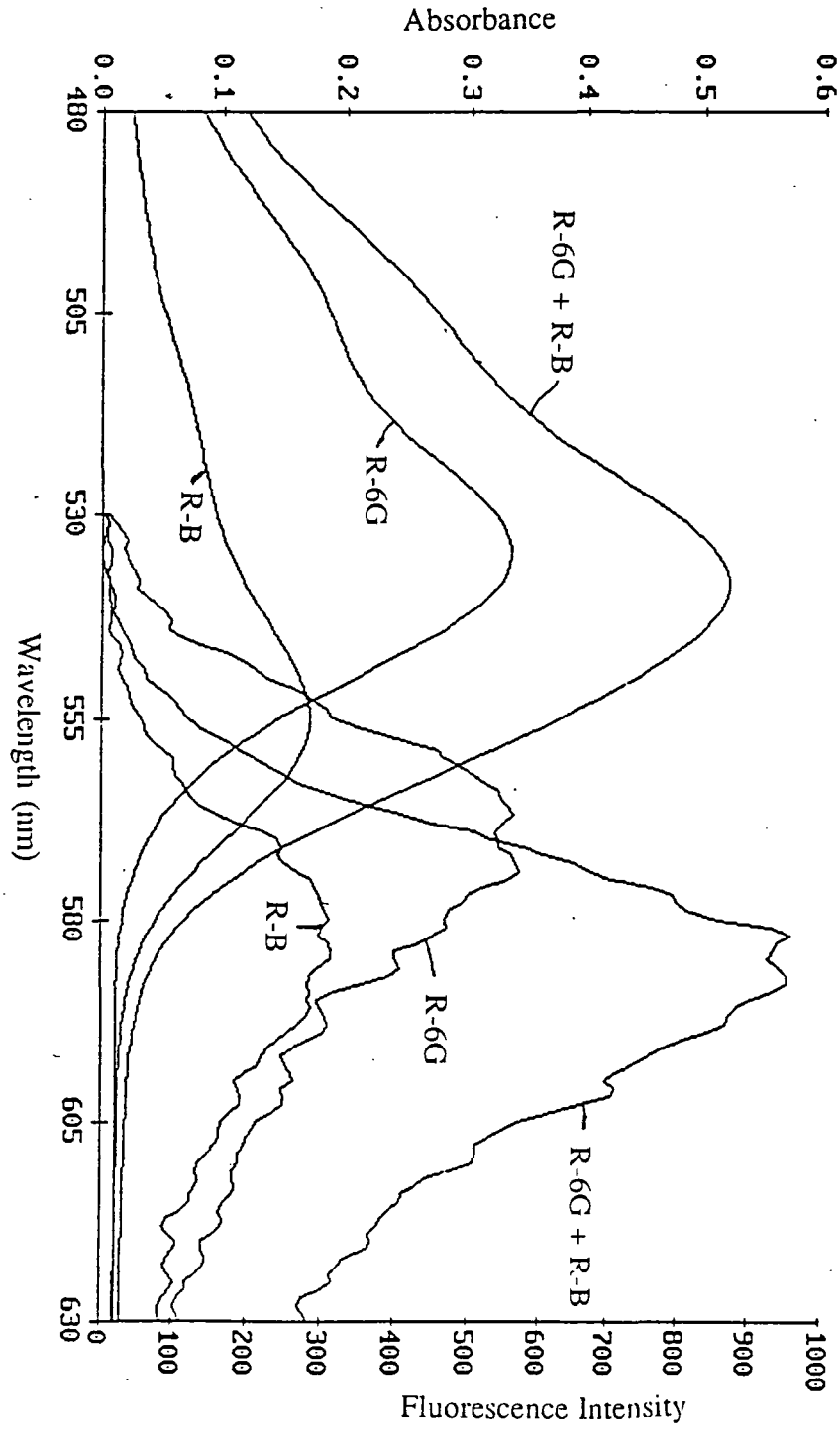

Figure (3.19) The absorption and fluorescence spectra of the pure R-B,R-6G and the 1 : 1 mixture

From the graphs and the table it can be seen that at high R-B concentrations, there is no contribution from the R-6G to the fluorescence emission of the mixed dye film. Also the fluorescence emission is red shifted about 10 - 20 nm from the maximum of the R-B. At low concentrations of R-B, a R-6G contribution to the fit is necessary for a reasonable match. But it can clearly be seen that the 1 : 1 mixture gives the maximum fluorescence, as much as three times that of R-B which has been excited at 514nm. This seems to be the most efficient system on the basis of these results.

The reason for the shift in fluorescence emission of the high R - B concentration films could be due to inner filter effects. Thus although the absorption spectra are linear combinations, the fluorescence emission spectra are not. This seems to suggest that the fluorescence of each individual dye is not independent of each other. Also from the nature of the results, in that the R-B dominates the fluorescence, it is possible to conclude that energy transfer is taking place, from R-6G to R-B.

A graph was plotted of the fluorescence of R-B against the absorption of R-B, which reflects the concentration of R-B, in the mixture. From figure (3.21) it can be seen that as the concentration of R-B is increased, the fluorescence increases to a maximum and then decreases. The maximum of the R-B contribution to the film fluorescence from the model system is at a ratio of 1 : 1. This also shows limitation due to concentration.

Thus from the two curves one can deduce two things, firstly there is energy transfer taking place from the R-6G to the R-B in the solid matrix. Secondly the most efficient system seems to be a 1 : 1 ratio of R-B : R-6G.

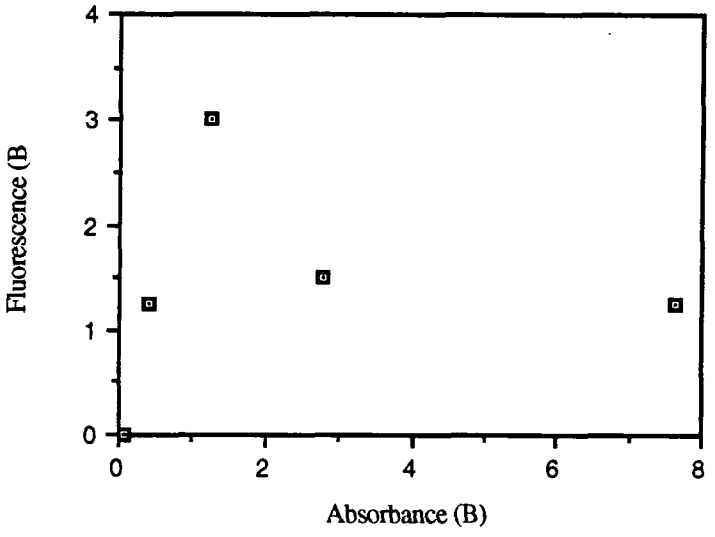

Figure (3.21) Fluorescence vs Absorption of R-B.

3.5.2.3 The effect of R300 concentration on the absorption and fluorescence spectra on the mixed BASF dye system.

A similar series of experiments were performed on newly developed dyes by BASF, called O240 and R300. These are perylene derivatives [Ivri J. et al., (1990)] and have been developed for their photo and thermal stability and efficiency for solar light collection and concentration. Also solid state dye laser action has been demonstrated [Reisfeld R. et al., (1989)] using the O240 dye.

The effect of different dye concentrations ratios was explored in order to determine which ratio gave the most efficient energy transfer. Solutions were made of the dyes in PMMA and the solvent used was dichloromethane, the amounts of dye used is given in the table (3.7).

R300 : O240	Wt. R300 (g)
4 : 1	0.02651
2 : 1	0.01325
1 : 1	0.00663
0.5 : 1	0.00331
0.25 : 1	0.00166

Table (3.7) Quantities of BASF dyes used.

The weight of O240 was kept constant at 6.63 mg and the weight of PMMA used was 2.651 g in 20 ml dichloromethane. The solutions were stirred for approximately 12 hours. From the solutions thin films were dipped at a withdrawal speed of 30 mm/min. The films were then left to dry at room temperature for 24 hours.

Using a Perkin Elmer Lambda 19 spectrophotometer, absorption measurements were recorded for each film, see figures (3.22 - 3.23). The absorption spectra for O240 shows pronounced structure reflecting the coupling of the electronic transition with the ~ 1300 cm^{-1} vibrational bending modes of the perylene skeleton. The three most prominent peaks are at 457.5, 489.4, and 526.2 nm.

The R300 dye, however, shows a different structure. The absorption spectrum shows a single peak at 565.6 nm, with a shoulder. The absorption spectra of the mixed films at the different dye concentration ratios show an increase in the contribution of R300 with increasing concentration. Thus to quantify the ratios of the dyes in the polymer film, linear combinations of the absorption spectra of the pure O240 and R300 were tried, to match the absorption spectra of the mixed dye samples. i.e.

$$\text{Abs (R300:O240)} = \alpha\text{Abs(1:0)} + \beta\text{Abs(0:1)}$$

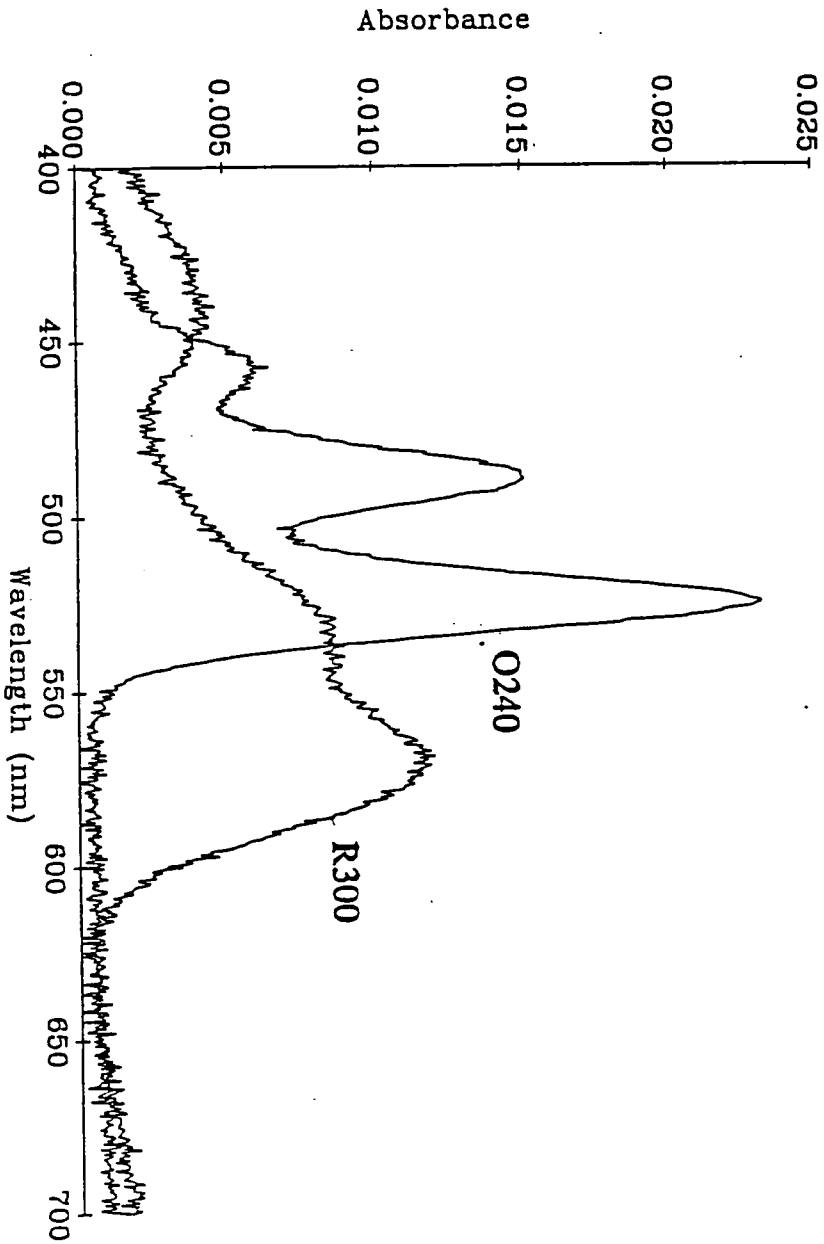

Figure (3.22) Absorption spectra of the BASF dyes R300 and O240.

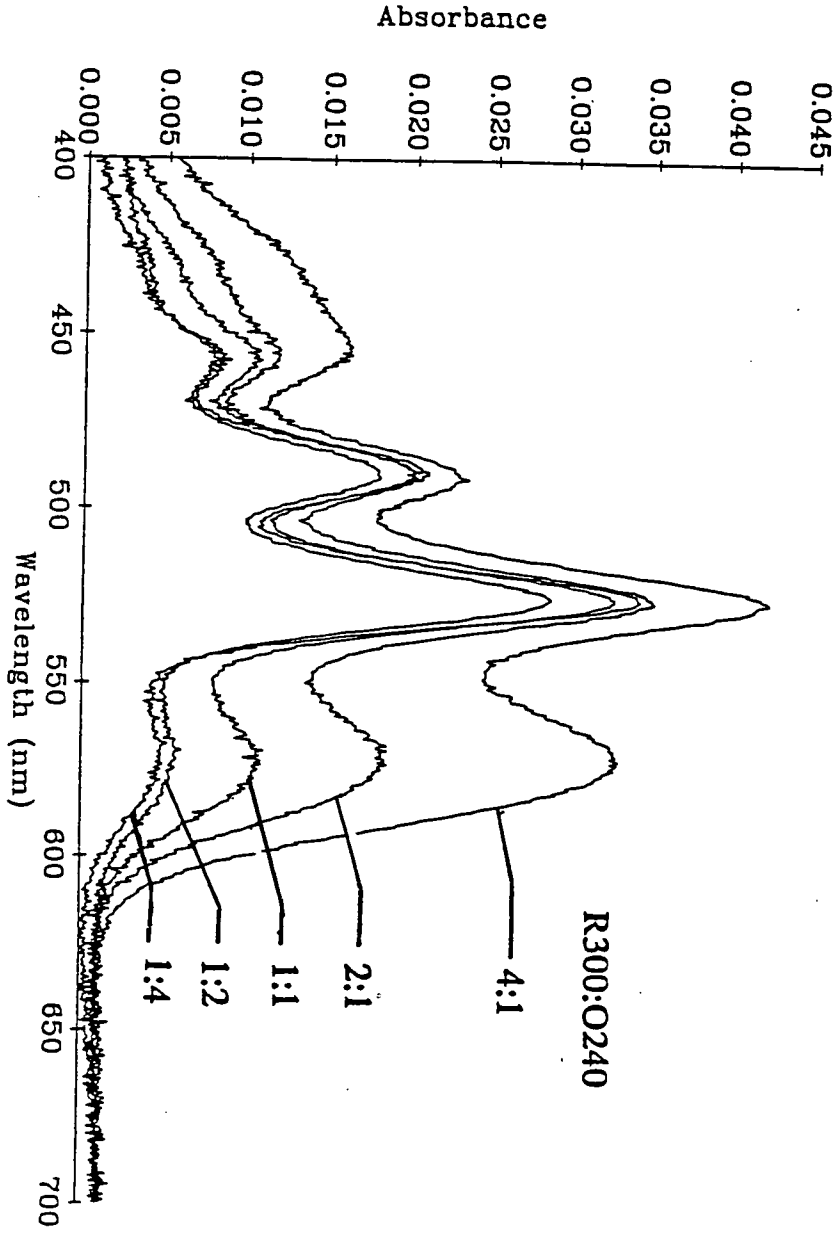

Figure (3.23) Absorption spectra of the mixed BASF dye films.

The background was removed from all the spectra to remove any unnecessary biases. Table (3.8) shows the result from this exercise.

From the table below it can be seen that a simple linear combination method can be used to match the individual absorption spectra of the dyes to the absorption spectra of the mixed dye film. This suggests that there are no interactions between the dyes which may have any affect on the profile of the absorption spectra. The actual ratios are close to those expected.

Expected R300 : O240	R300 α	O240 β	Actual R300 : O240
4 : 1	3.5	1.1	3.18 : 1
2 : 1	1.8	1.2	1.5 : 1
1 : 1	0.85	1.15	0.74 : 1
0.5 : 1	0.8	2.1	0.38 : 1
0.25 : 1	1.1	4.5	0.24 : 1

Table (3.8) Linear combinations of the individual dyes to match the absorption spectra.

Having determined that the absorption process of each dye is independent of the other, the next stage was to determine whether the fluorescence from the mixed films is also a simple linear combination of the individual dyes, and how the contribution of the individual components vary with the concentration ratio.

Using a Perkin Elmer Lambda 5 Fluorimeter the samples were excited at 486 nm and the fluorescence emission spectra of the mixtures were recorded. See figures (3.24 - 3.25) for the results. The results of the linear combinations of the fluorescence spectra are shown in table (3.9).

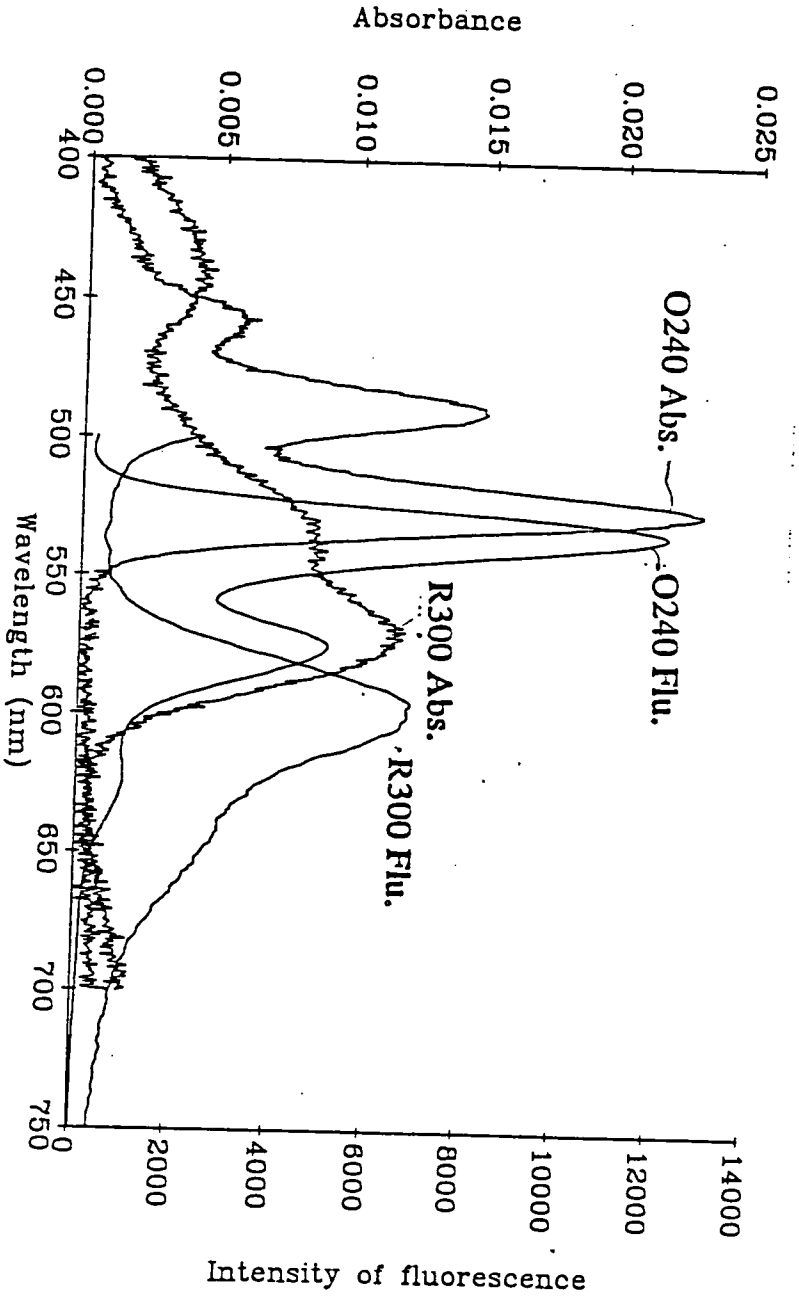

Figure (3.24) Absorption and fluorescence spectra of R300 and O240.

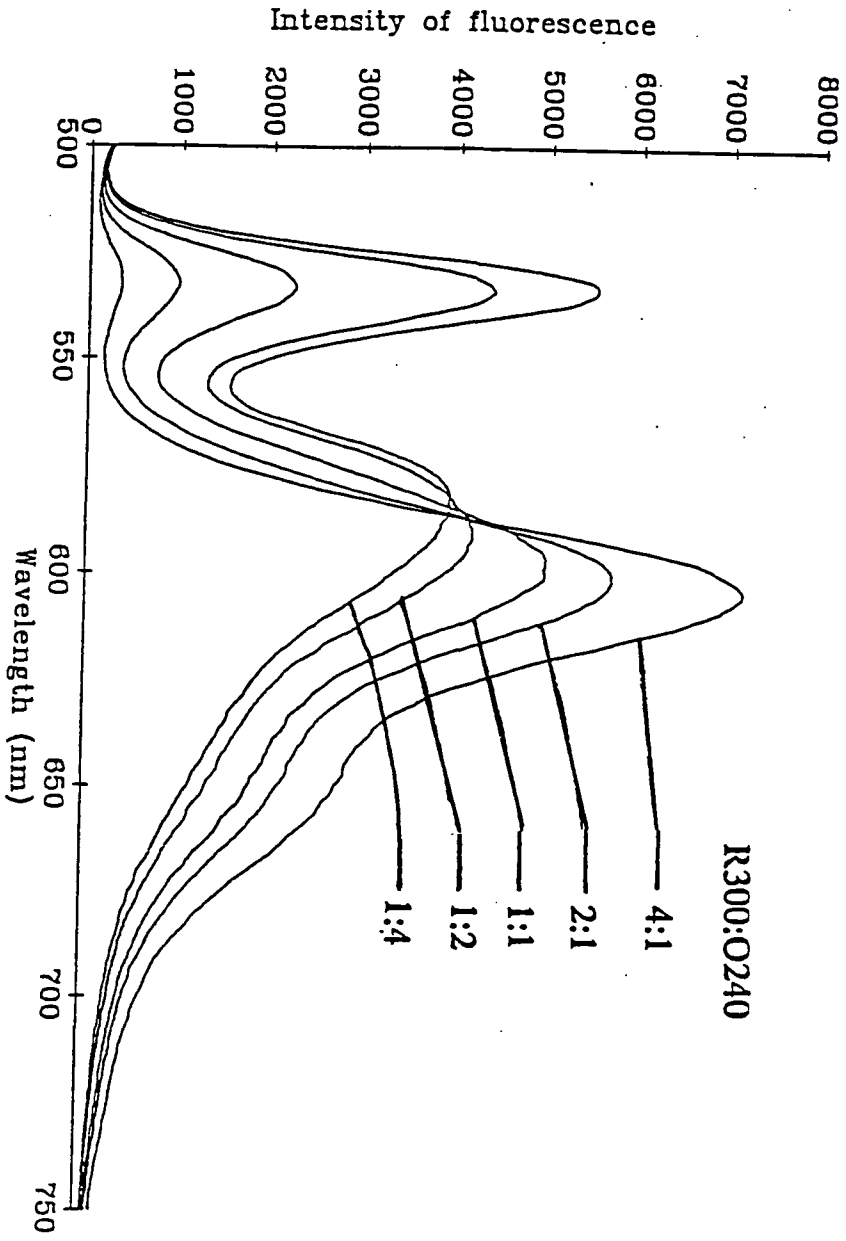

Figure (3.25) Fluorescence spectra of the mixed BASF dye films.

R300 : O240	R300 (±0.001)	O240 (±0.001)
3.18 : 1	10.3	0.01
1.5 : 1	8.48	0.036
0.74 : 1	7.27	0.164
0.38 : 1	5.3	0.359
0.24 : 1	4.3	0.455

Table (3.9) Linear combination of the individual dyes to match the fluorescence spectra.

From the graphs and table (3.9) it can be seen that at high R300 concentrations, there is very little contribution from the O240 to the fluorescence emission of the mixed sample. Also the fluorescence emission is red shifted from the maxima of the R300, this could be due to re-absorption effects due to the high concentrations of R300 used. At low concentrations there is a larger contribution from O240 to the emission.

A graph of the fluorescence dominance is shown in figure (3.26). From this graph it can be seen that the fluorescence of R300 dominates in the mixture at high concentration ratios, in spite of not being directly excited at the absorption maxima, unlike the O240 which is excited in the main absorption band, but does not seem to contribute. This is direct evidence of energy transfer between the two dyes. From the concentration range considered here the 3.18 : 1 ratio seems to be the most efficient system.

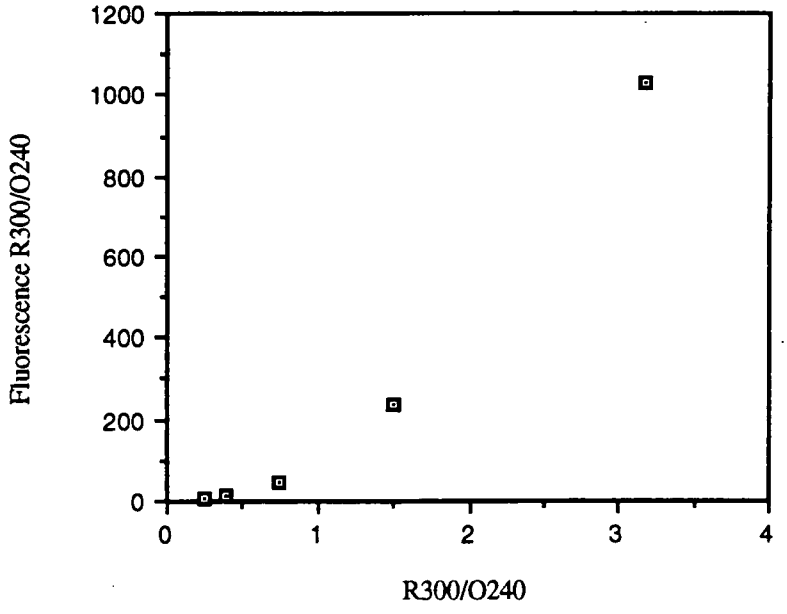

Figure (3.26) Fluorescence dominance curve.

So from this form of analysis, using the absorption and fluorescence spectra of the pure dyes and of the mixed samples, it is possible to determine that energy transfer is taking place between the two dye pairs considered. It also seems that this process is efficient in exciting the acceptor molecule, since the fluorescence intensity of the acceptor is so much higher in the mixed sample than in the pure sample.

3.6 Conclusion.

In this chapter the stringent requirements of the dye in a dye laser have been discussed. Also the advantages of using energy transfer as a mechanism of exciting the lasing dye have been outlined. In view of these points, absorption and fluorescence spectra were initially taken of pure dyes in different host polymer thin films, in order to select certain dyes as candidates for energy transfer.

Taking two dye pairs namely R-6G/R-B and the very stable O240/R300 BASF dyes, absorption and fluorescence spectra were recorded at different concentration ratios in a polymer thin film. This was done to observe, firstly the effect of energy transfer on the absorption and fluorescence spectra, and secondly to use this effect to determine the optimum concentration ratio for the dyes.

Although this is a very qualitative means of assessing the efficiency of energy transfer, it is however a necessary procedure for identifying and eliminating other possible non-radiative deactivation processes. Since they will show up in the absorption spectrum of the mixed dye sample.

Efficient non-radiative energy transfer was observed in both dye pairs considered and an optimum concentration ratio was determined . Most importantly it was seen how efficient energy transfer was in exciting the acceptor dye, since the fluorescence intensity of the acceptor was so much greater in the mixed samples than in the pure samples.

3.7 References.

Altman J. C., Stone R. E., Dunn B. and Nishida F.,"Solid state laser using a rhodamine doped silica gel compound.", IEEE Photo. Tech. Lett., Vol 3, No 3, pp 189 - 190, (1991).

Aoyagi Y. and Namba S.,"Laser oscillation in simple corrugated optical waveguide.", Appl. Phys. Lett., Vol 24, No 11, pp 537-539, (1974).

Avnir D., Levy D. and Reisfeld R.,"The nature of the silica gel as reflected by spectral changes and enhanced photostability of trapped rhodamine 6G.", J. Phys. Chem., Vol 88, pp 5956 - 5959, (1984).

Egami C., Nakagawa K. and Fujiwara H.,"Phase conjugation in Methyl-Orange-doped PVA films by photoinduced anisotropy.", Jap. J. Appl. Phys., Vol 29, No 8, pp 1544-1546, (1990).

Fletcher A. N., Pietrak M. E. and Bliss D. E.,"Laser dye stability, part 11. The fluorinated azacoumarin dyes.", Appl. Phys.. B., Vol 42, pp 79-83, (1987).

Gregg D. W. and Thomas S. J., "New lasing organic dyes flashlamp-pumped.", IEEE J. Quan. Elec., Vol 5, pp 302-303, (1969).

Gromov D. A., Dyumaev K. M., Manenkov A. A., Maslyukov A. P., Matyushin G. A., Nechitailo V. S. and Prokhorov A. M.,"Efficient plastic-host dye lasers.", J. Opt. Soc. Am., Vol 2, No 7, pp 1028 - 1031, (1985).

Ivri J., Burshtein Z., Miron E., Reisfeld R. and Eyal M.,"The perylene derivative BASF-241 solution as a new tunable dye laser in the visible.", IEEE. J. Quan. Elect., Vol 26, No 9, pp 1516-1520, (1990).

Kamat P. V. and Fox M. A.,"Photophysics and Photochemistry of Xanthene dyes in Polymer solutions and films.", J.Phys. Chem., Vol 88, pp 2297 - 2302, (1984).

Knabke G., Franke H. and Frank W. F. X.,"Electro-optical properties of a nonlinear dye in poly(methyl methacrylate) and poly(-methyl styrene).", J. Opt. Soc. Am. B., Vol 6, No 4, pp 761-764, (1989).

Kuzyk M. G. and Dirk C. W.,"Quick and simple method to measure third order nonlinear optical properties of dye doped polymer films.", Appl. Phys. Lett., Vol 54, No 17, pp 1628-1630, (1989).

Matsuda A. and Iizima S.,"Preferential doping of rhodamine 6G in a polyurethane optical solid circuit.", Appl. Phys. Lett., Vol 30, No 11, pp 571 - 573, (1977).

McKiernan J. M., Yamanaka S. A., Dunn B. and Zink J. I.,"Spectroscopy and laser action of rhodamine 6G doped aluminosilicate Xerogels.", J. Phys. Chem., Vol 94, pp 5652 - 5654, (1990).

Muto S., Fukasawa A., Ogawa T., Morisawa M. and Ito H.,"Breathing monitor using dye-doped optical fiber.", Jap. J. Appl. Phys., Vol 29, No 8, pp 1618-1619, (1990).

Muto S., Ito C. and Inaba H.,"Continuously tunable energy transfer laser operation in four-dye mixture systems.", Elect. Comm. Jap., Vol 66-C, No 11, pp 120-126, (1983).

Muto S., Shiba F., Iijima Y., Hattori K. and Ito C.,"Solid thin-film energy-transfer dye lasers.", Elect. Comm. Jap. Part 2., Vol 70, No 1, pp 21-31, (1987a).

Muto S., Uchida H. and Nakamura K.,"Characeristics of thin film energy transfer dye laser with DFB oscillator-amplifier system.", Elect. Comm. Jap. Part 2., Vol 70, No 2, pp 1512-1517, (1987b).

Okamoto N. and Tashiro S.,"Optical waveguides of polymethyl methacrylate doped with benzophenone and coumarin.", Opt. Comm., Vol 66, No 2,3, pp 93-96, (1988).

Pavlopoulos T. G., Shah M. and Boyer J. H.,"Efficient laser action from 1,3,5,7,8-pentamethylpyrromethane-BF_2 complex and its disodium 2,6-disulphonate derivative.", Opt. Comm., Vol 70, No 5, pp 425-427, (1989).

Reisfeld R., Brusilovsky D., Eyal M., Miron E., Burstein Z. and Ivri J.,"A new solid state tunable laser in the visible.", Chem. Phys. Lett., Vol 160, No 1, pp 43 - 44, (1989).

Salin F., Le Saux G., Georges P., Brun A., Bagnall C. and Zarzycki J.,"Efficient tunable solid state laser near 630 nm using sulforhodamine 640-doped silica gel.", Optics Letters, Vol 14, No 15, pp 785 - 787, (1989).

Tanaka H., Takahashi J., Tsuchiya J., Kobayashi Y. and Kurokawa Y.,"The high dispersion of organic dye into a transparent alumina film and its

application to photochemical and non-photochemical hole burnings.", J. Non-Crys. Sol., Vol 109, pp 164-170, (1989).

Urisu T. and Kajiyama K.,"Concentration dependence of the gain spectrum in methanol solutions of rhodamine 6G.", J. Appl. Phys., Vol 47, No 8, pp 3559-3562, (1976).

CHAPTER 4

Electronic energy transfer in polymer thin films.

4.1 Introduction.

The study of energy transfer between donor and acceptor dye molecules in solution and condensed media has both theoretical and practical importance. In photosynthesis, for example, dyes transfer optical energy from one spectral region to another. Dyes can increase the efficiency in solar energy conversion by absorbing the energy in a wide spectral region. Energy transfer can also improve the lasing efficiency of an acceptor dye by exciting it over a wide range of wavelengths, and so the threshold pump intensity required for the direct excitation of the acceptor dye is lowered. With a multiple dye mixture the effective tuning range of a dye laser can be increased. Energy transfer can also be useful in cases where the output wavelength is required to be far removed from the excitation wavelength. It is thus important to understand the mechanisms for energy losses and transfer in pure and binary dye mixtures. Experiments have shown that the excitation energy may be efficiently transferred from a photoexcited molecule (the donor) to an unexcited molecule (the acceptor).

In this chapter the theoretical description of energy transfer, in particular involving long range dipole - dipole interaction, will be discussed in some detail. A formulation is arrived at, expressed in experimentally determinable parameters, which can be used to measure the efficiency of the energy transfer process.

In order to investigate the extent of energy transfer in the mixed dye samples, the effect of the acceptor dye concentration on the donor dye fluorescence lifetime was measured. Time correlated single photon counting experiments were performed to

measure the fluorescence lifetimes of the dyes in the mixtures in the thin polymer film. The experimental techniques and apparatus will be described in detail in section (4.3). The results and conclusions of experiments on two dye pairs are presented. The experiments were performed at Imperial College, London and at Lancaster University, since the time correlated single photon counting equipment was not available at Durham University.

4.2 Electronic energy transfer : Theory.

The first observation of energy transfer was made by Cario and Franck, (1923) in their classical experiments on sensitized fluorescence of mercury and thallium atoms in the vapour phase. A mixture, when irradiated with light of the Hg resonance line showed emission spectra of both atoms. Since Th atoms did not absorb the exciting light, they could only be excited indirectly by an excitation transfer from Hg atoms. A transfer by re-absorption was impossible here. Therefore, this transfer was non-radiative with the Hg atom as the donor and the Th atom as the acceptor. The ambiguity of the occurrence of energy transfer between either distant atoms or during normal collision was resolvable in similar cases, as in the Hg sensitized fluorescence of Na. In this case the transfer occurs over distances very much larger than those in normal collisional separations.

The first observations of sensitized fluorescence in solution, though qualitative, were made by Perrin, (1929). Quantitative experiments were performed by Förster, (1949) with trypaflavine and rhodamine, where only the quenching in the donor fluorescence resulting from excitation transfer was followed quantitatively. Nevertheless, transfer over a separation of 70Å was established and the non - trivial nature of this transfer (see section (4.2.2)) was recognised by quenching experiments

which indicated a decrease in lifetime of the excited donor. Similar results were obtained by Galanin, (1951) for a large number of systems, where the decrease in donor lifetime was measured directly. The first measurements where the intensities of both fluorescence components could be followed quantitatively were those of Watson, (1950) with chlorophylls.

Perrin J., (1927) recognised that weak interaction between distant atoms or molecules may be sufficient for excitation transfer, provided some kind of resonance condition is fulfilled, and formulated a theory based on classical physics.

More recently, however, there has been considerable research on energy transfer looking at different dye systems in solution. Different experimental techniques have been used to investigate the nature of the energy transfer in dye mixtures. For example Lin and Dienes, (1973) studied excitation transfer as a function of acceptor concentration in the laser dye mixture of rhodamine 6G - Cresyl Violet by measuring the donor fluorescence lifetime. Kusumoto, (1978) studied energy transfer between 3,3'-diethylthiacarbocyanine iodide and rhodamine 6G by observing the reabsorption effect. Sebastian and Sathianandan, (1980) and Sabry and Mekawey, (1990) have looked at energy transfer between various dyes in solution by monitoring the donor emission peak wavelength. Singh, (1990) studied a dye mixture for energy transfer using a laser fluorimeter.

Energy transfer studies have also been carried out in the solid state. Muto, (1987) have looked at various dye pairs for energy transfer with a nitrogen laser as a pump source, which excites both dyes and therefore allows greater tuneability in the output, since the output is a combination of the total fluorescence. There has also been emphasis recently to formulate a generalised model for non-radiative energy transfer

between dyes Ali, (1989) and Speiser and Katraro, (1978) have shown that the output can be manipulated by varying either the donor or acceptor concentrations.

Table (4.1) summarises some of the features of the mechanisms involved in energy transfer. Experimental differentiation between these phenomenological types of energy transfer can be accomplished by measuring the donor fluorescence lifetime as a function of acceptor concentration, and some of the features listed in table (4.1).

	non-trivial transfer	reabsorption	complexing	encounter
Dependence of efficiency on increasing volume	none	increase	none	none
Dependence of rate on increasing viscosity	none	unchanged	none	decreased
Donor lifetime	decreased	unchanged	unchanged	decreased
Donor fluorescence spectrum	unchanged	changed	unchanged	unchanged
Donor absorption spectrum	unchanged	unchanged	changed	unchanged

Table (4.1) Mechanisms involved in energy transfer.

We shall now look in more detail into the mechanism of energy transfer between a donor dye and an acceptor dye.

Energy transfer can be defined as *any transfer of energy from an excited molecule to other species.*

$$D^* + A \dashrightarrow D + A^*$$

The energy transfer process may involve two steps with the intermediacy of a photon (radiative transfer) or may be a one step process (non-radiative transfer) requiring direct interaction of the excited donor with the acceptor.

4.2.1 Radiative transfer (The trivial process)

Radiative transfer of electronic energy involves the possibility of reabsorption of the donor emission. The process requires two steps with the intermediacy of a photon,

$$D^* \rightarrow D + h\nu$$

$$A + h\nu \rightarrow A^*$$

No direct interaction of the donor with the acceptor is involved. Obviously only energies corresponding to that part of the donor emission spectrum which overlaps with the acceptor absorption spectrum can be transferred. The efficiency of the energy transfer is governed by the quantum yield of emission from the donor and by the Beer - Lambert law regarding the absorption of this emission by the acceptor. The transfer can occur over very large distances (relative to molecular diameters) and the probability that an acceptor molecule reabsorbs the light emitted by a donor at a distance R varies as R^{-2}.

Radiative energy transfer may be characterised by (1) the invariance of the donor emission lifetime in the presence of an acceptor, (2) a change in the emission spectrum of the donor which can be accounted for on the basis of the acceptor absorption spectrum and (3) a lack of dependence of the transfer efficiency upon the viscosity of the medium.

4.2.2 Non-radiative transfer (Non - trivial transfer)

Non-radiative transfer of electronic energy involves the simultaneous de-excitation of the donor and excitation of the acceptor : a one step process which does not involve the intermediacy of a photon. Some interaction of the donor and acceptor is necessary and the ~~virtual~~ transitions in the donor and acceptor must be very close in energy. Efficient transfer may occur even with a small amount of interaction so that quite long range transfers are possible.

4.2.2.1 Resonant or Coupled Transitions.

In most of the mechanisms for non-radiative excitation transfer close resonance between the initial ($D^* + A$) and final ($D + A^*$) states is required. This condition is fulfilled if the transition in the donor ($D^* \rightarrow D$) and the transition in the acceptor ($A \rightarrow A^*$) involve nearly the same energy, the excitation transfer being the simultaneous occurrence of the two coupled or resonant transitions. If there is a difference in the electronic energy gaps for the two transitions, it may be made up by including the vibrational levels in the donor and acceptor.

Figure (4.1) represents a simplified energy level diagram of both molecules. During the absorption process, the donor is excited to a vibrational level of its first electronic excitation state. From there it is converted to lower vibrational levels of the same electronic state, by obtaining thermal equilibrium with the surrounding medium.

If the energy transfer (typically 10^{-8} sec.) is slower than the vibrational relaxation (typically 10^{-13} - 10^{-12} sec.) in the donor excited state and the temperature is not too high, the initial state has both the excited donor and acceptor in vibrationless

states. The excited donor molecule would normally return to the ground state by spontaneous radiative or non-radiative processes.

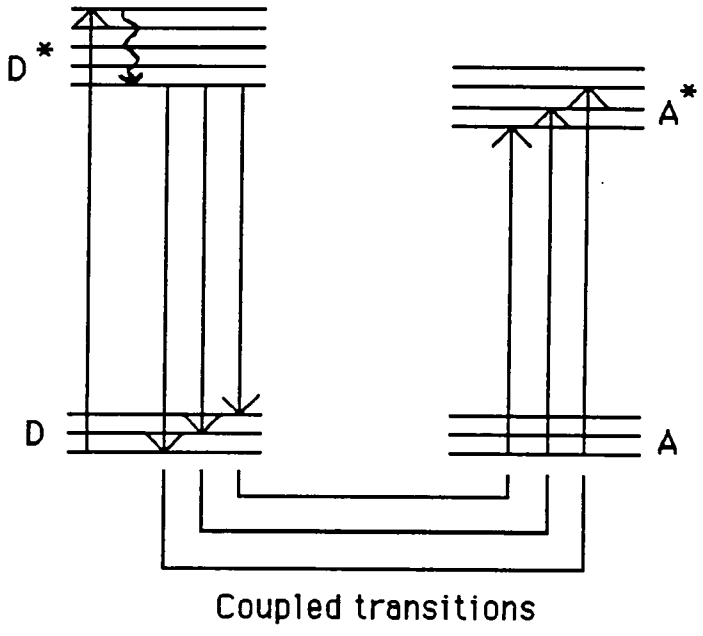

Figure (4.1) Energy level diagram showing a resonantly coupled transition.

If the energy difference for one of these possible de-activation processes in the donor molecule corresponds exactly to that for a possible absorption transition in a nearby acceptor molecule, then the energy transfer process is a vertical one, i.e., the transitions in both the donor and acceptor proceed in accordance with the Franck - Condon principle. With sufficient energetic coupling between these molecules, both emission and absorption may occur simultaneously, resulting in transfer of excitation from donor to acceptor. The energy transferred must correspond to a frequency which is common to the appropriate emission spectrum of the donor and the appropriate absorption spectrum of the acceptor. That is, it belongs to a region of overlap of the

two spectra. With increasing overlap, the number of possible coupled transitions increases and so also the probability for excitation transfer.

A spectral overlap integral J may be defined by :

$$J = \int_0^\infty F_D(\nu)\varepsilon_A(\nu)d\nu$$

F_D - spectral distribution of the donor emission.

ε_A - spectral distribution of the acceptor absorption.

each normalised to unity on a wavenumber scale so :

$$\int_0^\infty F_D(\nu)d\nu = \int_0^\infty \varepsilon_A(\nu)d\nu = 1$$

F_D and ε_A are chiefly determined by the Franck - Condon factors. Thus J is a measure of the number of possible final states together with the *Franck - Condon Factors* associated with the virtual transitions in the donor and acceptor which give rise to the various possible final states. Note that J as defined here has nothing to do with oscillator strengths of the transitions involved.

4.2.2.2 Donor - Acceptor Interactions.

Non-radiative excitation transfer can only occur if the initial (D^*+ A) state and final (D + A^*) state are degenerate or nearly so and if they are coupled by a suitable donor - acceptor interaction. The total interaction, β, is given as the matrix element of a perturbation between the initial (ψ_i) and final (ψ_f) states.

$$\beta = \int \psi_i \hat{H}' \psi_f d\tau = \int \psi_D.\psi_A \hat{H}' \psi_D \psi_A . d\tau$$

This includes all the electrostatic interactions of the electrons and nuclei of the donor and those of the acceptor. The total interaction can be expressed as a sum of the *coulomb* and *exchange* terms.

The dipole - dipole contribution of the coulomb term represents the interaction between the transition dipole moments of both molecules, the squares of which are proportional to the oscillator strengths of the radiative transitions in the isolated donor and acceptor molecules. The dipole - dipole interaction falls off as the inverse third power of the distance separating the interacting centres and can lead to interaction many times the molecular diameters.

The exchange interaction is a quantum - mechanical effect arising from the symmetry properties required of electronic wave functions with regard to the interaction of the space and spin coordinates of any two electrons in the donor - acceptor system. Since the exchange interaction represents the electrostatic interaction between two charge clouds, i.e. overlap, the interaction is necessarily of short range, on the order of collisional diameters. Hence, there is a very sharp fall off with donor - acceptor separation due to the approximately exponential decrease of electron density outside the boundaries of the molecules. Also the magnitude of the exchange interaction is not related to the oscillator strengths of the transitions in the donor and acceptor. If the transitions in the donor and acceptor are strongly forbidden the dipole - dipole term is very small and the exchange term usually predominates at close approach of donor and acceptor. However, when the transitions are fully allowed, the dipole - dipole term predominates.

For almost all cases in which the electronic energy transfer is slow compared to the vibrational relaxation in the donor and acceptor, the rate $n_{D^* \rightarrow A}$ for transfer is given

by equ (4.1) according to the time - dependent perturbation theory and based upon an interaction-of-continua model [Schiff L. I., (1949)].

$$n_{D^* \rightarrow A} = \frac{2\pi}{\hbar}\beta^2\rho_E \qquad (4.1)$$

ρ_E - density of states (number of resonant states per energy interval) and is related to the number of possible final states and thus to the extent of spectral overlap.

4.2.3 Transfer via dipole - dipole interaction.

Förster has developed a quantitative expression for the rate of long range electronic energy transfer due to dipole - dipole interactions shown in equation (4.2) :

$$k_{D^* \rightarrow A} = \frac{8.8 \times 10^{-25} K^2 \Phi_D}{n^4 \tau_D R^6} \int_0^\infty F_D(\nu)\varepsilon_A(\nu)\frac{d\nu}{\nu^4} \qquad (4.2)$$

ν is the wave number, $F_D(\nu)$ is the spectral distribution of the donor emission in quanta normalised to unity, $\varepsilon_A(\nu)$ is the molar extinction coefficient for the acceptor absorption, n is the refractive index of the medium, K is an orientation factor which equals $(\frac{2}{3})^{\frac{1}{2}}$ for a random distribution of donor and acceptor molecules, Φ_D is the quantum yield of donor emission, τ_D is the actual donor emission lifetime (in seconds), and R is the distance between the donor and acceptor molecules (in centimetres).

This formulation is based on the case where energy transfer is very much slower than vibrational relaxation, and considers only the dipole - dipole term in the coulomb interaction. The Förster relationship, equation (4.2), applies strictly only to those cases where the donor and acceptor are well separated and are immobile, the donor and acceptor exhibit broadened, relatively unstructured spectra, the spectral

overlap is significant [Katsuura K., (1965)], there are no important medium interactions, and the medium excited states lie much higher than those of the donor and acceptor.

In some cases the efficiency of the energy transfer ($\tau_D k_{D^*\rightarrow A}$) may be more critical than the rate of transfer. Since $\tau_D \propto 1/f_D$, and since $k_{D^*\rightarrow A} \propto f_D$, where f_D is the oscillator strength for the donor transition, the efficiency ($\tau_D k_{D^*\rightarrow A}$) of the excitation transfer should be nearly independent of the nature of the donor transition. Thus transfers involving spin forbidden transitions in the donors should be as efficient as those in which the donor transitions are allowed.

The efficiency of the Förster-type energy transfer is usually expressed in terms of a *critical radius* R_0, the distance between the donor and acceptor at which the rate of intermolecular energy transfer is equal to the sum of the rates for all other donor deactivation processes i.e.

$$k_{D^*\rightarrow A} = 1/\tau_D \qquad (4.3)$$

The expression for R_0 can be derived from equations. (4.2) and (4.3).

$$R_0^{\,6} = \frac{8.8\times10^{-25}K^2\Phi_D}{n^4}\int_0^\infty F_D(\nu)\varepsilon_A(\nu)\frac{d\nu}{\nu^4} \qquad (4.4)$$

The *critical concentration* of acceptor $C_A^{\,0}$ (moles/litre) at which the transfer is 50% efficient (the donor fluorescence is half quenched) is given by :

$$C_A^{\,0} = \frac{4.8\times10^{-10}n^2}{K}\left[\Phi_D\int_0^\infty F_D(\nu)\varepsilon_A(\nu)\frac{d\nu}{\nu^4}\right]^{-1/2} \qquad (4.5)$$

An approximate relationship between R_0 and $C_A^{\,0}$ is given by :

$$R_0(\text{Å}) = \frac{7.35}{(C_A^0)^{1/3}} \tag{4.6}$$

R_0 and $C_A{}^0$ do not depend on the donor transition strength since the efficiency of the excitation transfer has been shown to be independent of the strength of the donor transition.

In order to determine the rate of energy transfer from experimentally determinable parameters a Stern - Volmer relationship can be used [Lin C. and Dienes A., (1973)] :

$$\frac{\tau_{f^0}}{\tau_f} = 1 + k_{et}\tau_{f^0}[C_A] \tag{4.7}$$

where τ_{f0} - measured lifetime of the donor in the absence of the acceptor.

τ_f - measured lifetime of the donor in the presence of the acceptor.

C_A - acceptor dye concentration.

k_{et} - energy transfer rate in l/mol/s.

By re-arranging equation (4.7) to :

$$\tau_f^{-1} = \tau_{f^0}^{-1} + k_{et}[C_A] \tag{4.8}$$

it can be seen that a straight line plot of τ_f^{-1} vs $[C_A]$ will yield k_{et} as the gradient of the straight line, and τ_{f0} as the reciprocal of the y axis intercept. The critical concentration, $C_A{}^0$, can also be determined from equation (4.8), using the definition earlier as $\tau_f = {}^1/_2\tau_f^0$, hence also the critical radius, R_0, given by equation (4.6). Thus from these two values and equation (4.5), the value of the overlap integral can be determined.

The fluorescence lifetimes of the donor dye in the presence of the acceptor dye, at different concentration ratios, therefore has to be measured in order to determine the parameters of the energy transfer.

4.3 Experimental Details.

In order to measure the fluorescence lifetimes of dyes in the nanosecond region, sub-nanosecond pulse excitation is required with a fast electronic detection system to measure the fluorescence decay.

The technique of time correlated single photon counting, used at Imperial College London, enables lifetimes in the picosecond region to be measured. A schematic of the apparatus is shown in figure (4.2). The excitation source is a cavity dumped (Coherent model 7200/7220), mode - locked dye laser (Coherent model 701-3), synchronously pumped by a mode-locked (Coherent model 7600) cw Argon ion laser (Spectra Physics 164). Using rhodamine 6G in ethylene glycol, as the dye lasing medium, the output pulses are less than 10 picosecond duration and, at a repetition rate of 3.8 MHz, produce an average output power of ≈200 mW that is wavelength tuneable from 560 to 630 nm (vertically plane polarised). The samples are housed in a light tight environment. The fluorescence is collected perpendicular to the excitation beam, using fused silica collection optics which focuses the emission on to the slits of a 0.25 m monochromator (Rank Hilger D330) and is subsequently detected using either a microchannel plate photomultiplier, (MCP) (Hamamatsu R1564-UO1) or a side window photomultiplier (Hamamatsu R955) wired for single photon counting.

The time-to-amplitude converter, (TAC) (Ortec model 467) is run in an inverted mode of operation to take advantage of the high repetition rate of the laser. The stop

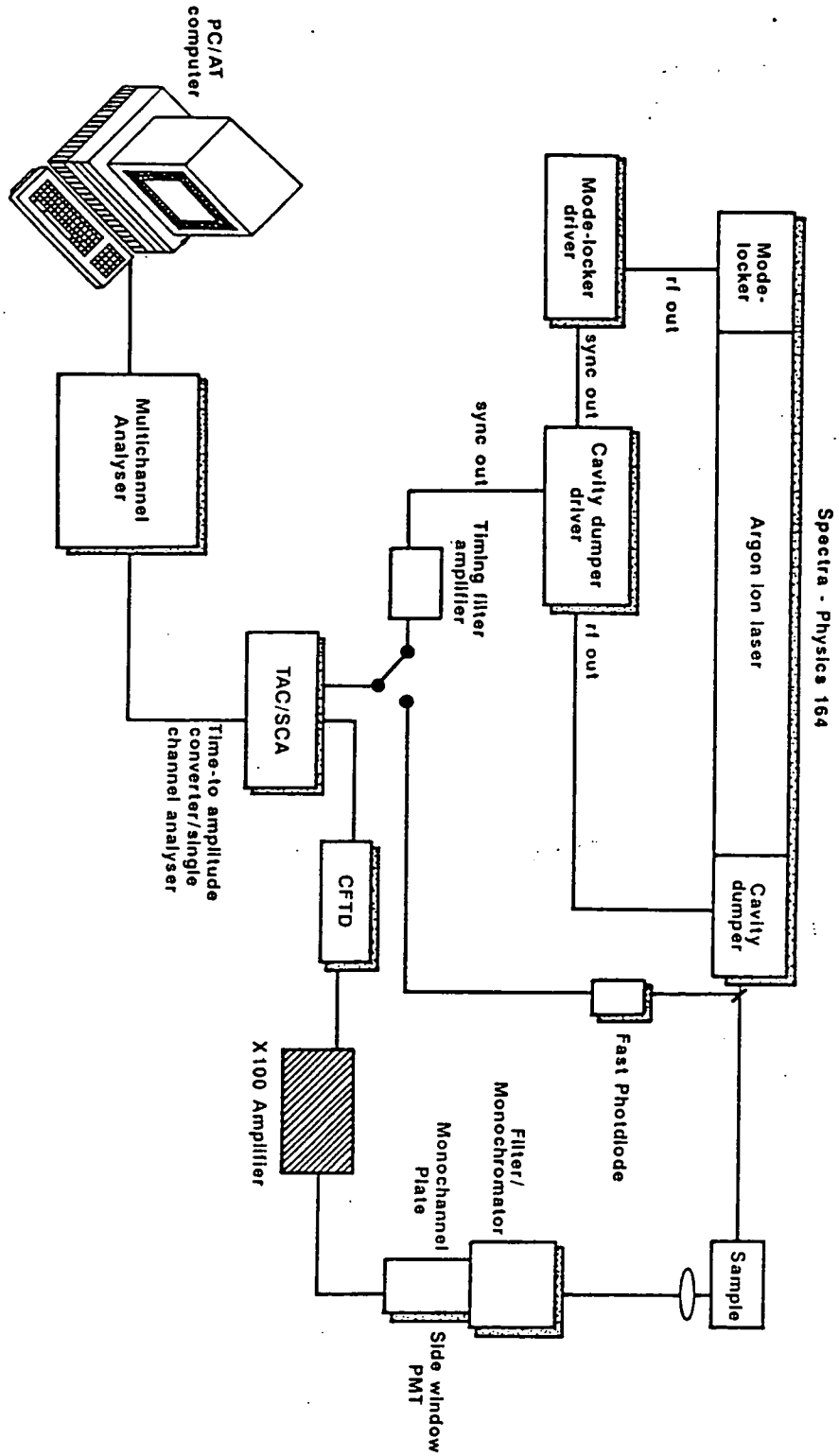

Figure (4.2) A schematic of the time correlated single photon counting apparatus used at Imperial College.

pulse is derived from synchronous TTL output from the cavity dumper driver (Coherent Model 7200), which is filtered and shaped using a timing filter amplifier (Ortec model 454), prior to being fed into the TAC. When using the MCP, to detect the fluorescence, the signal is amplified using a preamplifier with an overall gain of 100 (LeCroy VV101A). The signal is then processed using a constant fraction discriminator (Ortec model 584), and then fed into the start input of the TAC. The TAC output pulses are fed into the pulse height analysis input(s) of a multichannel analyser (Canberra series 35+) interfaced with a microcomputer (AST Premium 140 - IBM AT compatible).

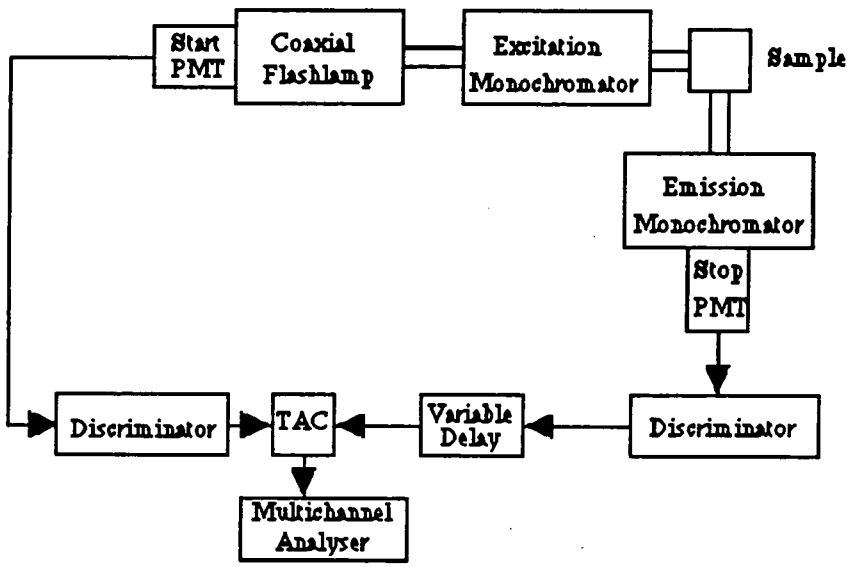

Figure (4.3) Schematic of experimental setup at Lancaster University.

The same technique of time correlated single photon counting was used at the Polymer Centre at Lancaster University. The apparatus was, however, different. The fluorescence lifetimes were measured using an Edinburgh Instruments 199 Fluorescence Spectrophotometer. A schematic diagram of the apparatus is shown in figure (4.3). The excitation source is a flashlamp with a repetition rate of approximately 40 MHz, with a pulse duration of 1-2 ns.

The heart of this method is a time to amplitude converter, which can be considered to be analogous to a fast stop watch. The sample is repetitively excited using a pulsed light source. Each pulse is optically monitored to produce a start signal which is used to trigger the voltage ramp of the TAC. The voltage ramp is stopped when the first fluorescence photon from the sample is detected. The TAC provides an output pulse whose voltage is proportional to the time between start and stop signals. A multichannel analyser converts this voltage to a time channel. Summing over many pulses the MCA builds up a probability histogram of counts versus time channels. The decay curve is then fitted to the relevent kinetic model using reconvolution analysis and the Marquardt algorithm.

In such instruments the frequency of photon detection is set at a rate which is about 1% of the repetition rate of the excitation source. This is to ensure that only one photon is detected for each excitation event and so the decay is not distorted.

When using the single photon counting technique, the instrument response function (the shape of the light pulse) must be measured. This is done by measuring scattered light from a bare microscope slide at the excitation wavelength. The actual decay measured G(t), is a convolution of the actual fluorescence decay, F(t), and the instrumental response function, P(t), i.e.

$$G(t) = F(t) \otimes P(t) = \int_0^{t_i} F(t')P(t_i - t')dt'$$

To analyse the data both the measured response and the instrumental response are fed into a computer which performs a reconvolution process, and fits a chosen mathematical model to the data by means of an iterative non-linear least squares method. The quality of fit of the data is checked using the χ^2, weighted residuals and

autocorrelation tests. The fluorescence decays are analysed using a Marquardt program [Spears K. G. et al., (1978)] which fits the decays to an exponential series i.e.

$$A + B_1e^{(-t/\tau_1)} + B_2e^{(-t/\tau_2)} + B_3e^{(-t/\tau_3)} + ...$$

Where τ_1, τ_2, τ_3, etc. represent the lifetimes to be fitted and B_1, B_2, B_3, etc. represent the relative contributions of the individual lifetimes defined as $(B_X\tau_X)/(\Sigma B_i\tau_i)$. Functions of this type provide good descriptions of the fluorescence decays, provided sufficient exponential terms are applied. There have been a number of models describing the energy transfer between two molecules under certain circumstances [Birks J. B., (1970)], and each model requiring specific conditions. Since the situation here of dye pairs with overlapping spectra in a solid polymer matrix does not provide a clear cut scenario for any particular model, and also since the situation can be compared to dye pairs in solution to a first approximation, a Stern - Volmer analysis has been adopted. This form of analysis can only be treated as approximate and to underline the effect of the acceptor concentration on the donor lifetime.

4.4 Experimental Results.

4.4.1 Dependence of the acceptor lifetime on the acceptor concentration in the mixed rhodamine dye system.

An experiment was performed to establish whether energy transfer was taking place between rhodamine 6G (R-6G) as the donor and rhodamine B (R-B) as the acceptor in a matrix of poly methylmethacrylate (PMMA) at various ratios, and to see the effect of varying the concentration of the acceptor dye in the mixture on the

fluorescence lifetime of the acceptor. This was to be determined using the fluorescence lifetime measuring apparatus at Imperial College.

4.4.1.1 Method.

The experiment was set up as shown in figure (4.2). The samples taken to Imperial College were of the ratios shown in Table (4.2). The weight of R-6G used was kept constant at 0.0096 g and the weight of PMMA used in each case was 2.651 g in 20 ml dichloromethane ($10\%^{w}/_{w}$). Also a 10^{-3} M solution of pure R-B in PMMA was made. Thin films were dipped onto glass microscope slides at a speed of 30 mm/min.

R-B : R-6G	wt. R-B (g)	conc. R-B (10^{-3}M)
4 : 1	0.03946	4
2 : 1	0.0192	2
1 : 1	0.0096	1
1 : 2	0.0048	0.5
1 : 4	0.0024	0.25
1 : 8	0.0012	0.125
1 : 0	0.0096	1

Table (4.2) Ratios, weights and concentrations of rhodamine B used.

The output from the dye laser was wavelength tuneable from 560 nm to 630 nm. 590 nm wavelength was chosen because at this wavelength there is predominantly R-B absorption and virtually no R-6G absorption, so that the R-B fluorescence could be analysed as a function of different concentration ratios. It was not possible with the

dye laser to obtain a wavelength where there was only R-6G absorption and no R-B absorption, i.e 488 nm.

4.4.1.2 Results.

The instrument response profiles were recorded at the excitation wavelength and the fluorescence decays were recorded, at a range of wavelengths from 600 nm to 675 nm, at 25 nm intervals, on a computer and saved on a floppy disc for later analysis. The lifetimes of the individual decays were determined using a computer program which fits a series of exponential decays to the data. The data recorded at each wavelength for a sample was globally analysed for a lifetime which fits at each wavelength. The program also produces χ^2 values for the fit. These values give an indication of the degree of the fit.

No signal could be detected from the R-6G sample, as one would have expected. The result of a global analysis on each sample across the emission wavelength range is given in table (4.3).

R-B : R-6G	τ_n (ns)	B_i	χ^2
2 : 1	τ_1 = 3.33 τ_2 = 1.62	66.83 33.17	1.292
1 : 1	τ_1 = 3.42 τ_2 = 1.53	80.68 19.32	1.046
1 : 2	τ_1 = 3.40 τ_2 = 1.35	85.65 14.35	1.027
1 : 0	τ_1 = 3.72 τ_2 = 1.91	86.52 13.48	1.145

Table (4.3) Globally analysed lifetimes for the different concentration ratios.

The pre-exponentials to the fitted functions of each decay curve show no variation of the relative contribution of each lifetime over the range of concentrations. The contribution of τ_1 is significantly greater than τ_2. Also the fact that the pre-exponentials and the lifetimes do not change their values very much over the range of wavelengths, substantiates the view that predominantly R-B is being excited, and the values are not dependent on the concentration of R-B.

A further global analysis was performed on the fluorescence lifetimes, of the three mixtures, measured at 600 and 625nm. This was done to see if there was any significant difference between the R-B fluorescence lifetimes measured in the three mixtures, i.e does the lifetime change with the concentration of R-B. The results were :

$$\tau_1 = 3.5 \text{ ns} , \tau_2 = 1.72 \text{ ns} , \chi^2 = 1.164.$$

From these results one can see that the two lifetimes are similar to those obtained before, with a reasonable χ^2 value. This suggests that globally (i.e. at each concentration) the two lifetimes have fitted well to the data, and so the lifetimes do not change significantly with the concentration of R-B. The pre-exponentials show that the contribution of τ_1 is still larger than τ_2.

A global analysis was performed on the fluorescence lifetimes of pure R-B and the 1 : 1 mixture. Since the concentration of R-B was the same in both, this was done to observe the effect of introducing R-6G to the mixture. The results were :

$$\tau_1 = 3.61 \text{ ns} , \tau_2 = 1.69 \text{ ns} , \chi^2 = 1.142.$$

From these results one can see that the two lifetimes are similar to those obtained before, with a reasonable χ^2 value. This suggests that the lifetime of R-B does

not change significantly with the introduction of R-6G. The pre-exponentials show that τ_1 is still larger than τ_2.

4.4.1.3 Conclusion.

From the results of this series of experiments the following points can be made. A pure R-B doped polymer film has given two lifetimes. This could be due to an artifact of the program whereby two lifetimes are necessary for a reasonable fit to the data. By predominantly exciting R-B it has been shown that its lifetime is independent of its concentration in the mixture, within the concentration range of interest. Also that it does not change significantly with the introduction of R-6G.

4.4.2 Dependence of the donor lifetime on the acceptor concentration in the mixed rhodamine dye system.

The aim of this experiment was to determine and quantify the energy transfer between rhodamine 6G and rhodamine B pairs in a PMMA matrix with different concentration ratios in terms of energy transfer rate. Also to calculate the Förster radius and the critical concentration.

4.4.2.1 Method.

The samples made were the same as those used in section (4.4.1). These dyes were dissolved into a matrix of PMMA at the same concentration ratios. Thin films were dipped from the solution onto glass microscope slides at a withdrawal speed of 30 mm/min.

The fluorescence lifetimes were measured using an Edinburgh Instruments 199 Fluorescence Spectrometer used in the Polymer Centre at Lancaster University. The

intensity of the light source was lower than the laser used at Imperial College, hence the decays took longer to collect.

4.4.2.2 Results

The excitation wavelength chosen was 480 nm. Since at this wavelength there is predominantly R-6G absorption, however there is also some R-B absorption. The fluorescence lifetime decays were recorded from all the samples prepared, and analysed in the same way as the data recorded at Imperial College. The decays were recorded at 570 nm, and are shown in figures (4.4 - 4.6). Table (4.4) shows a summary of the results recorded.

B : 6G ratio	Lifetimes (ns)	Relative contribution	χ^2
Pure R-6G	3.70 9.47	98.47 1.53	1.296
Pure R-B	1.70 4.00	12.48 87.52	1.063
1 : 4	3.56 7.49	94.97 5.03	1.435
1 : 2	3.54 7.67	93.50 6.50	1.225
1 : 1	0.32 3.36 6.96	3.91 84.55 11.54	1.216
2 : 1	0.55 3.20 7.32	9.66 78.26 12.07	1.259
4 : 1	0.24 2.48 6.71	14.70 64.12 21.18	1.475

Table (4.4) Lifetimes of rhodamine 6G with different ratios of rhodamine B.

4.4.2.3 Conclusion.

The table shows the fits to require two lifetimes in some cases and three lifetimes in other cases. The appearance of a third lifetime is possibly due to the program trying

to achieve a good fit. Since at 570 nm both dyes contribute to the emission spectrum with the R-6G predominating, the interpretation is that the lifetime with the highest contribution represents that of the rhodamine 6G. Hence to a first approximation the trend of the associated lifetime of rhodamine 6G decreases from 3.56 ns to 2.48 ns with increasing amount of rhodamine B present in the matrix. It can be seen that the lifetimes of the pure R-B are slightly different than those reported in table (4.3), this could be due to a combination of the systematic errors resulting from using two different apparatus for the same sample. These errors might have their origins in an excitation wavelength dependence for R-B.

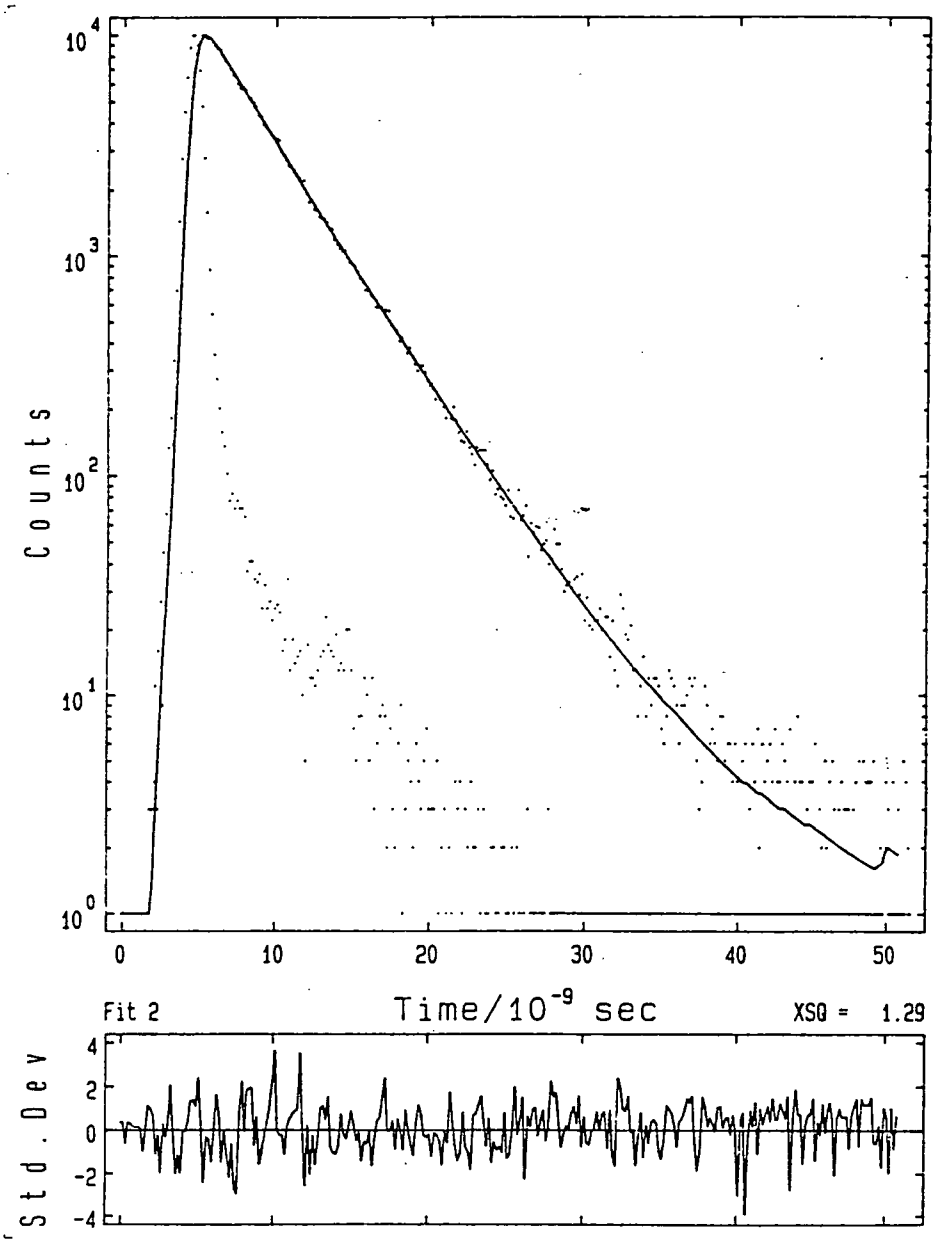

Figure (4.4) The fluorescence lifetime decay of rhodamine 6G.

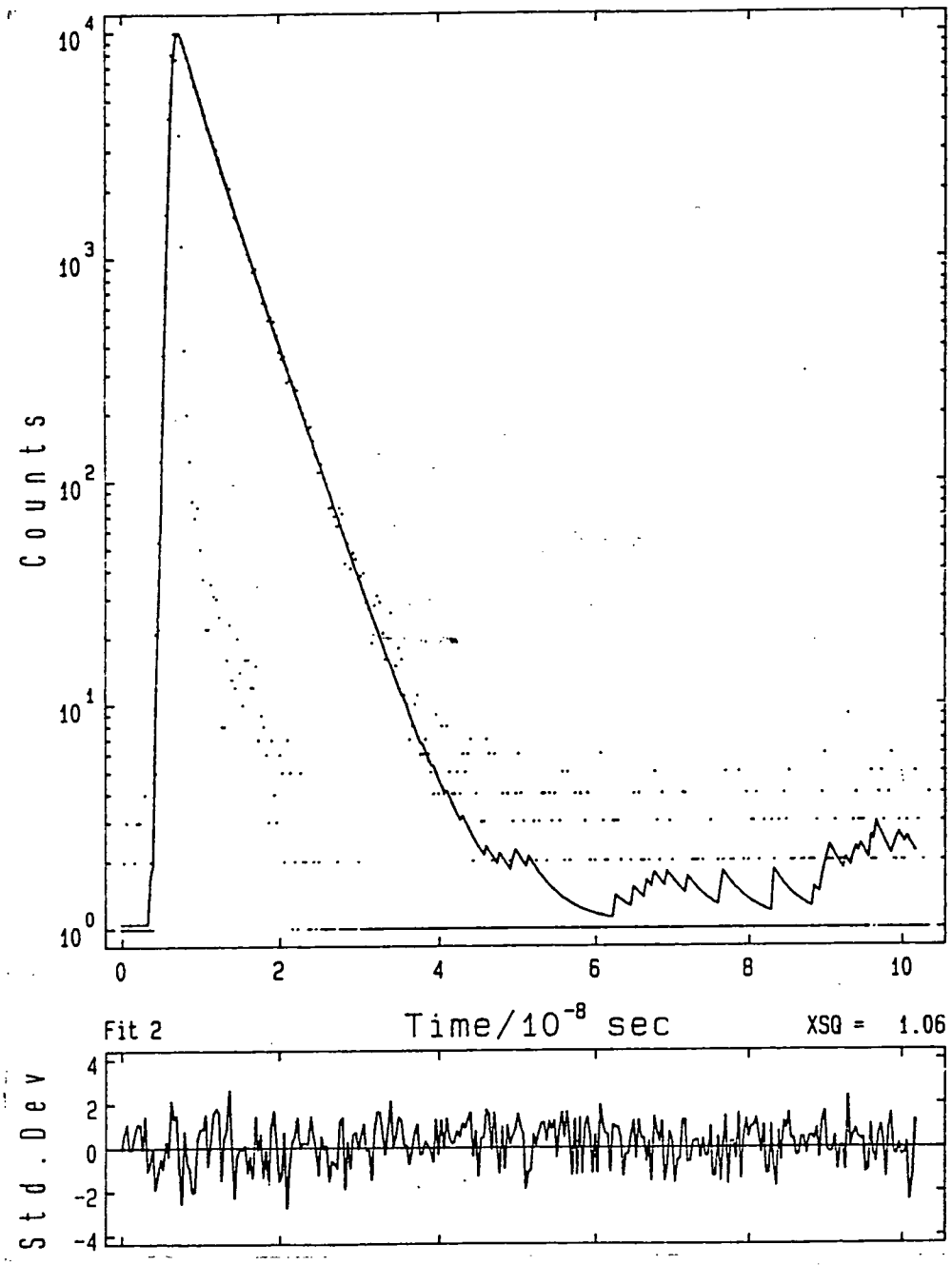

Figure (4.5) The fluorescence lifetime decay of rhodamine B.

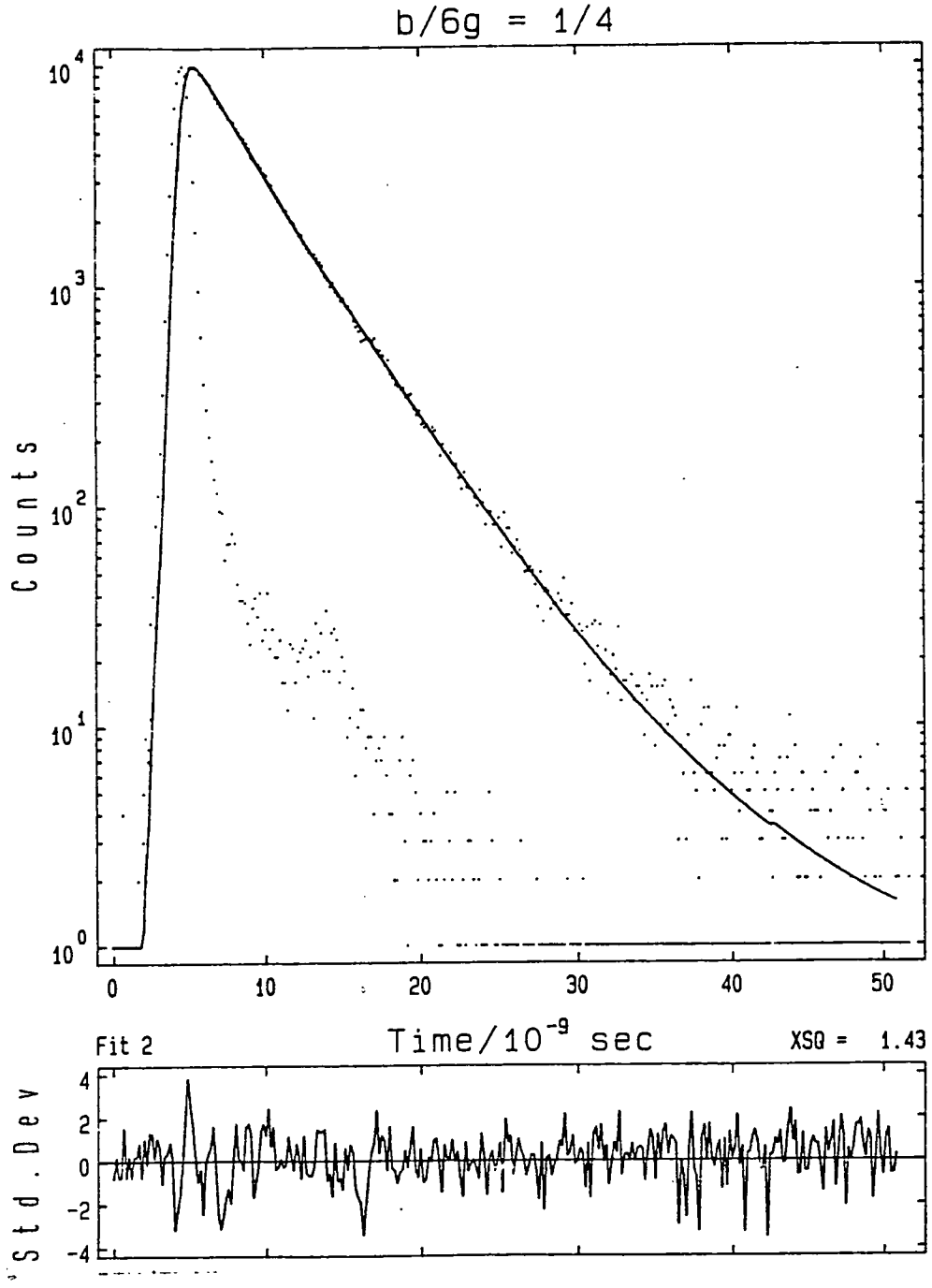

Figure (4.6) The fluorescence lifetime decays of the mixed dye system.

(a) B : 6G = 1/4 (b) B : 6G = 1/2 (c) B : 6G = 1 (d) B : 6G = 2 (e) B : 6G = 4 .

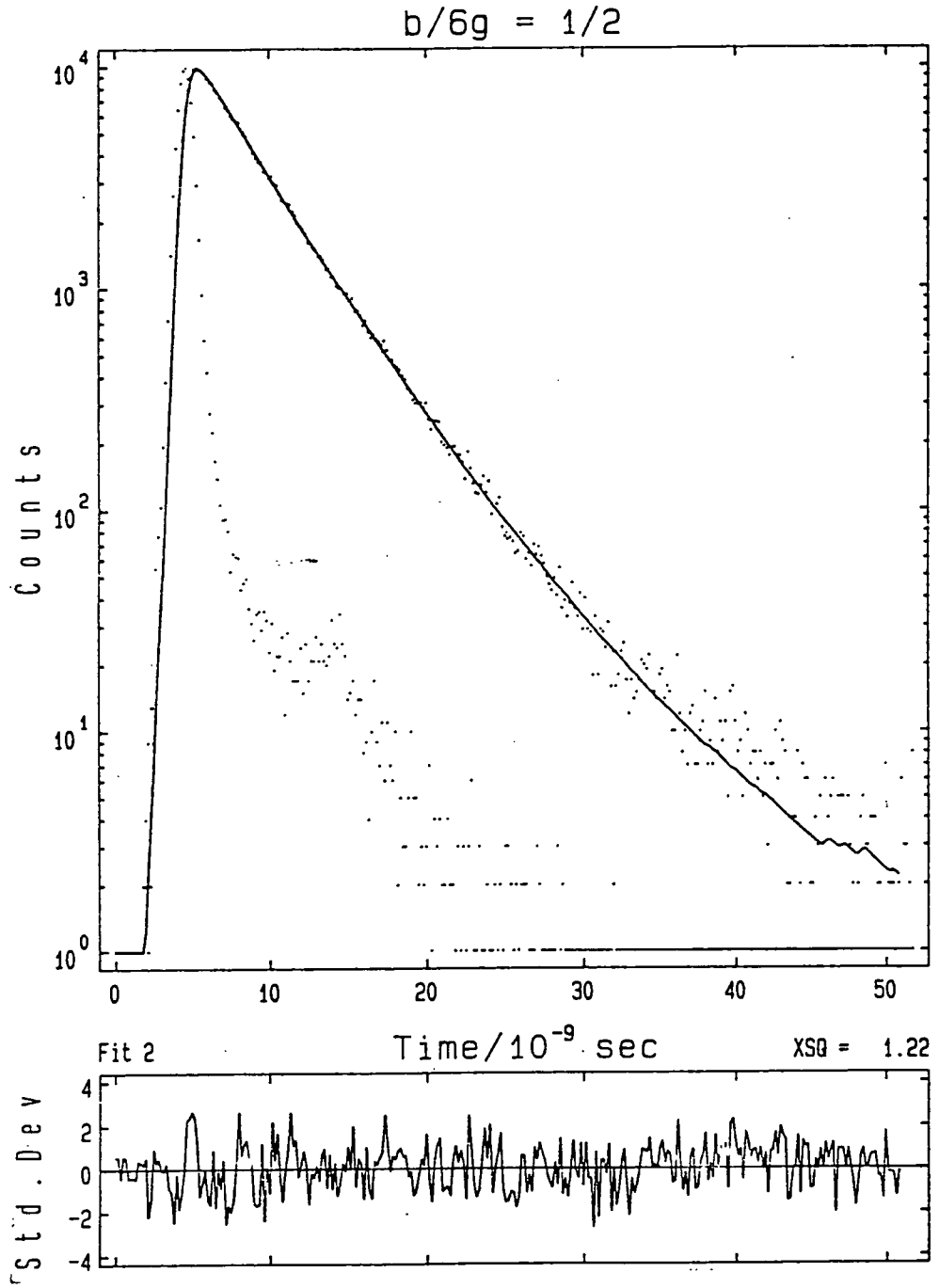
b/6g = 1/2
Counts
Time/10^-9 sec
Fit 2
XSQ = 1.22
Std. Dev

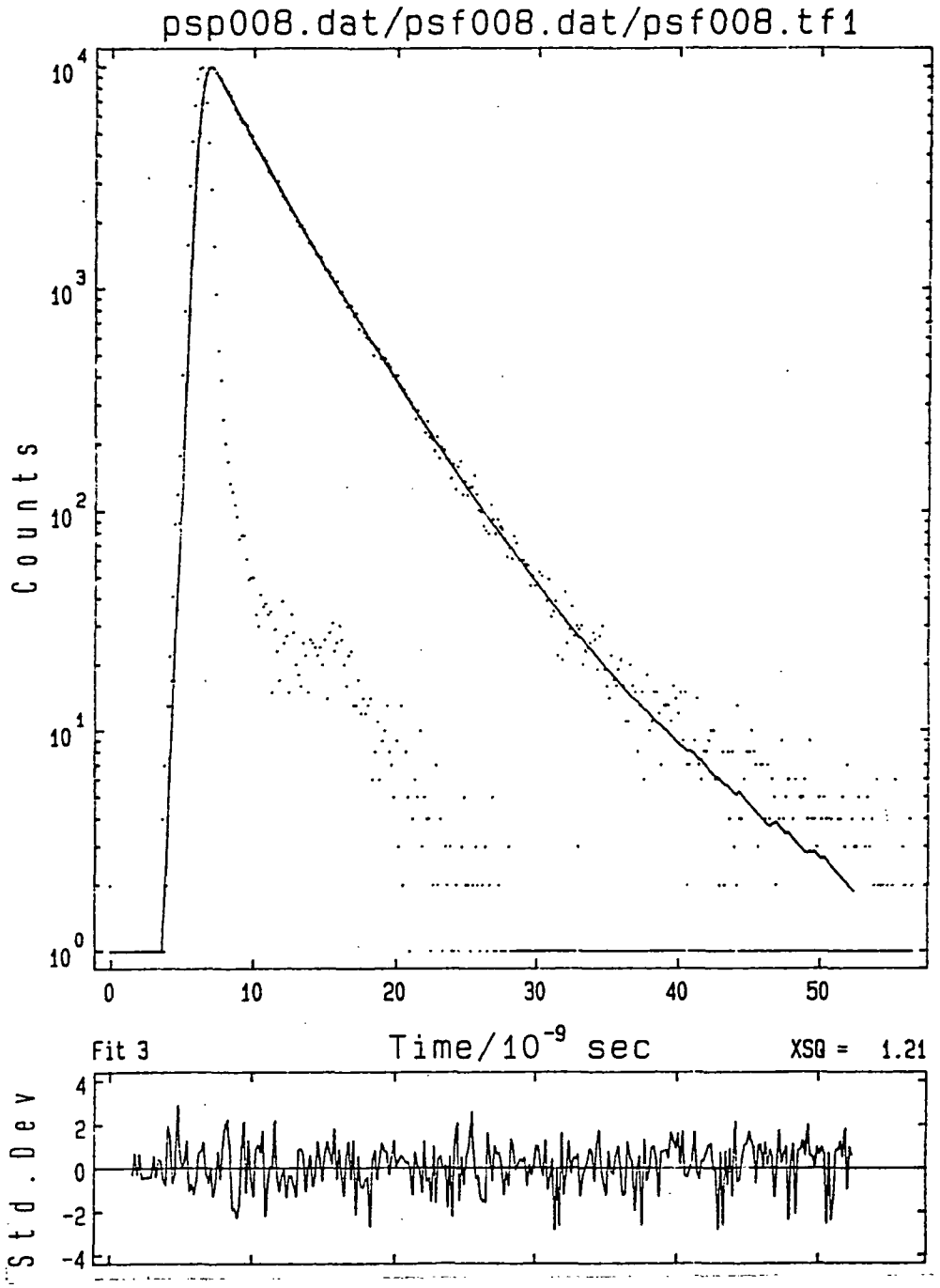
psp008.dat/psf008.dat/psf008.tf1
Counts
Time/10^-9 sec
Fit 3
XSQ = 1.21
Std. Dev

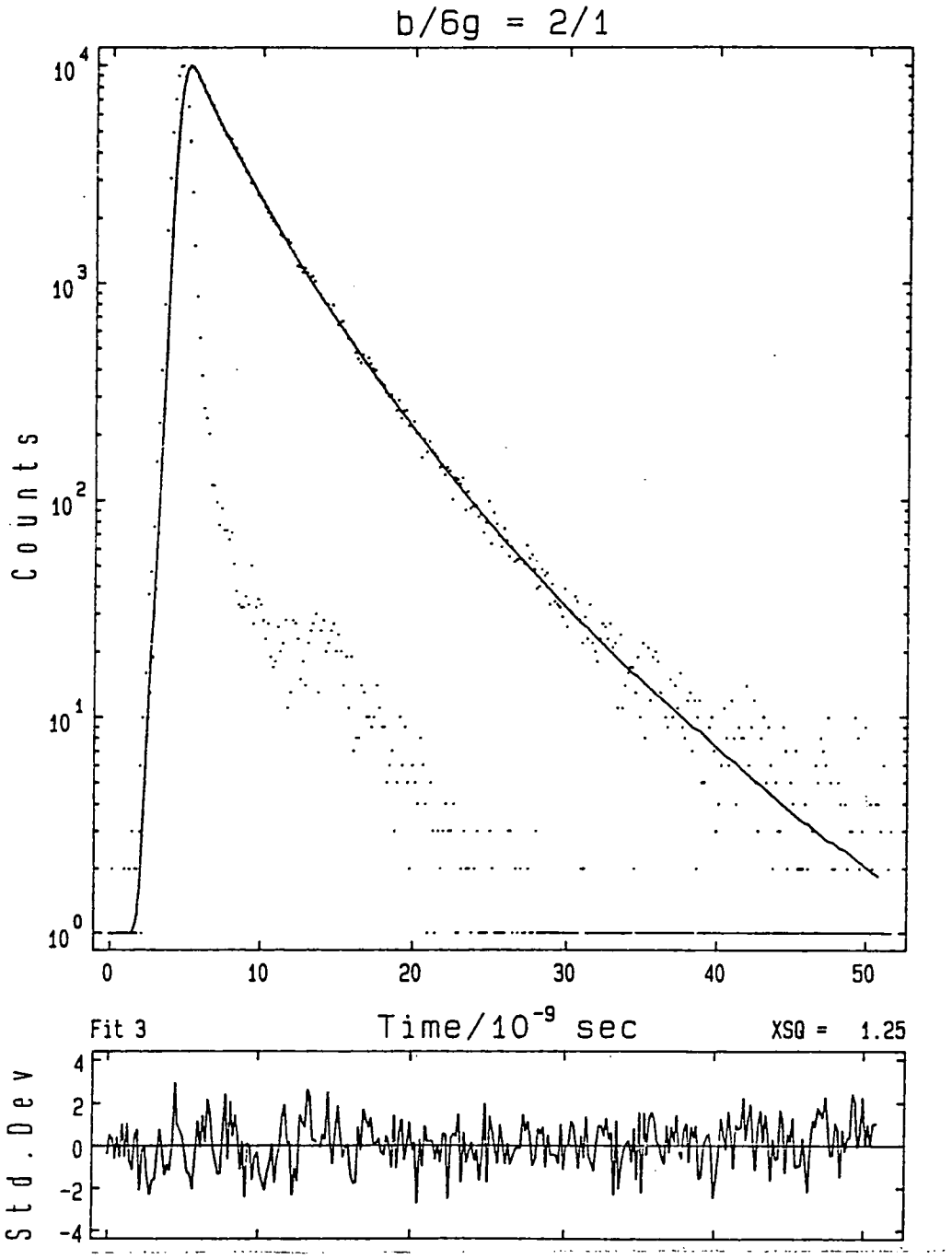
b/6g = 2/1
Counts
10^4
10^3
10^2
10^1
10^0
0
10
20
30
40
50
Fit 3
Time/10^{-9} sec
XSQ = 1.25
Std.Dev
4
2
0
-2
-4

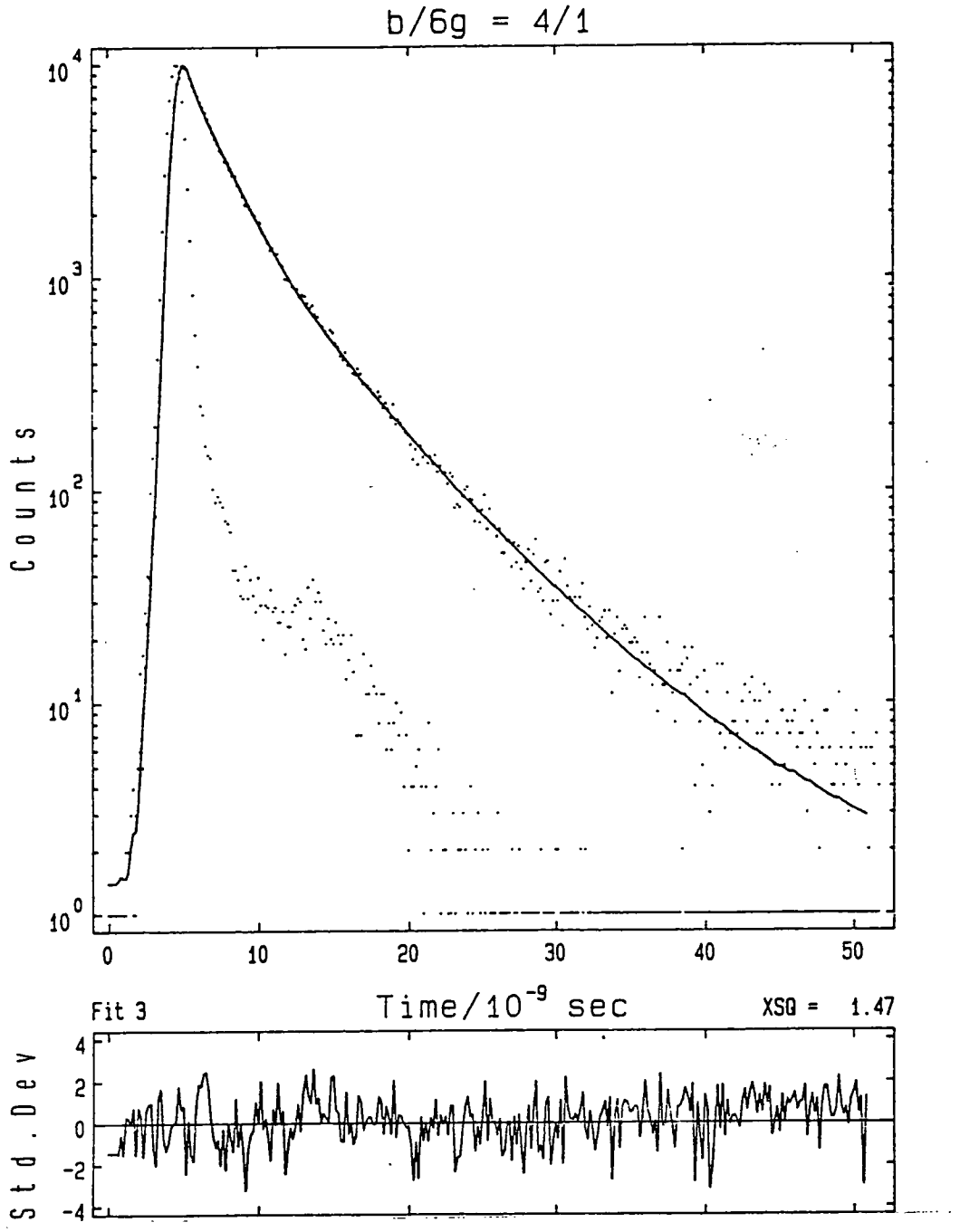
b/6g = 4/1
Counts
10^4
10^3
10^2
10^1
10^0
0
10
20
30
40
50
Fit 3
Time/10^{-9} sec
XSQ = 1.47
Std. Dev
4
2
0
-2
-4

A Stern - Volmer type plot was used to calculate the energy transfer rate and can be seen in figure (4.7).

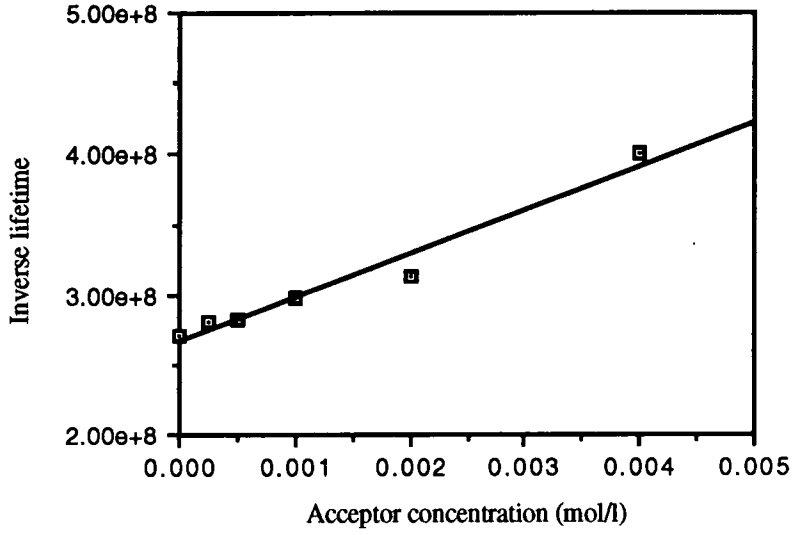

Figure (4.7) A Stern - Volmer plot for the rhodamine dye system.

The errors in the lifetimes can be estimated from the χ^2 values of the fits shown in table (4.4). A straight line fit for the data gave the following equation :

$$\tau_f^{-1} = 2.67 \times 10^8 + 3.2 \times 10^{10}[C_A] \qquad (4.9)$$

thus τ_{fo}^{-1} = 3.74 ns and k_{et} = 3.2 x 10^{10} l/mol/s. This value for k_{et} is in good agreement with a reported result [Muto S. et al., (1987)] from a similar rhodamine dye system in solution which was 7.5 x 10^{10} l/mol/s. The result obtained is somewhat smaller than in solution, this is partly due to the fact that there is no collisional transfer in this case.

From equation (4.9) it was found that C_A^0 = 8.34 * 10^{-3} M and R_0 = 36.2 Å. Also assuming n = 1.52, K = $\left(\frac{2}{3}\right)^{1/2}$ and Φ_D = 0.9, the overlap integral was calculated to be :

$$\int_0^\infty F_D(\nu)\varepsilon_A(\nu)\frac{d\nu}{\nu^4} = 2.95 * 10^{-14}$$

These values provide a good guide as to the efficiency of the energy transfer process and also allow comparison with other recorded values. The value obtained for the overlap integral is principally determined by the spectral distribution of the donor emission and the acceptor absorption.

4.4.3 Dependence of the donor lifetime on the acceptor concentration in the mixed BASF dye system.

The aim of this experiment was to study energy transfer between the BASF dye pair O240 (as the donor) and R300 (as the acceptor), in a polymer thin film, and to see the effect of varying the acceptor concentration on the fluorescence lifetimes of the donor. This was to be determined using the fluorescence lifetime apparatus at Imperial College. The polymer used was poly(methyl methacrylate) (PMMA). No previous reports of energy transfer between these two very efficient and stable dyes have appeared in the literature.

4.4.3.1 Method.

Thin films were dipped from solutions consisting of 2.651 g of PMMA in 20 ml dichloromethane with 0.00663 g of O240, i.e.0.25%$^{w}/_{w}$ of dye to polymer. The amount of R300 added to the mixture was varied as shown in table (4.5).

Thin films were dipped from the solutions at a withdrawal velocity of 30 mm/min onto glass microscope slides.

Using the time correlated single photon counting equipment, the fluorescence lifetimes were measured. The pump wavelength was chosen as 532 nm, and the fluorescence decays from the samples were measured at 577 nm and 618 nm, because these wavelengths correspond to the fluorescence maxima of the O240 and R300 respectively. The instrument response functions were recorded at 532 nm.

Solution	R300 : O240	wt R300 (g)
1	4 : 1	0.02651
2	2 : 1	0.01325
3	1 : 1	0.00663
4	1 : 2	0.00331
5	1 : 4	0.00166

Table (4.5) Ratios and weights of R300 used.

4.4.3.2 Results.

The fluorescence decays are shown in figure (4.8). The pure dyes show very different decays to each other. From the analysis of the pure samples the lifetime of O240 was found to be 3.6 ns and that of R300 was found to be 5.5 ns.

The fluorescence decays of the mixtures were analysed at the two different wavelengths at which they were recorded. From figure (4.9) it can be seen that the decays are completely different at the two different wavelengths for each sample. Table (4.6) shows a summary of the results recorded at 577 nm, since this wavelength represents the maximum of the O240 emission. From this table it can be seen that two lifetimes have been used to fit the decays. The short lifetimes have been used to fit the initial part of the decay, and the long lifetimes have been used to fit the tail of the decay.

The point of interest is the initial part of the decay, and one observes a decrease in the lifetime with increasing amount of R300. This is also observed from figure (4.10), which shows the decays at 577 nm, where as the amount of R300 in the mixture is increased the rate of decay also increases, and thus the fluorescence lifetime decreases.

R300 : O240 ratio	Lifetimes (ns)	Relative contribution	χ^2
Pure O240	3.60	100	2.098
Pure R300	5.52	100	1.704
1 : 4	1.13 3.65	30.4 69.6	1.718
1 : 2	0.96 3.75	39.8 60.2	1.684
1 : 1	0.80 3.88	54.7 45.3	1.88
2 : 1	0.64 3.93	51.8 48.2	2.063
4 : 1	0.58 4.26	59.2 40.8	1.961

Table (4.6) Lifetimes of O240 with different ratios of R300 recorded at 577 nm.

Under the experimental conditions the O240 is excited in preference to the R300. However, at 577 nm both dyes contribute to the emission spectrum. Thus the interpretation of these results is that the short lifetime is due to O240 which is de-excited by energy transfer to the R300. The longer component is due to a weighted average of the fluorescence of the R300 and a decreasing component due to O240 molecules at sites where energy transfer is inefficient.

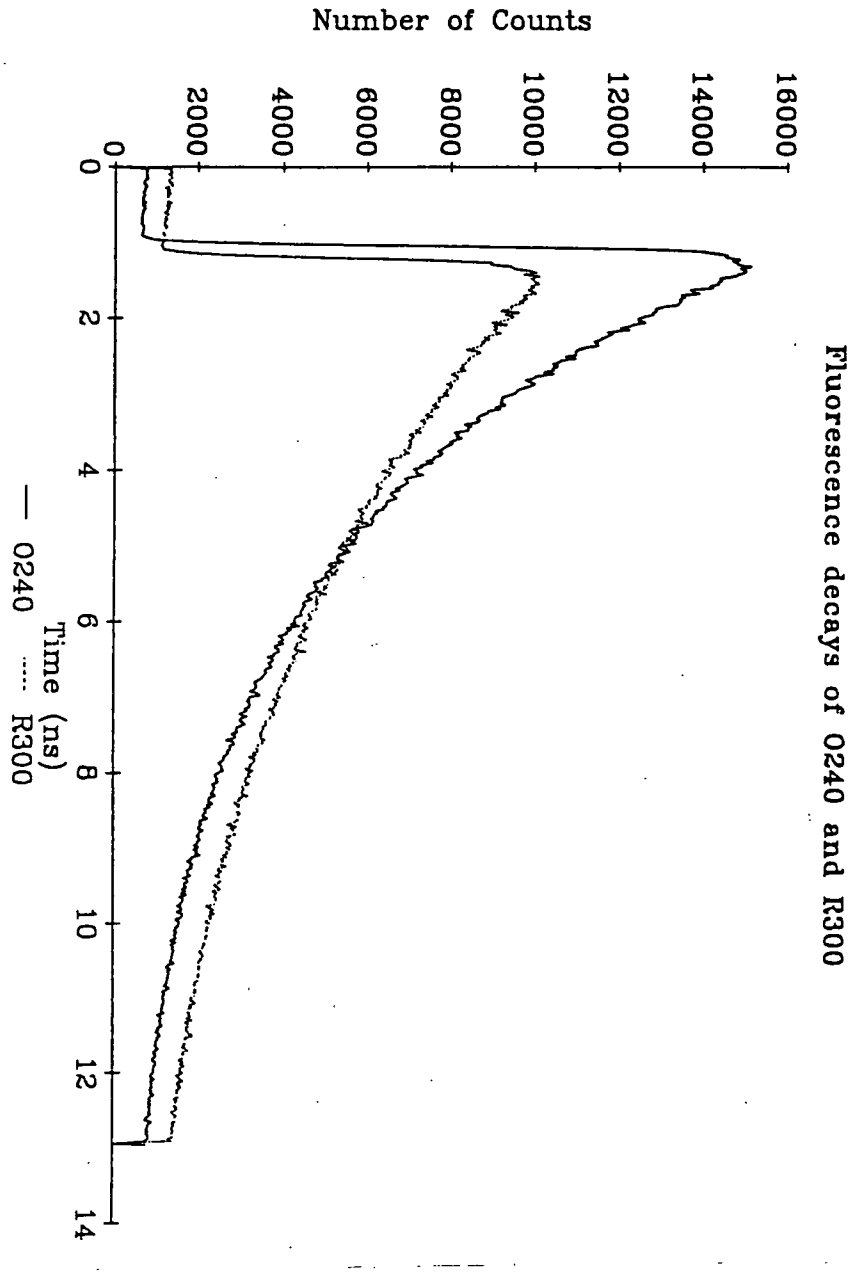

Figure (4.8) The fluorescence decays of O240 and R300.

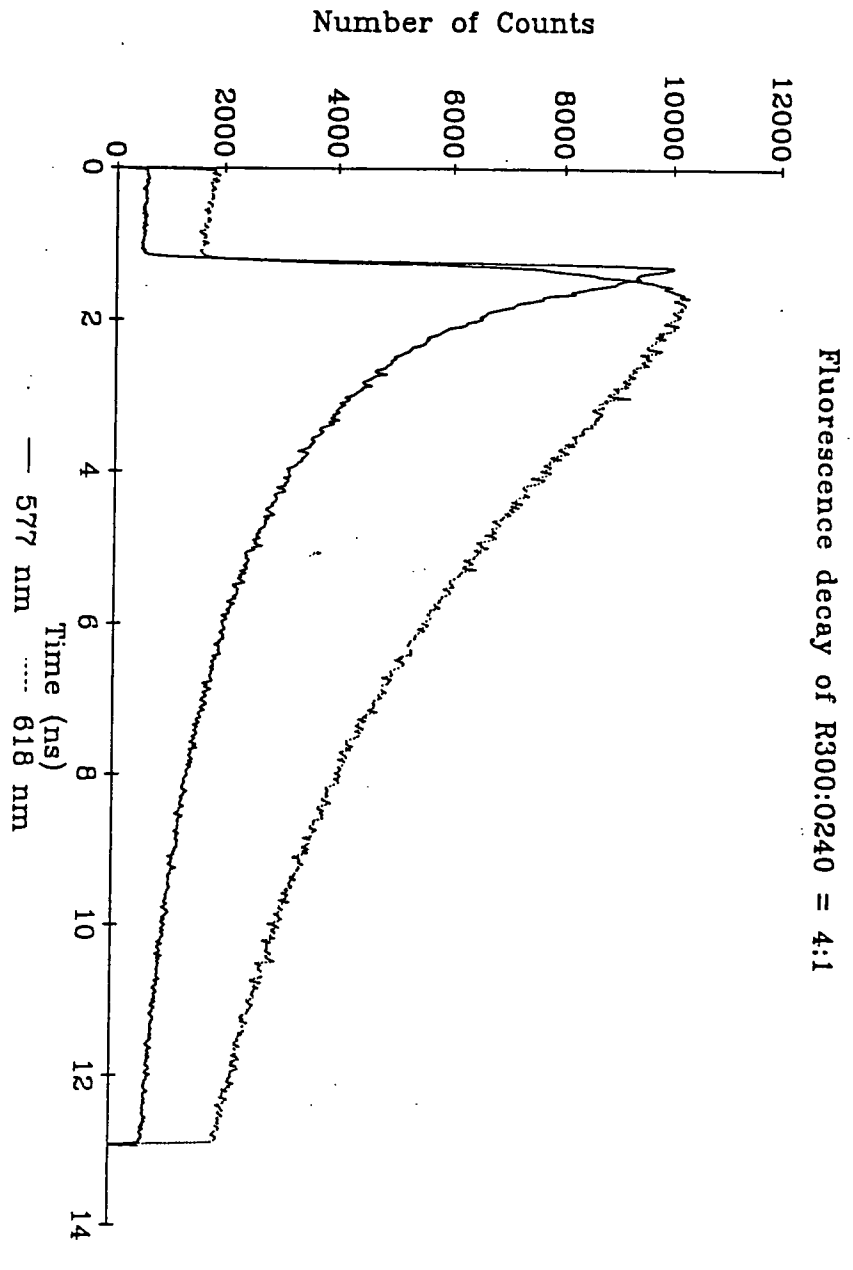

Figure (4.9) The fluorescence decays of the mixed BASF dye films recorded at 577 nm and 618 nm (a) R:0=4 (b) R:0=2 (c) R:0=1 (d) R:0=1/2 (e) R:0=1/4

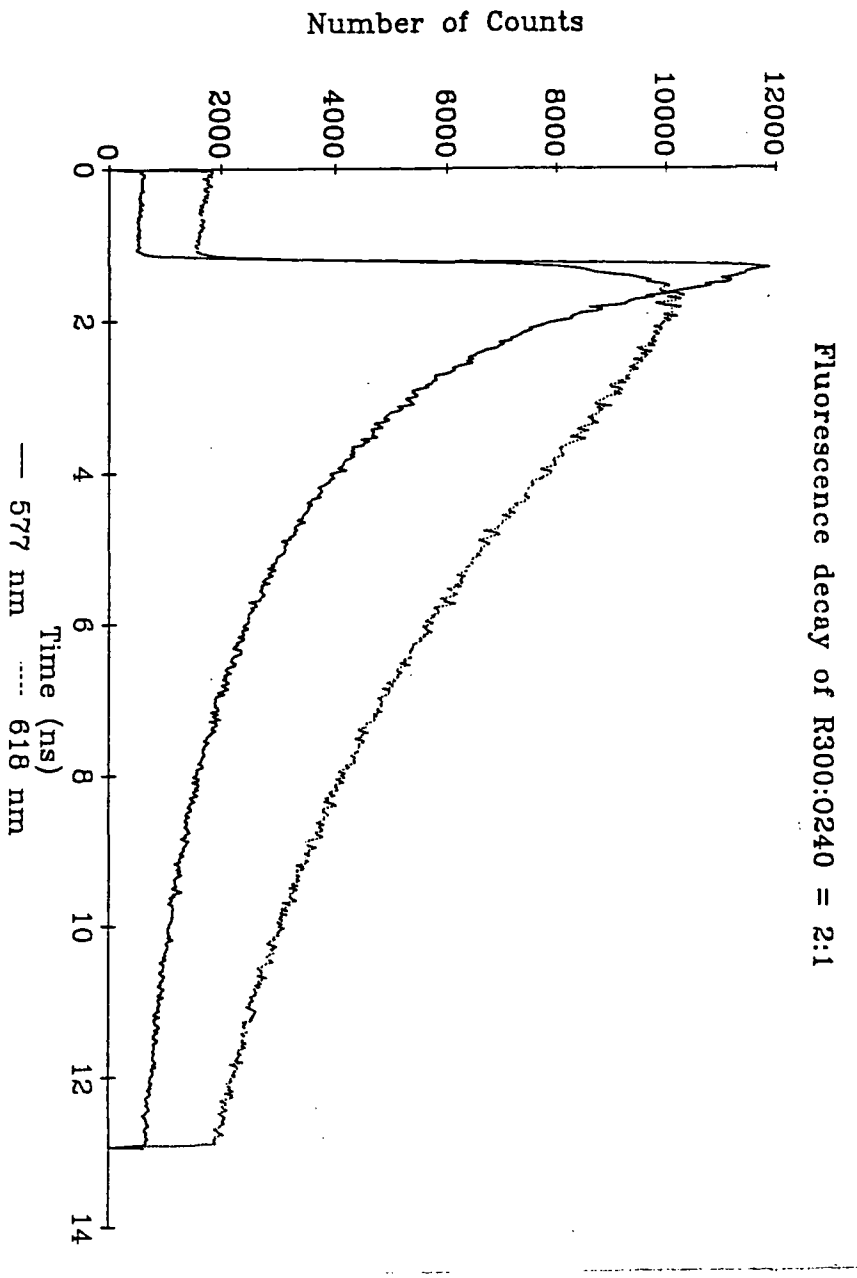
Number of Counts
0
2000
4000
6000
8000
10000
12000
0
2
4
6
8
10
12
14
Time (ns)
— 577 nm ---- 618 nm
Fluorescence decay of R300:0240 = 2:1

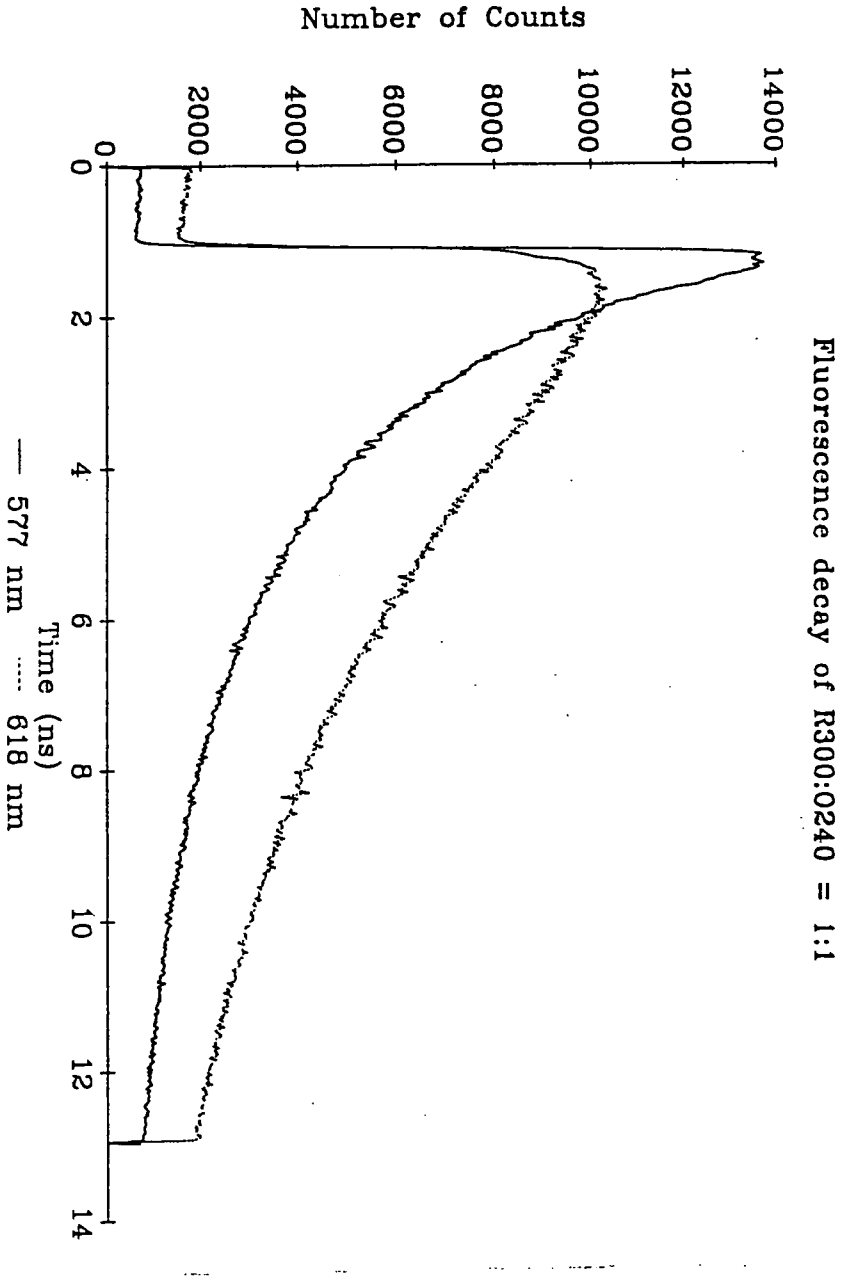
Number of Counts
0
2000
4000
6000
8000
10000
12000
14000
0
2
4
6
8
10
12
14
Time (ns)
— 577 nm ..... 618 nm
Fluorescence decay of R300:0240 = 1:1

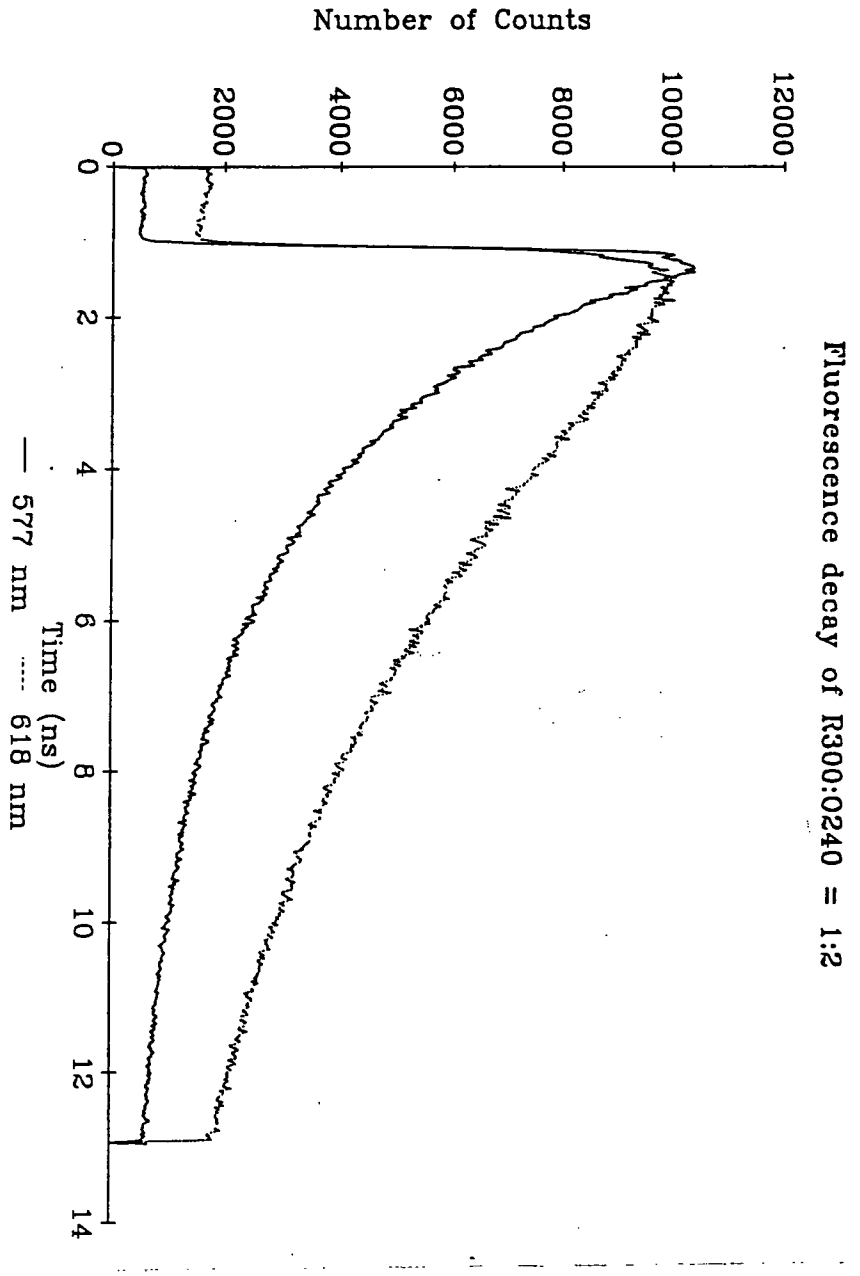
Number of Counts
0
2000
4000
6000
8000
10000
12000
0
2
4
6
8
10
12
14
Time (ns)
— 577 nm ---- 618 nm
Fluorescence decay of R300:0240 = 1:2

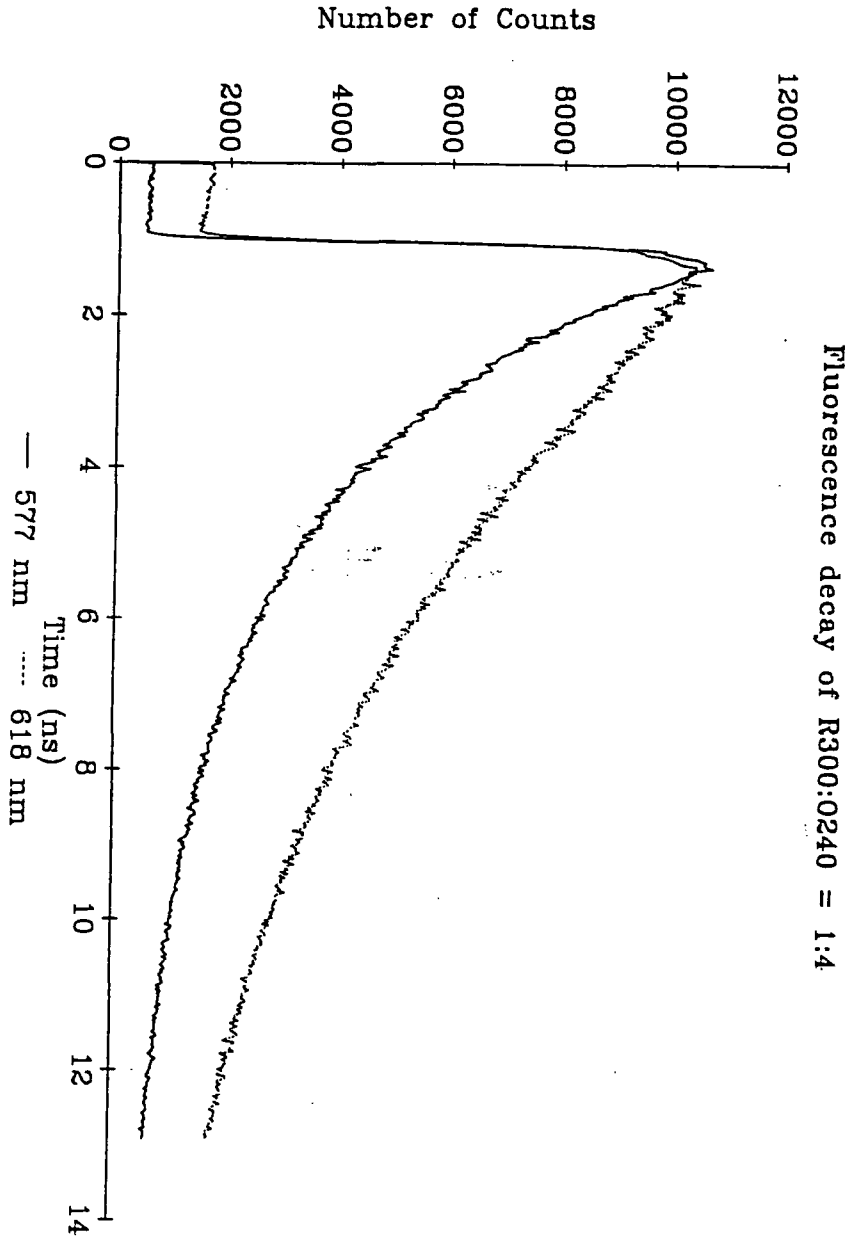
Number of Counts
0
2000
4000
6000
8000
10000
12000
0
2
4
6
8
10
12
14
Time (ns)
— 577 nm ···· 618 nm
Fluorescence decay of R300:0240 = 1:4

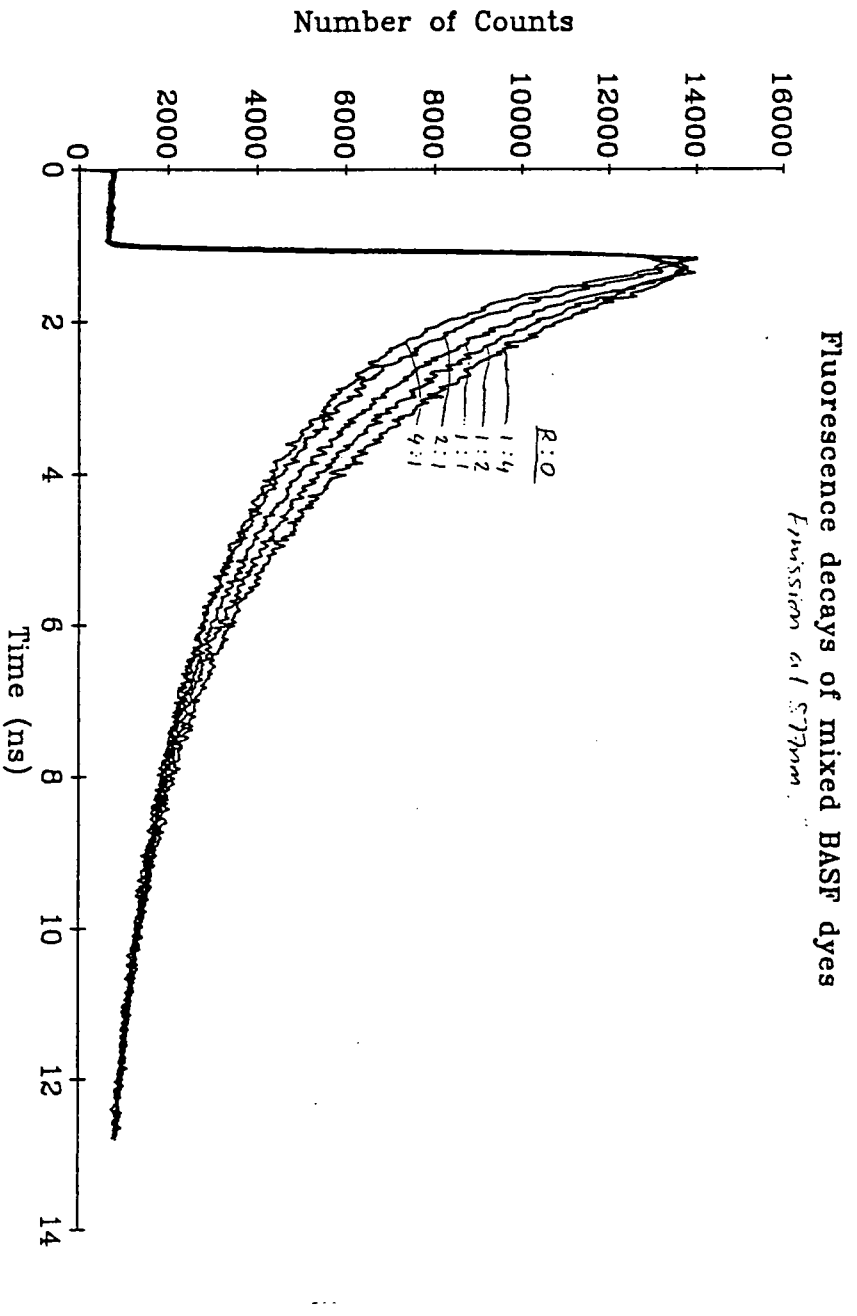

Figure (4.10) The fluorescence decays of the mixed dye films recorded at 577 nm.

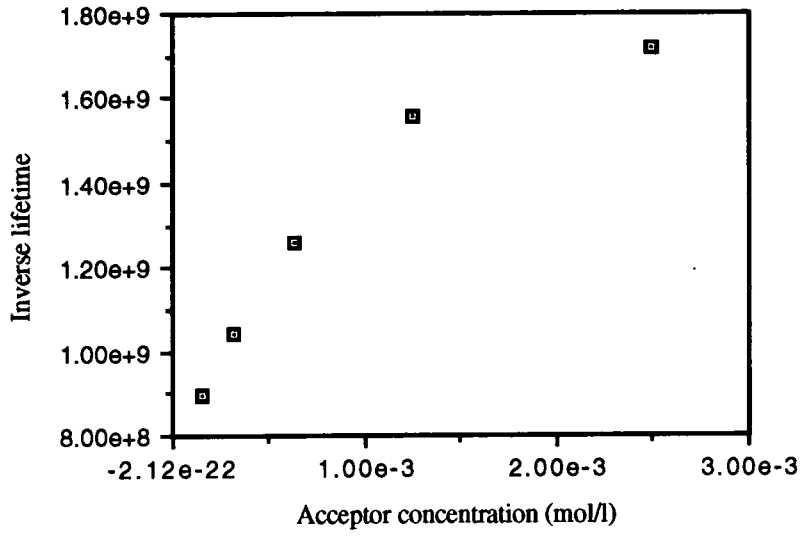

Figure (4.11) A Stern - Volmer plot for the BASF dye system.

From the lifetimes recorded a Stern - Volmer type plot was used to calculate the energy transfer rate. The plot can be seen in figure (4.11), from this graph it can be seen that the lifetime recorded for the high concentration system seems to have deviated from a reasonable linear progression. This could be due to the quality of the fit for the lifetime. From the χ^2 values of the fitted lifetimes it can be seen that the errors are large. Hence using the first four points, the following straight line was fitted :

$$\tau_f^{-1} = 8.43 * 10^8 + 5.9 * 10^{11}[C_A] \qquad (4.10)$$

thus $\tau_{f^o}^{-1}$ = 1.2 ns and $k_{et} = 5.9 * 10^{11}$ l/mol/s. This value for k_{et} illustrates more efficient energy transfer than the rhodamine system, although the errors in the precise value are large, since the whole concentration range was not considered. The critical concentration was calculated to be $1.42 * 10^{-3}$ M and the critical radius to be 65.3 Å. Using similar assumptions mentioned in section (4.4.2) the overlap integral was

calculated to be $9.14 * 10^{-13}$. Although the error in these values are likely to be large, they however are comparable to those obtained in the rhodamine system.

At 618 nm it can be seen from figure (4.12) that as the amount of R300 in the mixture is increased the decay shows an introduction of a risetime, this is illustrated by a curvature in the rise part of the fluorescence decay which becomes more pronounced with increasing R300 concentration. This is characteristic of the fact that the R300 dye, in the mixture, is being excited via another process other than direct excitation from the pump radiation. The actual fluorescence lifetime, however, does not change significantly with increasing R300 concentration, this fact has already been shown in the rhodamine system. Thus with these two pieces of information, i.e. the decrease in the lifetime of the donor dye with increasing concentration and the appearance of a risetime in the decay of the acceptor dye, one can deduce that energy transfer is taking place.

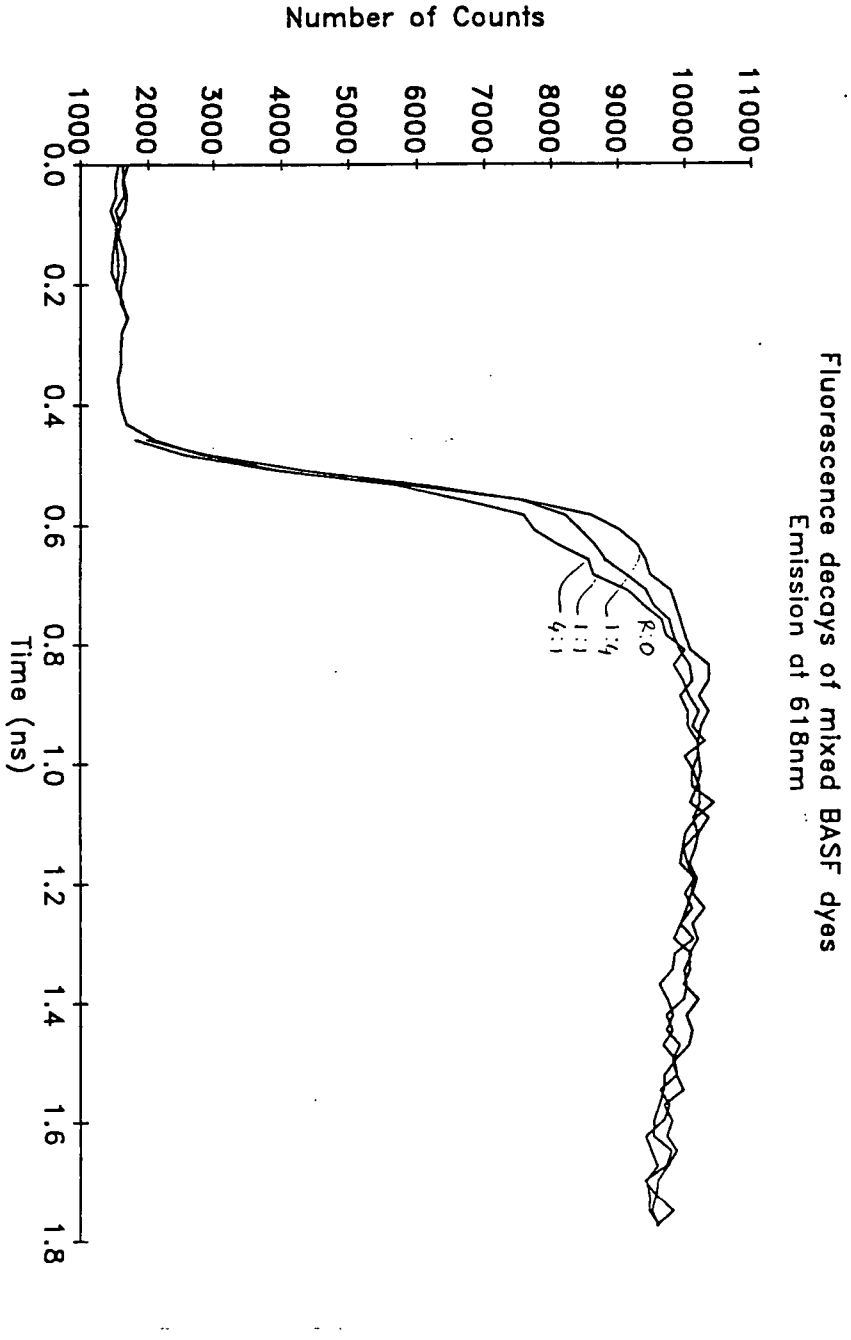

Figure (4.12) The fluorescence decays of the mixed dye films recorded at 618 nm.

4.5 Conclusion.

In this chapter the non-radiative Förster energy transfer mechanism between donor and acceptor dye molecules in a polymer matrix has been investigated in detail. The non-radiative energy transfer from a donor to an acceptor has been shown to be primarily a result of dipole - dipole interaction. The rate of energy transfer depends on a number of factors including the extent of spectral overlap and the distance between the molecules.

The fluoresence lifetime experiments performed along with the results are presented. It has been shown that the acceptor dye lifetime is independent of its concentration in the mixture, within the concentration range of interest, and does not change significantly with the introduction of the donor dye.

The fluorescence lifetime of the donor dye as a function of the acceptor dye concentration has been monitored. It has been shown that the donor dye lifetime decreases as the acceptor dye concentration increases. Also using a Stern - Volmer plot, the energy transfer rate and the critical radius and concentration have been calculated, and thus it has been shown that efficient energy transfer occurs between the dyes by the parameters given by the Stern - Volmer analysis.

It must be noted here that although a Stern - Volmer analysis has been used in a first approximation of the energy transfer mechanism, the values obtained for the lifetimes and efficiencies can only be used to serve as guidelines in forming an interpretation. The errors in the absolute numbers lie in the approximations made by the particular choice of model.

4.6 References.

Ali M. A., Ahmed S. A. and Chokhavatia A. S.,"Examination of a generalised model for radiationless energy transfer in dyes. Comparison of theory and experiments.", J. Chem. Phys., Vol 91, No 5, pp 2892-2897, (1989).

Birks J. B., "Photophysics of aromatic molecules", Chapter 11, Wiley, (1970).

Cario and Franck J., Z. physik., Vol 17, pp 202, (1923).

Förster T.,"Z. Naturforsch., Vol 4a, pp 321, (1949).

Galanin,"J. Exp. Th. fiz., Vol 21, pp 121, (1951).

Katsuura K.,"J. Chem. Phys., Vol 43, pp 4149, (1965).

Kusumoto Y., Sato H., Maeno K. and Yahiro S.,"Energy transfer dye laser : Confirmation of energy transfer by the reabsorption effect.", Chem. Phys. Lett., Vol 53, No 2, pp 388-390, (1978).

Lin C. and Dienes A.,"Study of excitation transfer in laser dye mixtures by direct measurement of fluorescence lifetime.", J. Appl. Phys., Vol 44, No 11, pp 5050-5052, (1973).

Muto S., Shiba F., Iijima Y., Hattori K. and Ito C.,"Solid thin-film energy-transfer dye lasers.", Elect. Comm. Jap. Part 2., Vol 70, No 1, pp 21-31, (1987).

Perrin J.,"Seances Acad. Sci., Vol 184, pp 1097, (1927).

Perrin J.,"Seances Acad. Sci., Vol 189, pp 1213, (1929).

Sabry M. M. F. and Mekawey F. M.,"Rhodamine 6G - resazurin energy transfer dye laser.", Jap. J. Appl. Phys., Vol 29, No 1, pp 101-102, (1990).

Schiff L. I.,Quantum Mechanics., New York, McGraw-Hill, (1949).

Sebastian P. J. and Sathianandan K.,"Donor concentration dependence of the emission peak in rhodamine 6G - rhodamine B energy transfer dye laser.", Opt. Comm. (Neth), Vol 35, No 1, pp 113-114, (1980).

Singh R. D., Sharma A. K., Unnikrishnan N. V. and Mohan D.,"Energy transfer study on Coumarin-30-rhodamine-6G dye mixture using a laser fluorimeter.", J. Mod. Opt., Vol 37, No 3, pp 419-425, (1990).

Spears K. G., Cramer L. E. and Hoffland L. D., "Subnanosecond time correlated single photon counting with tunable lasers", Rev. Sci. Instrum., Vol 49, No 2, pp 255-262, (1978).

Speiser S. and Katraro R.,"Computer simulation of an energy transfer dye laser.", Opt. Comm., Vol 27, No 2, pp 287-291, (1978).

Watson,"J. Chem. Phys., Vol 18, pp 802, (1950).

CHAPTER 5

Upconversion in dye-doped polymer waveguides.

5.1 Introduction.

Waveguides of rhodamine B-doped P-4VP were being studied as potential materials for solid sate dye lasers. A HeNe laser was being used to characterise the linear optical properties of the waveguide and fluorescence emission was observed from the waveguide at shorter wavelengths. The dye apparently had no absorption at this excitation wavelength. Thus a series of experiments were designed to identify the origin of this effect. The experiment where this effect was seen will now be explained below, followed by a brief outline of the proposed mechanisms to explain this effect.

The sample was prepared on a silicon wafer. The silicon wafer was cut to size and cleaned with acetone. A film of PMMA was dipped onto the silicon to a thickness of approximately 8-9 μm, to be used as a buffer layer for the waveguiding layer on top. This was baked in a vacuum oven for one hour at 100 °C to remove any residual solvent (dichloromethane). Then a film of rhodamine 6G and rhodamine B doped P4VP was dipped onto the PMMA layer and left to dry at room temperature for about one hour. In order to determine the thickness and refractive index of the film, the prism coupling method was used. The laser used was a 10mW Helium Neon (HeNe) laser, lasing at 632.8 nm. The modes were clearly visible but, instead of being red in colour from the HeNe, they were orange with some red. A 632.8 nm interference filter was placed in the path of the beam to remove any extraneous wavelengths from the laser. This had no affect on the mode, which was clearly visible and had not changed with the introduction of the filter. The orange light from the modes was detected using the

experimental set up as shown in figure (5.1). The spectrum recorded is shown in figure (5.2).

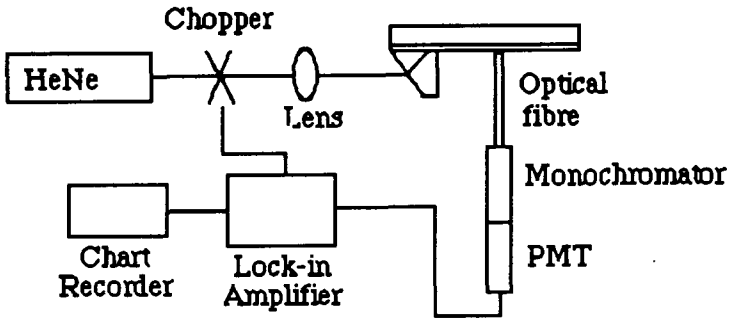

Figure (5.1) Experimental set up to record the spectrum of the emission.

This spectrum closely resembles the fluorescence spectrum of rhodamine B, with a peak at 590 nm. This suggests that the orange light detected was the fluorescence from rhodamine B.

From these results, a mechanism was proposed which involved two photon absorption (TPA) of the HeNe into a two photon level followed by relaxation to the first excited singlet state and then fluorescence. Another possible mechanism later identified was a thermal mechanism, whereby electrons in a thermally excited vibrational level in the ground electronic state are promoted to the first excited electronic state.

In this chapter the TPA mechanism will be explained in detail in section (5.2), and the thermal activation mechanism will be described in section (5.3), together with experiments to distinguish these processes.

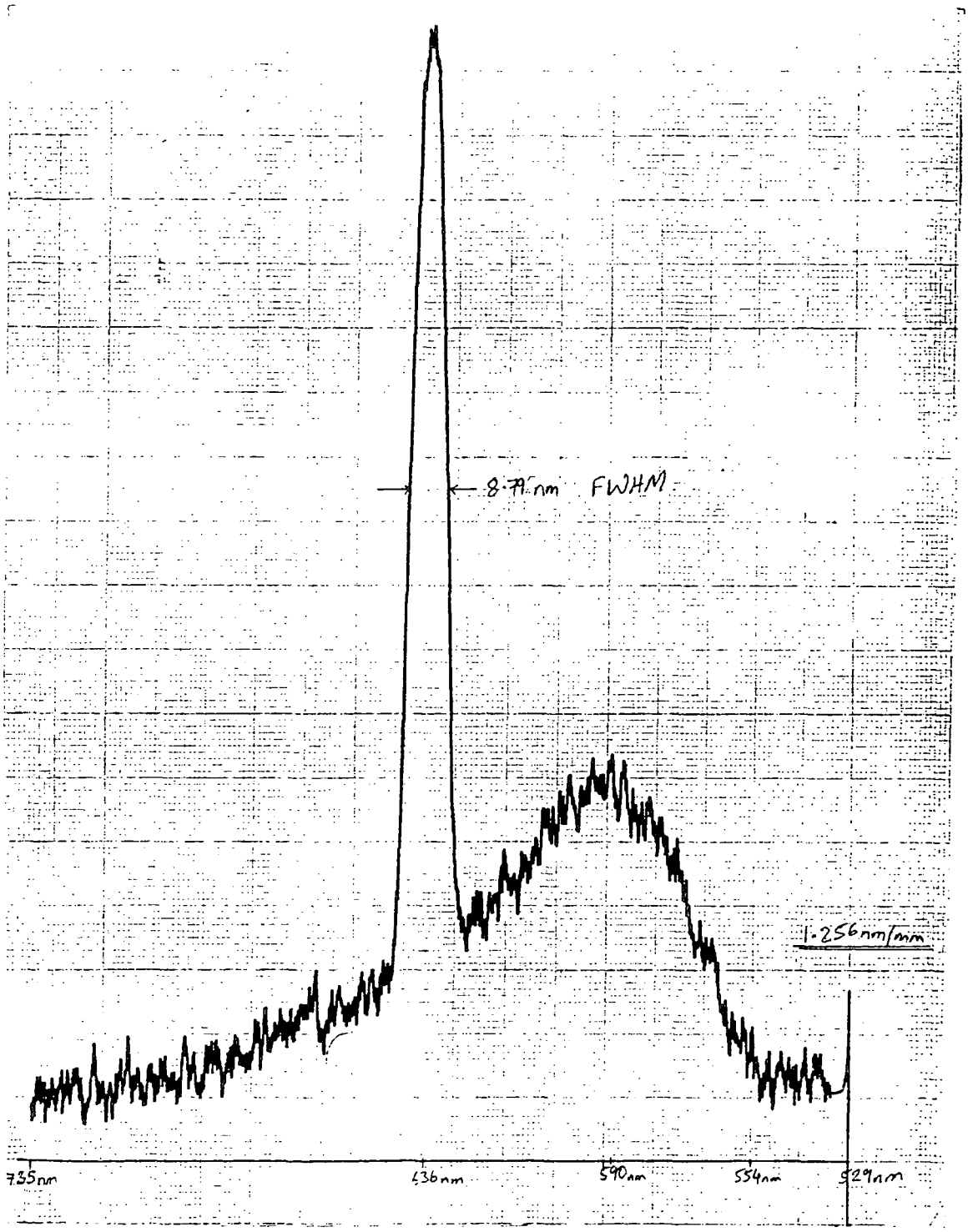

Figure (5.2) The recorded emission spectrum.

5.2 The Two Photon Absorption mechanism.

5.2.1 The model.

Two Photon Absorption (TPA) involves the simultaneous absorption of two photons by a single molecule, as described by Maria Göppert Mayer, (1931). A schematic diagram of the model is shown in figure (5.3).

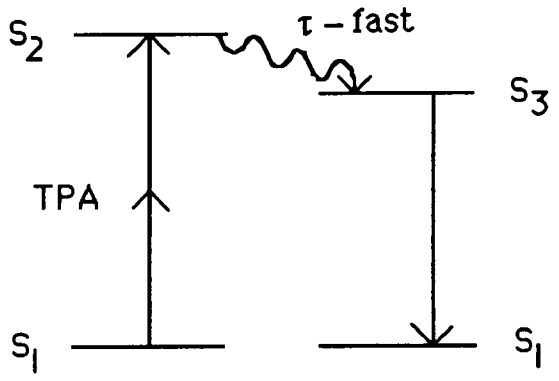

Figure (5.3) The proposed Two Photon Absorption model.

This model proposes that there is a TPA of 633 nm light promoting an electron to a level S_2 which is relatively short lived. The promoted electron then decays to the normal first excited electronic state from which it decays via fluorescence to the ground state. This model was investigated with the experiments which will be described in section (5.2.2).

TPA in $In_{1-x-y}Ga_xAl_yAs/InP$ waveguides has been studied by Villeneuve, (1990) and they have found that the attenuation of light as it propagates through the sample can be described as :

$$\frac{dI}{dz} = -\alpha I - \beta I^2 \qquad (5.1)$$

where α - linear absorption coefficient.

β - TPA coefficient.

I - peak intensity.

z - propagation distance through the waveguide.

The transmitted intensity through the sample is defined as the ratio of the peak transmitted intensity and the peak incident intensity and is given by :

$$T = \frac{I_{trans}}{I_{inc}} = \frac{(1-R)^2 \eta \exp(-\alpha L)}{1+\beta(1-R)\eta I_{inc} L_{eff}} \qquad (5.2)$$

where η - coupling efficiency into the waveguide.

R - Fresnel reflectivity off the front and end faces.

$L_{eff} = [1-\exp(-\alpha L)]/\alpha$

α - includes both linear absorption and scattering loss.

L - length of waveguide.

It is evident that a plot of inverse transmission, T^{-1} vs I_{inc} should consist of a straight line having a slope directly proportional to the TPA coefficient β.

Hence a series of experiments were performed investigating the transmission properties of rhodamine B (R -B) doped polymer waveguides.

5.2.2 The experiments.

The apparatus was set up as shown in figure (5.4). The sample was made from a solution of 0.02874g of R - B ($3*10^{-3}$ M) in 20 ml of dichloromethane with 3.5g of PMMA (i.e 0.8% weight ratio of dye to polymer). A thin film was dipped onto a fused silica microscope slide. The slide was mounted on a prism coupling stage in the normal manner.

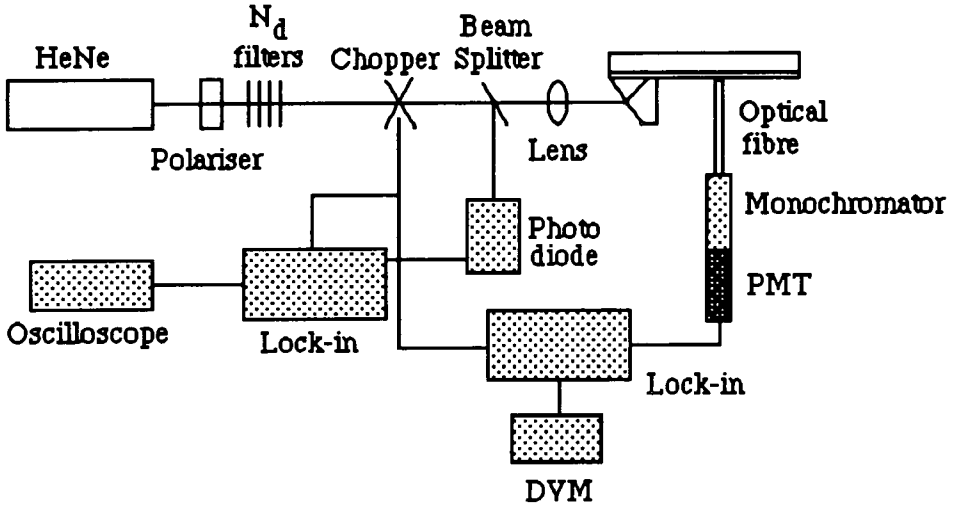

Figure (5.4) Experimental set up for intensity dependence studies.

A polariser was used to arrange for TE polarisation in the waveguide. The incident intensity was varied using neutral density filters. A chopper was used to improve the signal to noise ratio. The laser beam was focussed, using a lens, to a spot at the base of the prism. Once a mode had been located and the coupling angle optimised, the rotation stage was fixed into position. A multimode plastic optical fibre (numerical aperture - 0.47) was used to collect the emitted fluorescence by being placed in close proximity to the waveguide. The other end of the fibre was positioned at the entrance slit of a monochromator, with slit widths of 0.5 mm. A photomultiplier tube

(PMT) was taped flush to the exit slit of the monochromator so that the fit was light tight. The output from the PMT was fed to a lock-in amplifier, triggered by the chopper. The voltage from the lock-in amplifier was displayed on a digital voltmeter.

Initially the output from a lock-in was connected to a chart recorder, and the monochromator was used to scan the range of wavelengths to detect the spectrum of the emitted light. This is shown in figure (5.5). From the trace it can be seen that the resolution has improved, now roughly 6 nm, and the spike, corresponding to the 633 nm line is roughly of the same amplitude as the peak of the fluorescence. This is a good indication of the quality of the film, since there is very little scatter of the pump beam, and also underlines the incoherence of the emitted fluorescence.

To record the transmission properties the waveguide was cut, at a length of 2.1 cm, to allow the light to exit the mode. The monochromator was set to 633 nm and the output power as a function of the input intensity was recorded. The results are shown in figure (5.6).

The monochromator was then set up for 590 nm, and the fibre moved to an uncut part of the waveguide approximately 0.5 cm from the origin, in order to measure the intensity of fluorescence as a function of input intensity. The results are shown in figure (5.7).

Also, a pump/probe experiment was set up to observe the population of the S_1 state by TPA . The apparatus was set up as shown in figure (5.8). The HeNe was used as the pump beam to excite the fluorescence in the waveguide mode, and a Green HeNe (GreHeNe), lasing at 543 nm, was used as the probe beam, which would normally be absorbed by the R - B since it is in the main visible absorption band of the dye.

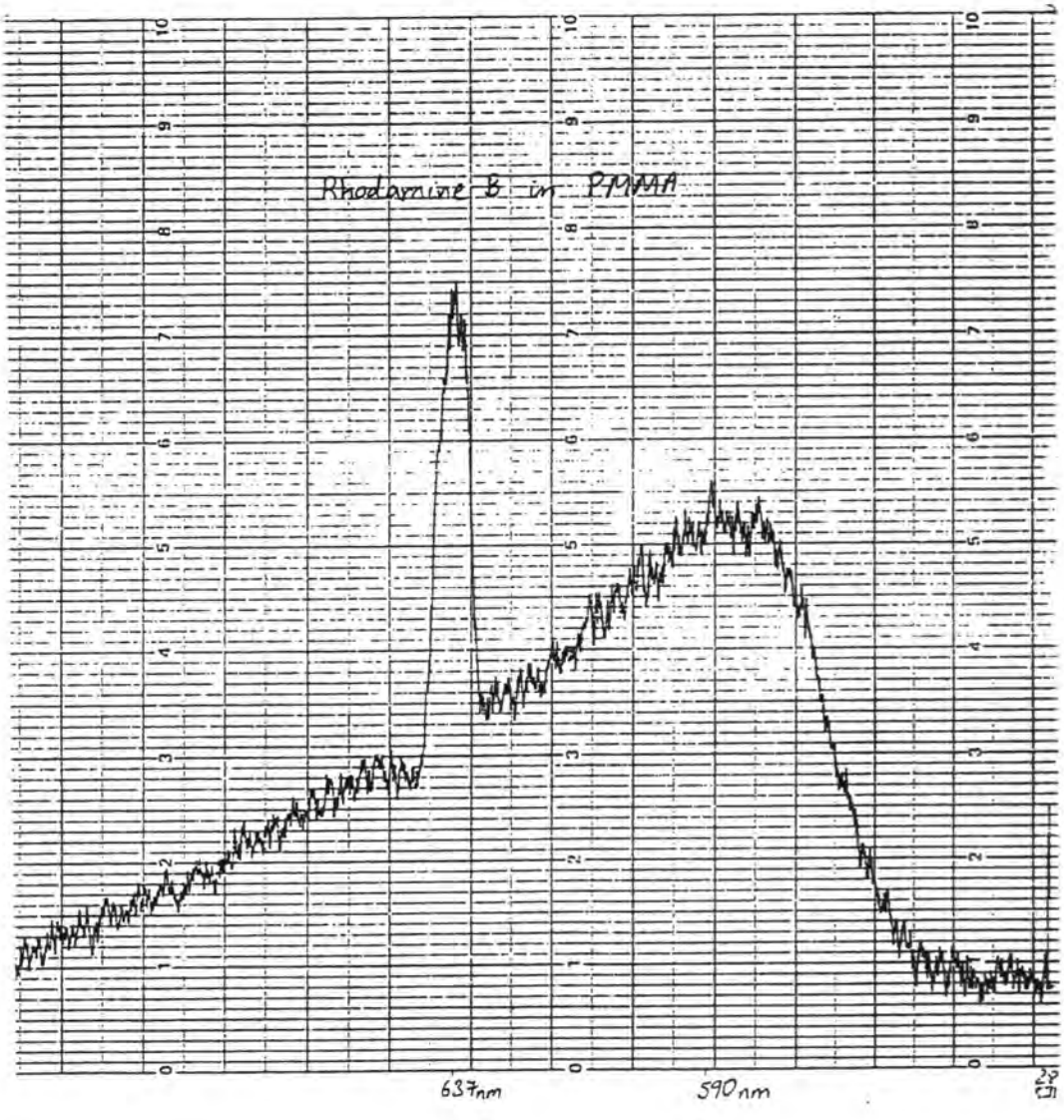

Figure (5.5) The recorded emission spectrum from an optimised set up.

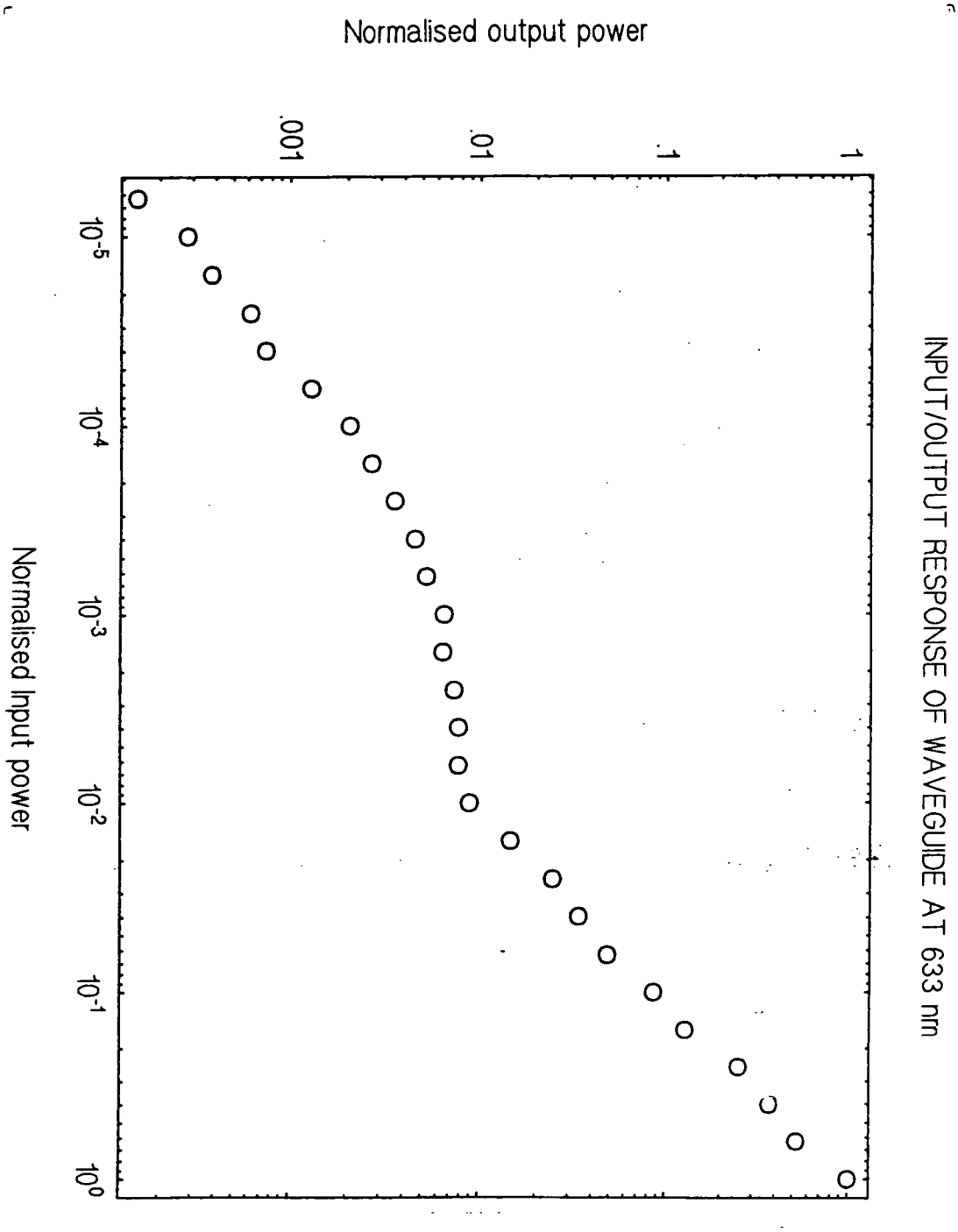

Figure (5.6) Output power of the HeNe as a function of the input intensity.

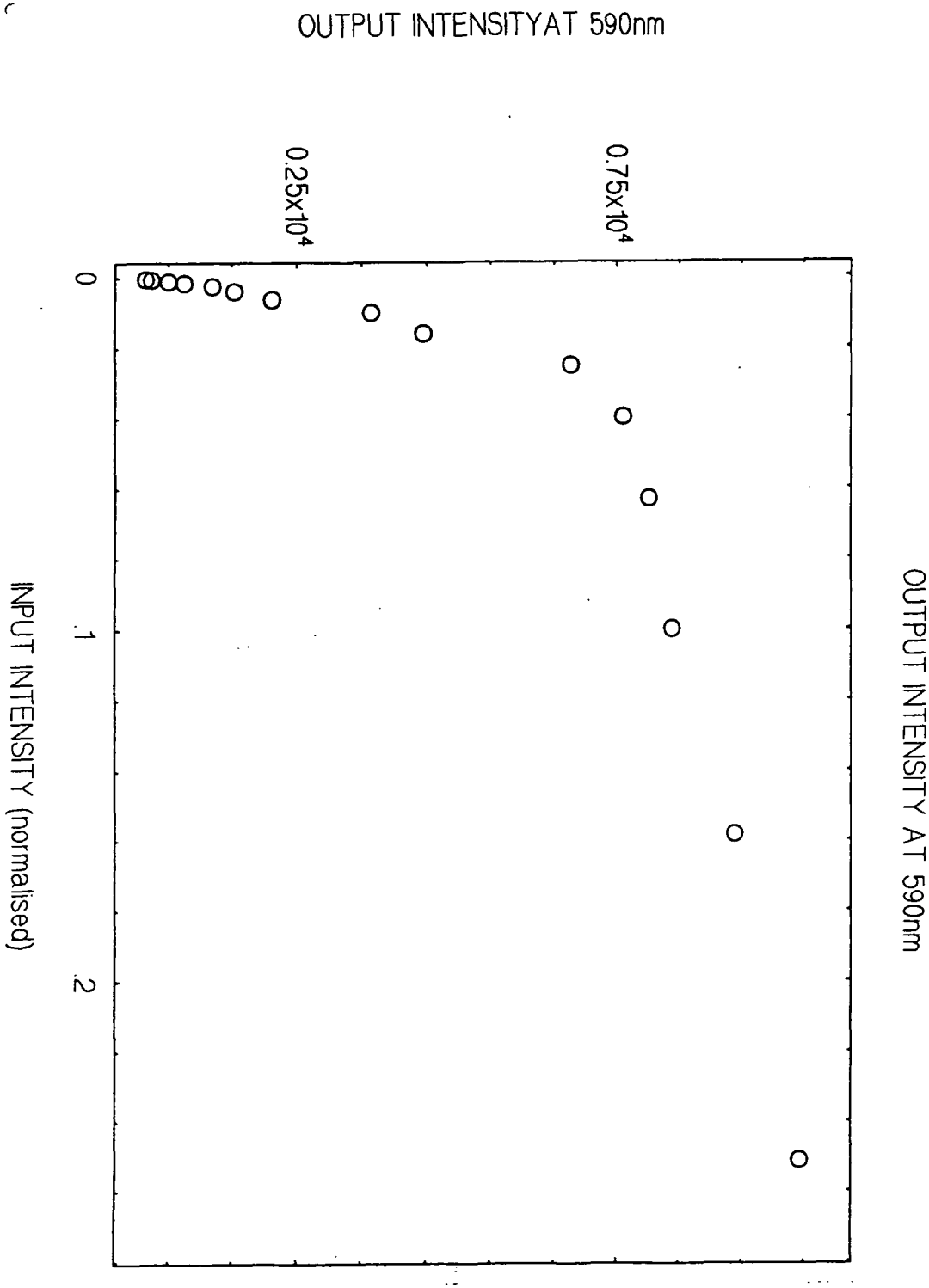

Figure (5.7) The intensity of fluorescence as a function of the input intensity.

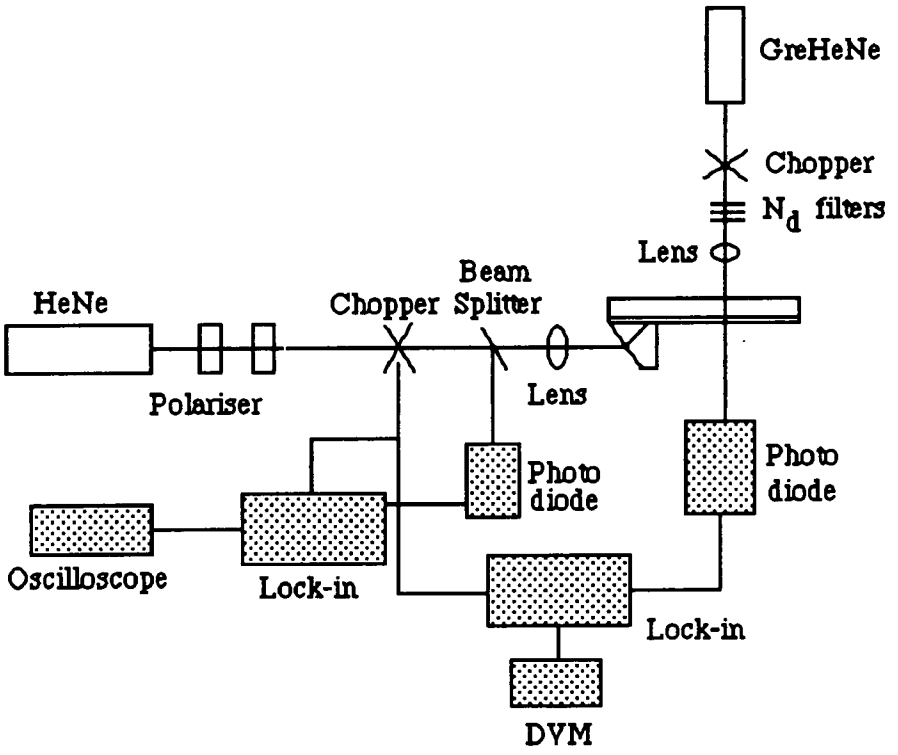

Figure (5.8) Experimental set up for the pump/probe experiment.

The GreHeNe was focussed on to the waveguide mode and the intensity of the transmitted GreHeNe detected by a photodiode. The intensity of the probe beam was kept low to avoid direct saturation of the S_1 state. The signal from the photodiode was sent to a lock-in amplifier which outputs a voltage to a digital voltmeter. The intensity of the HeNe was varied using a polariser and the intensity of the GreHeNe transmitted was monitored. The results are shown in figure (5.9).

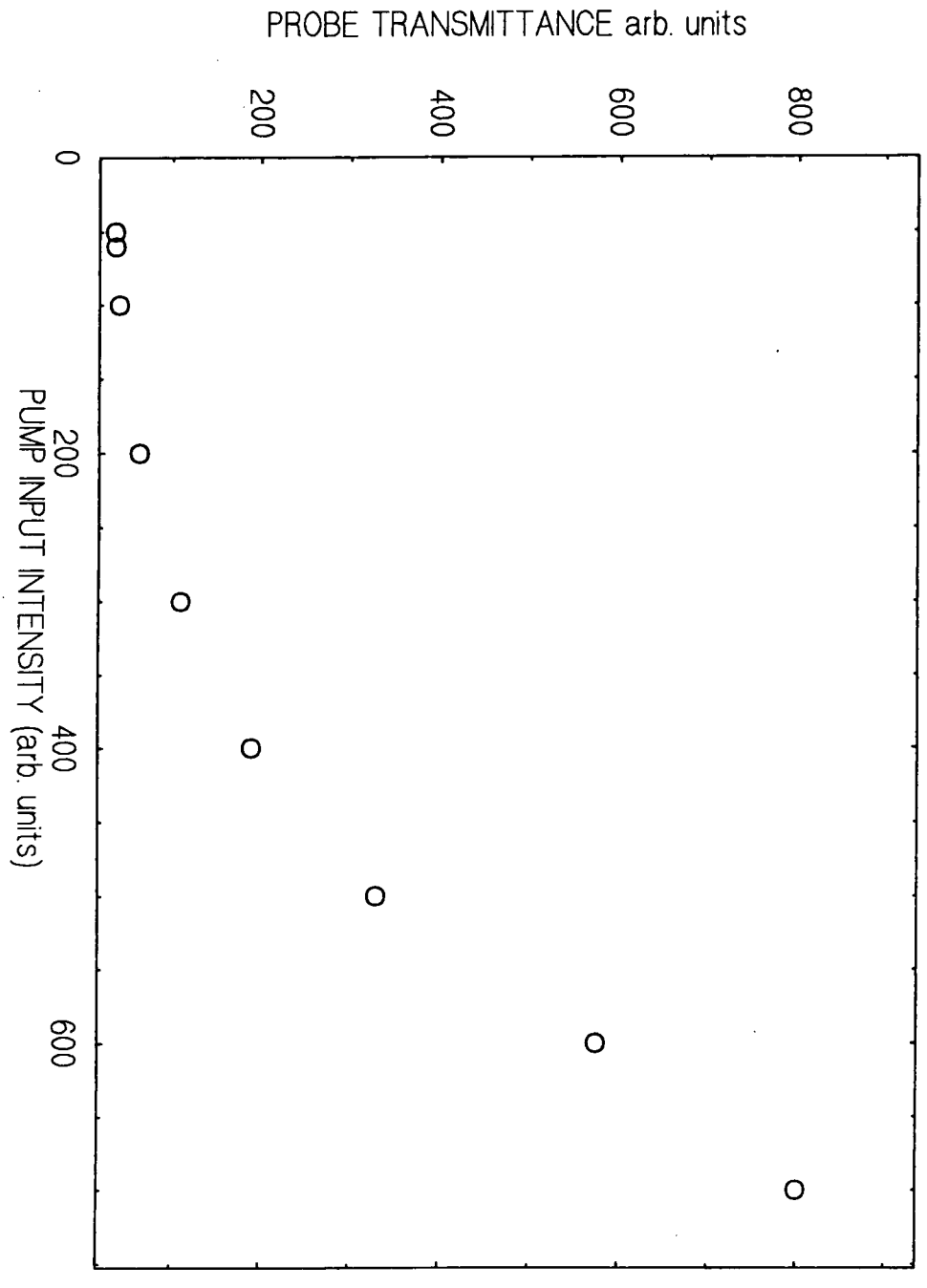

Figure (5.9) The intensity of the transmitted GreHeNe as a function of the intensity of the HeNe.

5.2.3 The results and further experiments.

From figure (5.6) it can be seen that there is a nonlinear response in the output at low input intensities, and at high input intensities the output increases rapidly. Taking a closer look at the low input intensity range and plotting T^{-1} vs input intensity, as shown in figure (5.10), a linear response is observed. This is as one would expect assuming a TPA model from equation (5.2). The increase in the transmission at higher input intensities implies a saturation of the S_2 level.

From figure (5.7) a saturation of the fluorescence intensity at high input intensities is observed. This seems to suggest that the decay from S_2 to S_3 is faster than the decay from S_3 to S_1. A closer examination of the low input intensities, as shown in figure (5.11), shows a quadratic response in the output with the input intensity which, again, is what one would expect to see if the excitation mechanism was TPA.

The result from the pump/probe experiment , shown in figure (5.9), shows that the transmission of the GreHeNe increases with the intensity of the HeNe. This result illustrates bleaching of the S_3 level, in our TPA model, by the HeNe.

Thus all these results taken together seem to correlate with the TPA model, and thus from figure (5.10) and from equation (5.1) it is possible to calculate a value for β . In our experiments the Fresnel reflections can be ignored since the light is prism coupled in and out scattered from a cut in the film and collected by an optical fibre. Thus equation (5.2) may be rewritten as :

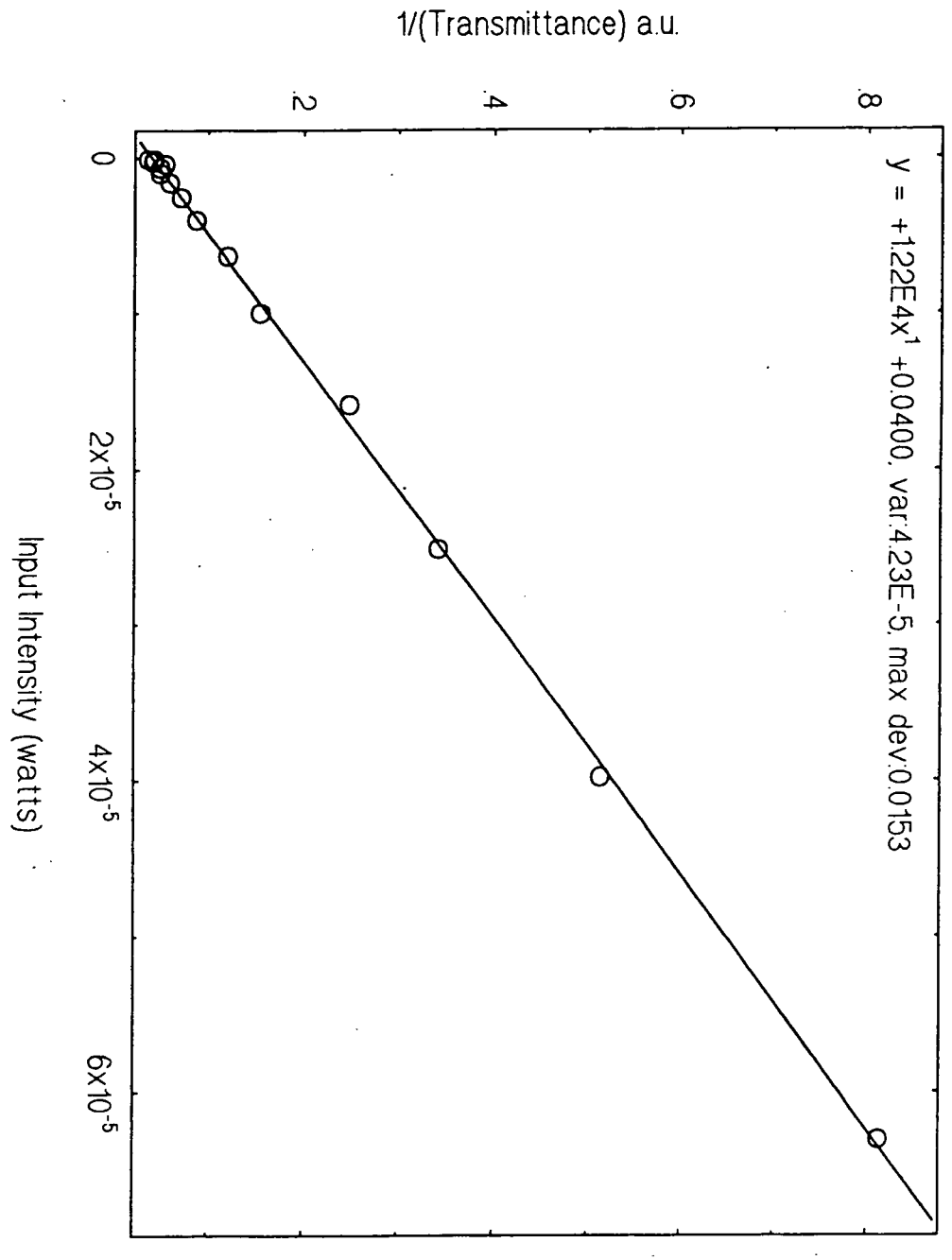

Figure (5.10) A plot of the inverse transmission versus input intensity.

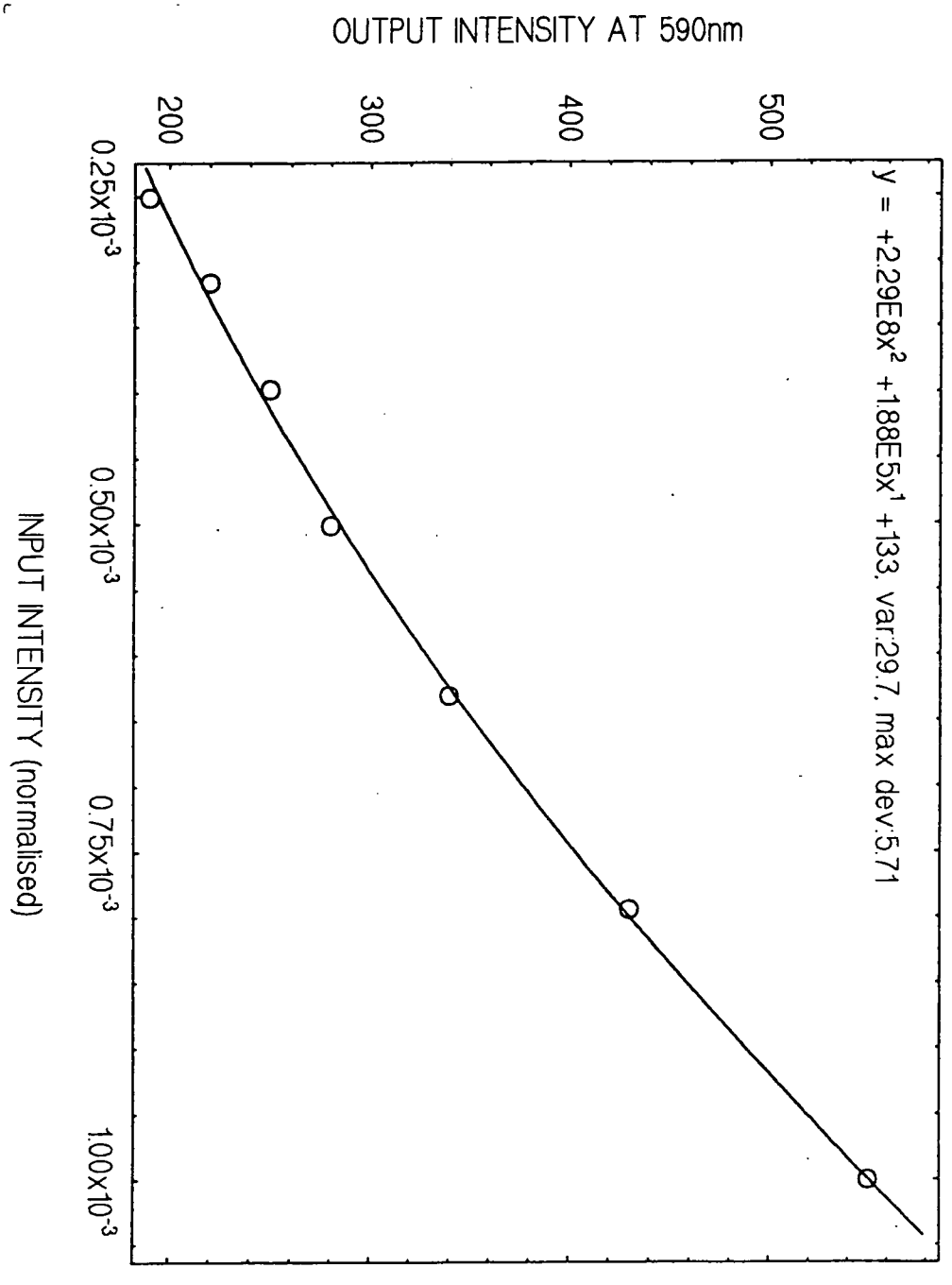

Figure (5.11) A closer examination of the low input intensities from figure (5.7).

$$T = \frac{\eta_1 \eta_2 e^{-\alpha L}}{1 + \beta \eta_1 I_{inc} \frac{\left(1 - e^{-\alpha L}\right)}{\alpha}} \tag{5.3}$$

The following assumptions were made :

Prism coupling efficiency, $\eta_1 = 0.4$,

Output coupling efficiency, $\eta_2 = 0.1$,

Length of waveguide L = 2.1 cm,

α = 1dB/cm = 0.226 cm^{-1}.

Thus equation (5.3) can be re-arranged to :

$$T^{-1} = 40.16 + 67.15 \beta I_{inc}$$

From our experiments we have a fit of $Y = 0.04 + 1.22*10^4 X$

Hence β = 181.68 cm/W or $1.8*10^{11}$ cm/GW.

This value is rather large, the value of β quoted by Villeneuve, (1990) for their semiconductor waveguides is 100 cm/GW. Thus with such a large difference in the values obtained a closer look at the mechanism was necessary. The transmission experiments were repeated but in slightly different conditions.

A new sample was made on a silicon substrate. Polyvinyl alcohol (PVA) was used as the buffer layer and for the waveguiding layer, R-B doped polycarbonate (PC)

was used. The PVA was dissolved in water, at approximately 5% weight ratio, heated and stirred and dipped onto the silicon at 20 mm/min. The film was baked in a vacuum oven for 30 minutes. Also a solution of 0.0096 g of R-B (10^{-3}M) and 3.96 g of PC in 20 ml dichloromethane (15% weight ratio), i.e. 0.24% weight ratio of dye to polymer, was made. A film was dipped on to the PVA layer at 30 mm/min. Once the sample was made, one end of the sample was cleaved to allow efficient out coupling of the light from the waveguiding layer. Prism coupling was used for input coupling.

Before any transmission experiments were carried out on the new sample the PMT was calibrated, so that the output could thus be measured in terms of watts. The PMT calibration graph is shown in figure (5.12). From this graph it can be seen that the calibration produced a straight line for neutral density filters with N_d values of 5.0 and above in front of the PMT.

Initially the transmission experiments were performed by prism coupling the HeNe into a waveguide mode and out coupling the light, from the cleaved face of the silicon, using a 40 times microscope objective lens. The light was then focussed onto the PMT. See figure (5.13) for a schematic of the apparatus.

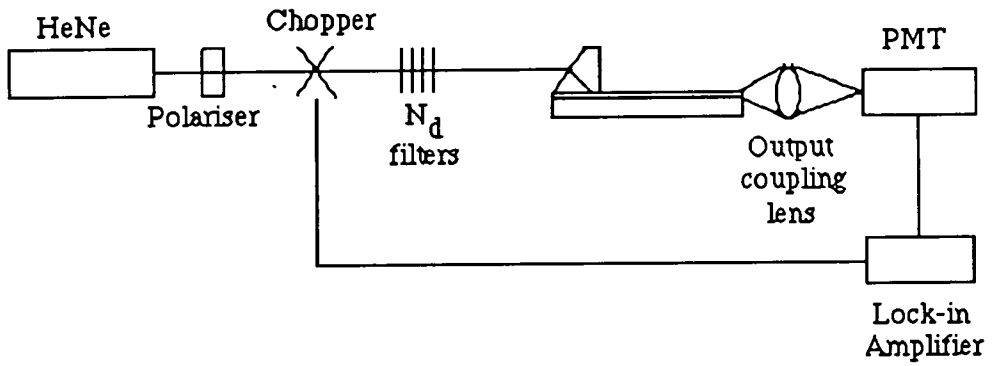

Figure (5.13) Experimental set up for intensity dependence studies.

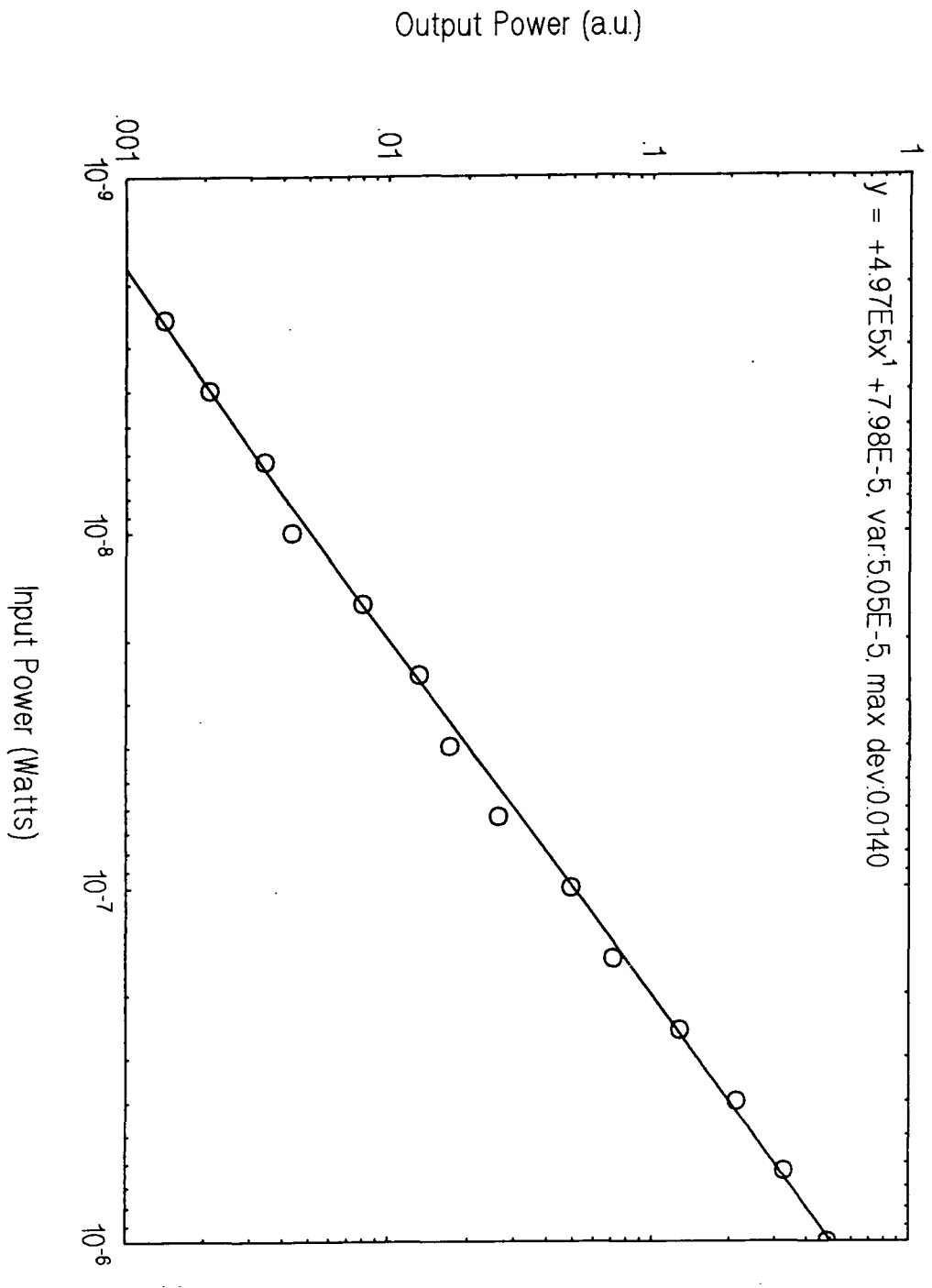

Figure (5.12) The calibration graph of the photomultiplier tube.

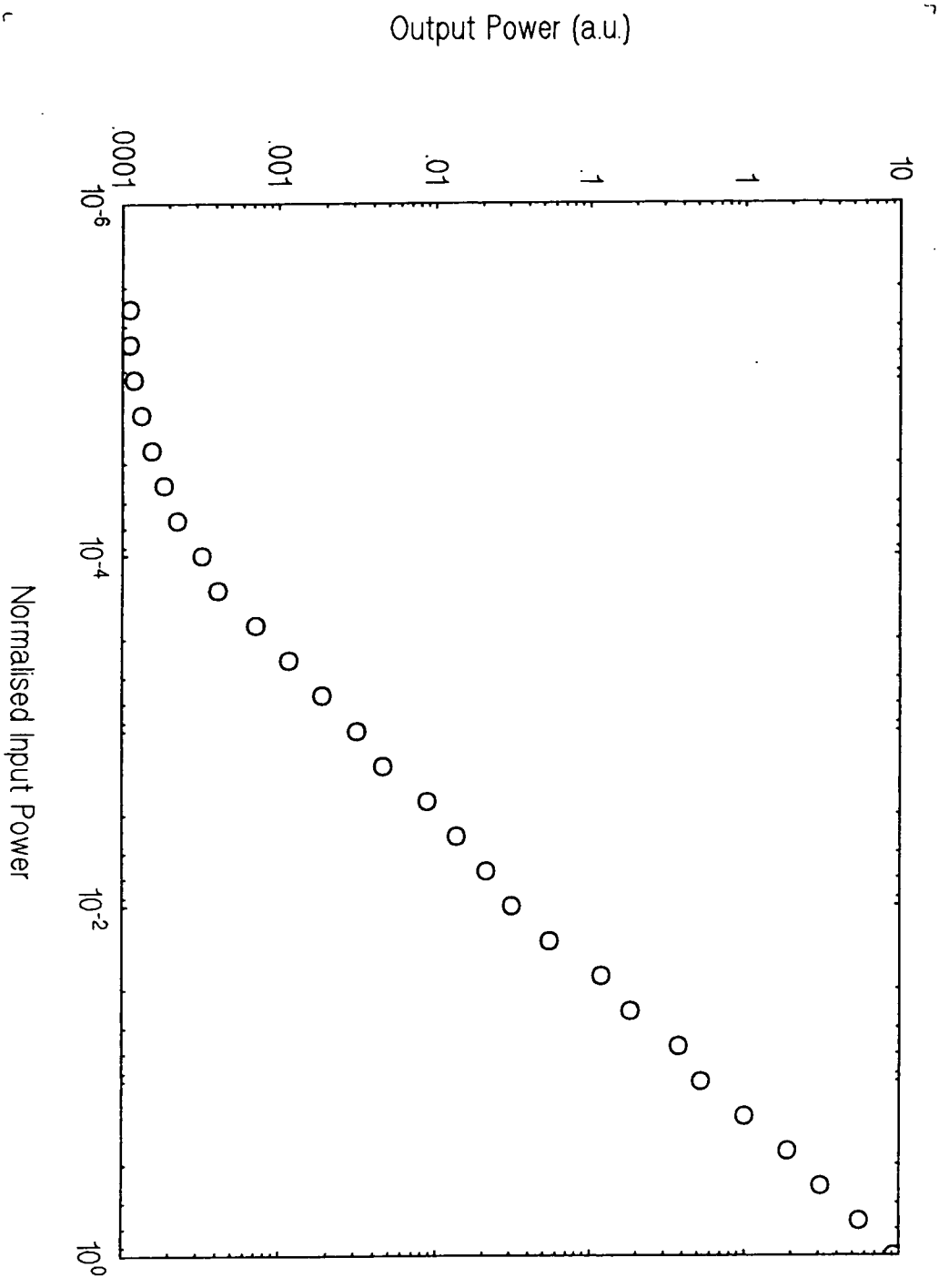

Figure (5.14) Output power of the HeNe as a function of the input intensity using prism coupling.

The intensity dependence of the transmission was measured by varying the N_d filters. The results are shown in figure (5.14). From these results a linear response can be seen, which would seem to rule out any nonlinear absorption processes that may be used to explain the upconversion observed. At lower input powers the output reaches the limit of detection.

As an alternative experiment the sample was cleaved on the input end face, and the HeNe end fired into a waveguide mode. The mode was again seen clearly as a visible streak of the R-B fluorescence. The HeNe was end coupled out and detected in the same way as before. A pinhole was used to block out any multiple reflections from the series of N_d filters used. The results of the transmission experiments are shown in figure (5.15). The experiment was repeated using an undoped sample, prepared and characterised in exactly the same way. These results are shown in figure (5.16).

Both sets of results seem to show a linear dependence of output power on input intensity. This is not in accord with what was seen before. This is significant, since the apparent nonlinearity estimated before, and seen in the experiments was very large. Thus by changing the host polymer to PC and the substrate to PVA on silicon would not seem to be enough to cause such differences in the results. Also the upconversion was still quite visible. Hence this led one to rethink the previous sets of experiments, and also the proposed TPA mechanism.

Since the linearities in the transmission with input intensity were quite repeatable, the nonlinearities observed before could be attributable to the limited linear range of the detectors used, i.e. PMT and the lock-in amplifiers. Thus any results taken outside this regime would be spurious.

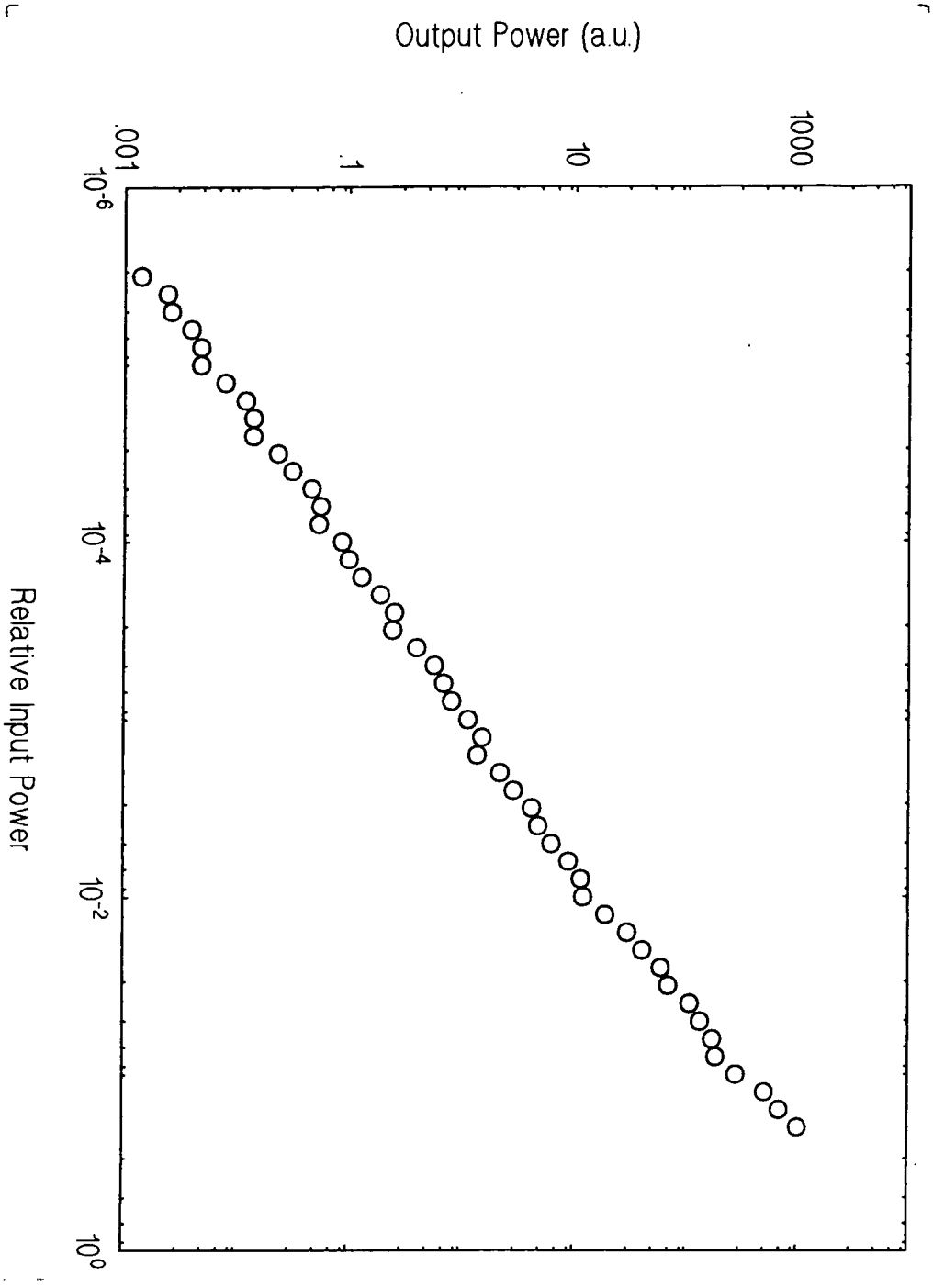

Figure (5.15) Output power of the HeNe as a function of the input intensity using end fire coupling.

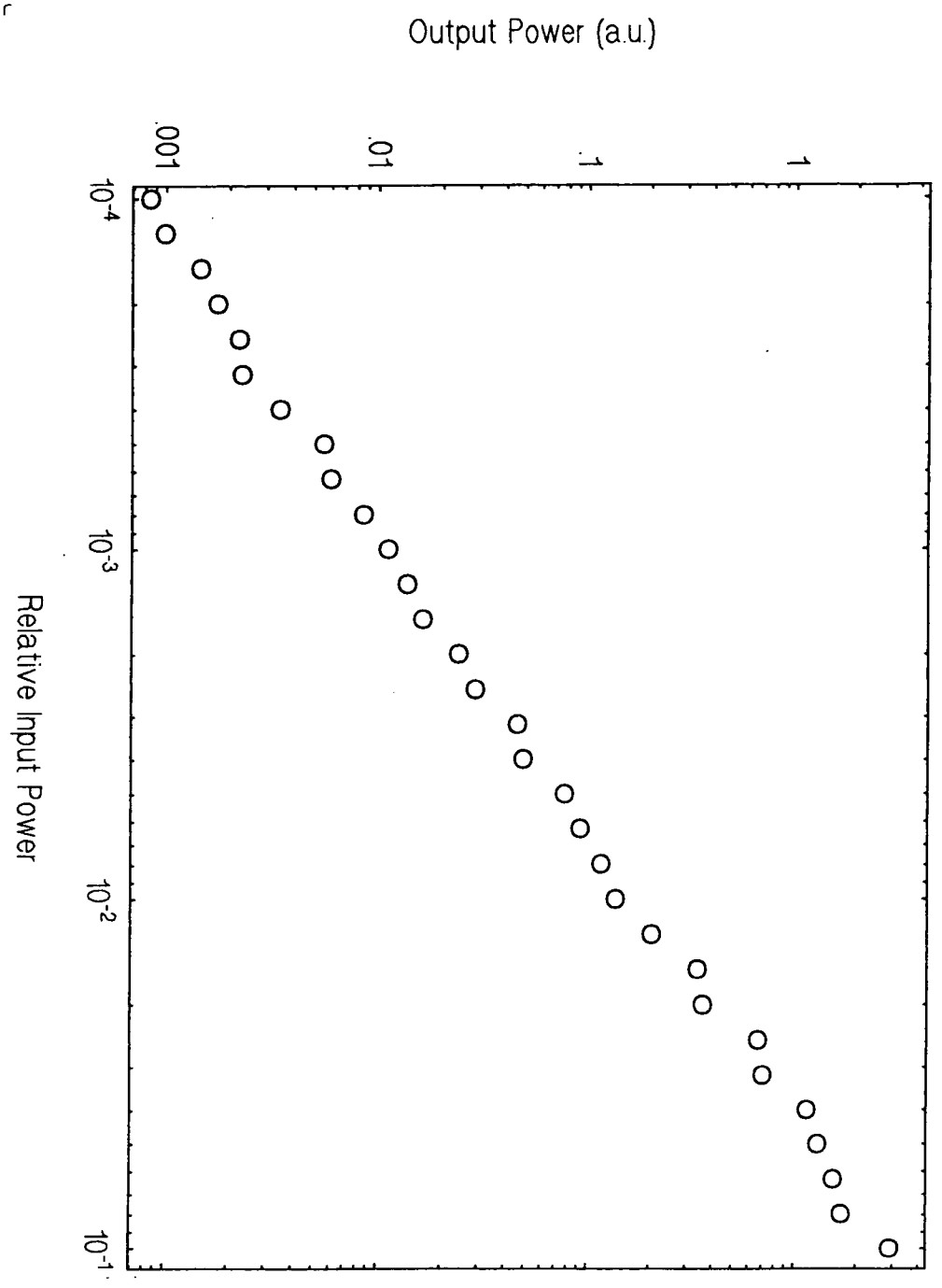

Figure (5.16) Output power of the HeNe as a function of the input intensity using end fire coupling, from an undoped sample.

Another factor to be taken into consideration is that work by Hermann and Ducuing, (1972) has shown the TPA cross section of R-B to be much smaller and more reasonable than the value calculated using the results reported here. The nonlinearities were seen at much higher intensities than used in the experiments reported here.

5.3 The Thermally Activated Excitation mechanism.

In the light of the experiments described above an alternative explanation was sought. These studies began with a look at the normal single photon absorption profile at 633 nm. In order to do this a block of PMMA - doped R-B was made by pouring a solution of the dye in polymer, 0.4% weight ratio, into a beaker and allowing the solvent to evaporate. This produced a solid sample at the base of the beaker approximately 1.5 mm thick. This was sufficiently thick for the spectrophotometer to detect any normal absorption at 633 nm. See figure (5.17) for the absorption spectrum obtained. It can be seen from the absorption profile that there is a small amount of absorption at 633 nm. The spectral shape of the absorption spectrum in the long wavelength tail is sometimes governed by thermal population [Meyers R. A., (1990)].

After consultation with Dr W. Blau at Dublin University, who had also seen this effect but under different conditions [Rossi B. et al., (1991)], a series of experiments were devised to explain the upconversion using a thermal model.

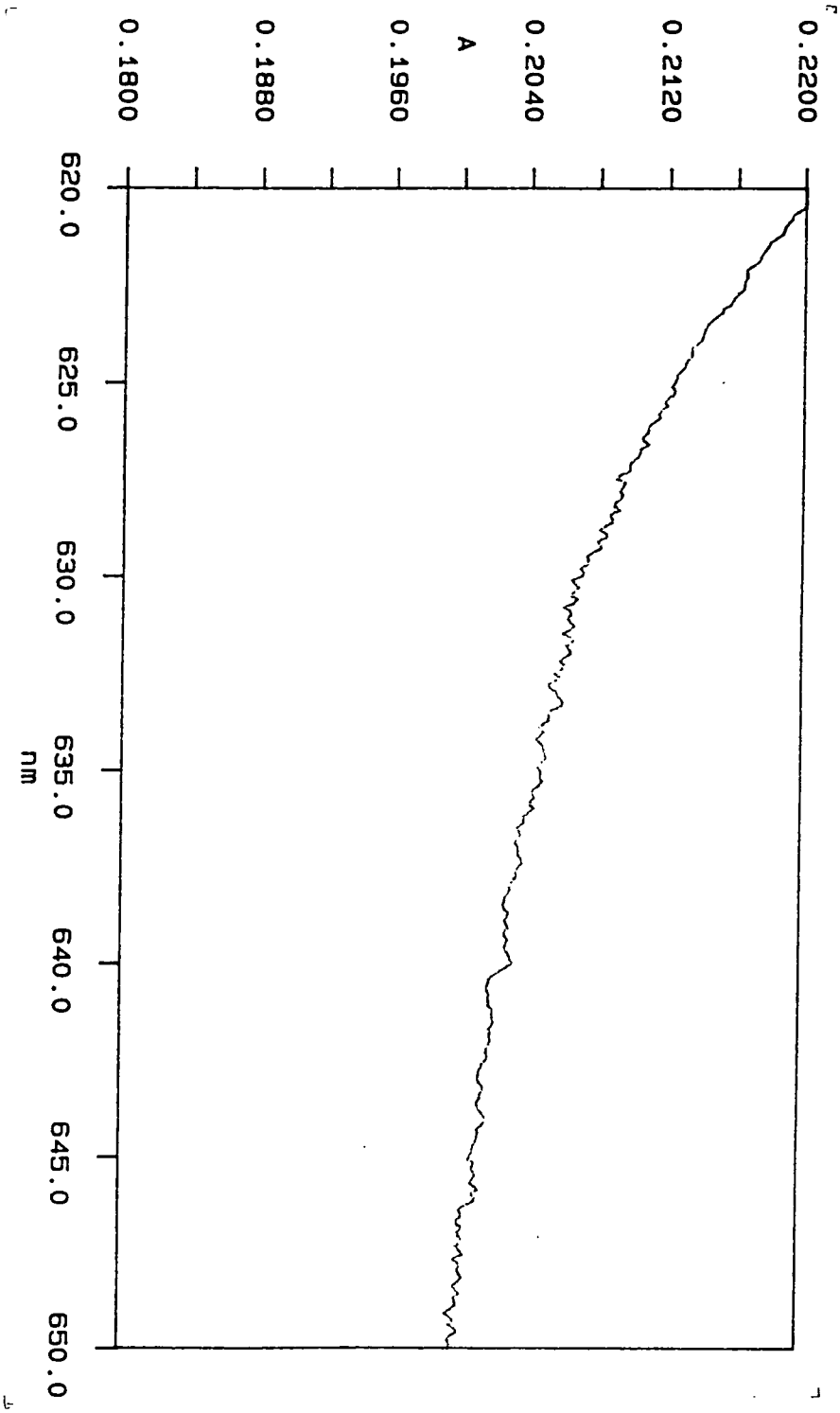

Figure (5.17) The absorption spectrum of a block of rhodamine B doped PMMA, approximately 1.5 mm thick.

5.3.1 The model

This model proposes thermally activated upconversion in the dye doped polymer waveguide. A schematic diagram of the model is shown in figure (5.18).

The thermal activation model involves the promotion of thermally excited molecules in the ground state to the first excited state. These molecules then drop back via the normal fluorescence process.

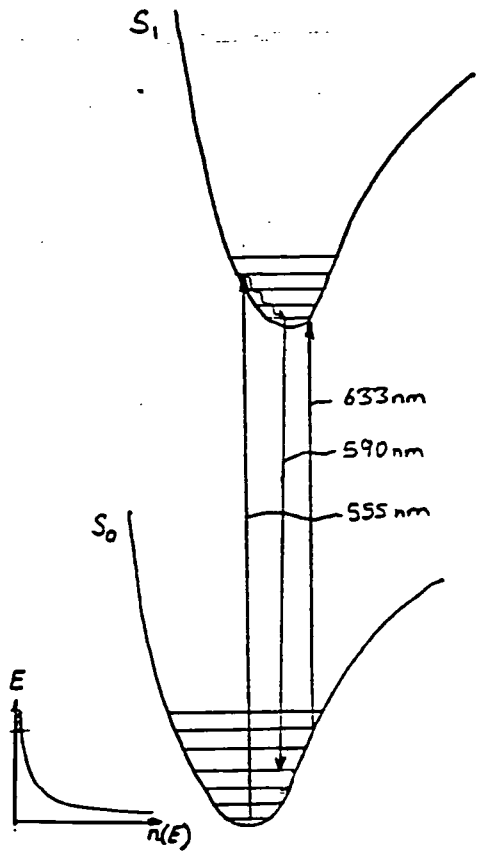

Figure (5.18) A schematic diagram of the proposed thermally activated upconversion model.

The population of molecules in the ground state follows a Boltzmann distribution, as shown in figure (5.19).

This graph illustrates the distribution of molecules in the vibrational levels of the ground electronic state at room temperature. The shaded region represents the molecules that can be promoted with 633 nm wavelength excitation light source. The ratio of thermalised molecules in the ground electronic state is given by :

$$\frac{N_u}{N_g} = e^{-\left(\frac{\Delta h\nu}{kT}\right)} \qquad (5.4)$$

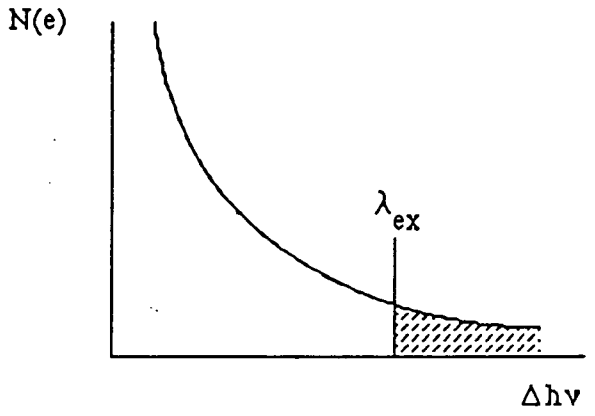

Figure (5.19) The distribution of molecules in the ground state.

where N_u - number of molecules in the upper vibrational level.

N_g - number of molecules in the ground vibrational level.

$\Delta h\nu$ - difference in energy between N_u and N_g. i.e. between 633 nm and the peak absorption wavelength.

From equation (5.4) it can be seen that by changing the temperature of the system the electronic distribution will change. Hence, also, will the number of molecules being promoted. This will result in changes of the fluorescence intensity with temperature.

5.3.2 The Experiments and Results

In order to investigate the dependence of the intensity of fluorescence with temperature, the apparatus used is shown in figure (5.20). The sample used was the same R-B doped PMMA block used earlier for the absorption measurements. A piece was cut off from the block and clamped securely to a flat heating block, and arranged so that there was no movement of the polymer during the heating process.

Using a 40 times microscope objective lens the HeNe beam was end fired in to the block. A visible fluorescence streak was observed along the sample. The fluorescence was detected using a multimode optical fibre, n.a. 0.47, at the origin of the waveguide.

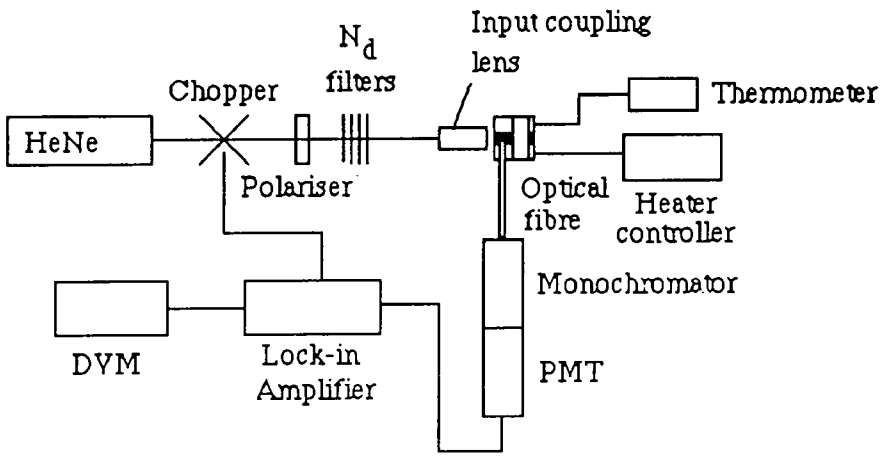

Figure (5.20) Experimental set up for thermal dependence studies.

The temperature controller was used to increase the temperature of the heater and thus the temperature of the sample. Since the sample was in intimate contact with the heater the temperature of the heater, as read with the thermometer, was assumed to be the same as the sample. At each temperature setting the intensity of the fluorescence detected was measured. The results are shown in figure (5.21).

From figure (5.21) it can be seen that the fluorescence intensity increases with temperature in a reasonably linear fashion. With decreasing temperature the intensity of fluorescence also decreased. The difference in the intensities between increasing and decreasing the temperature can be possibly attributable to the degradation of the dye at the higher temperatures. This fact was a limitation to the highest temperature achievable. The linear dependence is not in agreement with the theory outlined earlier.

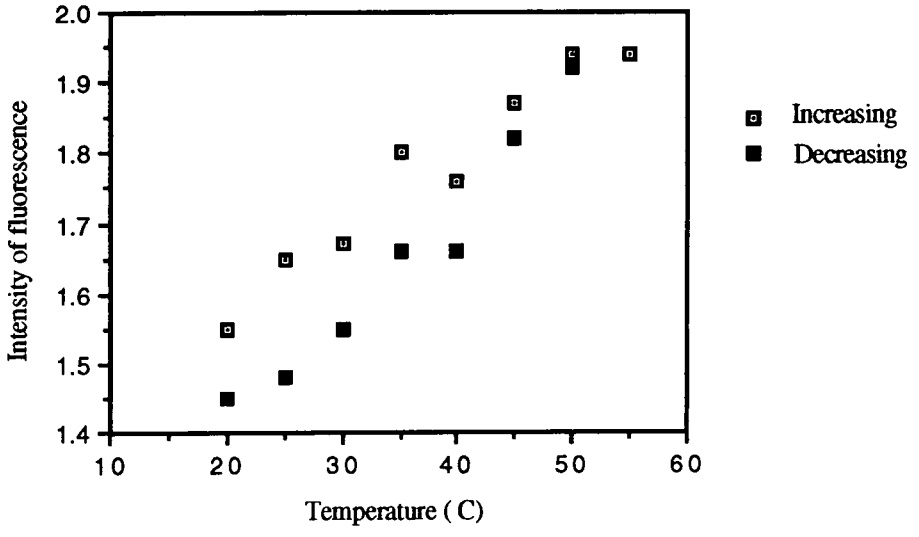

Figure (5.21) Results from the temperature dependence studies on the fluorescence.

The actual temperature range is, however, limited and it is not possible to draw any conclusions as to the exact formal nature of the mechanism. Thus it was important to also decrease the temperature of the system and monitor the intensity of fluorescence. This experiment was performed at Imperial College, since there was a cryostat which allowed the system to be cooled down to 78 K. The apparatus used is shown in figure (5.22).

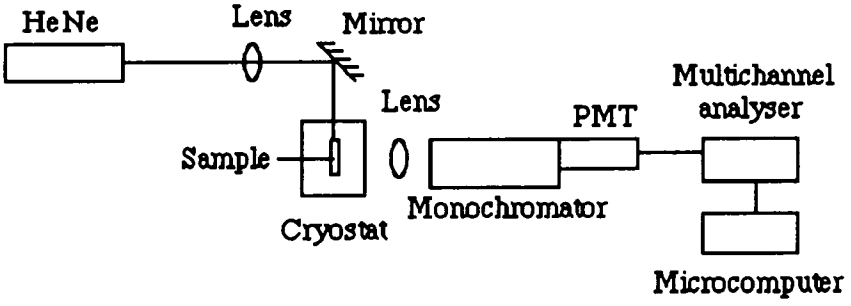

Figure (5.22) A schematic diagram of the equipment used to measure the intensity of fluorescence at very low temperatures.

The sample used was the same rhodamine B doped PMMA block used earlier. It was placed in a cryostat and liquid nitrogen was poured in to cool the system down. Using a 10 cm focal length lens the HeNe beam was focussed into the side of the sample and a collecting lens was used to focus the fluorescence emission onto the entrance slit of a monochromator. A photomultiplier tube at the exit slit was used to detect the signal. This was connected to a multichannel analyser to display the results, which were then stored onto a microcomputer.

Initially the monochromator was used to scan the emission wavelengths at different temperatures, the results are shown in figure (5.23). Here it is clearly seen that as the temperature of the system decreases so the intensity of the fluorescence spectrum

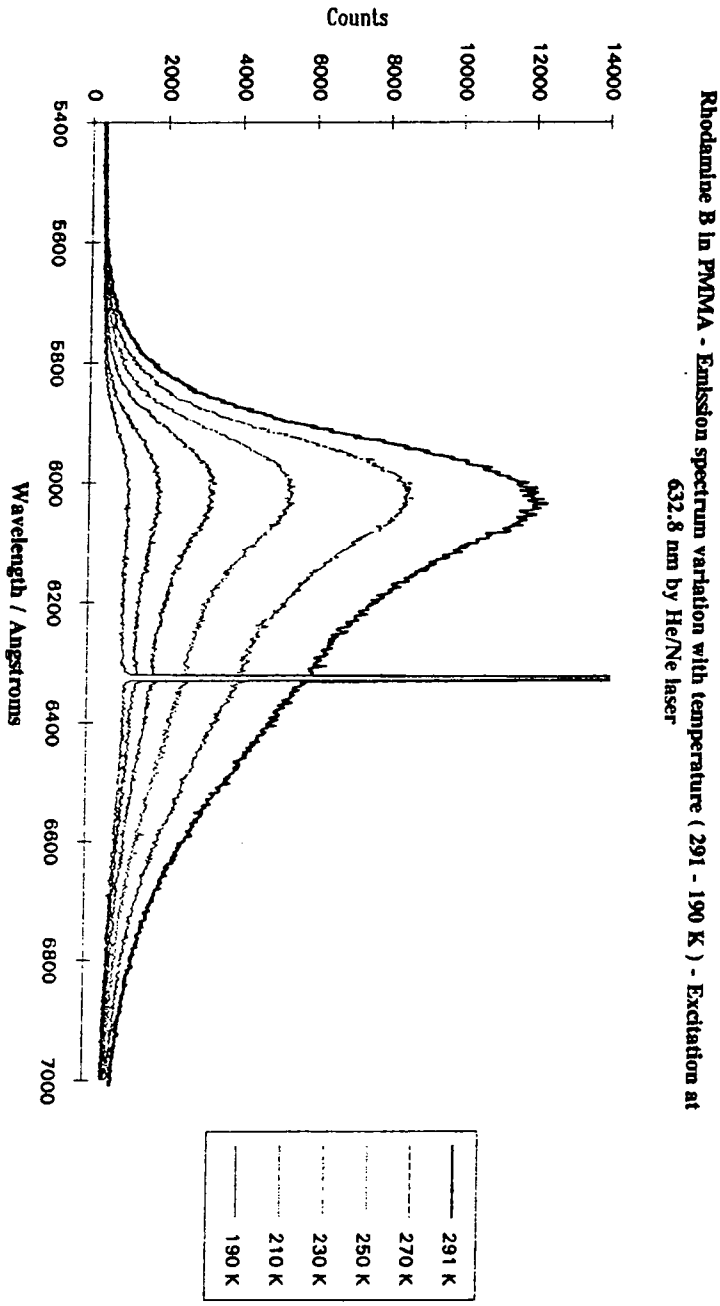

Figure (5.23) The fluorescence spectra of rhodamine B, excited at 633 nm, as a function of reduced temperature.

decreases. It disappears completely at 78K. This is very good evidence that the absorption is thermally activated.

The monochromator was then set to 590 nm and the intensity of the fluorescence at 590 nm was monitored as a function of temperature. The multichannel analyser was set to average over a set number of channels, the intensity it recorded. Figure (5.24) shows the result obtained. Here it is clearly seen that as the temperature decreases so does the fluorescence intensity, and is completely diminished by 180 K.

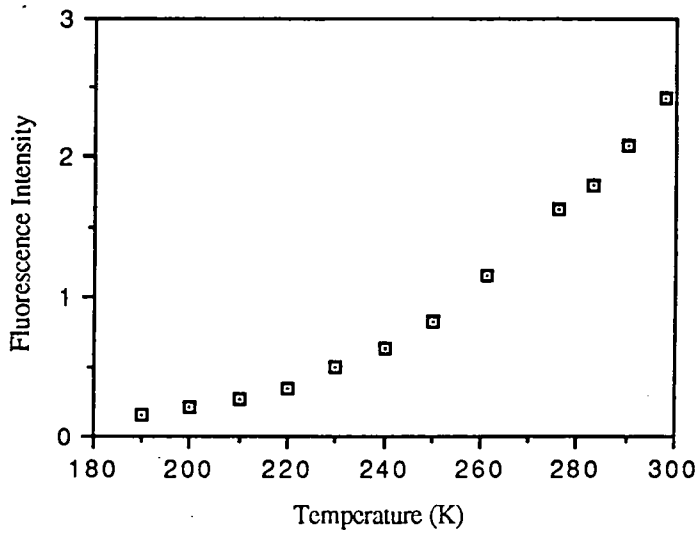

Figure (5.24) Intensity of fluorescence as a function of temperature.

From this data and using the model given by equation (5.4) a log(I) vs 1/T graph was plotted, i.e equation (5.4) can be re-arranged to:

$$\ln I = \ln A - \frac{\Delta E}{kT}$$

Figure (5.25) shows a plot of ln I vs Inverse temperature.

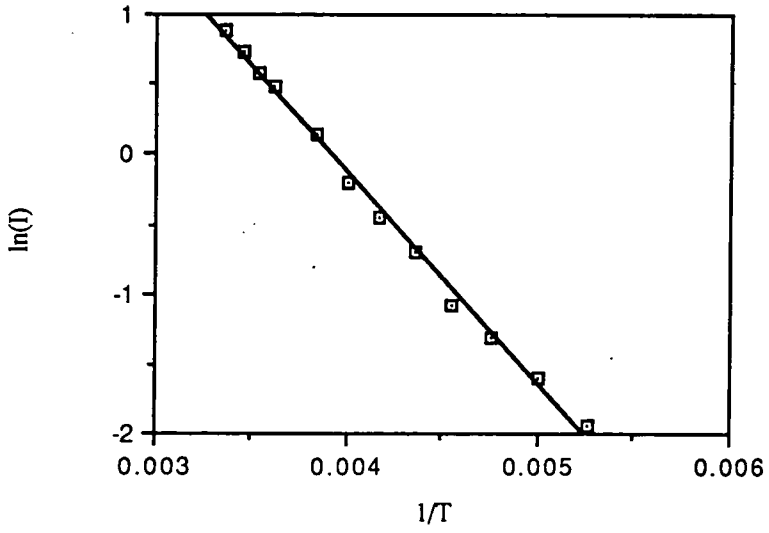

Figure (5.25) A plot of log(I) vs 1/T for the low temperature data

The data was fitted to a straight line with the following function :

$$y = 5.92 - 1514\,x$$

Hence $\frac{\Delta E}{k} = 1514$, since $k = 1.38 \times 10^{-23}\ JK^{-1}$ so $\Delta E = 0.13$ eV.

Thus the energy difference between the vibrational ground state molecules and those excited by 633 nm light is 0.13 eV. A schematic diagram of the energy levels involved is shown in figure (5.26). The assumption made here is that the thermalised molecules are excited to the lowest lying vibrational levels in the excited electronic state. This assumption is in close agreement with the energies calculated, i.e. 1.96 eV (HeNe wavelength) + 0.13 eV = 2.09 eV. This is close to the peak of the fluoescence energy, 2.10 eV, which represents the energy difference via radiative decay.

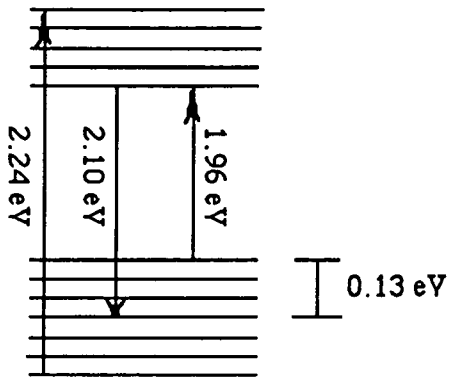

Figure (5.26) A schematic diagram of the energy level scheme for the thermal model.

Using the same rhodamine B doped PMMA block a series of absorption spectra were recorded as a function of temperature. These spectra were recorded by Julia Elliot, at Imperial College. The spectra are shown in figure (5.27). This figure quite clearly shows the shift of the absorption tail to shorter wavelengths with decreasing temperature. This is in accord with the proposed model, since any thermalised molecules would drop in energy and thus the absorption at long wavelengths would decrease, since these molecules would not be promoted to the first excited electronic state.

From this series of thermal experiments it has been shown that there is a logarithmic dependence of the intensity of fluorescence with temperature, with excitation in the long wavelength tail of the absorption band. This has been further supported by absoprtion studies at different temperatures. A log(I) vs 1/T plot produces a straight line with a gradient of 0.13 eV. This fact also implies a Boltzmann relation in the intensity of fluorescence, and hence the population of the higher ground vibrational level in figure (5.26). The 0.13 eV represents the minimum energy required by an electron to be promoted by excitation with 633 nm light.

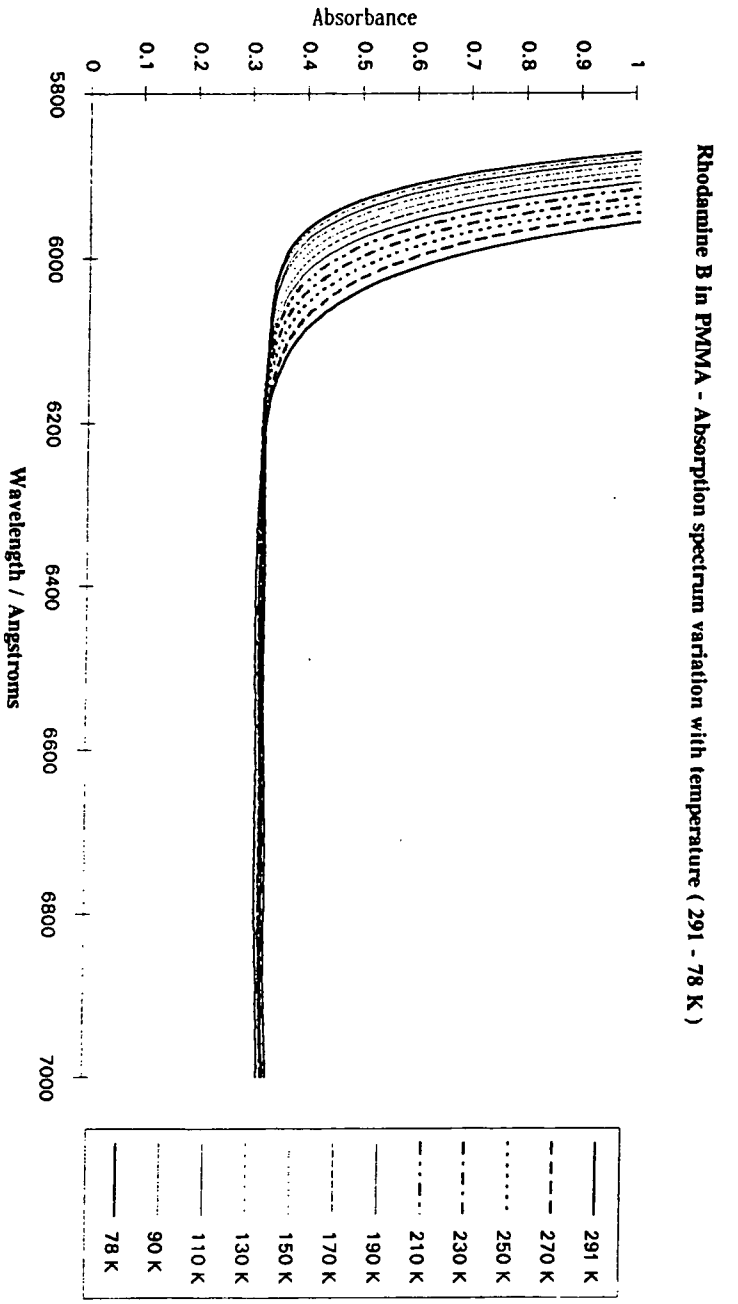

Figure (5.27) The absorption spectra of rhodamine B as a function of temperature.

With the quality of the fit, and the closeness of the values calculated on this very simple model, this series of experiments have confirmed that the upconversion observed is predominantely a thermally activated process.

5.4 Conclusion.

In this chapter the observation of upconversion in a dye doped polymer waveguide was made which was not immediately explicable. Hence, this led to a series of proposed models and experiments to test these models. From the models proposed the thermal activation of upconversion seemed to best fit the data recorded.

The results from the pump/probe experiment reported in section (5.2.2) have not been resolved in light of the thermal model. This experiment requires careful repeating under strict conditions. The result implies bleaching of the first excited state, but it has been shown that the HeNe only excites a small proportion of the molecules from the ground state, not enough to bleach the first excited state and hence reduce the absorption coefficient at the GreHeNe wavelength, thus increasing its transmittance through the sample.

5.5 References.

Hermann J. P. and Ducuing J.,"Dispersion of the two photon cross section in rhodamine dyes.", Opt. Comm., Vol 6, No 2, pp 101-105, (1972).

Meyers R. A., "Encyclopedia of lasers and optical technology", Academic Press, California, (1990).

Rossi B., Byrne H. J. and Blau W.,"Degenerate four wave mixing in rhodamine doped epoxy waveguides.", Appl. Phys. Lett., Vol 58, No 16, pp 1-3, (1991).

Villeneuve A., Sundheimer M., Finlayson N., Stegeman G. I., Morasca S., Rigo C., Calvani R. and De Bernardi C.,"Two photon absorption in InGaAlAs/InP waveguides at communications wavelengths.", Appl. Phys. Lett., Vol 56, No 19, pp 1865-1867, (1990).

CHAPTER 6

Conclusion.

The main aim of this research was to characterise potential materials for designing wavelength tuneable light sources for integrated optics. As potential materials several polymers have been investigated for their suitability to integrated optics. For tuneability in output organic dyes, used as amplifying media in dye lasers, have also been investigated for their suitability. Energy transfer between donor and acceptor dye pairs can improve the lasing efficiency of the acceptor dye. Thus this mechanism was investigated in the solid state.

The theoretical considerations, and fundamental concepts of waveguiding in thin films have been presented. Also various techniques of processing the materials and forming the thin films in a sufficient enough quality to be able to waveguide have been outlined. Different input and output coupling techniques have been discussed. Particular attention has been paid to prism, end fire and grating coupling.

A grating structure has been fabricated using an SEM. Poly (methyl methacrylate) was used as an electron sensitive material, and using the electronic scanning facility of the SEM a grating could be etched on to the polymer. The grating formed had a pitch of 1.6 μm. This is a quick and relatively simple technique to produce gratings, that does not involve the accuracy of interference techniques.

The experimental results from the characterisation of the linear optical properties of polymeric thin films are presented. From a solution of the polymer in a solvent, thin films were formed by dipping the substrate into the solution and withdrawing at a controlled rate in a clean room. This produced excellent quality thin films from

thicknesses of 0.1 - 10 μm. The thin films were then characterised for their linear optical properties. Prism coupling was used to couple the light in and out. This form of characterisation provides a good scanning process for potential polymers and is a reliable guide as to the performance of these polymers. From the results it has been shown that polymers are good materials for light guides. Also the dipping procedure allows for easy doping of the polymer thin film for different desired optical properties.

The mechanism of non-radiative Förster energy transfer, between donor and acceptor dye pairs, has been investigated, as a means of efficiently exciting the acceptor dye. The energy transfer has been shown to be primarily a result of dipole-dipole interaction between the dyes. Also increasing the extent of spectral overlap between the donor fluorescence and acceptor absorption, is an important factor in optimising the efficiency of the energy transfer process.

Initially the absorption and fluorescence spectra of several dyes were recorded to observe the extent of spectral overlap. From this study two dye pairs were further investigated. These were rhodamine 6G/rhodamine B and the newly developed BASF dyes O240/R300. The absorption and fluorescence spectra were recorded at different concentration ratios in thin polymer films. The effect of energy transfer on the absorption and fluorescence spectra was observed and also the optimum concentration ratio for the dye pairs was determined. From this form of analysis, efficient non-radiative energy transfer was observed and qualitatively assessed.

A more quantitative study was performed on the same dye pairs by measuring the fluorescence lifetimes of the dyes in the polymer thin film. The technique of time correlated single photon counting was used. The philosophy of the technique, along with a description of the apparatus used, has been explained.

From the results of these experiments it was seen that the acceptor dye lifetime is independent of its concentration in the mixture, within the concentration range of interest, and does not change significantly with the introduction of the donor dye. Also the fluorescence lifetime of the donor dye decreases as the acceptor dye concentration increases. Stern - Volmer plots have been used to calculate the energy transfer rate of the systems. Also the Förster formulation has been used to calculate the critical radius and the critical concentration of the systems. From the results obtained and by comparision of the results of other systems, it has been shown that both dye pairs show efficient energy transfer.

A series of experiments were performed to test proposed models which were used to explain an upconversion observed in a dye doped polymer waveguide. Here a dye doped into a polymer waveguide was excited in the long wavelength tail of the absorption band, and fluorescence of shorter wavelengths than the pump was observed. Of the models tested the thermal model best describes the observation.

The shape of the long wavelength tail of the absorption band is sometimes governed by thermal population. It has been shown that it is possible to promote thermalised molecules by excitation in the long wavelength tail of the absorption band. Furthermore from the thermal dependence experiments it has been shown that the absorption tail shifts to shorter wavelengths with decreasing temperature. As a consequence of this the fluorescence intensity also decreases. A Boltzmann distribution has been applied to the occupation of the ground electronic state vibrational levels. This has been directly observed from the fluoescence intensity studies, which show an exponential increase in the intensity of fluorescence with temperature.

Further Work.

The polymers have been characterised in a slab waveguide form, to better characterise the optical properties of these materials, however channel waveguiding is required for better confinement of the waveguide modes. This method will also allow structures to be built to control the light. Thus research investigating channel guide formation and characterisation of channel waveguides is needed to develop device structures incorporating channels.

A prototype grating structure has been made, but it would be interesting to make integrated grating structures not only to allow input and output coupling but also to provide distributed feedback of the fluorescence to select a single wavelength. This would lead to the building of a prototype solid state dye laser. So more research is needed to optimise this procedure, investigating all the parameters responsible for the formation of an efficient grating.

Efficient energy transfer has been observed between the dyes pairs investigated. The next step would be to incorporate lasing structures into the thin films. This could be achieved using a grating structure, or external mirrors. The former would be advantageous since then the laser would be truly integral. Even better would be to combine the grating structure with a channel waveguide.

It would also be interesting to look at different polymers and dyes which fluoresce at different wavelengths, and to investigate other possibly more stable dyes as potential materials for a solid state energy transfer dye laser.

The thermally activated upconversion observed here has also been seen in the BASF R300 dye, it would be interesting to observe the extent of upconversion in

various dyes. Also a more accurate picture of the energies of the ground electronic state vibrational levels is required. This could be achieved by energy level calculations based on molecular orbial theory. From this type of analysis a more theoretical approach can be used to predict the temperature dependence.

CHAPTER 7

Appendix.

Molecular structures of the rhodamine and BASF dyes used.

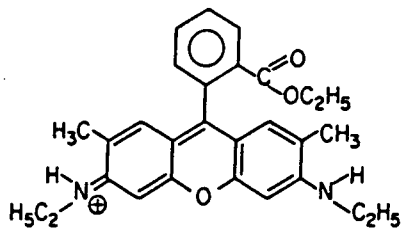

rhodamine 6G

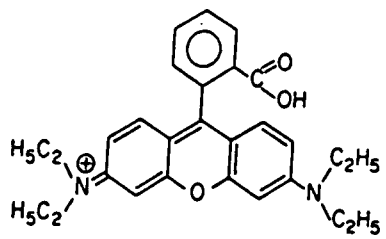

rhodamine B

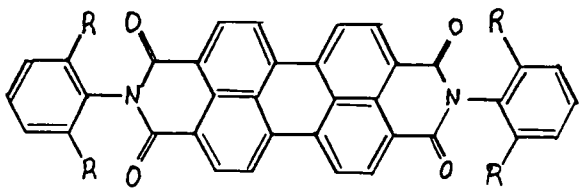

R = $-CH(CH_3)_2$ – BASF 0240[1]

R = – BASF R300

BASF declined to reveal the formula for the R300 dye without a confidentiality agreement.

(1). IVRI J., Burshtein Z., Miron E., Reisfeld R. and Eyal M., "The Perylene derivative BASF 241 solution as a new tunable dye laser in the visible", IEEE J. Q. Elect., Vol 26, No 9, pp1516-1520, (1990).